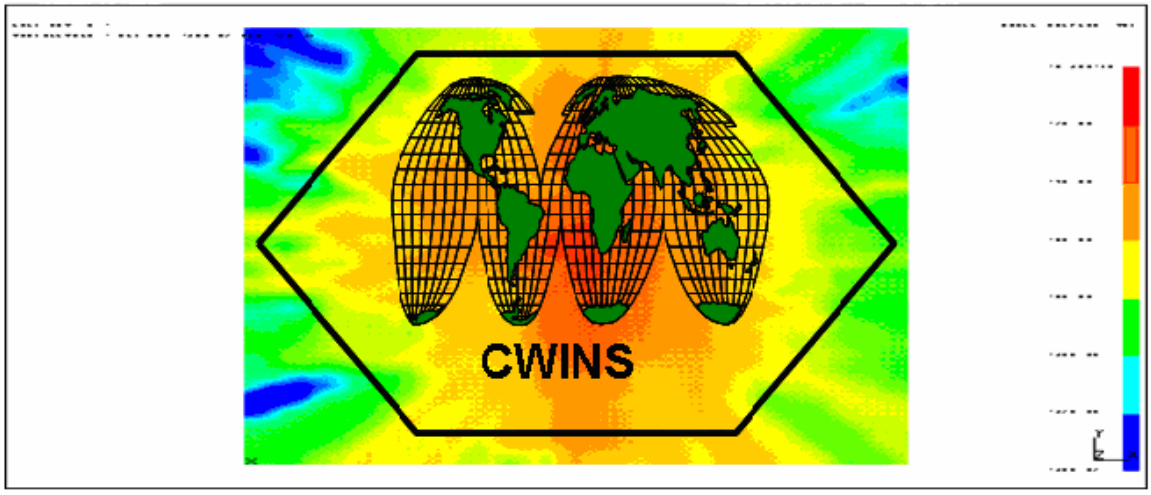

Indoor Geolocation Program - Since 1997

Facilities and Contributions

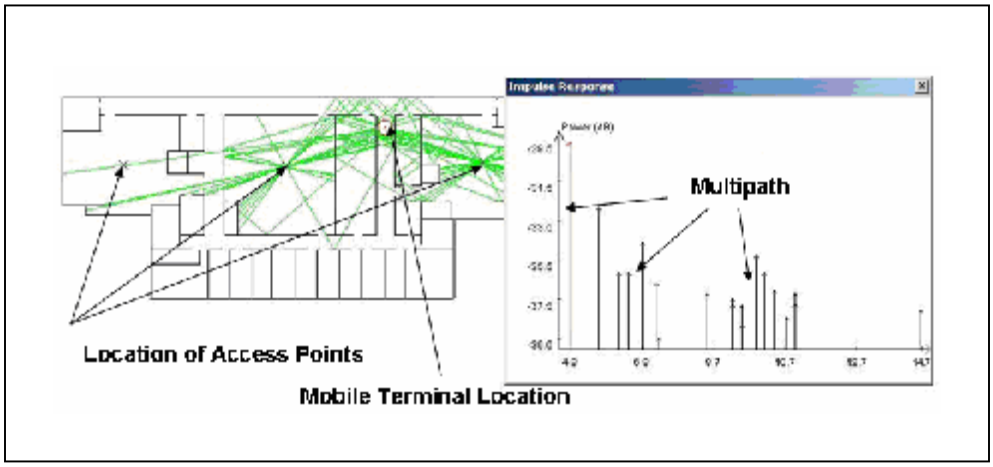

July 2005

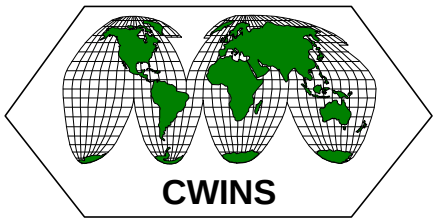

Center for Wireless Information Network Studies

Electrical and Computer Engineering Department, Worcester Polytechnic Institute, Worcester, MA 01609

Part I: Overview of the Program

This brochure describes the indoor geolocation research program at the Center for Wireless Information Network Studies (CWINS), Worcester Polytechnic Institute. The material is divided into two parts. The first part provides an overview of the indoor geolocation program, the history of CWINS, a summary of related research grants, and descriptions of the measurement, modeling, and test facilities available at the Center. The pioneering work of the center in indoor geolocation has resulted in several PhD and MS theses and a number of seminal publications. The first part of the brochure also includes a comprehensive bibliography of the published research work of the Center related to the indoor geolocation. The second part of the brochure provides reprints of selected seminal research papers in indoor geolocation published by members of the Center, reflecting the diversity and depth of the research program.

Overview of the Indoor Geolocation Program

The Indoor Geolocation research program at WPI began in 1997 with a joint project conducted by CWINS and TASC/Litton as a part of DARPA's Small Unit Operation Situation Awareness System (SUO/SAS) program. The pioneering research work of CWINS on radio channel modeling for indoor geolocation application in SUO/SAS program demonstrated the challenges to precise indoor geolocation posed by severe multipath conditions. Since 1997, in addition to active participation in DARPA's leading projects in indoor geolocation Prof. Pahlavan, the director of CWINS, has had close interaction with pioneering indoor positioning commercial companies such as PinPoint, InTrak, Ekahau, Skyhook, and PanGo. The successor to the SUO/SAS project was another joint research initiative between CWINS and the Center for Wireless Communications (CWC), University of Oulu, Finland in 1999 which addressed indoor positioning exploiting the OFDM signals used in IEEE802.11a and HIPERLAN-2 WLANs. In the year 2000 CWINS received a DoD DURIP equipment grant to develop a real-time hardware platform for performance evaluation of modern telecommunication and geolocatoin systems. In the same year CWINS received an NSF award to establish a foundation for indoor geolocation science and technology. This work resulted in the first application of the super-resolution algorithms to RF indoor positioning and the first models relating the distance measurement error using time-of-arrival (TOA) estimation to the bandwidth of an indoor geolocation system. In 2002, the Center received an equipment grant from NSF to update its facilities for UWB measurements operating at frequencies up to 40GHz. In 2004 the Center and IWT won a DoD-sponsored SBIR award for development of precision indoor geolocation using UWB technology. In this work UWB channel models and positioning algorithms in variety of environments are under development. In 2005, CWINS and Draper Laboratory won a DARPA award to work on innovative algorithms for indoor positioning. The current focus of the Center's research is on extending the knowledge base of channel modeling for indoor geolocation, use the propagation models to develop realistic algorithms for precision indoor positioning, and identifying important new applications for this technology.

Key features of the indoor geolocation program at CWINS are:

- Pioneering experience in indoor radio channel measurement and modeling for indoor geolocation and UWB technology
- A unique real-time laboratory testbed for performance analysis of positioning algorithms using Ray Tracing software and the PROPSIM real-time RF multipath channel simulator
- Pioneering experience in application of super-resolution algorithms to accurate indoor geolocation using RF signals
- Experience in development of positioning algorithms for TOA and received signal strength (RSS) systems
- Experience with both commercial and DoD requirements and applications

History of CWINS

The Center for Wireless Information Network Studies (CWINS) is a world-renowned compact wireless research laboratory having a long and successful history of research alliances with industrial and other academic organizations. The Center has performed research for governmental agencies and has developed close ties with many world-leading organizations in the wireless industry. The core competence of the center is in indoor radio channel propagation measurement modeling and in the development of testbeds and tools for design and performance monitoring of location-aware broadband wireless indoor networks. The unique measurement and test facilities at CWINS have been acquired gradually through several NSF and DoD grants, industrial donations, and WPI's cost sharing program for research equipment grants.

The research program in wireless information networks at WPI was established by Professor Kaveh Pahlavan in 1985 and was the first research program of this type in the United States. In 1986, the program was awarded the first NSF grant addressing modern indoor wireless communications. In 1989, the center participated in founding the annual *IEEE International Symposium on Personal, Indoor and Mobile Radio Communications (PIMRC)*, first convened in the UK, and in 1992 and 1998 organized the conference in Boston. In 1991, CWINS organized the *First IEEE Workshop on Wireless LANs*, which was held at WPI. In 1994, the Center initiated the *International Journal on Wireless Information Networks*, the first journal in this field. In 1995, Prof. Pahlavan and Dr. Allen Levesque published *Wireless Information Networks* (John Wiley and Sons), the first graduate-level textbook on wireless networks. In 1995 the Center formed the Wireless LAN Research Laboratory (WLRL) as an industrial research alliance to address the newly growing interest in WLAN technology. In 1996, Prof. Pahlavan was elected as a Fellow of the IEEE for his contributions in wireless office information networks. In 1997, the Center expanded the scope of activity to perform pioneering research on indoor and short-range geolocation applications for the Small Unit Operation Situation Awareness System (SUO/SAS) program under DARPA sponsorship. Also in 1997, the Center initiated a long-term active collaboration with the University of Oulu, Nokia, and several other leading wireless companies in Finland. In 1999, Prof. Pahlavan was the first non-native of Finland to receive the prestigious recognition as Nokia Fellow. In 2000, he was the first scholar to receive the Fulbright-Nokia Fellowship. In 2003 Prof. Pahlavan was co-chair of the International Workshop on Ultra Wideband Systems, Oulu, Finland and in 2004 he served as co-chair of the International Workshop on Wireless Adhoc Networks, Oulu, Finland. In 2005 he is serving as General Chairman of the IEEE International Conference on Mobile Adhoc Sensor Systems, Washington, D.C.

In the past two decades, numerous organizations worldwide have cooperated with CWINS in sponsoring research and development projects, educating their staffs, and arranging for corporate consulting. More details of CWINS activities are available at www.cwins.wpi.edu.

Measurement, Modeling, and Test Facilities

The experimental research program at CWINS utilizes advanced measurement, modeling, and test equipment, which has been acquired gradually since the 1985 inception of the wireless research program through external funding as well as supplemental funding from WPI's cost sharing program. Since 1995 CWINS has received two NSF equipment grants that allowed purchase of around $550K of equipment, one DoD DURIP equipment grant for approximately $250K, and a number of industrial contributions on the order of $100K each. Using CWINS' comprehensive research equipment for multi-layer performance evaluation of location aware broadband wireless networks, a variety of channel-measurement and testbed facilities have been developed and used in the indoor geolocation research program. These measurement and testbed facilities are the foundation for modeling channel behavior for design and performance evaluation of positioning algorithms using TOA, RSS, and MIMO technologies.

Figure 1 shows the Agilent 50GHz 85107B Network Analyzer System and several UWB antennas acquired through NSF research equipment grants. This equipment is used for measurement of the UWB radio channel propagation characteristics, for the analysis of the behavior of TOA in multipath-rich indoor areas, also shown in Figure 1. These measurements are used for channel modeling and performance evaluation of indoor geolocation algorithms in several DARPA sponsored projects at the Center.

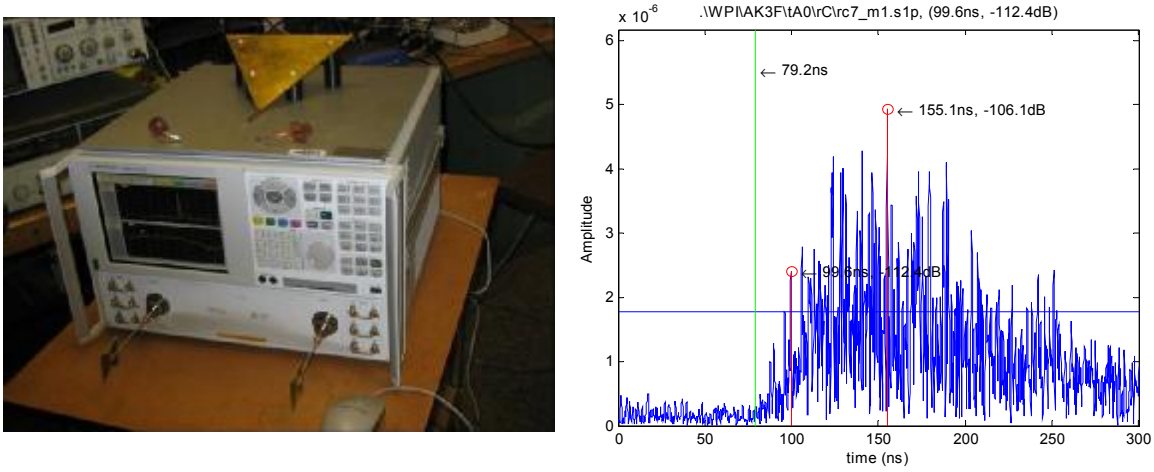

Figure 1: 50GHz Agilent Network Analyzer, UWB antennas, and a sample measurement of the multipath characteristics of an indoor radio channel for indoor geolocation applications.

Figure 2 shows CWINS' unique real-time laboratory testbed for evaluating the effects of multipath on the performance of indoor positioning systems. Three WLAN access points (APs) are connected to three of the eight channels of the PROPSIM C8 real-time channel simulator acquired through a DoD DURIP research equipment grant. The outputs of the channel simulators are combined and fed to the WLAN PCMCIA card of a laptop

running the Ekahau positioning engine. The computer controlling the PROPSIM channel simulations is running CWINS proprietary 2D Ray Tracing (RT) software with its graphical user interface (GUI). The desired location of the APs, the laptop, and the training points needed to calibrate Ekahau software are fed to the GUI of the RT software. The RT generated channel impulse responses are then fed to the PROPSIM C8 to simulate the multipath conditions of the channel in the real-time. Figure 2 also shows a sample performance results for the Ekahau software for 1, 2, and 3 APs and 4, 10, and 27 training points. This repeatable environment can be simulated for comparative performance evaluation of other algorithms and technologies

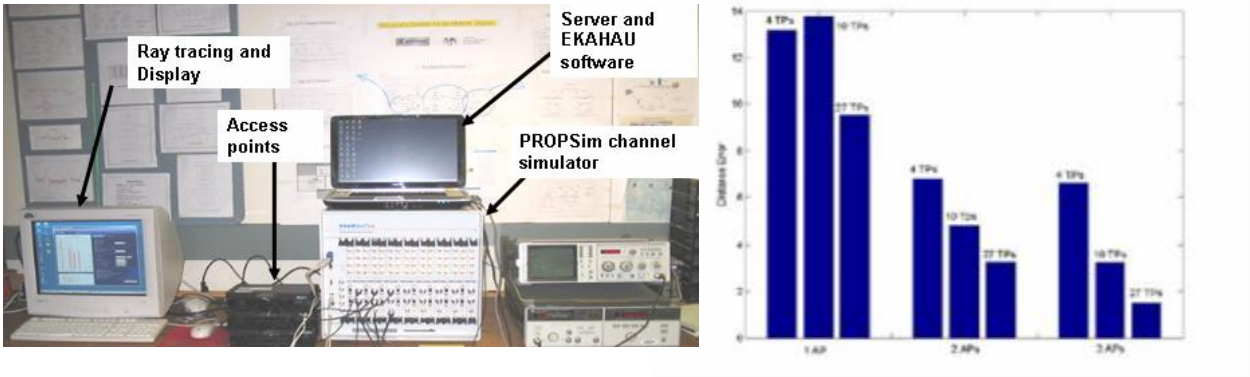

Figure 2: Indoor geolocation laboratory testbed and a sample performance plots for the Ekahau software.

More recently the CWINS laboratory has used its latest NSF research equipment grant to expand its facilities to incorporate RF isolation Azimuth chambers into its performance evaluation facilities in real-time simulated fading multipath conditions. This facility allows cabled laboratory test of wireless technologies using highly-RF-isolated Azimuth chambers, allowing for repeatable and automated test of wireless technologies. Figure 3 shows the unique testbed at CWINS using the Azimuth RF-isolated chamber and PROPSIM real-time multipath channel simulator. This setup allows RF-isolated laboratory test in extensive multipath conditions for wireless devices operating from 350MHz up to 6GHz, with bandwidths of up to 70MHz. This testbed can be used for automated performance evaluation of various features of wireless devices such as coverage, roaming, and positioning accuracies. Figure 3 shows a sample throughput versus path-loss performance of a WLAN measured by Azimuth test facilities.

Figure 3: RF isolated multipath testbed at CWINS using Azimuth RF chamber and PROPSIM real time channel simulator.

The following table summarizes the major pieces of equipment available in CWINS, which can be used for experimental research in channel measurement and modeling and performance evaluation of wireless networks.

Major Equipment at CWINS: Item Description
Proprietary 3-D and 2-D Ray Tracing Software
2-D PlaceTool for WLAN Planning
Ekahau Positioning Engine 2.0
PinPoint 3D- Local Positioning System
PropSim – C8 Wideband Multi channel Simulator
Agilent 85107B Network Analyzer System, 45MHz to 50 GHz
HP-8753B 6 GHz Network Analyzer
HP-85047A S-Parameter Test Set
HP-3780A 10 Mbps Pattern Generator and Error Detector
Azimuth 801W Test System for WLANs
Brix Network Performance Evaluation System
HP Open View Network Node Manager
HP Internet Advisor - LAN/WAN Protocol Analyzer
Tektronix 11402 Digitizing Oscilloscope
HP-8082A Pulse Generator
Mobiwave BPA-D10 Bluetooth Protocol Analyzer - Software
AiroPeek NX for windows - WLAN Protocol Analyzer
Axis 9010A Bluetooth Access Point
Agilent E4419B Dual Channel EPM Series Power Meter
Agilent E440A PSA Series Spectrum Analyzer, 3Hz to 26GHz
Kalpana Ethernet Switch Pro 16
Cisco 4000 Series Router
IEEE 802.15.4 radio modules for adhoc networking experiments
Numerous IEEE 802.11 a,b,g access points and PCMCIA cards
Numerous laptops and PCs for network formations

Indoor Geolocation Related Research Grants

Kaveh Pahlavan (CWINS/WPI) and Robert Tingely (Drapers Laboratory)
DARPA: BAA 04-031
Title of Award: Innovative Indoor Geolocation Using RF Multipath Diversity.
Award amount (and period): $370K Phase I, $754K Phase II (begun March 2005)

In a BAA 04-031 project between CWINS/WPI and Draper Laboratory, the primary objective is to enable accurate, robust localization and tracking of people/assets/objects in indoor environments. This will be accomplished by developing a signal processing methodology and algorithms which address several fundamental limitations of existing active, passive, or aided concepts. This development will be based on localization and tracking of electronic tags capable of receiving and retransmitting (with or without alteration) signals received from known signal sources located within a local network. The key innovation is to more fully exploit the diversity of measurement phenomena and unique waveform characteristics of indoor RF multipath signals. Measurements of received signal strength, angle of arrival, time of arrival, time difference of arrival and Doppler will be exploited, as appropriate, for each individual multipath signal element. CWINS works on the analysis and modeling of the multipath and performance of traditional algorithms and Draper Laboratory works on algorithms exploiting multipath diversity.

Jim Silverstrim (IWT, Forest, VA), Kaveh Pahlavan (CWINS/WPI)
DARPA/DoD SBIR: BAA 03-029
Title: Innovative Methods for Geolocation and Communication with UWB Mobile Radio Networks
Award amount (and period): $70K Phase I, $700K Phase II (begun Feb. 2004)

In this project CWINS and IWT, a small wireless radio development firm, join forces to design an MB-OFDM UWB system with indoor positioning capabilities. The main contribution of CWINS is to characterize UWB RF propagation in various environments and develop indoor positioning algorithms that support accurate indoor positioning in an adhoc networking environment. IWT will design the hardware for implementation of the actual communication network. Phase I of this project was completed successfully and we are awaiting the start of Phase II. In this project Prof. Pahlavan's group used the UWB measurements in 3-6GHz bands to develop a novel model for indoor geolocation. The model was then used for evaluation of indoor geolocation algorithms.

Kaveh Pahlavan and Emmanuel Agu (CWINS/WPI)
NSF GRANT NO. CISE-0303592
Title of Award: An Integrated Multi-Layer Wireless LAN Testbed
Award amount (and period): $284K plus $95K WPI cost sharing (Sept. 2003 to Aug. 2006)

In this project CWINS has been funded to purchase equipment that will significantly enhance its research activities in wireless networks for multi-media applications. The principle feature of this equipment enhancement is an experimental wireless LAN testbed that will be used to serve as a test environment for multi-layer design and performance monitoring. In this testbed, researchers working at all protocol layers of the network will conduct their research to evaluate the impact of wireless broadband access on the design and performance analysis. Multimedia services such as voice, text and image streams will be provided to terminals dispersed over the geographical area covered by the testbed. The planned equipment includes a network analyzer, spectrum analyzer, and RF power meter for physical layer scenario development up to 50GHz, which includes all bands currently considered for UWB systems. Other planned equipment includes wireless access points, a central router and switch, network management and monitoring

software, laptop computers, PDAs, wireless LAN IP phones, and head-mounted displays as well as a traffic generator and protocol analyzers for packet generation and performance monitoring. The wireless LAN Network Interface Cards (NICs) include IEEE 802.11 as well as Bluetooth cards for both laptop computers and PDAs.

Kaveh Pahlavan (CWINS/WPI)
NSF Grant No.: ECS-0084112
Title: Indoor Geolocation Science for 4G Wireless Information Networks
Award amount (and period): $270K (Aug. 2000 to Sept. 2003)

The principal research goal of this project was to provide a foundation for the indoor geolocation science needed in the design and performance evaluation of indoor geolocation systems. Two specific research objectives in this project were (1) To analyze the multipath characteristics of the indoor radio propagation that affect the performance of indoor geolocation systems through empirical broadband measurements in typical sites, and design of statistical measurement-based and geometrical models for the behavior of the channel. (2) To use the results of objective 1 to lay a foundation for the design and performance evaluation of distributed indoor geolocation systems capable of locating objects in smart indoor spaces where numerous unreliable sources interact to provide an accurate location of each element. For the first objective indoor channel measurements of the TOA of the first path at GHz frequencies were performed to prepare a database for future research in this field. The measurement data base includes LOS and OLOS measurements. Results of these measurements were used to analyze the effectiveness of the super-resolution algorithms. Also, a novel model for the distance measurement error for indoor geolocation was developed under this project.

Kaveh Pahlavan, Allan Levesque and Jacques Beneat (CWINS/WPI)
Sponsored by DoD DURIP program
Title: A Hardware Platform for Real Time Wireless Channel Simulation for Modern Telecommunication and Geolocation Military Applications
Award Amount (and Period): $278K (April 2000 to May 2001)

Using the funding in this project CWINS purchased a PROPSim C8 hardware platform for development of a real time RF channel simulation environment. PROPSim is currently the world's leading hardware platform used for real time simulation of wireless channel behavior for cellular networks and WLANs. In addition to simulation for traditional communication systems, the platform can simulate geolocation and smart antenna environments vital to modern military and commercial communication projects. The simulator allows us to test modern telecommunication and geolocation systems quickly and thoroughly under controlled, realistic, and repeatable channel conditions in the laboratory, thereby reducing the time and cost of field tests through improved and better focused test planning.

Kaveh Pahlavan (CWINS/WPI)), Matti Latva-Aho (CWC/U. of Oulu, Finland)
Sponsored by TEKES, Nokia and Sonera, Finland
Title: Wireless Indoor Geolocation and Voice Over IPv6 (WINGIP)
Award Amount (and Period): $420K (Jan. 1997 to Dec. 1998)

In this project CWINS, WPI and CWC, University of Oulu Finland received funding from TEKES, Nokia, and Finnish Air force to work on traffic engineering and architecture of IGT-WIN systems. This project was focused on practical telecommunication aspects in the design of PHY and MAC layers and in the general architecture of the network. Design of system architecture and traffic engineering for IGT-WIN networks were in its infancy. A good solution for this problem involves understanding the worldwide evolution of products and standards. For this reason CWINS-CWC team that has interaction with Nokia and other leading commercial wireless companies is an ideal team to pursue this design. The specific goals of this project were to study the architecture of the existing geolocation products, study the progress in PHY and MAC layer design for Bluetooth and Home RF projects, design PHY and MAC layers to support both geolocation and telecommunication applications, and design an architecture for the Vo-IP network. The project resulted in several graduate theses in the US and Finland.

Paul Creamer and Joe Pizano (TASC, Bedford, MA), Kaveh Pahlavan and Jim Matthews (CWINS/WPI)
DARPA Grant No.: BAA 97-14 (SUO/SAS)
Title: Urban Geolocation System Architecture Analysis and Demonstration
Award amount (and period): $1.2M (June 1997 to Dec. 1998)

The objective of this project was to implement an urban geolocation demonstrator. In the course of the project, it was discovered that due to severe multipath conditions in urban and indoor areas traditional GPS receivers are unable to provide an accurate measurement of the location of objects within the buildings. Preliminary results of ray tracing simulation and initial measurements showed that in many situations the signal arriving from the direct path (DP) is not the strongest signal arriving at the receiver. Traditional receivers, however, lock to the path associated with the strongest received signal. Therefore, the estimated distance found with traditional receivers may correspond to an arbitrary distance that includes a number of reflections of the signal before it arrives at the receiver. This observation revealed a need for research in modeling of the indoor radio channel and design of new signal structures and algorithms for indoor geolocation that led to other indoor geolocation projects pursued at WPI. The preliminary results of this project were presented in several DARPA open review workshops, two DARPA reports, and several pioneering papers and presentations.

Publications in Indoor Geolocation

Selected Journals/Book Chapters

- K. Pahlavan and A. Levesque, ***Wireless Information Networks***, John Wiley and Sons, Chapter 13: RF Location Sensing, Second Edition 2005.
- X. Li and K. Pahlavan, "Super-resolution TOA estimation with diversity for indoor geolocation", ***IEEE Trans on Wireless Comm.***, Dec. 2003.
- K. Pahlavan, X. Li, and J. Makela, "Indoor Geolocation Science and Technology", ***IEEE Comm Soc. Mag.***, Feb. 2002.
- K. Pahlavan and P. Krishnamurthy, ***Principles of Wireless Networks – A Unified Approach***, Chapter 14: Wireless Positioning Systems, Prentice Hall, 2002.
- R. Tingley and K. Pahlavan, "Measurement of the Time-Space Characteristics of Indoor Radio Channel", ***IEEE Trans. on Instrumentation and Measurements***, September 2000.
- K. Pahlavan, P. Krishnamurthy and J. Beneat, "Wideband Radio Propagation Modeling for Indoor Geolocation Applications", ***IEEE Communications Magazine***, April 1998.
- K. Pahlavan and A. Levesque, ***Wireless Information Networks***, 1st edition, John Wiley and Sons, 1995. First comprehensive textbook published in wireless networks.

Conferences

- B. Alavi, K. Pahlavan, N. Alsindi, and X. Li, " Indoor Geolocation Distance Error Modeling using UWB Channel Measurements", The 16th Annual IEEE International Symposium on Personal Indoor and Mobile Radio Communications (PIMRC-2005), September 11 - 14, 2005, Berlin, Germany.
- B. Alavi and K. Pahlavan, "Analysis of Undetected Direct Path in Time of Arrival Based UWB Indoor Geolocation", Proceedings of IEEE 62nd Semiannual Vehicular Technology Conference, September 25-28, 2005.
- B. Alavi, K. Pahlavan, X. Li, and N. Alsindi, "Indoor Geolocation Distance Error Modeling with UWB Technology," Proceedings of IASTED 2nd International Conference on Communication and Computer Networks, CCN 2004, Nov. 8-10 2004.
- M. Heidari and K. Pahlavan, Performance Evaluation of Indoor Geolocation Systems Using PROPSim Hardware and Ray Tracing Software, IWWAN, Oulu, Finland, June, 2004.
- M. Kanaan and K. Pahlavan, CN-TOA a New Algorithm for Indoor Geolocation, IEEE PIMRC, Sep 2004.
- M. Heidari and K. Pahlavan, "A Testbed for Real-Time Performance Evaluation of Indoor Geolocation Systems" IEEE Wireless and Microwave Technology (WAMI), 2004 April 15,16, 2004.

- M. Kanaan and K. Pahlavan, A comparison of wireless geolocation algorithms in the indoor environment, Proceedings of the IEEE WCNC, April 2004.
- N. Alsindi and K. Pahlavan, “Performance of TOA Estimation Algorithms in Different Indoor Multipath Conditions”, Proceedings of the IEEE WCNC, April 2004.
- A. Hatami and K. Pahlavan, In-building Intruder Detection for WLAN Access, The IEEE Aerospace and Electronic Systems Society conference, PLANS, Monterey, CA, April 2004.
- Emad D. Zand, K. Pahlavan and Jacques Beneat, Frequency Domain Measurement for Indoor Geolocation,to be submitted for IEEE PIMRC September 2003.
- B. Alavi and K. Pahlavan, “Bandwidth effect on distance error modeling for indoor geolocation”, IEEE-PIMRC 2003., Volume: 3, 7-10 Sept. 2003, Pages:2198 – 2202.
- B. Alavi and K. Pahlavan, "Modeling of the Distance Error for Indoor Geolocation", IEEE WCNC, 2003.
- X. Li, K. Pahlavan, and J. Beneat, “Performance of TOA estimation techniques in indoor multipath channels”, IEEE PIMRC, Portugal, Sep. 2002.
- X. Li, K. Pahlavan, "Indoor Super Resolution TOA Measurement in Frequency-Domain", IEEE Workshop on WLANs, Boston, Sep. 27-28 2001.
- X. Li and K. Pahlavan, M. Latva-aho, and M. Ylianttila, "Indoor Geolocation using OFDM Signals in HIPERLAN/2 Wireless LANs", IEEE PIMRC'2000, London, Sep. 2000.
- X. Li and K. Pahlavan, M. Latva-aho, and M. Ylianttila, "Comparison of Indoor Geolocation Methods in DSSS and OFDM Wireless LAN Systems", IEEE VTC'2000, Boston, Sep. 2000.
- K. Pahlavan, X. Li, M. Ylianttila, R. Chana, and M. Latva-aho, "An Overview of Wireless Indoor Geolocation Techniques and Systems", MWCN'2000, Paris, May 2000.
- J. Beneat, K. Pahlavan, and P. Krishnamurthy, "Radio Channel Characterization for Geolocation at 1 GHZ, 500MHZ, 90 MHZ, and 60 MHZ In SUO/SAS", MILCOM99, Atlantic City, NJ, November 1999.
- P. Krishnamurthy, and K. Pahlavan, "Distribution of Range Error and Radio Channel Distribution of Range and Radio Channel Modeling for Indoor Geolocation Applications", IEEE PIMRC'99 Osaka, Japan, September 12-15, 1999.
- P. Krishnamurthy, J. Beneat, M. Marku, and K. Pahlavan, "Modeling of the Wideband Indoor Radio Channel Geolocation Applications in Residential Areas", IEEE VTC'99, July 1999.
- P. Krishnamurthy, and K. Pahlavan, "Analysis of the Probability of Detecting the DLOS Path for Geolocation Applications in Indoor Areas", IEEE VTC'99, July 1999.
- P. Krishnamurthy, K. Pahlavan and J. Beneat, “Radio Propagation Modeling for Indoor Geolocation Applications”, IEEE PIMRC'98 Boston, MA, September 8-11, 1998.

- K. Pahlavan, "Emergence of the Location Aware LAN-PAN-HAN Industry", IEEE Workshop on Wireless LANs, Boston, MA, Sep. 27, 2001.
- K. Pahlavan, "Trends in Indoor Geolocation", SAAB Workshop on Short Range Location System, Sweden, May 2000.

Theses Related to Indoor Geolocation Supervised by Prof. Pahlavan

- “A Test-bed for Real-time Performance Evaluation of Indoor Geolocation Systems in Laboratory Environment”, Mohammad Heidari, MS. Thesis, May 2005.
- “Performance of TOA Estimation Algorithms in Different Indoor Multipath Conditions”, Nayef Alsindi, MS. Thesis, May 2004.
- “Measurement of TOA Using Frequency Domain Techniques for Indoor Geolocation”, E. Zand, M.S. Thesis, WPI, May 2003.
- “Super-resolution TOA estimation with diversity for indoor geolocation”, X. Li, Ph.D. Thesis, May 2003.
- “Voice over IP in a Wireless LAN Environment”, J. Feigin, MS Thesis, 2000.
- “Time-Space Characteristics of Indoor Radio Channel”, R. Tingley, Ph. D. Dissertation, 2000.
- “Analysis and Modeling of the Wideband Radio Channel for Indoor Geolocation Applications”, P. Krishnamurthy, Ph. D. Dissertation, 1999.
- “Using Ray-Tracing Techniques in Site-Specific Statistical Modeling of Indoor Radio Channels”, M. Hassan-Ali, Ph. D Dissertation, 1998.

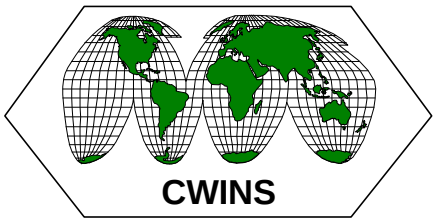

Center for Wireless Information Network Studies

Electrical and Computer Engineering Department, Worcester Polytechnic Institute, Worcester, MA 01609

Part II: Reprint of Selected Publications

In this part of the report we provide reprints of 14 selected and best-cited papers coming out of the indoor geolocation research program at CWINS. These papers are divided into three categories. Two tutorial papers in the *IEEE Communication Society Magazine* in 1998 and 2002 provide an overview of the indoor geolocation issues. The next category is six papers in channel measurement and modeling related to indoor geolocation. These papers describe measurements and models for the radio propagation parameters that affect the performance of the wireless networks as well as models for distance measurement errors observed in TOA based precision indoor geolocation systems. The last section consists of six papers on algorithms, testbeds, and performance of indoor geolocation systems. These six papers provide the basis for performance evaluation of super-resolution signal processing algorithms as well as a number of TOA based and RSS based indoor geolocation algorithms based on the measurements and models describes in the papers of the previous section. We start this part with a 15th reprint describing CWINS. This paper was published in the special issue of the *ACM SIGMOBILE Mobile Computing and Communication* on worldwide research laboratories working in wireless networking.

Overview of CWINS

- K. Pahlavan, "An overview of the center for wireless information network studies at Worcester Polytechnic Institute, MA, USA," *ACM SIGMOBILE Mobile Computing and Communications Review*, Volume 4, Issue 2, April 2000.

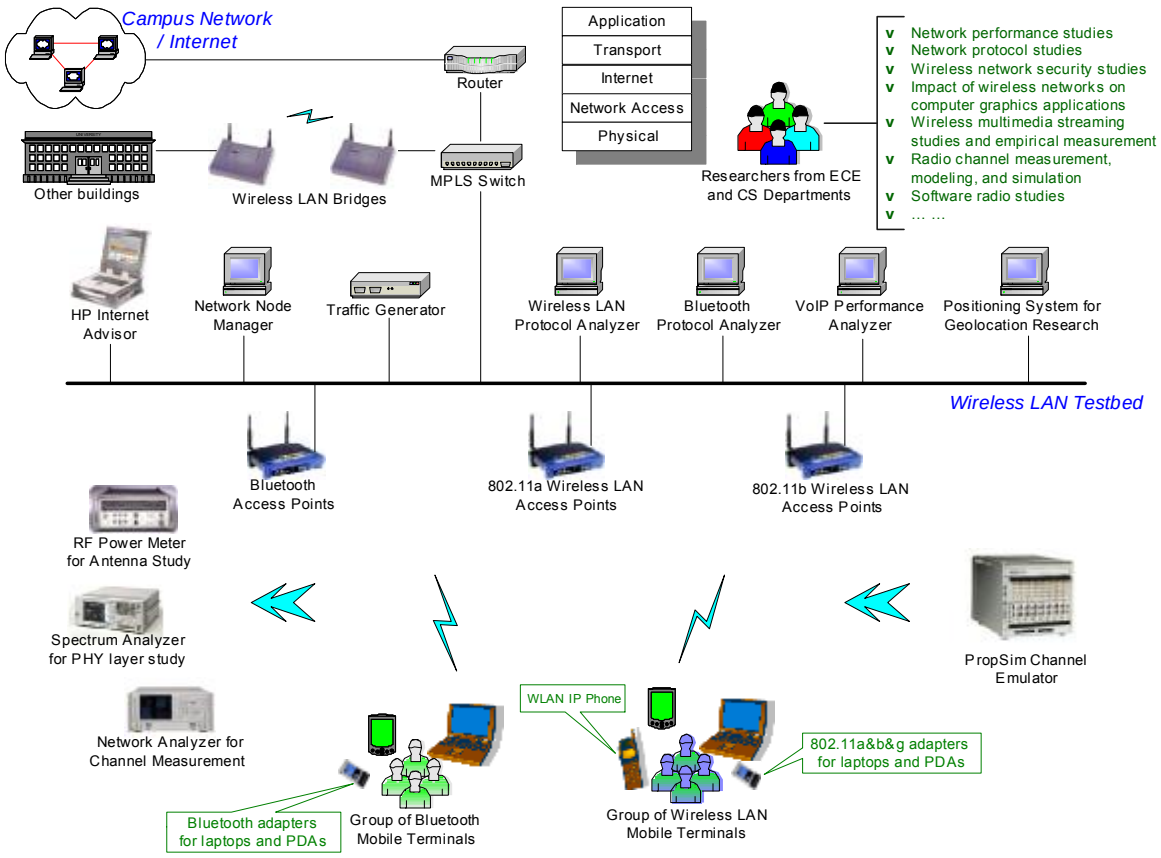

An Overview of the Center for Wireless Information Network Studies at Worcester Polytechnic Institute, MA, USA

Kaveh Pahlavan, Director and Founder, CWINS
Professor, Electrical and Computer Engineering Department, WPI
kaveh@ece.wpi.edu
www.cwins.wpi.edu

The Center for Wireless Information Network Studies (CWINS) is a well renowned compact wireless research laboratory with a successful history of research alliances with other industrial and academic groups. The center has performed research for government agencies and has close ties with the world-leading organizations in the wireless industry. The core competence of the center is in indoor radio channel propagation measurement modeling and in the development of testbeds and tools for design and performance monitoring of wireless indoor networks. For over a decade, by publishing an international periodical journal, organizing several workshops and participating in organizing a yearly international conference, the center has contributed significantly to information exchange among important sectors of the wireless industry.

History

The research program in wireless information networks at WPI was established in 1985 as the first research program of this sort in the United States. In 1986, the program was awarded the first NSF grant in modern wireless communications to start pioneering work on channel modeling, transmission and multiple access methods for wireless indoor networks. In 1989 and 1990, the center participated in founding the IEEE International Symposium on Personal, Indoor and Mobile Radio Communications (PIMRC) and the IEEE International Symposium on Spread Spectrum Techniques and Applications (ISSSTA) in the UK. In 1991, the center organized the first IEEE Workshop on Wireless LANs, which was held at WPI. In 1992, the center organized the Third IEEE PIMRC in Boston. In 1994, the center initiated the International Journal on Wireless Information Networks, the first journal in this field. In 1995, Prof. Pahlavan and Dr. Levesque published "Wireless Information Networks", John Wiley and Sons, the first graduate level textbook in wireless networks. During 1996-98, the Wireless LAN Research Laboratory was formed under CWINS to serve as an industrial research alliance in answer to the growing interest in wireless LAN technology. In 1996, Prof. Pahlavan was elected Fellow of the IEEE for his contributions in wireless office information networks. In 1997, the center expanded the scope of research to perform pioneering research for indoor and short-range goelocation applications for the Small Unit Operation Situation Awareness System program under DARPA. Also in 1997, the center initiated a long-term active collaboration with the University of Oulu, Nokia, and several other leading wireless companies in Finland.

Research Objectives and Directions

The main objective of the center is to perform basic research in broadband wireless local access. The pioneering research work in indoor radio propagation measurements and modeling and developing experimental testbeds and performance evaluation facilities for comparative studies of evolving wireless indoor networks is now finding its way into applications for wireless home networking. The center strikes a balance between basic and applied research by maintaining contacts with national and international research organizations as well as leaders in the commercial industry.

Projects

The projects conducted at CWINS are focused on two main areas of research: radio propagation and modem design for physical layer, and traffic engineering and performance monitoring of broadband indoor wireless networks.

Radio propagation measurement and modeling at CWINS started in 1986 with the development of a wideband indoor radio channel measurement system and time domain modeling of wideband indoor radio propagation. Shortly after that, the center introduced frequency domain modeling using a network analyzer that since then has become a popular method for indoor radio propagation measurement. These efforts were funded by NSF, HP and Raytheon. Later, the center developed a spread spectrum channel sounder for GTE Laboratories for performance monitoring of urban cellular systems. More recently, time-space channel measurement characteristics of indoor radio propagation have been studied at the center for smart antenna and indoor geolocation applications. In the early 1990s a first 2-D ray-tracing program for radio

propagation prediction in indoor areas was developed and calibrated using the results of measurements obtained in the earlier research. This program was extended to 3-D ray-tracing for microcellular applications in 1993. Results of these efforts have been used by NYNEX Science and Technology, GTE Laboratories, ERS, and more recently by DARPA's SUO/SAS project and United Technology Research Center. In 1996 the center developed an indoor deployment tool for wireless LANs for the WLRL, a consortium of five industrial partners. In 1994, CWINS started a real-time channel simulation for indoor propagation program using its own proprietary prototype. This year, the center has received an award from DoD to purchase the most advanced commercially available real-time channel simulation hardware platform that will be used to simulate all channel measurements and modeling efforts of the previous years. The latest contribution of the center to the research community is the recognition of the fact that the exiting channel models developed for telecommunication applications are not suitable for performance evaluation of geolocation systems operating in multipath environments. Through a research program initiated by the DARPA's SUO/SAS program and later supported by Nokia, the Finnish Airforce, and TEKES, the center has launched a program for the measurement and modeling of the indoor radio channel for geolocation applications.

Starting in 1986, CWINS performed theoretical studies of wireless network access methods, capture effects, voice and data integration, and performance of WLANs. In 1993, with the support of NYNEX, a benchmark software tool was developed to provide real-time performance monitoring such as throughput and time data of CDPD networks. In 1995, the center was awarded a grant from NSF to deploy and evaluate the performance of an experimental wireless LAN tested. This unique subnet wireless LAN testbed was designed to examine a variety of technologies for point-to-point inter-LAN bridges as well as different technologies used for mobile laptop applications. This led to an experimental performance evaluation of WLANs where throughput, delay and other characteristics were measured taking into account the effects of walls, floors, and number of users. In 1996 with the support of WLRL, the CDPD benchmark tool was augmented to be used for WLANs. Using this tool and HP Open View, HP Protocol Analyzer, empirical data was collected and modeled. This enabled the center to lay a foundation for wireless traffic engineering. In 1997, the center started a long-term collaboration with the University of Oulu, Nokia and other Finnish companies. The first project called Wireless LANs for UMTS (WiLU) had a goal to evaluate inter-technology handoff requirements for the third generation pan-European standard UMTS. The work focused on developing handoff algorithms between WLANs and GPRS. In 1999, a second project called Wireless Indoor Geolocation and IP traffic analysis (WINGIP) had two main objectives. The first objective was to investigate and model the performance of voice applications over existing WLANs and IP networks. A measurement system for voice oriented applications was designed and used with the NSF WLAN testbed to collect data, and a complete OPNET simulation was created and checked against measurements. The second objective was to investigate the feasibility and performance of including geolocation services over fourth generation wireless networks, in particular using OFDM in HIPERLAN2. In 1999, the center started investigating the area of home networking, with particular interest in the Bluetooth, HomeRF, IEEE 802.11, a and b, IEEE 802.15 Wireless Personal Area Networks (WPAN), and other wireless home networking initiatives.

Research Staff

The center is a compact and highly selective organization, the staff of the center includes two full-time, three part-time, several contributing faculty members and 5-10 graduate and undergraduate students. The founder and director of CWINS is Kaveh Pahlavan, Professor of Electrical and Computer Engineering and Computer Science, WPI, and International Professor of Electrical Engineering, University of Oulu, Finland. Dr. Jacques Beneat is a full-time research scientist at CWINS, mainly involved in radio propagation measurements and modeling and real-time channel simulation. Dr. Allen Levesque, is a Research Professor in wireless communication systems, Dr. James Mathews is a consultant in radio design, Craig Mathais of Farpoint Group, is a consultant in commercial aspects of Wireless LANs. A number of ECE and CS department faculty members at WPI have participated in CWINS projects.

Sample list of publications

1. K. Pahlavan, et. al. "Handoff in Hybrid Mobile Data Networks", IEEE Personal Communication Magazine, April 2000 (invited paper).

2. K. Pahlavan, P. Krishnamurthy, and J. Beneat, "Wideband Radio Propagation Modeling for In-

door Geolocation Applications", IEEE Communications Magazine, April 1998 (invited paper).

3. K. Pahlavan, A. Zahedi, and P. Krishnamurthy, "Wideband Local Access: WLAN and WATM", IEEE Communications Magazine, Special Series on Wireless ATM, November 1997 (invited paper).

4. A. Falsafi, K. Pahlavan, and G. Yang, "Transmission Techniques for Wireless LANs", IEEE Journal on Selected Areas in Communications, November 1996 (invited paper).

5. K. Pahlavan, T. H. Probert, and M. E. Chase, "Trends in Local Wireless Networks", IEEE Communications Magazine, March 1995 (invited paper).

6. K. Pahlavan and A. Levesque, "Wireless Data Communication", IEEE Proceedings, September 1994 (invited paper).

7. K. Pahlavan, S. Howard, and T. Sexton, "Adaptive Equalization of Indoor Radio Channel", IEEE Transactions on Communications, January 1993.

8. S. J. Howard and K. Pahlavan, "Autoregressive Modeling of Wideband Indoor Radio Propagation", IEEE Transactions on Communications, September 1992.

9. K. Zhang and K. Pahlavan, "An Integrated Voice-Data System for Wireless Local Area Networks", IEEE Transactions on Vehicular Technology, April 1990.

10. K. Pahlavan, "Wireless Office Information Networks", IEEE Communications Magazine, June 1985 (A modified version of this paper was published in the ACM Transactions on Office Information Systems, July 1988. It was also published as the opening paper in "Advances in Local and Metropolitan Area Networks", edited by William Stalling, IEEE Press, 1994).

Facilities

The center has several radio channel measurement systems suitable for indoor telecommunications, smart antenna and geolocation applications over a broad range of frequencies. The center has extensive ray-tracing capabilities suitable for indoor, urban and tunnel applications. The center is augmenting its real-time channel simulation capabilities to be suitable for indoor and urban telecommunication, smart antenna and geolocation applications.

The center has a complete experimental wireless LAN sub-network with router, switch, access points, wireless inter-building bridges, and laptops with wireless adapter cards. It has proprietary and commercial wireless network application monitoring tools suitable for wireless traffic engineering and voice over IP studies.

There are extensive computer facilities in the CWINS laboratory, the ECE department, and WPI. WPI is a member of the Internet 2 Consortium.

Sponsoring organizations

The center has received support from government agencies such as the National Science Foundation and DARPA, from the local industry such as GTE Laboratories, TASC/Litton, Bell Atlantic Mobile, BBN, Sierra Comm, Raytheon Company, DEC, and Alta Group of Cadence, and from national industry such as Savi Technologies (CA), Apple Computers (CA), Radio LAN (CA), Hewlett-Packard (CA), Motorola (IL), Texas Instruments (TX), and United Technologies Research Center (CN). It has received support from international agencies and industry such as Nokia (FI), Elektrobit (FI), Sonera (FI), TEKES (FI), Finnish Air Force (FI), NTT (JAPAN), and Jolt (ISRAEL). The companies that sponsored the WLRL alliance were Aironet, Cushcraft, Harris Semiconductors, Persoft, and DEC. The center has also provided corporate consulting and training to several national and international companies.

Statement on Impact

The research at the CWINS has resulted in more than 150 technical papers, several book chapters and the text book *Wireless Information Networks*, the first comprehensive text book published on modern WIN systems. The research has resulted in over a dozen Ph. D. dissertations, numerous M.Sc. and extended undergraduate senior projects. The students who complete their graduate degrees learn multi-disciplinary skills and teamwork practices in a fast-paced information technology hungry environment that permits them to move quickly and productively into the competitive workplace. CWINS has enjoyed great success in placement of its graduates in start-up companies, academia, and corporations active in the expansion of wireless information networks (such as Qualcomm, Nokia, David Sarnoff Labs, Bellcore, Motorola, GTE Laboratories, Rockwell International, PCSI, Raytheon, etc.).

Overview of the Challenges in Indoor Geolocation

- K. Pahlavan, X. Li, and J. Makela, "Indoor Geolocation Science and Technology", *IEEE Comm Soc. Mag.*, Feb. 2002.
- K. Pahlavan, P. Krishnamurthy and J. Beneat, "Wideband Radio Propagation Modeling for Indoor Geolocation Applications", *IEEE Communications Magazine*, April 1998.

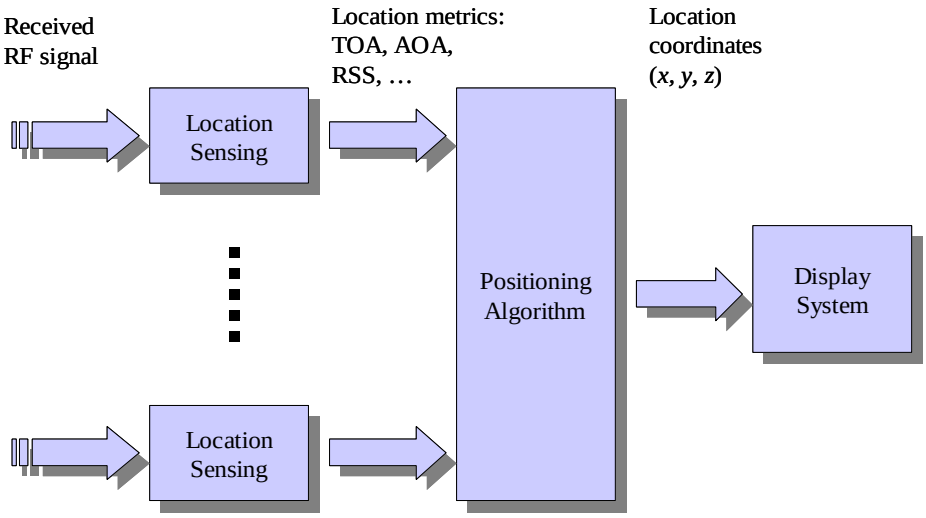

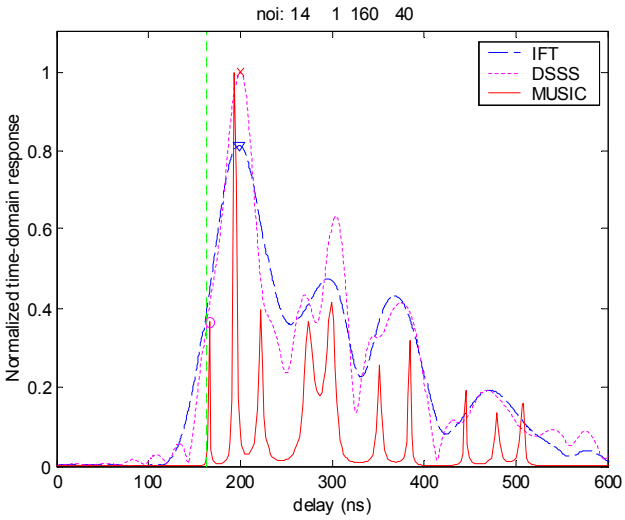

Indoor Geolocation Science and Technology

Kaveh Pahlavan and Xinrong Li, Worcester Polytechnic Institute
Juha-Pekka Mäkelä, University of Oulu, Finland

ABSTRACT

This article presents an overview of the technical aspects of the existing technologies for wireless indoor location systems. The two major challenges for accurate location finding in indoor areas are the complexity of radio propagation and the ad hoc nature of the deployed infrastructure in these areas. Because of these difficulties a variety of signaling techniques, overall system architectures, and location finding algorithms are emerging for this application. This article provides a fundamental understanding of the issues related to indoor geolocation science that are needed for design and performance evaluation of emerging indoor geolocation systems.

INTRODUCTION

Recently, there is increasing interest in accurate location finding techniques and location-based applications for indoor areas. The Global Positioning System (GPS) [1] and wireless enhanced 911 (E-911) services [2] also address the issue of location finding. However, these technologies cannot provide accurate indoor geolocation, which has its own independent market and unique technical challenges. In 1997, while engaged in the Defense Advanced Research Projects Agency's (DARPA's) Small Unit Operation/Situation Awareness System (SUO/SAS) program, the lead author of this article and his research group noticed the need for fundamental research in accurate indoor geolocation [3]. The follow-up initiative of the group attracted the attention of Nokia and other Finnish organizations to the commercial importance of indoor geolocation. In recognition of this importance, an NSF grant was awarded to establish a scientific foundation in this field.

Accurate indoor geolocation is an important and novel emerging technology for commercial, public safety, and military applications [4]. In commercial applications for residential and nursing homes there is an increasing need for indoor geolocation systems to track people with special needs, the elderly, and children who are away from visual supervision, to navigate the blind, to locate in-demand portable equipment in hospitals, and to find specific items in warehouses. In public safety and military applications, indoor geolocation systems are needed to track inmates in prisons and navigating policeman, fire fighters, and soldiers to complete their missions inside buildings. These incentives have initiated interest in modeling the radio channel for indoor geolocation applications [3, 5], development of new technologies [6], and emergence of first-generation indoor geolocation products [7]. To help the growth of this emerging industry, there is a need to develop a scientific framework to lay a foundation for design and performance evaluation of such systems.

Figure 1 illustrates the functional block diagram of a wireless geolocation system. The main elements of the system are a number of location sensing devices that measure metrics related to the relative position of a mobile terminal (MT) with respect to a known reference point (RP), a positioning algorithm that processes metrics reported by location sensing elements to estimate the location coordinates of MT, and a display system that illustrates the location of the MT to users. The location metrics may indicate the approximate arrival direction of the signal or the approximate distance between the MT and RP. The angle of arrival (AOA) is the common metric used in direction-based systems. The received signal strength (RSS), carrier signal phase of arrival (POA), and time of arrival (TOA) of the received signal are the metrics used for estimation of distance. As the measurements of metrics become less reliable, the complexity of the position algorithm increases. The display system can simply show the coordinates of the MT, or it may identify the relative location of the MT in the layout of an area. This display system could be software residing in a private PC or a mobile locating unit, locally accessible software in a local area network (LAN), or a universally accessible service on the Web. Obviously, as the horizon of accessibility of the information increases, design of the display system becomes more complex.

This work is supported in part by the National Science Foundation under Grant ECS-0084112.

There are two basic approaches to designing a wireless geolocation system. The first approach is to develop a signaling system and a network infrastructure of location sensors focused primarily on geolocation application. The second approach is to use an existing wireless network infrastructure to locate an MT. The advantage of the first approach is that physical specification, and consequently quality of the location sensing results, is under control of the designer. The MT can be designed as a very small wearable tag or sticker, and the density of the sensor infrastructure can be adjusted to the required accuracy of the location finding application. The advantage of the second approach is that it avoids expensive and time-consuming deployment of infrastructure. These systems, however, need to use more intelligent algorithms to compensate for the low accuracy of the measured metrics. Both approaches have their own markets, and design work on both technologies has been pursued in the past few years [2, 4, 7, 8].

To develop a scientific foundation, we need to examine the performance of different signaling techniques and geolocation approaches. This performance evaluation needs a suitable model for radio propagation that reflects the characteristics of the channel affecting the accuracy of location sensing and system positioning. In the next three sections we address technical issues related to channel modeling, location sensing, and positioning algorithms for indoor geolocation systems.

Channel Characteristics for Indoor Geolocation

The indoor radio propagation channel is characterized as site-specific, severe multipath, and low probability for availability of a line of sight (LOS) signal propagation path between the transmitter and receiver [9]. The two major sources of errors in the measurement of location metrics in indoor environment are multipath fading and no LOS (NLOS) conditions due to shadow fading [3].

Radio propagation channel models are developed to provide a means to analyze the performance of a wireless receiver. The performance criteria for telecommunication and geolocation systems are quite different [3]. The performance criterion for telecommunication systems is the bit error rate (BER) of the received data stream, while for geolocation systems the performance measure is the estimated accuracy of location coordinates. The accuracy of location estimation is a function of the accuracy of location metrics and the complexity of positioning algorithms. Since the metrics for geolocation applications are AOA, RSS, and TOA, models for geolocation application must reflect the effects of channel behavior on the estimated value of these metrics at the receiver. The existing narrowband indoor radio channel models designed for telecommunication applications [9] can be used to analyze the RSS for geolocation applications. The AOA part of the emerging 3D channel models developed for smart antenna applications [10, 11] might be used for modeling of the AOA for indoor geolocation applications. However, the existing wideband indoor multipath channel measurements and models [9] are not suitable for analysis of the behavior of TOA for geolocation applications.

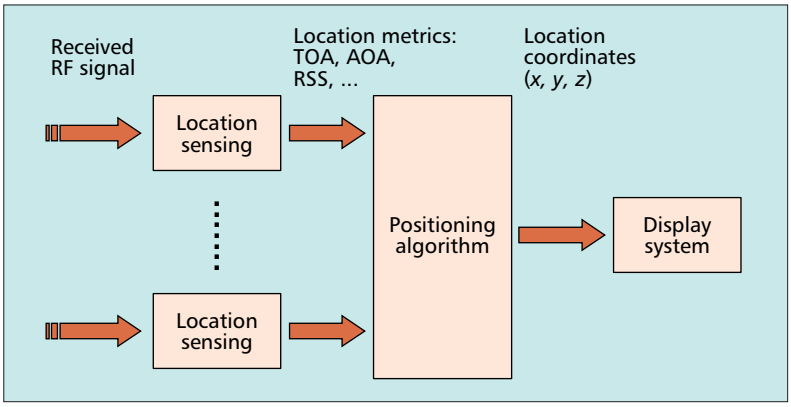

Figure 1. *A functional block diagram of wireless geolocation systems.*

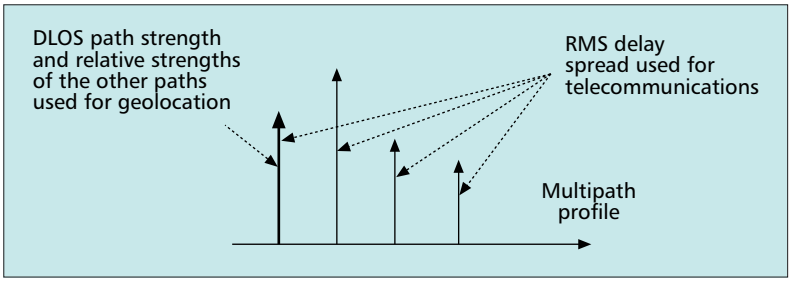

Figure 2. *The multipath profile of an indoor radio propagation channel.*

The existing statistical wideband indoor multipath models, such as the JTC model [9], represent multipath characteristics of the channel with a discrete channel profile similar to the one shown in Fig. 2. The strength and arrival time of the paths are so determined that the root mean square (RMS) delay spread and consequently BER of a telecommunication receiver obtained from the simulations using these profile represents values similar to those obtained from empirical measurements. If these models are used for performance evaluation of TOA-based geolocation systems, the statistics of distance errors do not reflect the results obtained from empirical data [3]. Besides, to confirm the modeling results of a radio channel, empirical measurement is essential to check the validity of the model. In the literature there are a number of measurements of the wideband characteristics of indoor radio channels for frequencies from 1 to 60 GHz [9]. However, none of these measurements are useful for geolocation applications because they do not have a well-calibrated estimate of the arrival time of the direct LOS (DLOS) path and a very accurate measurement of the real physical distance between the transmitter and receiver [12]. The only available short-range measurements calibrated for geolocation applications are those reported in [12], which are used in this article to analyze the performance of super-resolution techniques in the next section.

While we do not have any good models for the multipath characteristics of indoor radio channels for geolocation applications, there are three classes of recent statistical modeling approaches that can be used to develop reliable models in the future, which are wideband 2D

In indoor areas, due to obstruction by walls, ceilings, or other objects, the DLOS propagation path is not always the strongest path and even in some casess, for example, NLOS, it may not be detectable with a specific receiver implementation. In such cases, dramatically large errors occur in TOA estimation.

multipath modeling [3, 5], 3D geometrical statistical modeling [10], and 3D measurement-based statistical modeling [11]. In measurement-based 2D statistical modeling, the measurement data are used to define a multipath profile by

$$h(\tau) = \sum_{k=0}^{L_p - 1} \alpha_k \delta(\tau - \tau_k), \quad (1)$$

where L_p is the number of multipath components, and $\alpha_k = |\alpha_k| e^{j\phi_k}$ and τ_k are complex amplitude and propagation delay of the kth path, respectively. The strength and statistical characteristics of the first path and its relative strength with respect to other paths fit similar results obtained from empirical data. The measurement systems for this approach are the same as those used for telecommunication applications [7, 9]. However, these systems are calibrated for accurate measurement of the TOA of the DLOS, and for each measurement the physical distance between the transmitter and receiver is accurately recorded. Preliminary measurement and modeling work in this field is reported in [5, 12]; larger calibrated measurement databases and more practical multipath models need further investigation.

In 3D modeling, the mathematical model for the channels is represented by

$$h(\tau, \theta) = \sum_{k=0}^{L_p - 1} \alpha_k \delta(\tau - \tau_k, \theta - \theta_k), \quad (2)$$

where θ_k is the AOA of the kth path [11]. While in 2D modeling each path was associated with a TOA, in 3D modeling each path is associated with a TOA and an AOA. The 3D models can be developed either based on geometric analysis of the statistics of the paths arriving from different directions or out of empirical 3D channel measurement data. The 3D geometrical statistical models, developed for smart antenna applications, use an analytical approach to relate propagation parameters to the structure of scattering in the environment [10]. In this approach, a mathematical description of radio propagation based on statistical building features and a geometric optics approximation of Maxwell's equations are employed to derive relevant radio propagation models such as distributions of the TOA, AOA, and RSS. The statistics of the AOA and RSS in these models can be used directly for indoor geolocation applications. Further research in this area is needed to develop statistical models for the TOA of the DLOS path and its relation to other paths to make them useful for the analysis of positioning errors in TOA-based geolocation systems.

In 3D measurement-based statistical modeling, measured channel characteristics are used to develop models for AOA, TOA, and RSS. The major challenge of this approach is the implementation of a system to measure the 3D characteristics of the channel. Recently two techniques have been studied for this purpose. The first technique mechanically rotates a directional antenna to measure the strength of the signal arriving from different directions, and the second technique measures a set of eight channel impulse responses using an antenna array and calculates the AOA using signal processing techniques [11]. Preliminary 3D modeling of an indoor area using a limited database in a building is available in [11]. More extensive measurement and modeling in this field can result in realistic models for indoor geolocation applications.

Location Sensing Techniques

As discussed in the introduction, the location sensing elements measure RSS, AOA, and TOA as location metrics. The indoor radio channel suffers from severe multipath propagation and heavy shadow fading, so the measurements of RSS and AOA provide less accurate metrics than does TOA [4]. As a result, similar to GPS systems, independent systems designed for indoor geolocation normally employ the more accurate TOA as the location metric. Systems using existing infrastructures installed for wireless LANs or the third-generation (3G) indoor systems may use RSS, AOA, or less accurate TOA measurements to fully exploit the existing hardware implementation designed for traditional telecommunication applications [8]. In indoor areas, due to obstruction by walls, ceilings, or other objects, the DLOS propagation path is not always the strongest; in some cases (e.g., NLOS), it may not even be detectable with a specific receiver implementation [3]. In such cases, dramatically large errors occur in TOA estimation. To accurately estimate the TOA in indoor areas, we need to resort to different and more complex signaling formats, frequency of operation, and signal processing techniques that can resolve the problems. The following subsection is devoted to accurate TOA estimation techniques.

Estimation of TOA for Indoor Ranging

The TOA-based systems measure distance based on an estimate of signal propagation delay (i.e., TOA) between a transmitter and a receiver since in free space or air, radio signals travel at the constant speed of light. The TOA can be measured by either measuring the phase of received narrowband carrier signal or directly measuring the arrival time of a wideband narrow pulse. The wideband pulses for measuring TOA can be generated either directly [6] or using spread spectrum technology [7]. In the following, we present these techniques in three classes: narrowband, wideband, and ultra wideband techniques.

Narrowband Signals and Phase Measurement Systems — In the narrowband ranging technique, the phase difference between received and transmitted carrier signals is used to measure the distance between two points. The phase of a received carrier signal, ϕ, and the TOA of the signal, τ, are related by $\tau = \phi/\omega_c$, where ω_c is the carrier frequency in radian. It is well known that the differential GPS (DGPS) using measured reference carrier phase at the receiver improves the location accuracy of the traditional GPS from about 20 m to within 1m [1]. However, unlike the DGPS, where the DLOS signal path is always present, the severe multipath condition of the indoor geolocation environment causes substantial errors in phase measurements. When a narrowband carrier signal is transmitted in a multipath environ-

ment, the composite received carrier signal is the sum of a number of carriers, arriving along different paths, of the same frequency but different amplitude and phase. The frequency of the composite received signal remains unchanged, but the phase will be different from that of the DLOS signal [9]. An immediate conclusion is that phase-based distance measurement using a narrowband carrier signal cannot provide accurate estimate of distance in a heavy multipath environment.

Wideband Signals and Superresolution Techniques — The direct-sequence spread-spectrum (DSSS) wideband signal has been used in ranging systems for many years [1]. In such a system, a signal coded by a known pseudo-noise (PN) sequence is transmitted by a transmitter. Then a receiver cross-correlates received signal with a locally generated PN sequence using a sliding correlator or a matched filter [7, 9]. The distance between the transmitter and receiver is determined from the arrival time of the first correlation peak. Because of the processing gain of the correlation process at the receiver, the DSSS ranging systems perform much better than competing systems in suppressing interference from other radio systems operating in the same frequency band. In single-path radio propagation channels, only disturbed by additive white Gaussian noise, the Cramer-Rao lower bound is commonly used for performance assessment of cross-correlation-based TOA estimation techniques. However, due to the complexity of multipath indoor radio propagation channels, such a bound is not directly applicable to indoor geolocation systems. Instead, the resolution of TOA estimation in DSSS ranging systems is roughly determined by the base width of the PN correlation function, or equivalently the signal bandwidth [7]. For example, if a bandwidth of 200 MHz is used, the absolute distance estimation errors are less than 1.5 m if the DLOS signal is detectable.

Due to the scarcity of the available bandwidth in practice, in some indoor geolocation applications, the DSSS ranging systems cannot provide adequate accuracy. On the other hand, it is always desirable to achieve higher ranging accuracy using the same bandwidth. Inspired by high-resolution spectrum estimation techniques, a number of researchers have studied super-resolution techniques for time-domain analysis such as [13]. A frequency-domain superresolution technique can be used to determine the TOA with high resolution from frequency channel response. In practice, discrete samples of frequency channel response can be obtained by sweeping the channel at different frequencies [9], by taking advantage of an existing multicarrier (orthogonal frequency-division multiplexing, OFDM) communication system, or in a DSSS system by deconvolving received signal over the frequency band of high signal-to-noise ratio [13].

To understand the concept of frequency-domain super-resolution technique, we take the Fourier transform of Eq. 1 so that the frequency channel response is obtained as

$$H(f) = \sum_{k=0}^{L_p-1} \alpha_k e^{-j2\pi f \tau_k}. \qquad (3)$$

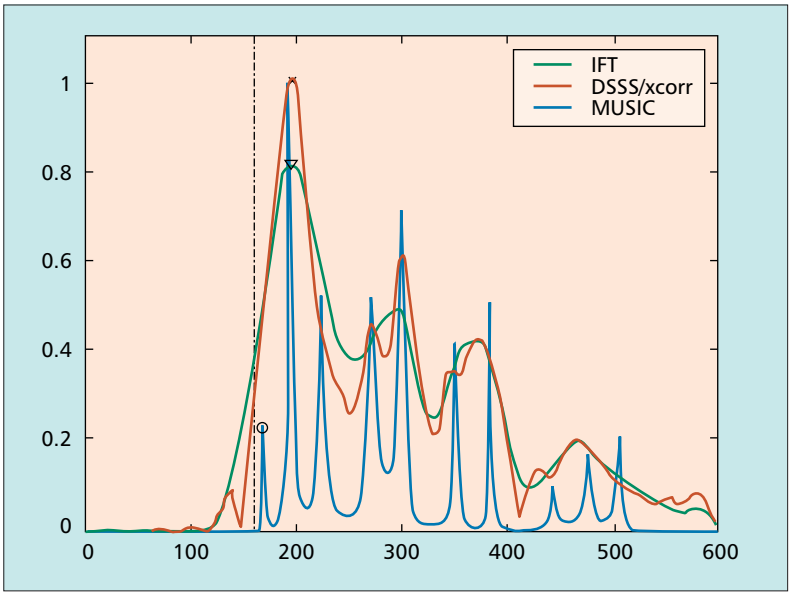

Figure 3. *Estimated TOA of the DLOS path and normalized time domain responses obtained using three different techniques. The vertical dash-dot line denotes the expected TOA. The x-axis is delay in ns.*

If we exchange the role of time and frequency variables in Eq. 3, we observe that it becomes the harmonic signal model, which is well known in the spectrum estimation literature. Therefore, all spectrum estimation techniques used for harmonic signal models can be applied to frequency domain measurement data of radio propagation channel to determine the delay of multipath signals.

In order to demonstrate the usefulness of the super-resolution technique we compare its performance based on measured indoor channel characteristics reported in [12] with two other time delay estimation techniques. The MUSIC algorithm is used as an example of super-resolution techniques. In the first of these, the frequency domain channel response is directly converted to the time domain using inverse Fourier transform (IFT) [9], and then the arrival time of the DLOS is detected. The second technique uses the traditional cross-correlation techniques with DSSS signals (DSSS/xcorr). Figure 3 shows simulation results using the three techniques over sample channel measurement data. We observe that the MUSIC algorithm shows much higher time domain resolution than the other two and accurately detects the arrival time of the DLOS path, while the other two fail. Figure 4a presents mean and standard deviation of ranging errors vs. the bandwidth of the system over channel measurement data in several different buildings reported in [12]. Figure 4b presents percentage of measurement locations where absolute ranging errors are smaller than 3 m. In general, the superresolution technique has the best performance and is preferred, especially when the signal bandwidth is small. It should be noted that while using the superresolution technique and large bandwidth improves statistical performance, it couldn't eliminate large ranging errors at some locations because of NLOS conditions between transmitter and receiver. This needs to be dealt with in the positioning process to achieve high positional accuracy, as presented

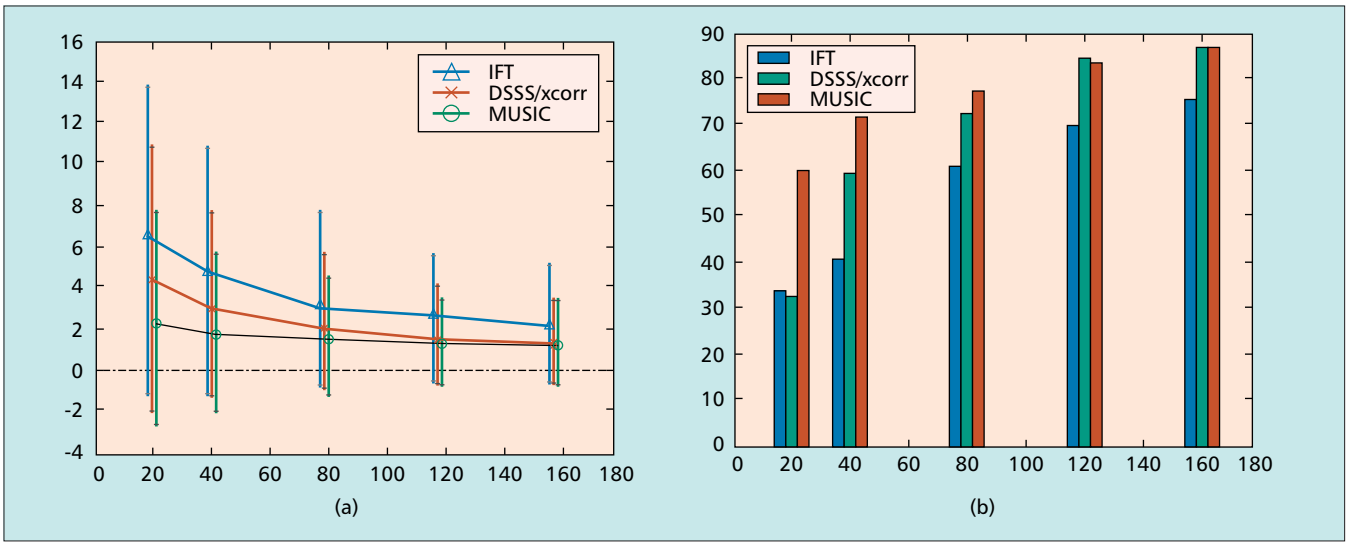

Figure 4. *Simulation results: a) mean of ranging errors in meter vs. bandwidth in MHz using three different TOA estimation techniques; the vertical line corresponds to one standard deviation; b) percentage of measurement locations where absolute ranging errors are smaller than 3 m vs. bandwidth in MHz.*

in the next section. Using the superresolution technique increases the complexity of system implementation, and there are a number of issues in practical implementation that need to be further investigated. More details of this study will be available in a separate publication.

The Ultra Wideband Approach — As mentioned before, signal bandwidth is one of the key factors that affect TOA estimation accuracy in multipath propagation environments. The larger the bandwidth, the higher the ranging accuracy. Ultra wideband (UWB) systems, which exploit bandwidths in excess of 1 GHz, have attracted considerable attention as a means of measuring accurate TOA for indoor geolocation applications [6]. Due to the high attenuation associated with the use of a high-frequency carrier, the frequency band considered for a UWB system is typically focused on 2–3 GHz unlicensed. With results of propagation measurement in a typical modern office building, it has been shown that the UWB signal does not suffer multipath fading [14], which is desirable for accurate TOA estimation in indoor areas. The actual deployment of UWB systems in the United States is subject to FCC approval, which was due in late 2001. The main concern of the FCC authorities is the interference of UWB devices with, among other licensed services, the GPS systems that operate at approximately the 1.5 GHz frequency band. Similar to the spread spectrum signals, the UWB signal has a low, flat, and noise-like power spectrum. But given the weak satellite signals that must be processed by GPS receivers, the noise-like UWB signal is still harmful for GPS systems in close vicinity. A significant amount of research work is underway to assess the effect of UWB interference on GPS receivers.

Positioning Algorithms

As discussed earlier, the measurement accuracy of location metrics in indoor areas depends on location sensing technologies and site-specific indoor radio propagation conditions. Due to imperfect implementation of location sensing techniques, lack of bandwidth, and the complexity of the multipath indoor radio propagation channel among others, there are always varying errors associated with measurements of location metrics. To achieve high positional accuracy when the measurements of location metrics are unreliable, the errors encountered in the measurement process have to be mitigated in the positioning process. In the next two subsections we discuss the traditional positioning algorithms used with reliable measurements of location metrics and more intelligent pattern recognition techniques that can be used to improve the positioning performance when the measurements of location metrics are unreliable.

Traditional Techniques

In the indoor radio channel, it is difficult to accurately measure AOA, POA and RSS so that most of the independent indoor positioning systems mainly use TOA based techniques. With reliable TOA-based distance measurements, simple geometrical triangulation methods can be used to find the location of the MT [2, 4]. Due to estimation errors of distances at RP receivers caused by inaccurate TOA measurement, the geometrical triangulation technique can only provide a region of uncertainty, instead of a single position fix, for estimated location of the MT. To obtain an estimate of location coordinates in the presence of measurement errors of location metrics, a variety of direct and iterative statistical positioning algorithms have been developed to solve the problem by formulating it into a set of nonlinear equations [2].

In some indoor geolocation applications, the purpose of positioning systems is to provide a visualization of possible mobile locations instead of an estimate of location coordinates [7]. On the other hand, positional accuracy is not constant across the area of coverage, and poor geometry of relative position of MT and RP can lead to high geometric dilution of precision [15].

The output of statistical methods is an estimate of mobile location coordinates, and the changes of the shape of the region of uncertainty are not revealed by this method. When the region of uncertainty information as well as the estimate of location is needed, both geometric and statistical triangulation algorithms are used [15].

For traditional outdoor geolocation, intelligent techniques, such as Kalman filter-based techniques for tracking and fusion of multiple metrics, are normally used to improve positioning performance [1]. In essence, these techniques are readily applicable to indoor geolocation systems. However, the indoor application environment has some unique features, discussed in the next section, which make the traditional positioning algorithms less attractive. On the other hand, these unique features of indoor applications enable the design of intelligent positioning algorithms that can significantly improve the positioning performance in indoor areas.

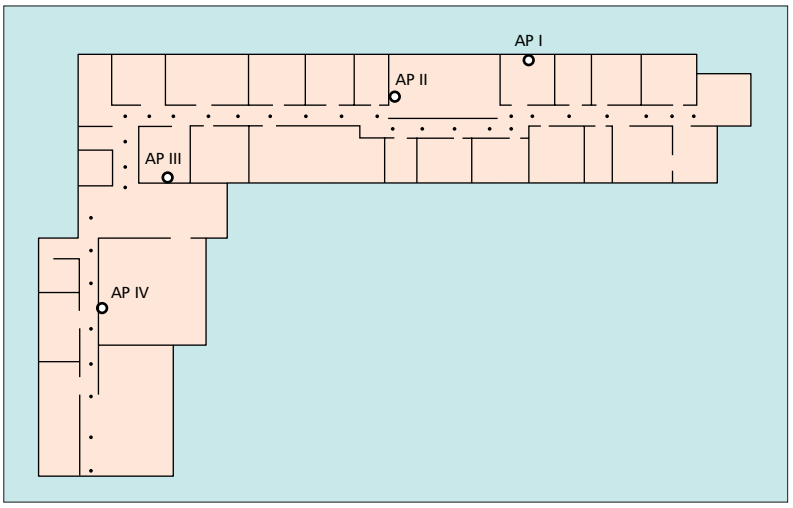

Figure 5. *Partial layout of the TLab and CWC, University of Oulu, as well as the locations of the four 802.11b APs and the measurement points.*

Pattern Recognition Techniques

For indoor geolocation applications, the service area is restricted to inside and the close vicinity of a building, and nowadays the building floor plan is normally accessible as an electronic document. The availability of electronic building floor plans is one of the features of indoor applications that can be exploited in positioning algorithms. For example, while tracking an MT in a building, with the aid of a building floor plan situations involving crossing walls or jumping through floors can easily be identified and eliminated. Another unique feature of indoor applications is that the size of the coverage area is much smaller than outdoor applications. This makes it possible to conduct comprehensive planning of the placement of sensors. Careful planning of a sensor network can significantly reduce measurement errors of location metrics caused by NLOS propagation. The structural information of the sensor network can also be employed in intelligent positioning algorithms similar to the use of building floor plans. The small coverage of the system also makes it possible to conveniently conduct extensive premeasurement in the areas of interest. As a result, the premeasurement-based location pattern recognition (also called *location fingerprinting*) technique is gaining increasing attention for indoor applications [8]. On the other hand, in most indoor applications, such as finding needed equipment or locating patients in critical condition, the MT is used in a quasi-stationary way. For these situations, pattern recognition work better than traditional triangulation techniques and Kalman filter-based tracking techniques.

The basic operation of pattern recognition positioning algorithms is simple. Each building has unique signal propagation characteristics; each spot in a building would have a unique signature in terms of RSS, TOA, and/or AOA, observed from different sensors in the building. A pattern recognition system determines the unique pattern features (i.e., the location signature) of the area of interest in a training process, and then this knowledge is used to develop rules for recognition. The challenge for such algorithms is to distinguish locations with similar signatures. To build the signature database, a terminal is carried through the service area transmitting signals to a monitoring site through all location sensing elements. The service area is divided into nonoverlapping zones or grids, and the algorithm analyzes the received signal patterns and compiles a unique signature for each zone.

For quasi-stationary applications, the simplest way of pattern recognition is the nearest-neighbor method. In this method the Euclidean distance measure is calculated between the measured metrics, RSS, TOA, and/or AOA, and all entities in the signature database. The location estimate is determined to be the one associated with the minimum Euclidean distance [8]. A simple experiment has been conducted to demonstrate the usefulness of this technique. Figure 5 presents a partial layout of the Telecommunications Laboratory (TLab) and the Center for Wireless Communications (CWC) at the University of Oulu, Finland. The locations of four 802.11b access points (APs) and 31 measurement locations along a long corridor, with about 2 m separation between adjacent points, are illustrated in the figure. An MT is carried along the corridor, and the RSS is measured at each location. Figure 6 shows the measured RSS at all four APs as the terminal travels from the right corner close to AP-I to the end of the vertical corridor after AP-IV. Then the nearest-neighbor pattern recognition method is applied to the measurement data. In this experiment the standard deviation of the positioning error was 2.4 m, and at about 80 percent locations the positional error was less than 3 m. Similar results in a different building are available in [8].

When the area of coverage becomes large and a large number of sensors are involved, the size of the location signature database increases dramatically, which makes the use of simple nearest-neighbor pattern recognition computationally cumbersome. More complex algorithms, including fuzzy logic, neural network, subspace techniques, and hidden Markov model-based techniques among others, are being investigated to reduce overall computational complexity and improve performance. When the 3G systems using spread spectrum signals and RAKE receivers are employed for indoor geolocation, it is possible to

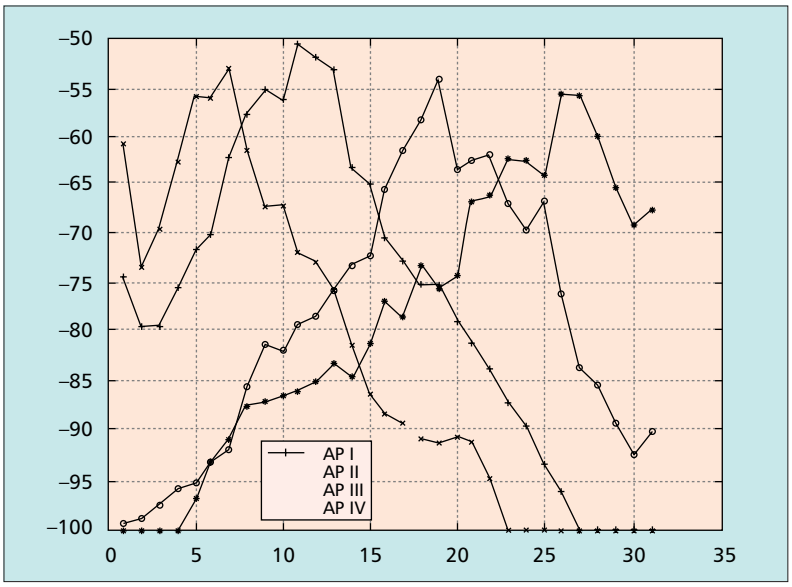

Figure 6. *Measured RSS in dBm at the four APs.*

use the measured time and signal strength of all fingers in place of RSS to improve the positioning performance.

CONCLUSIONS

Indoor geolocation is an emerging technology that needs a scientific foundation. To provide such a foundation we need to characterize the radio propagation features that impact the performance of the indoor geolocation systems. Two classes of indoor geolocation systems are emerging. The first class has its own infrastructure, uses reliable TOA measurement using wideband, superresolution, or UWB location sensing approaches, and employs triangulation techniques for positioning. The second class uses the existing infrastructure of a wireless system (a wireless LAN or cellular system), more unreliable metrics, premeasurement data, and pattern recognition algorithms. The challenge for TOA-based systems is to develop a signaling system and infrastructure that is inexpensive to design and deploy, complies with frequency regulations, and provides a comprehensive coverage for accurate ranging. Even though building and updating the signature database are much easier in indoor environments than in wide urban areas, the major drawback of pattern recognition techniques still lies in substantial efforts needed in generation and maintenance of the signature database in view of the fact that the working environment changes constantly. In general, both techniques demonstrate promising positioning performance for the emerging indoor geolocation applications.

ACKNOWLEDGMENTS

The authors would like to thank DARPA, Nokia, Finnish Air Force, TEKES, and NSF for support of different parts of our research in this area. We also thank members of the CWINS at WPI, and the TLab and CWC at the University of Oulu, who have contributed to our technical understanding of this field. In particular we thank Dr. P. Krishnamurthy, Dr. J. Beneat, M. Marku, Dr. R. Tingley, Dr. M.H. Hassan-Ali, and Dr. J. Matthews of WPI, Dr. P. Misra of MIT Lincoln Laboratories, P. Creamer and J. Pizano of TASC/Litton, and Dr. M. Latva-aho, M. Ylianttila, and R. S. Chana of the University of Oulu.

REFERENCES

[1] E. D. Kaplan, *Understanding GPS: Principles and Applications*, Artech House, 1996.
[2] J. Caffery and G. Stuber, "Subscriber Location in CDMA Cellular Networks," *IEEE Trans. VT*, vol. 47, no. 2, May 1998, pp. 406–16.
[3] K. Pahlavan, P. Krishnamurthy, and J. Beneat, "Wideband Radio Channel Modeling for Indoor Geolocation Applications," *IEEE Commun. Mag.*, vol. 36, no. 4, Apr. 1998, pp. 60–65.
[4] K. Pahlavan and P. Krishnamurthy, *Principles of Wireless Networks — A Unified Approach*, Prentice Hall, 2002.
[5] P. Krishnamurthy, "Analysis and Modeling of the Wideband Radio Channel for Indoor Geolocation Applications," Ph.D. dissertation, Worcester Polytechnic Inst., 1999.
[6] R. Fontana, "Advances in Ultra Wideband Indoor Geolocation Systems," *3rd IEEE Wksp. WLAN*, Boston, MA, Sept. 2001.
[7] J. Werb and C. Lanzl, "Designing a Positioning System for Finding Things and People Indoors," *IEEE Spec.*, vol. 35, no. 9, Sept. 98, pp. 71–78.
[8] P. Bahl and V. Padmanabhan, "RADAR: An In-Building RF-Based User Location and Tracking System," *IEEE INFOCOM*, Israel, Mar. 2000.
[9] K. Pahlavan and A. Levesque, *Wireless Information Networks*, John Wiley & Sons, 1995.
[10] M. Hassan-Ali and K. Pahlavan, "A New Statistical Model for Site-Specific Indoor Radio Propagation Prediction Based on Geometric Optics and Geometric Probability," *IEEE JSAC Wireless*, Jan. 2002.
[11] R. Tingley and K. Pahlavan, "Time-space Measurement of Indoor Radio Propagation," *IEEE Trans. Inst. Measurements*, vol. 50, no. 1, Feb. 2001, pp. 22–31.
[12] J. Beneat, K. Pahlavan, and P. Krishnamurthy, "Radio Channel Characterization for Indoor and Urban Geolocation at Different Frequencies," *IEEE PIMRC*, Osaka, Japan, Sept. 1999.
[13] M. Pallas and G. Jourdain, "Active High Resolution Time Delay Estimation for Large BT Signals," *IEEE Trans. SP*, vol. 39, no. 4, Apr. 1991, pp. 781–88.
[14] M. Win and R. Scholtz, "On the Performance of Ultra-Wide Bandwidth Signals in Dense Multipath Environment," *IEEE Commun. Letters*, vol. 2, no. 2, Feb. 1998, pp. 51–53.
[15] S. Tekinay, E. Chao, and R. Richton, "Performance Benchmarking for Wireless Location Systems," *IEEE Commun. Mag.*, vol. 36, no. 4, Apr. 1998, pp. 72–76.

BIOGRAPHY

KAVEH PAHLAVAN [F] (kaveh@wpi.edu) is a professor of ECE and CS, and director of the CWINS Laboratory at Worcester Polytechnic Institute, Worcester, Massachusetts. He is also a visiting professor of TLab and CWC, University of Oulu, Finland. He is the principal author of *Wireless Information Networks*, John Wiley & Sons, 1995 (with A. Levesques) and *Principles of Wireless Networks — A Unified Approach*, Prentice Hall, 2002 (with P. Krishnamurthy). He has published numerous papers, served as a consultant to a number of companies, and sits on the boards of a few companies. He is editor-in-chief of *IJWIN*, the founder of the IEEE Workshop on Wireless LANs, and a co-founder of the IEEE PIMRC conference.

XINRONG LI (xinrong@wpi.edu) received his B.E. and M.E. from the University of Science and Technology of China, Hefei, China, and the National University of Singapore in 1995 and 1999, respectively. He is pursuing his Ph.D. degree in wireless communications and networks at WPI. His recent research has been focused on indoor geolocation and wireless networks.

JUHA-PEKKA MAKELA (juha-pekka.makela@ee.oulu.fi) received his M.S. degree from the University of Oulu, Finland, in 1997. He is working as a research scientist at CWC, University of Oulu, and is pursuing his Ph.D. degree in the field of mobility management and geolocation applications for 4G wireless networks. His research interests include intelligent handoff techniques, ad hoc networks, and mobility-related issues in IP-based networks.

Wideband Radio Propagation Modeling for Indoor Geolocation Applications

Kaveh Pahlavan, Prashant Krishnamurthy, and Jacques Beneat
Worcester Polytechnic Institute

ABSTRACT A framework for statistical modeling of the wideband characteristics of the frequency-selective fading multipath indoor radio channel for geolocation applications is presented. Multipath characteristics of the channel are divided into three classes according to availability and the strength of the direct line of sight (DLOS) path with respect to the other paths. Statistics of the error in estimating the time of arrival of the DLOS path in a building is related to the receiver's sensitivity and dynamic range. The effects of external walls on estimating the location of the DLOS path are analyzed.

Indoor radio channels suffer from extremely serious multipath conditions that have to be modeled and analyzed to enable the design of radio equipment for a variety of applications. The objective of wideband radio propagation modeling for telecommunications and geolocation applications are quite different. As a result, available models for radio channel propagation are not adequate for analyzing the performance of geolocation systems. In radio propagation studies for telecommunication applications, the main objective is to determine the relationship between distance and total received power in all paths, and to find out the multipath delay spread of the channel. The distance-power relationship is used to determine the coverage of the radio and the multipath delay spread to evaluate the data rate limitations of the receivers [1]. The objective of radio propagation studies for geolocation applications is to determine the relative power and time of arrival (TOA) of the signal arriving from the direct line of sight (DLOS) path versus the signal arriving from other paths. The relative power and TOA of the paths, and the channel noise and interference are used to analyze the error in estimating the distance between the transmitter and the receiver if the DLOS path is not detected correctly.

With the increased popularity of wireless services in the 1990s new applications in a variety of fields have evolved. These applications were incentives for radio propagation measurement and modeling in indoor and outdoor areas. In the telecommunications industry, indoor radio propagation studies were motivated by voice-oriented wireless private branch exchange (PBX) and personal communications services (PCS) applications as well as data-oriented wireless LANs and wireless ATM services [2]. Wideband radio propagation studies were more focused on wideband data applications such as LAN extension, inter-LAN bridges, nomadic access, ad hoc networking, and fusion of computers and communications [3]. Research in wideband indoor radio channel modeling for telecommunications applications in the past decade resulted in numerous measurements, statistical models, and ray tracing software to identify the wideband characteristics of different classes of buildings such as factory floors, office buildings, and residential houses [1].

More recently, applications for indoor geolocation are becoming popular [4]. In mental hospitals and jails there is a growing need to identify the location of specific patients or inmates. In warehouses, laboratories, and hospitals there is a need to identify the location of portable and in-demand pieces of equipment. Public safety departments are thinking of identifying the location of people at the site of a crime or accident [5–7]. Fire department officers are keen on identifying the locations of victims of accidents and firefighters inside a building. Small unit operation (SUO) military teams are keen on situation awareness systems (SASs) capable of identifying the location of individual warfighter systems (IWSs) inside buildings [8]. Quantitative study of the feasibility of alternative indoor geolocation systems for these applications requires measurement and modeling of the indoor radio channel to predict and analyze the availability of the DLOS path in different parts of a building. In the same way that the bit error rate (BER) is the ultimate measure for comparing performance of different digital communication receivers, accuracy of measurement of the TOA of the DLOS path is a measure of the performance of geolocation receivers. In this article we provide a new framework to model the radio propagation characteristics for analysis of the TOA of the DLOS path.

Three Classes of Locations

In wideband indoor radio propagation studies for telecommunication applications often channel profiles measured in different locations of a building are divided into line of sight and obstructed line of sight because the behavior of the channel in these two classes has substantially different impacts on the performance of a telecommunications system. A logical way to classify channel profiles for geolocation applications is to divide them into three categories. The first category is the dominant direct path (DDP) case, in which the DLOS path is detected by the measurement system and is the strongest path in the channel profile. In this case, traditional GPS (Global Positioning System) receivers [9–11] can lock onto the DLOS path and detect its TOA accurately. The second category is the nondominant direct path (NDDP) case, where the DLOS path is detected by the measurement system but is not the dominant path in the channel profile. For these profiles traditional GPS receivers, expected to lock onto the strongest path, will make an erroneous decision on the TOA. The amount of error made by a traditional receiver is the distance associated with the difference between the TOA of the strongest path and the TOA of the DLOS path. For the second category, locations with NDDP profiles, a more complex RAKE type receiver [1] can resolve the multipath and make an intelligent decision on the TOA of the DLOS path. The third category of channel profiles are unde-

0163-6804/98/$10.00 © 1998 IEEE

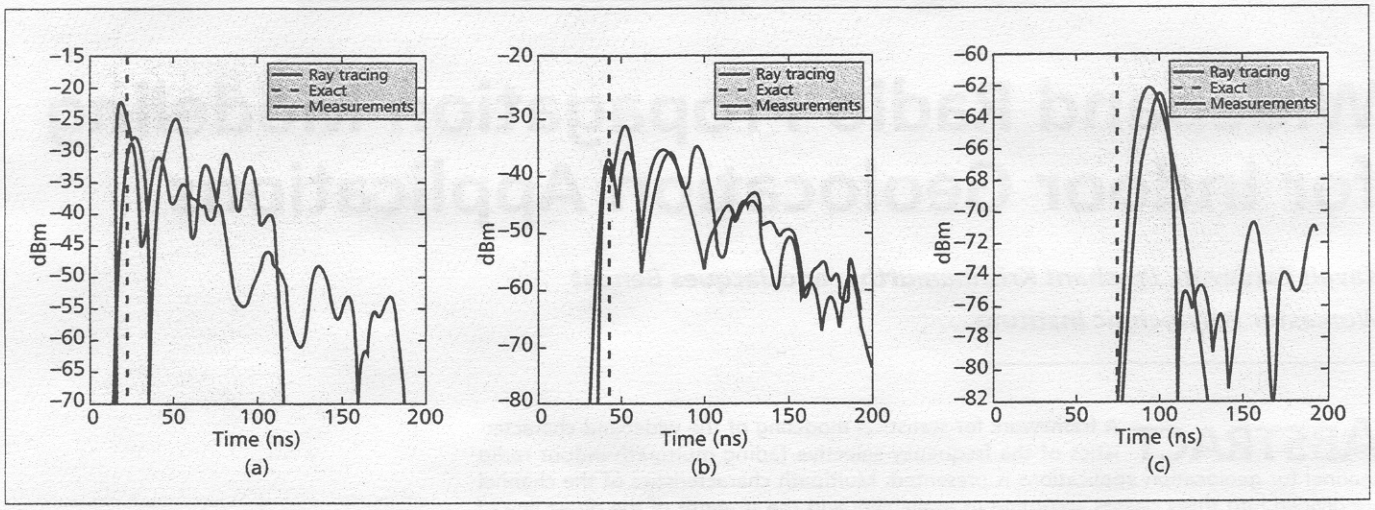

■ **Figure 1.** *Three classes of channel profiles: a) DDP, b) NDDP, and c) UDP.*

tected direct path (UDP) profiles. In these profiles the measurement system cannot detect the DLOS path, and therefore neither traditional GPS nor RAKE-type receivers can detect the DLOS path. If we define the ratio of the power of the strongest path to the power of the weakest detectable path of a profile as the dynamic range of a receiver, in NDDP profiles the strength of the DLOS path is within the dynamic range of the receiver, and in UDP profiles it is not. If practical considerations regarding the dynamic range are neglected, one can argue that we have only two classes (DDP and NDDP) of profiles because the DLOS path always exists, but sometimes we cannot detect it with a practical system.

Description of the Measurements

The measurement system we have used is the frequency domain measurement system described in [12]. The centerpiece of this system is a network analyzer that sweeps the channel from 900–1100 MHz. The output signal is first amplified with a 27 dBm amplifier and then connected to the transmitter antenna by a long cable. The receiver antenna passes the signal through a chain of low-noise amplifiers that are connected to the input port of the network analyzer. The network analyzer records the frequency response of the channel and, by taking the Fourier transform, provides the impulse response we refer to as a *channel time profile* or simply *profile*. The sensitivity of the network analyzer is –80 dBm. Running massive simulations requires exhaustive results from the measurement system, which is extremely expensive. To avoid this difficulty, we use the CWINS ray tracing (RT) software described in [13–15] to draw our statistical conclusions. Recently, RT has also been used for development of wideband statistical models for indoor telecommunications applications [15]. In general, all the details of building and furniture as well as movement of people are not included in any RT programs. We increase details of the building to the extent that results of empirical data from the measurement system at selected points agree with results of RT for the particular application. From that point onward, we use results of RT for massive simulations to draw reasonable statistical conclusions [1, 14, 16]. For telecommunications applications we are interested in the total received power and root mean square (rms) multipath delay spread of the channel. For geolocation applications we have included adequate details of the building to match the power of the DLOS path and to an extent the power in the remaining paths.

Figure 1 shows samples for the three classes of profiles obtained from RT and the measurement system on the first floor of the Atwater Kent (AK) Laboratories at Worcester Polytechnic Institute. The floor plan of this building and the location of the transmitter and receivers are shown in Fig. 2.

In the DDP case the transmitter and receiver are in the same area, in the NDDP case a couple of walls separate them, and in the UDP case several walls are between them. As shown in Fig. 1, results of measurement and RT show close agreement in the DDP and NDDP cases. The DLOS path is within 2–4 dB, the range of variations of the paths is within a few dB, and the arriving paths from RT have a reasonable match to the result of measurements. For the UDP case RT accurately predicts the lack of the DLOS path, and the dynamic range is within a few dB, but the rest of the paths follow less accurately compared to the other two cases. As we mentioned earlier, these differences are caused by effects of movement and other details not included in the RT program. However, in geolocation applications we are mainly concerned with statistical behavior of the DLOS path and the dynamic range of the signal. For these purposes RT proves to be a reliable tool for modeling.

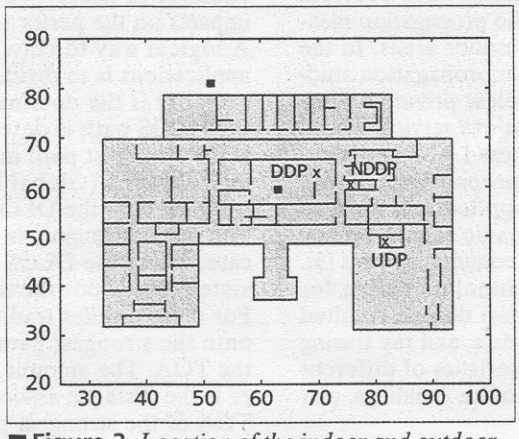

■ **Figure 2.** *Location of the indoor and outdoor transmitters (small squares) and receivers (X) for the sample measurements and ray tracing shown in Fig. 1.*

Statistical Behavior of the Channel

To investigate the statistical behavior of the strength of the DLOS path, RT simulations were performed for 1600 receiver locations in a grid covering the first floor of the AK Laboratories, the floor plan of which is shown in

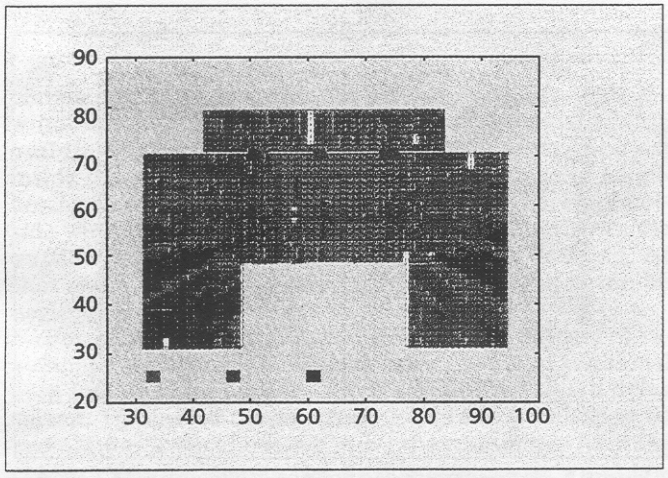

■ **Figure 3.** *Locations in the building exhibiting the three classes of multipath profiles for a receiver sensitivity of –80 dBm and 40 dB dynamic range.*

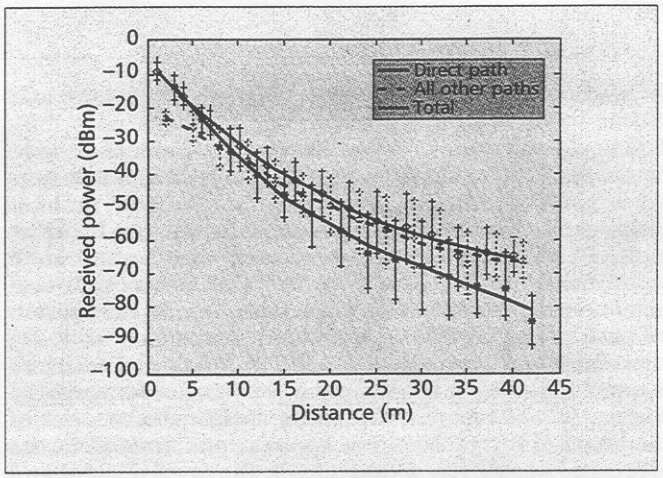

■ **Figure 4.** *Received power as a function of distance in the AK Laboratories first floor for the indoor transmitter location shown in Fig. 2.*

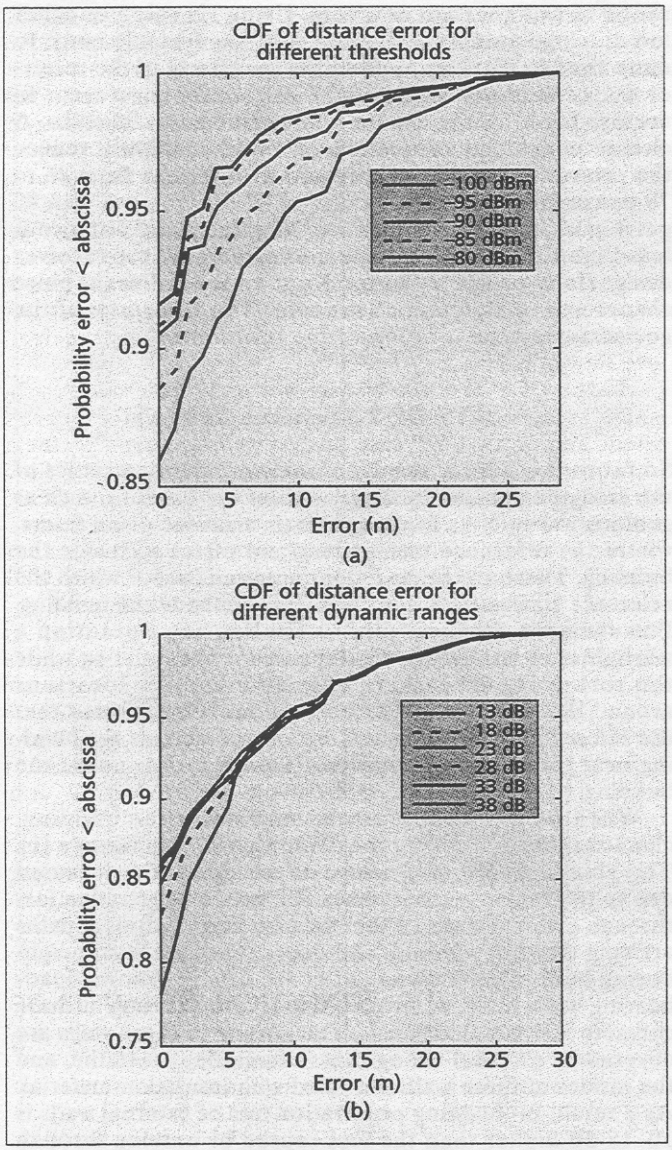

■ **Figure 5.** *CDF of the error in predicted distance for the indoor transmitter: a) as a function of different receiver sensitivities and a fixed dynamic range of 40 dB; b) as a function of different receiver dynamic ranges and a fixed sensitivity of –80 dBm.*

Fig. 2. The transmitter is located at the center of the building, and the receiver is moved to different points on the grid. The AK building was built in 1906 and had two major remodelings and additions in 1934 and 1981. Therefore, in some areas within the building we have more than one exterior-type wall. The exterior walls of this building are heavy brick, the interior walls are made of aluminum stud and sheet rock, the floors are made with metallic beams, the doors and windows are metallic, and many other metallic objects (such as relatively large electric motors, equipment, and vending machines) are spread over different laboratory areas and corridors of the first floor. The excessive number of metallic objects and heavy and multiple external walls makes this building a very harsh environment for radio propagation.

Figure 3 shows the classes of channel profiles obtained in different locations of the building. The red, green, and blue areas correspond to the DDP, NDDP, and UDP profiles, respectively. As we discussed earlier, in the red areas traditional geolocation systems work properly, in the green areas more complicated RAKE type receivers are needed to accurately extract the TOA of the DLOS path, and in the blue areas we need additional transmitters to measure the distance accurately. The reader should be reminded that in practice a geolocation system involves at least three transmitters spread over opportunistically selected locations in the building. This figure provides an intuitive understanding of the range of operation of one reference transmitter operating inside a harsh indoor environment.

We next examine the strength of the DLOS path compared to the combined strength of all other paths and the total received power, including the power in the DLOS path. Figure 4 shows the received power (in dBm) versus distance for the DLOS path, all other paths combined, and total power for all locations of the floor plan. The vertical lines on the curves correspond to the one standard deviation of the received signal strength for that distance.

Over a distance of 45 m in this building, the range of received power in the DLOS path is around 75 dB, while the range of received power in combined other paths and total received power is around 40 dB. The range of received power in the DLOS path is noticeably larger than that of the other paths combined and total received power. An immediate conclusion from this observation is that the receivers designed for geolocation applications in a frequency-selective fading multipath environment should accommodate wider dynamic ranges for the received signal power.

Effects of Receiver Design

The main objective of a geolocation radio receiver is to detect the TOA of the DLOS path. The DLOS path always exists, but in practice for a given receiver sensitivity, dynamic range, and bandwidth, we cannot correctly measure the TOA of the DLOS path all the time. Assuming that the bandwidth is sufficiently large to resolve all the paths, if a receiver cannot detect the DLOS path it will assume that the first detected path is the DLOS path, and will make an erroneous decision on estimating the TOA. This error can easily be mapped to the error in measuring the distance between the transmitter and receiver. To further analyze the behavior of the channel for geolocation applications we look at the effects of sensitivity and dynamic range of a wideband receiver on the probability of detection of the DLOS path and the cumulative distribution function (CDF) of the error in measurement of the distance between the transmitter and receiver.

Detection of the TOA is a function of multipath structure, receiver specification, signal-to-noise ratio, and the algorithm used to detect the DLOS path. We assume a wideband RAKE-type receiver capable of resolving the entire multipath profile of the channel. This receiver declares the TOA of the first detected path as the TOA of the DLOS path. We identify this receiver by its sensitivity and dynamic range. Sensitivity provides the minimum power level of a path that can be detected. Dynamic range provides the difference in dB between the strongest and weakest detectable paths. For example, when assuming a sensitivity of –80 dBm and a dynamic range of 15 dB, the DLOS path is detectable if its power is stronger than –80 dBm and is not more than 15 dB below the power of the strongest path. If these two conditions are not satisfied, the receiver detects the first available path that fits this condition. When the receiver detects another path the difference between the distances measured based on the TOA of the erroneously detected path and the TOA of the DLOS path is considered as the error in detection.

Figure 5a shows the CDF of the distance error as a function of receiver sensitivity for a fixed dynamic range of 40 dB, using the same locations described in Fig. 3. A change in receiver sensitivity from –80 dBm to –100 dBm will change the probability of correct detection of the DLOS path from 86 to 92 percent. The majority of errors occur for shorter distances, for example, a receiver with –100 dBm sensitivity makes an error of less than 2 m 95 percent of the time, although, with a low probability, the receiver may make errors up to 30 m. The larger errors belong to cases where several walls separate the transmitter and receiver. In these cases, often the overall received signal is extremely weak and all paths arrive after several reflections and transmissions through the walls. Again, the reader should note that the errors in Fig. 5 are the errors of a single receiver and not the error of the geolocation system. Practical geolocation systems usually provide redundancies by installing additional reference transmitters and use intelligent algorithms to avoid erroneously reported distances [11]. As a result, the system error can be reduced so that it is significantly less than the error of each individual receiver. When the overall architecture of the geolocation system is specified, statistics provided in Fig. 5 can be used to analyze and determine the actual error of the system.

In the implementation of a receiver, the dynamic range is related to the sidelobes of the pulses that are used for measurement of the TOA. For example, if Nyquist pulses are used, the sidelobes are about 13 dB below the main peak. Therefore, if a path is more than 13 dB below the strongest path it cannot be detected, and the dynamic range of this receiver is 13 dB. Using Hanning or other low-sidelobe pulses, we can increase the dynamic range to more than 40 dB. Figure 5b shows the effects of the receiver dynamic range on the CDF of the distance error in meters for a receiver with a sensitivity of –80 dBm. A change in dynamic range from 38 dB to 13 dB will reduce the probability of detection of the DLOS path from 86 to 78 percent. For a dynamic range of 13 dB, in more than 90 percent of locations the error in measuring the distance is less than 5 m. Analysis of this sort is useful for receiver designers to evaluate the trade-off among different pulse shapes and relate them to the overall performance of the geolocation system.

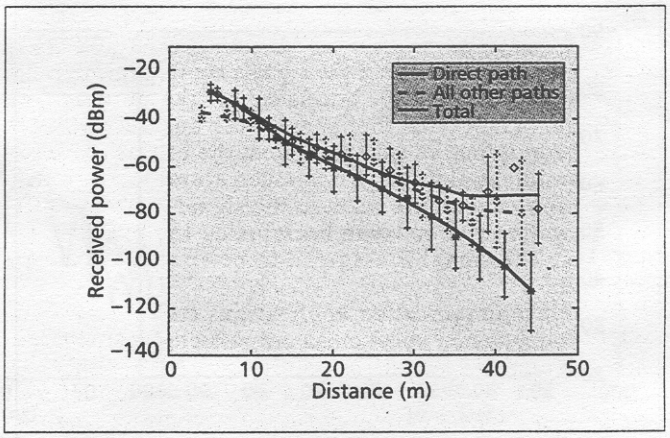

■ **Figure 6.** *Received power as a function of distance in AK Laboratories first floor for the outdoor transmitter location shown in Fig. 2.*

Effects of External Walls

So far in this article, we have analyzed characteristics of the radio channel for indoor-to-indoor applications, such as geolocation systems for hospitals or manufacturing floors, where the reference transmitters are installed inside the building. There are other indoor applications for which the reference transmitters must be located outside the building. For example, in a military or firefighting operation a warfighter or firefighter could be inside the building while the rest of the troops are outside in nearby locations around the building. In these situations it is expected that the reference transmitters will be located outside the building near the external walls while the receiver is inside the building.

When we move the transmitter outside the building, characteristics of radio propagation change significantly [1]. This abrupt change of propagation characteristics is caused due to two major reasons: excessive indoor penetration loss through external walls of the building, and additional paths arriving through windows and doors reflected from neighboring buildings. External walls are usually thicker loadbearing walls made of heavier material which may include concrete and metallic beams. The outside of these walls are covered by external siding that is sometimes metallic, and the insides of these walls are filled with insulation material. As a result, in- building penetration loss of external walls is 10–15 dB higher than the loss caused by passing through traditional internal walls [1]. When the transmitter is outside the building, because of this extra power loss due to in-building penetration, the paths that arrive after penetration though several walls become significantly weak and, at

certain points, weaker than the signals coming through the windows and doors after bouncing off the neighboring buildings. When both the transmitter and receiver are inside the building we usually neglect the effects of neighboring buildings and the signal penetrations through outside windows and doors because the signal must cross the outside walls twice to come back inside the building. At that stage the signal is assumed to be so weak it can be neglected.

For telecommunication applications the effects of in-building penetration phenomena are reflected in additional path loss and an increase in average rms multipath delay spread. To observe the effects of in-building penetration on geolocation applications, we move the transmitter from the center of the building to the outside location shown in Fig. 2 and repeat our previous experiments and analysis. Figure 6 shows the received power versus distance in meters and the best fit curve for the DLOS path, combined other paths, and total received power. The range of the received signal power for the DLOS path is 90 dB as compared to about 40 dB for the combined other paths and total received power. When compared to the results of Fig. 3 for indoor-to-indoor situations, the range of the power of the DLOS path in the outdoor-to-indoor case is significantly larger, while the range of total received power and the combined power in the other paths remains approximately the same. In many locations inside the building, the DLOS path has to pass through many walls, including a heavy outside wall, while other paths can enter the building through open doors and windows. In other words, we may have many locations in the building where we have reasonable power coming through the external windows and doors but the DLOS path is extremely weak.

Figure 7 shows the CDF of the error in predicted distance for a variety of sensitivities and dynamic ranges. When compared with the graphs for indoor-to-indoor applications shown in Fig. 5, the curves in Fig. 7 offer two classes of errors, one less than ~ 10 m and the other more than about 30 m. In the first group of profiles, when the DLOS path is not detected, the next detected path has arrived after penetration through the closest wall to the transmitter, so the arrival time is less than 30 ns (10 m) delayed from the arrival time of the DLOS path. In the second group the falsely detected first path arrives through windows and doors from external reflections, so the overall path length is more than 90 ns (30 m). Therefore, the error is either between the paths coming through penetration or those coming through windows and doors, and these two classes provide a distinct behavior in the error caused by the receiver.

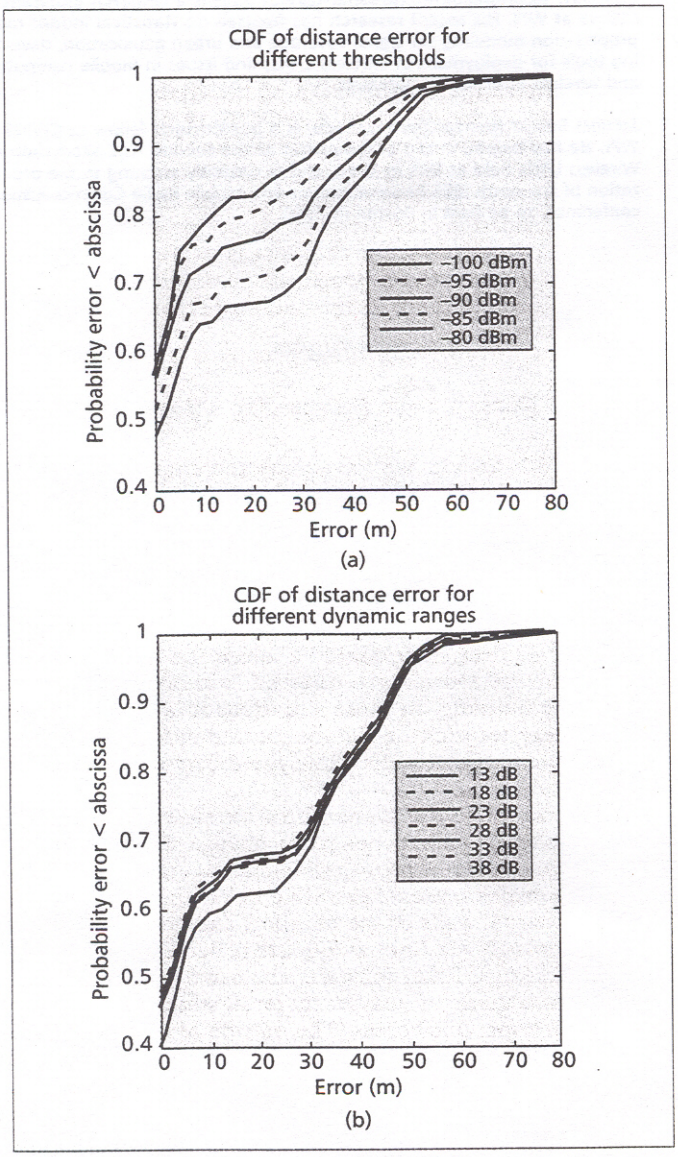

■ **Figure 7.** *CDF of the error in predicted distance for the outdoor transmitter: a) as a function of different receiver sensitivies and a dynamic range of 40dB; b) with a threshold of –80 dBm and different dynamic ranges.*

CONCLUSIONS

Because of the frequency-selective multipath fading characteristics of the indoor radio channel, design of an accurate indoor geolocation system is a challenging task. To provide a foundation for quantitative performance evaluation of such systems a methodology for statistical modeling of this channel for geolocation applications is presented. To relate the performance of traditional GPS receivers to the more complex RAKE-type receivers, the multipath profiles in an indoor area were divided into three classes: DDP, NDDP, and UDP. In the DDP case both RAKE-type and traditional GPS receivers operate properly. In the NDDP case only RAKE receivers function accurately, and in the UDP case neither of the receivers is satisfactory. The statistics of the occurrenceof the three classes of channel profiles in a building with harsh radio propagation characteristics were presented. The statistics of error in measuring the distance as a function of the sensitivity and dynamic range of the receiver as well as effects of outside walls were presented. As we move reference transmitters to the outside of the building, the statistics of the error in estimating the TOA of the DLOS will change significantly. The signal arriving from windows and doors through reflection from neighboring buildings will cause larger errors in prediction of the TOA of the DLOS path.

ACKNOWLEDGMENTS

The authors would like to express their appreciation to DARPA's SUO-SAS program for partial support of this project and approval for public release with unlimited distribution. We are thankful to Dr. Mark McHenry of DARPA for his comments and suggestions. We also thank Paul Creamer and Joseph Pisano, our collaborators at TASC, Reading, Massachusetts, and Dr. James W. Matthews and Ahmad

Hatami, our associates at CWINS, WPI for fruitful discussions and a variety of help. We also appreciate Yan Xu's contribution in running the RT program for the outdoor-to-indoor scenario.

REFERENCES

[1] K. Pahlavan and A. Levesque, *Wireless Information Networks*, New York: Wiley, 1995.
[2] K. Pahlavan, A. Zahedi and P. Krishnamurthy, "Wideband Local Access: WLAN and WATM," *IEEE Commun. Mag.*, Nov. 1997.
[3] K. Pahlavan, T. Probert and M. Chase, "Trends in Wireless Local Networks," *IEEE Commun. Mag.*, Mar. 1995.
[4] MicroTRAX tracking and location system Web site, http://www.harris.com/microtrax.
[5] M. J. Meyer *et al.*, "Wireless Enhanced 9-1-1 Service — Making It a Reality," *Bell Labs Tech. J.*, pp. 188–202, Autumn 1996.
[6] "Report on the New Jersey Wireless Enhanced 911 System Trial," State of New Jersey, Dept. of Law and Public Safety, June 16, 1997.
[7] Trueposition Systems, http://www.trueposition.com.
[8] DARPA Tactical Technology Office: Situation Awareness System Open Review #1 and #2: http://web-ext2.darpa.mil/tto/sas-docs.htm.
[9] P. K. Enge, "Global Positioning Systems: Signals, Measurements and Performance," *Int'l. J. Wireless Info. Networks*, vol. 1, no.2, Apr. 1994.
[10] I. A. Getting, "The Global Positioning System," *IEEE Spectrum*, Dec. 1995, pp. 36–47.
[11] E. D. Kaplan, ed., *Understanding GPS: Principles and Applications*, Boston: Artech House, 1996.
[12] S. J. Howard and K. Pahlavan, "Measurement and Analysis of the Indoor Radio Channel in the Frequency Domain," *IEEE Trans. Instr. Meas.*, no. 39, 1990, pp. 751–55.
[13] T. Holt, K. Pahlavan and J. Lee, "A Graphical Indoor Radio Channel Simulator Using 2-D Ray Tracing," *Proc. PIMRC '92*, Oct. 1992, pp. 411–16.
[14] G. Yang and K. Pahlavan, "Sectored Antenna and DFE Modem for High Speed Indoor Radio Communications," *IEEE Trans. Vehic. Tech.*, Nov. 1994.
[15] M. Hasan-Ali and K. Pahlavan, "Site-Specific Wideband Indoor Channel Modelling Using Ray Tracing Software," *Elect. Lett.*, vol. 33, no. 23, Nov. 1997, pp. 1983–84.
[16] A. Falsafi, K. Pahlavan and G. Yang, "Transmission Techniques for Wireless LANs," *IEEE JSAC*, Apr. 1996.

BIOGRAPHIES

KAVEH PAHLAVAN [F] (kaveh@wpi.edu) is a professor of electrical and computer engineering and director of the Center for Wireless Information Network Studies (CWINS) at Worcester Polytechnic Institute (WPI), Massachusetts. His recent research has been focused on indoor radio propagation modeling and analysis of multiple access and transmission methods for wireless local networks. He is editor-in-chief and founder of the *International Journal of Wireless Information Networks*, and has contributed to numerous technical papers and two patents. He has been program chair and organizer of IEEE conferences and workshops including PIMRC '98 this year. Additional information is available at http://www.cwins.wpi.edu.

PRASHANT KRISHNAMURTHY (prashant@wpi.edu) is a research assistant at CWINS at WPI. His recent research has focused on statistical indoor radio propagation modeling for signal coverage and urban geolocation, developing tools for deployment of wireless LANs, and issues in mobile computing and wireless information networks.

JACQUES BENEAT (beneat@ece.wpi.edu) is a postdoctoral fellow at CWINS at WPI. He has helped in the organization of the Second IEEE Workshop on Wireless LANs held at WPI in 1996, and is currently assisting in the organization of the ninth IEEE Personal Indoor and Mobile Radio Communications conference, to be held in Boston in 1998.

Channel Measurement and Modelining

- B. Alavi, K. Pahlavan, N. Alsindi, and X. Li, ” Indoor Geolocation Distance Error Modeling using UWB Channel Measurements”, The 16th Annual IEEE International Symposium on Personal Indoor and Mobile Radio Communications (PIMRC-2005), September 11 - 14, 2005, Berlin, Germany.
- N. Alsindi, X. Li, and K. Pahlavan, “Performance of TOA Estimation Algorithms in Different Indoor Multipath Conditions”, Proceedings of the IEEE WCNC, April 2004.
- B. Alavi and K. Pahlavan, “Bandwidth effect on distance error modeling for indoor geolocation”, IEEE-PIMRC 2003, Volume: 3, 7-10 Sept. 2003, Pages: 2198 – 2202, 2003.
- R. Tingley and K. Pahlavan, "Measurement of the Time-Space Characteristics of Indoor Radio Channel", *IEEE Trans on Instrumentation and Measurements*, September 2000.
- J. Beneat, K. Pahlavan, and P. Krishnamurthy, "Radio Channel Characterization for Geolocation at 1 GHz, 500MHz, 90 MHz, and 60 MHz In SUO/SAS", MILCOM99, Atlantic City, NJ, November 1999.
- P. Krishnamurthy, and K. Pahlavan, "Analysis of the Probability of Detecting the DLOS Path for Geolocation Applications in Indoor Areas", IEEE VTC'99, July 1999.

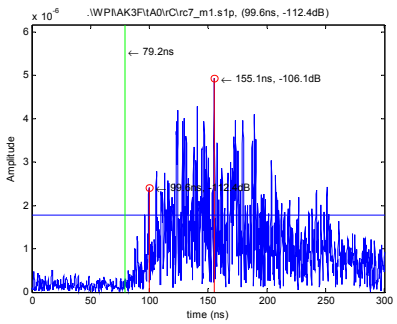

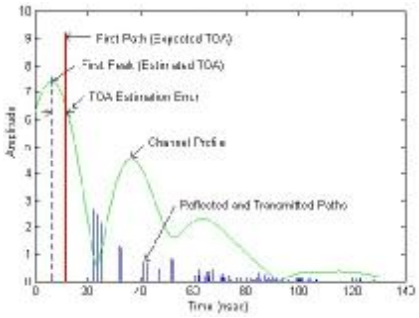

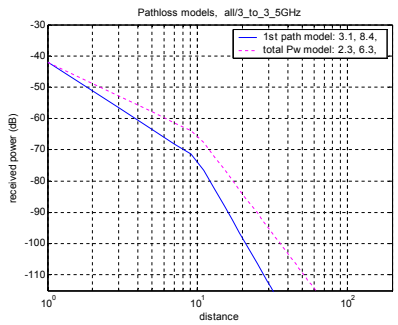

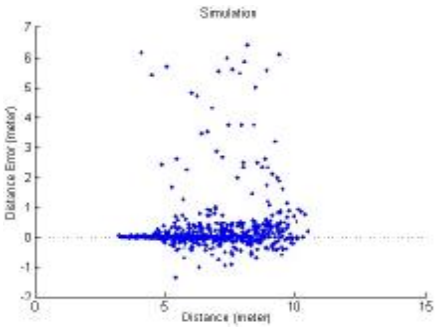

Indoor Geolocation Distance Error Modeling using UWB Channel Measurements

Bardia Alavi, *Student Member IEEE*, Kaveh Pahlavan, *Fellow, IEEE*,
Nayef A. Alsindi, *Student Member IEEE*, Xinrong Li, *Member IEEE*
Center for Wireless Information Network Studies
Electrical Engineering Department
Worcester Polytechnic Institute
Worcester, MA 01609, USA
{bardia, kaveh, nalsindi}@wpi.edu, xinrong@unt.edu

ABSTRACT

In this paper we introduce a model for the distance error measured from the estimated time of arrival (TOA) of the direct path (DP) in a typical multipath indoor environment. We use the results of our ultra-wideband (UWB) measurement database in a sample office environment. To begin modeling, first we separate the causes of the error into multipath and undetected direct path (UDP), and then we model them separately considering the variation of bandwidth of the system. We show that the behavior of the distance error consists of two parts; one that is from multipath, and the other one from UDP. Both errors can be modeled as Gaussian, so the final distance error is a mixture of two Gaussian distributions. We also related the statistics of the distributions to the bandwidth of the system.

KEYWORDS

Wireless networks, positioning, geolocation, ultra-wideband, channel modeling

I. INTRODUCTION

Geolocation systems are becoming more and more popular. Recently the interests in location finding systems are growing. Two existing location finding systems, namely Global Positioning System (GPS) and wireless enhanced 911 (E-911), have been used to provide relatively accurate positioning for the outdoor environment [1]. These technologies, although accurate, could not provide the same accuracy when applied to indoor positioning. The different challenging indoor environment necessitates alternative systems to provide accurate positioning. Therefore, the design and development of indoor positioning systems requires in-depth modeling of the indoor wireless channel, which is more specific to positioning application.

As mentioned, although many channel models for indoor environment exists in the literature; their application to geolocation is weak [2]. Therefore there is a great need in channel models for application to indoor geolocation.

On the other hand, in recent years due to approval of Federal Communication Commission (FCC) for using 3.1-10.6 GHz for commercial use, Ultra-Wideband (UWB) techniques are attracting more interest. Recently UWB has been chosen for the physical layer of the new standard of wireless personal area networks (WPAN) standard [3].

In [4] it has been shown that increasing the bandwidth of the geolocation system can improve the accuracy of the positioning. In this paper we use UWB technology to introduce a channel model for indoor geolocation.

This paper is a continuation of [5] and [4], in which a model for relating measured ranging errors using TOA to the distance between two terminals was investigated. In [5] the concept of distance error and modeling was introduced. Then in [4] the effect of system bandwidth on performance of geolocation systems was studied. In this paper we continue the work on modeling the distance error by considering a UWB system where its bandwidth varies from 3 to 6 GHz. The modeling approach to the problem is also changed and the emphasis is to have a more physical model rather than mathematical. In order to introduce a practical model there is always a trade off between simplicity versus accuracy and it will be discussed later in more detail. The other difference is to use the results of real measurements instead of Ray Tracing simulation that make the claims conclusive.

The structure of the rest of the paper is as follows. Section

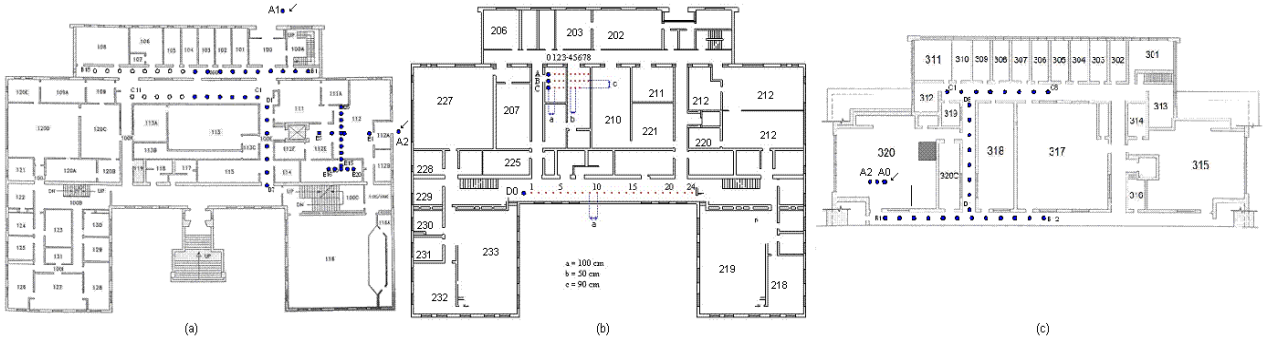

Figure 1. Floorplan of the measurements in Atwater Kent (AK)(a) First Floor – Tx: A1, A2 (b) Second Floor – Tx: A0, B0, C0, D0 (c) Third Floor – Tx: A0-2

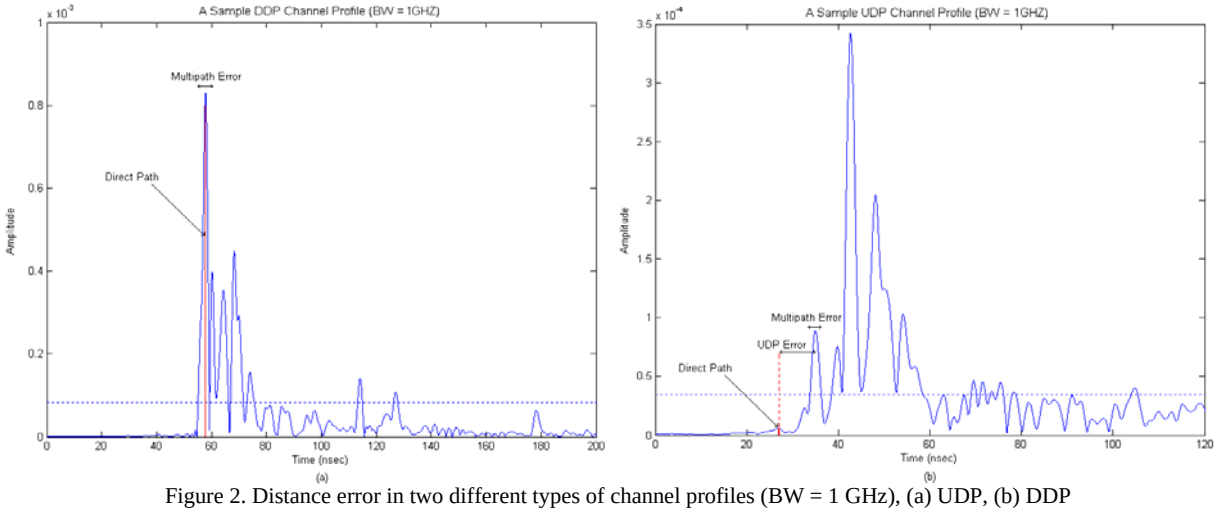

Figure 2. Distance error in two different types of channel profiles (BW = 1 GHz), (a) UDP, (b) DDP

II is about the measurement system and scenario. Section III consists of the modeling part, which includes the modeling framework and strategy, and finally Section IV is the conclusion.

II. DESCRIPTION OF UWB MEASUREMENT SYSTEM AND MEASUREMENT SCENARIO

A. *Measurement System and Scenario*

Magnitude and phase frequency domain measurement method was used to measure channel characteristics. The procedure of this method is described in [6]. In our new UWB measurement system we used a pair of UWB omni directional antennas and Agilent Technologies E8363B vector network analyzer. The bandwidth of the measurements is 3-6 GHz.

In order to generate a database of channel impulse responses of a typical indoor area, the measurements were done in a typical indoor office environment with total of 405 points. They were carried out in the first, second, and third floor of Atwater Kent Laboratory building of Worcester Polytechnic Institute. Figure 1 shows the floor plans of the measurements and positions of transmitters (Tx) and receivers (Rx). The pairs of Tx and Rx were chosen in a way to cover Line-of-Sight (LOS) and Obstructed LOS (OLOS) cases and also Undetected First Path (UDP) cases [2] [7]. The whole measurement campaign consisted of many measurement sets. During each measurement set the position of Tx was constant and Rx was changing from a place to another. Also to reduce the stochastic property of channel profiles each measurement pair were measured two or three separate times. The distance between consecutive Rx's varies depending on the measurement set. It is 0.5, 1, or 2 meters.

III. DISTANCE ERROR MODELING

A. *Modeling Framework*

Assuming that the actual distance between the transmitter and the receiver is *d*, and the estimated distance is $\hat{d}_w$, we define the distance error $\varepsilon_{d,w}$ as,

$$\varepsilon_d = \hat{d} - d \ . \qquad (1)$$

The subscript *w* is for system bandwidth and comes from [4] that mentions estimated distance and hence distance error, both highly depend on the system bandwidth.

B. *Modeling Strategy*

As it was mentioned in the introduction, in this paper the emphasis in modeling is on having a more physical model rather than only mathematical fitting. The modeling is about a physical phenomenon, experimentally measured, so the modeling should be able to justify the behaviors as much as possible.

By looking at Fig. 2 two types of channel profiles are shown. Figure 2-(a) shows a situation where the direct path (DP) is detected and Fig. 2-(b) shows a case that the DP is not detected. In both cases we detect the first available peak, which is the peak above the threshold.

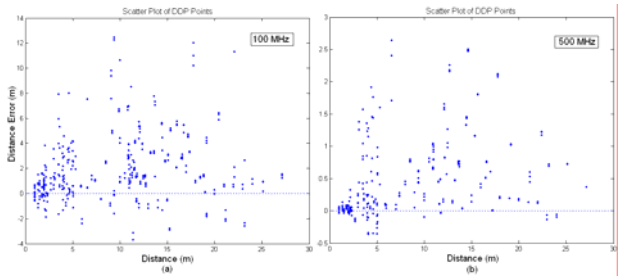

Figure 3. Scatter Plots of distance error for DDP, (a) 100 MHz, (b) 500 MHz

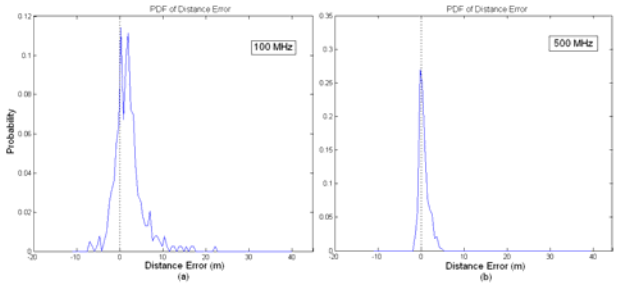

Figure 4. PDF's of distance errors for DDP, (a) 100 MHz, (b) 500 MHz

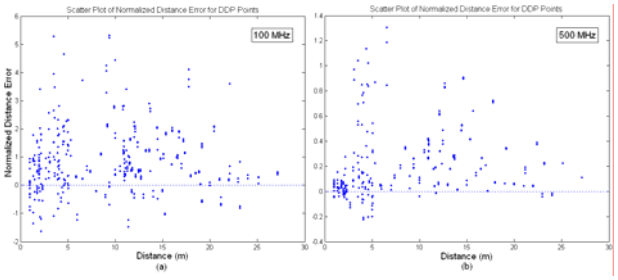

Figure 5. Scatter plots of normalized distance error for DDP points, (a) BW = 100 MHz, (b) BW = 500 MHz

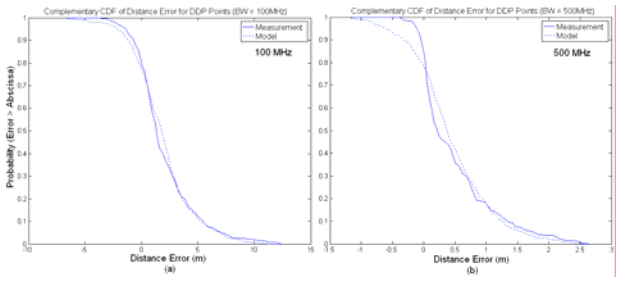

Figure 6. CDF comparisons between measurements and model for DDP points, (a) BW = 100 MHz, (b) BW = 500 MHz

The threshold is determined by the noise power and the side-lobe amplitude of the peaks that depends on the selected window. In our experiment we used hamming window that has -31dB side-lobe amplitude. But to remove the random noise effects we used a 5 dB margin that makes it -26 dB.

In the first case, the first peak is mainly created by the first path. But because of the multipath effect it can be deviated to both sides. In [5] and [4] it is discussed that this type of error is modeled as a zero mean Gaussian with a factor of distance; since it is also distance dependent. We consider this error as multipath error. It can be shown that multipath error can be reduced with increasing the bandwidth.

Looking in the second case, the first peak does not contain the first path anymore. In fact the first path is been weakened so much that it is below the threshold. Now we have another type of error that we call it UDP error. It is interesting that still we have our multipath error on top of the UDP error, which changes the position of the detected peak.

To approach this phenomenon, we model the distance error as a summation of a multipath error part, which is shown with ε_m and always exists, and a UDP error part, ε_{UDP}, that some times happens as follows

$$\varepsilon_{d,w} = \varepsilon_{m,w} + \xi_w \cdot \varepsilon_{UDP,w} \qquad (2)$$

In (2) ξ is a random variable (RV) that is based on having a UDP situation or not, it is either "1" or "0". In the next two subsections we will provide more details on modeling each type of error.

C. Modeling of Multipath Error

To model the multipath error we need to look into channel profiles that the DP is detected. These channel profiles are called Detected DP (DDP) and only have the multipath error, so $\varepsilon_{d,w} = \varepsilon_{m,w}$ is true for this case. Figure 3 shows the scatter plots of $\varepsilon_{d,w}$ versus distance, d, for DDP channel profiles and two different bandwidths 100 MHz and 500 MHz. As we can see by increasing the distance, $\varepsilon_{d,w}$ increases. But the increase pace seems to be slower than linear, which was observed from Ray-Tracing (RT) results in [4]. Also we can observe that the symmetry around the horizontal axis is not preserved as in the RT case. This can be justified by the fact that the arriving paths next to the DP are all on one side of the DP and hence their effect on the peak can not be even.

Figure 4 shows the probability density function (PDF) of the corresponding scatter plots. We can observe that by increasing the system bandwidth the variance of the error decreases. Also we can see that the mean is not zero, which explains the asymmetry, which is another consequence of having all neighbor arriving paths after DP.

Similar to [5] and [4] in order to model the increase of $\varepsilon_{m,w}$ with increasing distance, we introduce a new parameter γ_w, the normalized distance error. The normalized distance error is defined as follows:

$$\gamma_w = \frac{\varepsilon_{m,w}}{\log(1+d)} \qquad (3)$$

In (3) the summation with one is used to avoid the negative part of logarithm or facing division by zero situations. We want to use the specific property of the logarithm that has slower increasing pace than linear; this property is true for the arguments greater than 1. The scatter plots of γ_w are shown in Fig. 5. It can be seen that the normalized one has relatively constant spread across the distance axis.

We used Gaussian distribution to model the distribution of γ_w; Fig. 6 shows the complementary cumulative distribution function (CDF) comparison between the measurement results and the model, for the DDP points.

So, the multipath error has been modeled as

$$\varepsilon_{m,w} = G(m_w, \sigma_w)\log(1+d) \qquad (4)$$

Where, $G(m_w, \sigma_w)$ is a Gaussian number with mean m_w and variance σ^2_w. Table 1 shows the values of m_w and σ^2_w for different bandwidths obtained from the measurements.

D. Modeling of UDP Errors

In order to model the UDP errors we need to have ideas about behaviors of ξ and $\varepsilon_{UDP,w}$. For ξ we can find a good approximation for probability of occurring UDP. In order to model this we calculate probability of UDP as a function of distance and bandwidth. For the distance we consider two cases for the probability, one for distances less than 10 meters and the other for distances of more than 10 meters. The 10 meter distance criteria comes from the fact that as the receiver goes farther from the transmitter probability of having UDP point increases [8] [9]. Then to calculate this probability we divide the number of UDP points in that region by the total number of points in the same region.

Table 1 shows this approximation for different bandwidths. As you can see probability of UDP in distances of more than 10 meters is much higher than the other case. Another interesting observation is that by increasing the bandwidth, probability of having UDP ($P_{UDP,w}$) increases, this is because

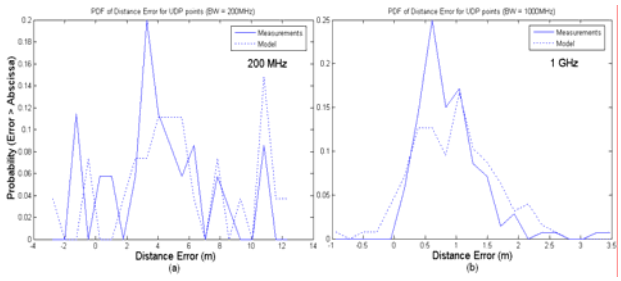

Figure 7. PDF's of distance error for UDP points, (a) BW = 200 MHz, (b) BW = 1 GHz

in higher bandwidths, arriving neighbor paths are resolved, separated and usually their individual power is less than their combined power. So, there is an important conclusion that by increasing the bandwidth we can not always have a better situation. In fact, as it happened in this case we can have more UDP points.

So, ξ will be an RV with the following distribution:

$$f(\xi) = (1 - P_{UDP,w})\delta(\xi) + P_{UDP,w}\delta(\xi - 1) \qquad (5\text{-a})$$

$$P_{UDP,w} = \begin{cases} P_{closeUDP,w} & d \le 10\,m \\ P_{farUDP,w} & d > 10\,m \end{cases} \qquad (5\text{-b})$$

where $P_{close\ UDP,w}$ and $P_{far\ UDP,w}$ can be found in Table 1.

To model $\varepsilon_{UDP,w}$ we look into PDF of $\varepsilon_{UDP,w}$ for different bandwidths. Figure 7 shows these PDFs. To examine the effect of UDP error, alone, we used the UDP points from the database.

We used Gaussian distribution to model the distribution of $\varepsilon_{UDP,w}$. Fig. 8 shows the complementary CDF comparison between the measurement results and the model for the UDP points. So, the UDP error has been modeled as

$$\varepsilon_{UDP,w} = G(m_{UDP,w}, \sigma_{UDP,w}) \qquad (6)$$

Where, $G(m_{UDP,w}, \sigma_{UDP,w})$ is a Gaussian number with mean $m_{UDP,w}$ and variance $\sigma^2_{UDP,w}$. Table 1 shows the values of m_w and $\sigma^2_{UDP,w}$ for different bandwidths obtained from the measurements.

E. The final Model for Distance Error

So far, we have separated two different causes for distance error and modeled each one of them separately. In this subsection we use the results of both previous parts to finalize our model.

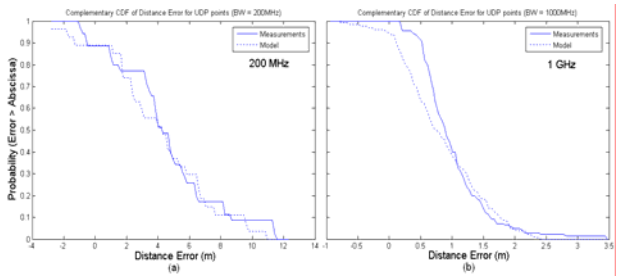

Figure 8. CDF comparisons between measurements and model for UDP points, (a) BW = 200 MHz, (b) BW = 1 GHz

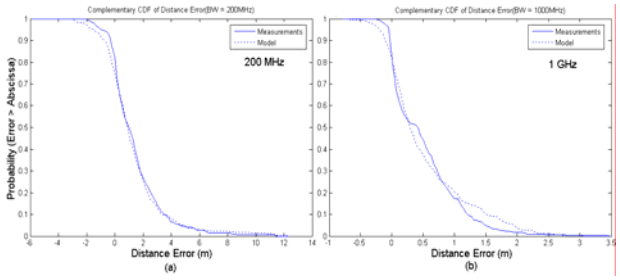

Figure 9. CDF comparisons between measurements and model for total points, (a) BW = 200 MHz, (b) BW = 1 GHz

Despite our previous works [5] [4] [10], the modeling strategy in this paper is not based on partitioning the area into LOS and OLOS. On the other hand we used the concept of UDP and the modeling is based on UDP/DDP situation, which is more essential for distance error modeling.

As noted in (2) the distance error $\varepsilon_{d,w}$ is modeled as a summation of two different errors that each of them has been identified. The final model can be expressed as follows:

$$\hat{d} = d + G(m_w, \sigma_w) \cdot \log(1 + d) + \xi_{w,d} \cdot G(m_{UDP,w}, \sigma_{UDP,w}) \qquad (7\text{-a})$$

$$f(\xi) = (1 - P_{UDP,w}) \cdot \delta(\xi) + P_{UDP,w} \cdot \delta(\xi - 1) \qquad (7\text{-b})$$

Figure 9 shows the comparison of complementary CDFs between measurements and model results for two correspondent bandwidths and Fig. 10 shows the scatter plots of measurements and model for bandwidths 200 and 1000 MHz. As we can see the model decently follows the measurements.

So, one can use the proposed model to estimate the accuracy of distance estimation in a Time-Of-Arrival (TOA) based indoor geolocation system.

IV. CONCLUSION

In this paper, we introduced a model for the estimated distance from TOA of the first path in an indoor multipath environment typically used for WPAN applications. Using results of UWB channel measurements we showed how in a typical indoor environment the model relates the distance error to the bandwidth of the system, and occurrence of UDP can affect the distance error.

We separated the causes of the distance error into multipath and UDP and modeled each of them with respect to the system bandwidth. We concluded that an increase in both the distance and the bandwidth of the system can increase the chance of having UDP. However, increasing bandwidth decreases distance error. As a result a compromise in system bandwidth has to be made between probability of UDP occurrence and TOA estimation performance. We also demonstrated that the results of the model closely fit the empirical data.

REFERENCES

[1] M. J. Meyer *et al*., "Wireless Enhanced 9-1-1 Service – Making It a Reality," *Bell Labs Tech. J.*, pp. 188-202, autumn 1996.

[2] K. Pahlavan, P. Krishnamurthy, and J. Beneat, "Wideband Radio Channel Modeling for Indoor Geolocation Applications," *IEEE Commun. Mag.*, vol. 36., no. 4, Apr. 1998, pp. 60-65.

[3] S.S. Ghassemzadeh, L.J. Greenstein, A. Kavcic, T. Sveinsson, and V. Tarokh, "UWB indoor path loss model for residential and commercial buildings," *IEEE VTC 2003*-Fall,Volume: 5, 6-9 Oct. 2003, Pages:3115 - 3119

[4] B. Alavi and K. Pahlavan, "Bandwidth effect on distance error modeling for indoor geolocation",*IEEE-PIMRC 2003*., Volume: 3, 7-10 Sept. 2003, Pages:2198 – 2202.

[5] B. Alavi and K. Pahlavan, "Modeling of The Distance Error for Indoor Geolocation", *IEEE-WCNC 2003*, Volume: 1, 16-20 March 2003, Pages:668 – 672.

[6] S.J. Howard and K. Pahlavan, "Measurement and analysis of the indoor radio channel in the frequency domain", *Instrumentation and Measurement, IEEE Transactions on*, Volume: 39, Issue: 5, Oct. 1990, Pages:751 – 755.

[7] N.A. Alsindi, X. Li, K. Pahlavan, "Performance of TOA Estimation Algorithms in Different Indoor Multipath Conditions", *IEEE-WCNC 2004*, Volume: 1, 16-20 March 2004.

[8] D. Cassioli; M. Z. Win, A. F. Molisch, "The ultra-wide bandwidth indoor channel: from statistical model to simulations", *Selected Areas in Communications, IEEE Journal on* , Volume: 20 , Issue: 6 , Aug. 2002 Pages:1247 – 1257.

[9] X. Li, K. Pahlavan, B. Alavi, N. Alsindi, "Measurement and Characterization of Indoor UWB Channels for Positioning Applications", submitted to IEEE Communications for publication November 2004.

[10] E.D. Zand and K. Pahlavan, "Measurement of TOA using frequency domain characteristics for indoor geolocation", *IEEE-PIMRC 2003*, Volume: 3, 7-10 Sept. 2003, Pages:2213 – 2217.

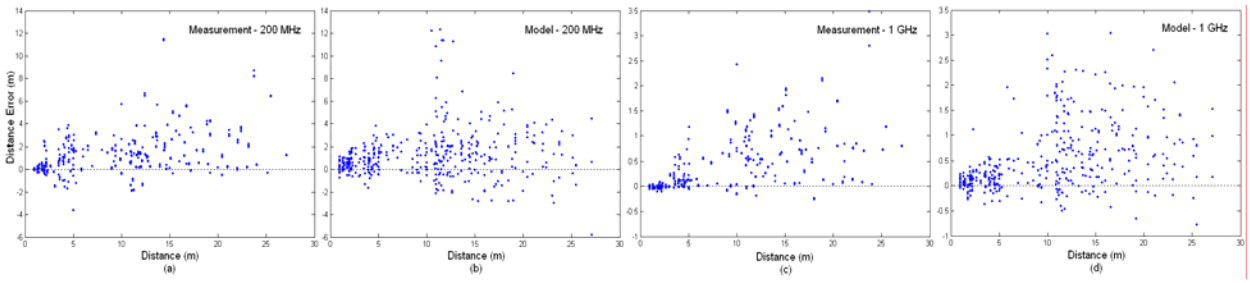

Figure 10. Scatter plots of total points (DDP + UDP), (a) Measurements, 200 MHz, (b) Model, 200 MHz, (c) Measurements, 1 GHz, (d) Model 1 GHz

Table 1. Typical values of model parameters derived from the measurements

W (MHz)	m_W(cm)	σ_W(cm)	$P_{close\ UDP,W}$	$P_{far\ UDP,W}$	$m_{UDP,W}$(cm)	$\sigma_{UDP,W}$(cm)
20	3.66	515	0	0.005	-12.83	0
50	1.57	205	0	0.009	24.48	21.1
100	0.87	115	0	0.091	5.96	358.5
200	0.47	59	0.006	0.164	3.94	289.0
500	0.21	26.9	0.064	0.332	1.62	80.9
1000	0.09	13.6	0.064	0.620	0.96	60.4
2000	0.02	5.2	0.070	0.740	0.76	71.5
3000	0.004	4.5	0.117	0.774	0.88	152.2

Bandwidth Effect on Distance Error Modeling for Indoor Geolocation

Bardia Alavi Kaveh Pahlavan
Center for Wireless Information Network Studies
Electrical Engineering Department
Worcester Polytechnic Institute
Worcester, MA 01609, USA
{bardia, kaveh}@wpi.edu

***Abstract*— In this paper we introduce a model for the distance error measured from the estimated time of arrival (TOA) of the direct path (DP) between the transmitter and the receiver in a typical multipath indoor environment. We use the results of a calibrated Ray Tracing software in a sample office environment. First we divide the whole floor plan into LOS and Obstructed LOS (OLOS), and then we model the distance error in each environment considering the variation of bandwidth of the system. We show that the behavior of the distance error in LOS environment can be modeled as Gaussian, while behavior of the OLOS is a mixture of Gaussian and Exponential distribution. We also related the statistics of the distributions to the bandwidth of the system.**

Keywords-wireless networks, positioning, geolocation, indoor communications, channel modeling

I. INTRODUCTION

Indoor geolocation is a new emerging technology. Recently, accurate location finding techniques and location-based applications for indoor areas are becoming more interesting. The applications vary from WLANs security to patient positioning in hospitals.

A general geolocation system consists of three major elements: location-sensing module, positioning algorithm module, and the display module. The location-sensing part which is used in multiple sample modules due to trianglization, receives the RF signal, extracts appropriate features and delivers them to the positioning algorithm part. Trianglization is a technique that finds the position of the mobile terminal (MT) from its relative distances to the reference points (RP). Furthermore, the accuracy of the MT positions can be enhanced by increasing the number of RPs which increases the number of circles.

Depending on the environment and applications, features vary from one to another. For locationing applications, features can be directly related to the distance between MT and RP, such as Time of Arrival (TOA), or indirectly related to the distance such as Received Signal Strength (RSS), or they can even be related to the direction of the path between MT and RP, such as Angle of Arrival (AOA).

The second module is the positioning algorithm, and it processes the metrics reported by the location sensing elements to estimate the location coordinates of MT. The display system illustrates the location of the MT to the users [1].

Among distance measurement metrics and features for geolocation systems, TOA is the most popular one [2]. However, except for the preliminary work in [3] there is no model available in the literature for the distance error that can be used for performance evaluation of these algorithms. In addition to WPAN application, these models can also be useful for other applications such as design of indoor geolocation algorithms [4].

This paper is a continuation of [3] to introduce a model for relating measured ranging errors using TOA to the distance between two terminals and studies the effect of bandwidth in performance of the system.

The structure of the chapters and sections of this paper is as follows. Chapter I, which this text belongs to, provides an introduction for the geolocation technologies. Chapter II gives some information about the Ray Tracing software (used for simulation), the way multipath makes errors in TOA estimation and the simulation scenario. Chapter III is about LOS and OLOS modeling and Chapter IV is the conclusion.

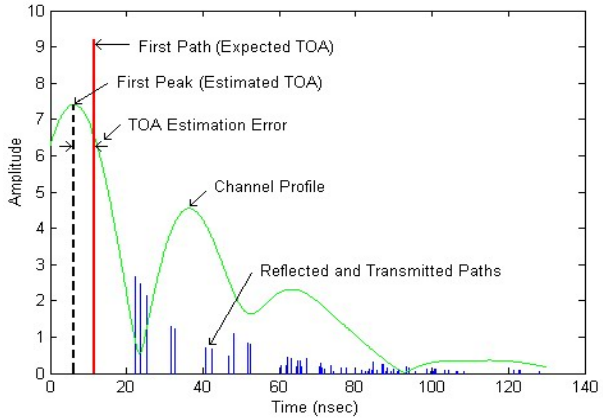

Figure 1. Effects of multipath in estimation of the distance from TOA of the first path

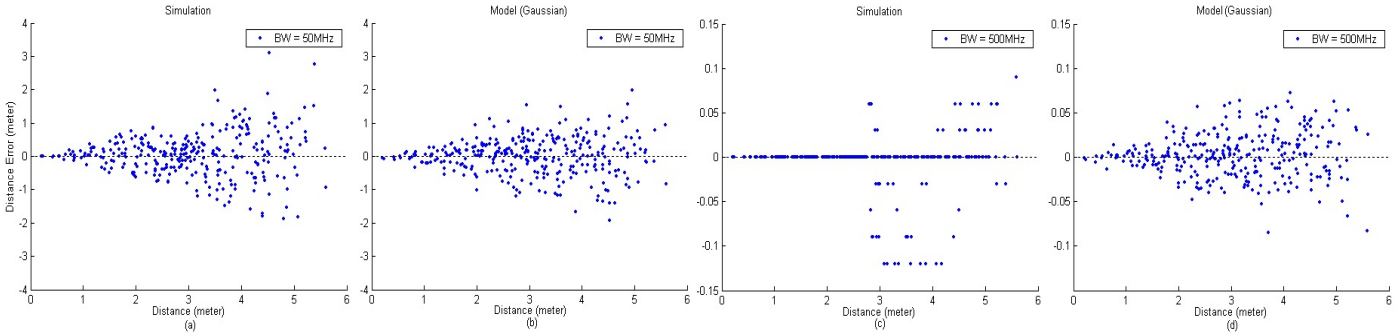

Figure 2. Scatter plots of distance error for (a) Simulation, w = 50 MHz (b) Model, w = 50 MHz (c) Simulation, w = 500 MHz (d) Model, w = 500 MHz

II. DISTANCE ERROR CALCULATION USING RAY TRACING (RT)

A. *Distance Estimation in Multipath Environment*

The major problem of radio propagation in all of the telecommunication systems is the multipath effect. Like other telecommunication systems, geolocation systems also suffer from the multipath effect. To illustrate how multipath effect can cause error in calculating the distance from TOA, assume that the transmitted signal *p(t)* travels in a multipath environment, and after many transmissions and reflections arrives at the receiver as *s(t)*, which is given by

$$s(t) = \sum_{n=1}^{L} \alpha_n p(t-\tau_n) e^{j\phi_n} \quad (1)$$

where α_n's, τ_n's and ϕ_n's are attenuation, delay and phase related to each particular received path and L is the total number of received paths [5].

Figure 1 clarifies this issue by describing the relationship among arriving paths, channel profile, expected and estimated TOA of the first path, and TOA estimation error. The real distance is obtained from multiplication of expected TOA of the first path by the speed of light ($c = 3\times10^8\ m/s$). Similarly, from the estimated TOA of the first path, which is the first peak we can derive the estimated distance, and finally the distance measurement error can be obtained from TOA estimation error. In this figure, the channel profile is produced by assuming that a 40MHz raised cosine pulse with a roll-off factor of 0.5 was transmitted.

To simulate the strength and the arrival time of the paths, similar to [6], we use the Ray Tracing (RT) software. The use of the RT software makes it is possible to simulate the behavior of the signal traveling from the receiver to the transmitter based on optical rules. By locating a pair of Tx-Rx, RT simulates all the paths to Rx including necessary information such as received path amplitude, time delay, arrival angle, departure angle, phase, number of reflections, and number of transmissions. Detailed explanation about RT can be found in [5].

B. *Simulation Scenario*

To generate a large database of the channel impulse responses of a typical indoor area we used a calibrated floor plan [7] for RT. Similar to [3] the floor plan is taken from the second floor of Atwater Kent Laboratory, Worcester Polytechnic Institute, Worcester, MA. The calibration process is aimed to fit the empirical data with the results of RT simulation by adjusting propagation parameters representing physical characteristics of the material used in the building. The position of the transmitter is constant during the whole simulation procedure and it is located in the middle of the floor plan. For locating the receivers, several hundred points were selected from a grid with approximately 20cm minimum distance between the adjacent points.

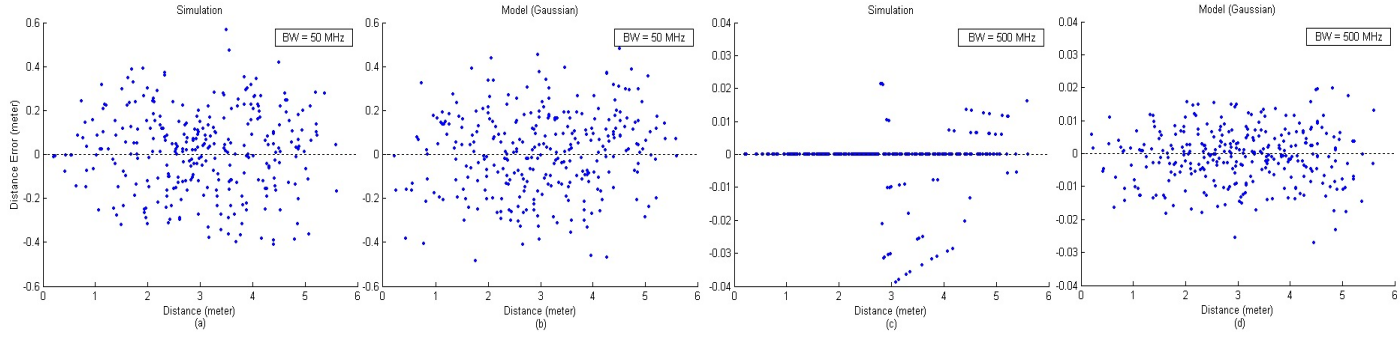

Figure 3. Scatter plots of LOS normalized distance error for (a) Simulation, w = 50 MHz (b) Model, w = 50 MHz (c) Simulation, w = 500 MHz (d) Model, w = 500 MHz

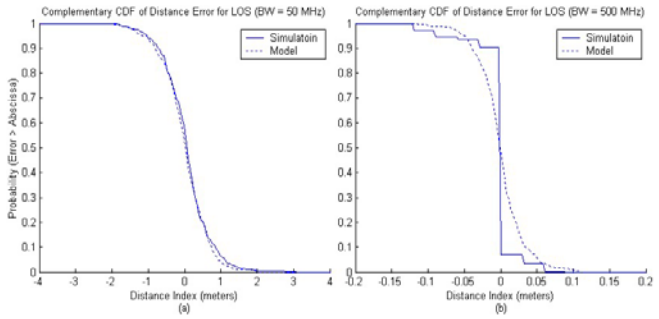

Figure 4. Comparison between complementary CDFs of distance error for LOS, (a) w = 50 MHz, (b) w = 500 MHz

III. DISTANCE ERROR MODELING

A. *Modeling Strategy*

The behavior of the channel in LOS and OLOS is basically different. This difference stems from the fact that in OLOS case the Direct LOS (DLOS) path, which in positioning is of particular importance, often is not the strongest path. But in LOS situation the DLOS path has the highest amplitude because it not only has the lowest path length and therefore the least path loss due to distance, but it also hasn't experienced any loss because of reflection or transmission.

Furthermore, to analyze the channel behavior in each region differently we divided the whole floor plan into LOS and OLOS. In LOS region the minimum distance is close to zero and the maximum distance is around 5.5 meters. In OLOS region the distance varies between 3 to 11 meters.

Unlike [3] in this paper the modeling emphasis is on studying the effect of bandwidth on distance estimation error. Assuming that the system has bandwidth of "w" we are to find the distance for the channel profile. Then the estimated distance is $\hat{d}_w$ and the distance error is $\varepsilon_{d,w}$, which is defined as

$$\varepsilon_{d,w} = \hat{d}_w - d \tag{2}$$

where *d* is the real distance. This definition is consistent for both LOS and OLOS cases.

In the next two sections we explain the modeling of the distance errors in LOS and OLOS environments.

B. *LOS Modeling*

Figures 2-(a), (c) show the scatter plots of $\varepsilon_{d,w}$ derived from the simulation results for two different bandwidths 50 and 500 MHz. As we discussed in [3], to overcome the increase of $\varepsilon_{d,w}$ with increasing the distance, we introduce a new parameter γ_w, the normalized distance error. The normalized distance error is defined in (3), and for the LOS case it is shown as γ_{Lw}.

Table 1. Typical values of model parameters and the fitting error for different bandwidths for LOS

w (MHz)	σ_{Lw} (cm)	ε_{fit} (cm)
30	34.33	29.40
40	34.33	15.34
50	19.06	5.57
100	6.48	2.59
200	2.6	2.54
500	0.83	1.60
1000	0.27	0.58
2000	2.1e-14	3.4e-14
3000	2.1e-14	3.3e-14

$$\gamma_{Lw} = \frac{\varepsilon_{d,w}}{d} \tag{3}$$

This definition results in a general form of representing the estimated distance in terms of normalized distance error, which is shown in (4).

$$\hat{d} = d\left(1 + \gamma_{Lw}\right) \tag{4}$$

Similar to [3], we assume that γ_{Lw} has zero mean Gaussian distribution with variance derived from the simulation results, which has the form of

$$f\left(\gamma_{Lw}\right) = \frac{1}{\sqrt{2\pi}\sigma_{Lw}} e^{-\frac{\gamma_{Lw}^2}{2\sigma_{Lw}^2}} \tag{5}$$

where σ_{Lw} is the standard deviation (STD) of γ_{Lw}.

Figures 3-(a), (c) show the corresponding normalized distance errors to Figs. 2-(a), (c), derived using (3), which are for bandwidths 50 and 500 MHz, respectively. Figures 3-(b), (d) are the generated normalized distance errors from the introduced model; they correspond to Figs. 3-(a), (c) respectively and have the same number of points and variances as their simulation version. To generate the distance error sets from (3) we can conclude

$$\varepsilon_{d,w} = \gamma_{Lw} \times d \tag{6}$$

and using the distance set that we used for the simulation phase, we can derive the distance errors. The results are shown in Figs. 2-(b), (d). To measure the similarity of the introduced model with the results of simulation, cumulative distribution function (CDF) has been used. The CDF curves for two bandwidths 50 and 500 MHz are shown in Figs. 4-(a), (b). It can be seen that for higher bandwidths the CDF curve doesn't resemble the Gaussian shape. This is due to quantization error in the time axis of channel profiles. In addition, decreasing the time step can solve this problem but the amount of distance error and the fitting error (discussed in the next paragraph) is so small that it makes this approximation quite accurate. This quantization effect can be clearly seen on figures 2-(c) and 3-(c).

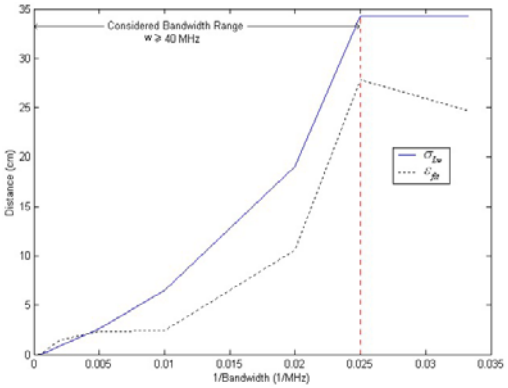

Figure 5. Standard deviation of normalized distance error (σ) and the average fitting error (ε) vs. 1/Bandwidth for LOS

To show how closely the CDF curve of the model follows the CDF curve of the simulation, we defined a new parameter, which is called average fitting error or ε_{fit}. The average fitting error is defined as the average of the horizontal difference between the curves of the simulation and the model and it is derived from the area created between these two curves. Table 1 shows the standard deviation of the normalized distance error and the average fitting error for 9 different bandwidths from 30 to 3000 MHz. Figure 5 shows the two parameters σ_{Lw} and ε_{fit} versus *1/w*, as it can be seen the model fits well until the lower limit of 40 MHz. Based on these results and from polynomial fittings (7) introduces an equation to find σ_{Lw} in cm, where A_L=52691, B_L=0.43, m_L=10^{-4}, and w is the bandwidth in MHz $(w \geq 40MHz)$.

$$\sigma_{Lw} = A_L\left(\frac{1}{w} - m_L\right)^2 + B_L \qquad (7)$$

C. OLOS Modeling

Figures 6-(a), (c) show the scatter plots of $\varepsilon_{d,w}$ derived from the simulation results of OLOS environment for two different bandwidths 50 and 500 MHz. Here, we again used the concept of normalized distance error, because for the

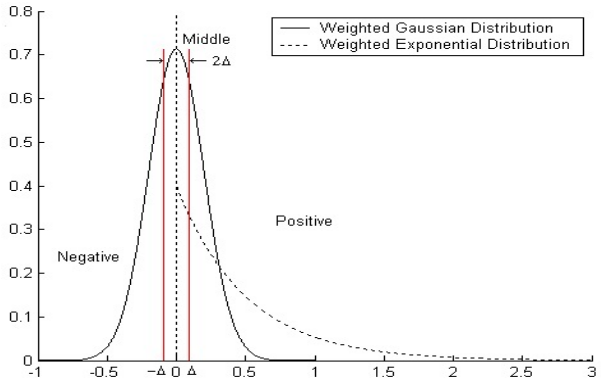

Figure 7. Assumed distribution for the OLOS with the partitioning

major number of points increase in the distance error along with distance is still visible. So, the equations (3) and (4) can be applied for OLOS case, but the normalized distance error is shown as γ_{Ow}.

To estimate the distribution of γ_{Ow} we made the same assumption as in [3], which was a mixture of zero mean Gaussian and Exponential. The distribution of γ_{Ow} can be written in a compact form as

$$f(\gamma_{Ow}) = W_{Gw}\frac{1}{\sqrt{2\pi}\sigma_{Ow}}e^{\frac{\gamma_{Ow}^2}{2\sigma_{Ow}^2}} + W_{Expw}\left(\frac{\gamma_{Ow}+|\gamma_{Ow}|}{2\gamma_{Ow}}\right)\lambda_w e^{-\lambda_w\gamma_{Ow}} \qquad (8)$$

where W_{Gw} and W_{Expw} are the weights of the Gaussian and Exponential parts, σ_{Ow} is the STD of Gaussian distribution, and λ_w is the Exponential distribution parameter.

To extract the parameters for OLOS we used the same technique that has been used in [3] with a small modification. As it can be seen from table 1, for high bandwidths distance error dramatically decreases, in such a way that it goes beyond the simulation resolution. In those cases the data does not seem to be correct anymore and most of the points have equal distance error, which makes the distribution have a delta function close to zero, which causes errors in parameter calculations. To overcome this problem we

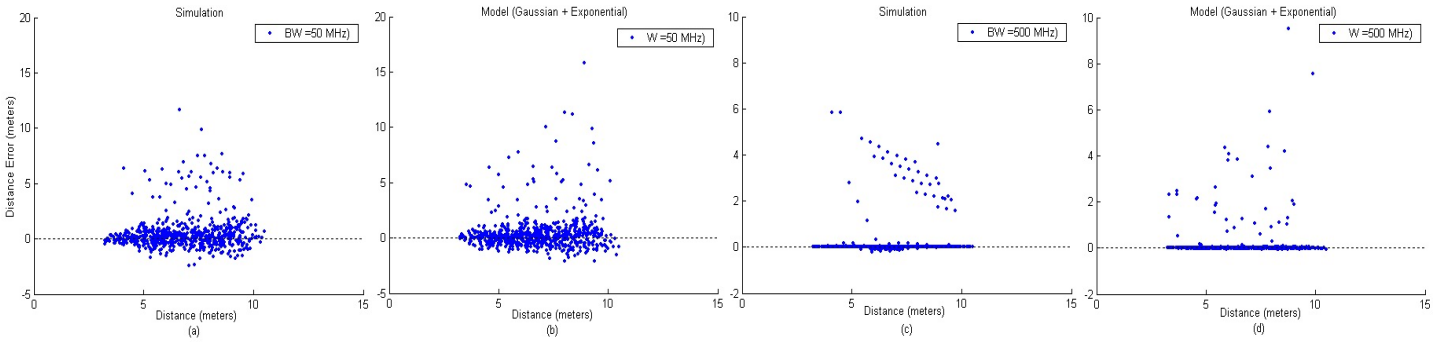

Figure 6. Scatter plots of OLOS normalized distance error for (a) Simulation, w = 50 MHz (b) Model, w = 50 MHz (c) Simulation, w = 500 MHz (d) Model, w = 500 MHz

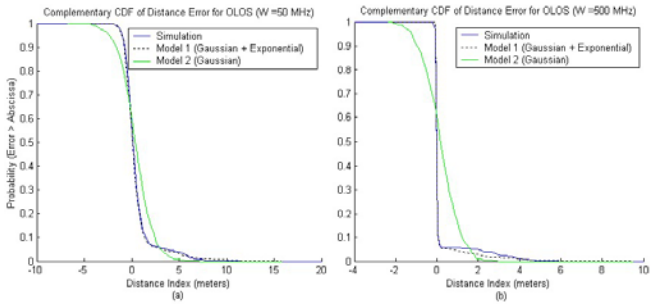

Figure 8. Comparison between complementary CDFs of distance error for OLOS, (a) w = 50 MHz, (b) w = 500 MHz

divided the distance error region into three sections, middle, negative, and positive. The middle section is a very narrow (with a constant width of Δ=0.002) region between the positive and negative regions. Then, we counted half of the middle points as negative and half as positive. Figure 7 shows the distribution and the partitioning technique. To derive the parameters, first from the number of negative and positive points we find the values of W_{Gw} and W_{Expw}, Then we calculate the mean of the negative section assuming that mean of the middle points is -Δ/2, and after calculating σ_{Ow} we calculate the mean of the positive part assuming that mean of the middle points is Δ/2 to derive λ_w.

Figures 6-(b), (d) are the generated distance errors using the normalized distance errors as in (3) from the introduced model; they correspond to Figs. 6-(a), (c) respectively and have the same number of points as their simulation version. It can be seen that the Exponential part in distance errors has not decreased like the Gaussian part. To compare these scatter plots, Figs. 8-(a), (b) show the CDFs of distance error for 50 and 500 MHz bandwidths for the OLOS case. To illustrate that the Gaussian model used for LOS does not fit for the OLOS case we include its CDF curve in the figures as well. For 50 MHz bandwidth ε_{fit} is 11 cm for Gaussian Exponential mixture and 65 cm for Gaussian, while for 500 MHz they are 6 and 63 cm.

Table 2 shows the typical values of model parameters for different bandwidths, and the corresponding average fitting error values. To use the polynomial fitting we need to sketch them versus 1/*w*, as it is shown in Fig. 9. For the OLOS case the considered bandwidth range, which is used for

Table 2. Typical values of model parameters and the fitting error for different bandwidths for OLOS

w (MHz)	σ_{Ow} (cm)	(m^{-1}) λ_w	ε_{fit} (cm)
30	18.86	1.75	32.85
40	13.71	1.92	16.70
50	9.27	1.98	11.13
100	2.67	4.67	8.84
200	0.78	3.50	10.70
500	0.29	2.31	6.37
1000	0.15	2.07	9.02
2000	0.13	2.93	6.64
3000	0.13	2.27	7.25

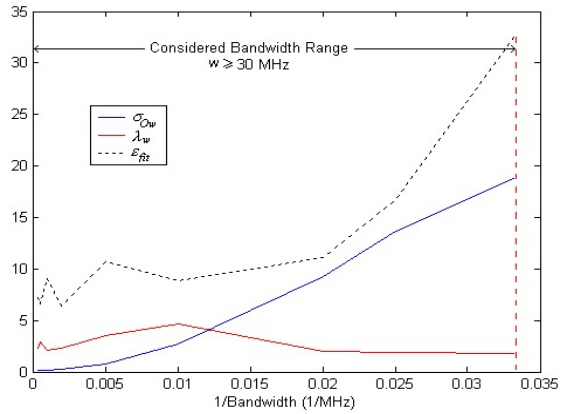

Figure 9. model parameters for OLOS (σ and λ) and the average fitting error (ε) vs. 1/Bandwidth

polynomial fit, is from 30 to 3000 MHz. From the results of second order polynomial fit similar to (7), (9) introduces an equation to find σ_{Ow} in cm, where A_O=9052, B_O=2.6, m_O=0.16, and *w* is in MHz.

$$\sigma_{Ow} = A_O\left(\frac{1}{w} - m_O\right)^2 + B_O \qquad (9)$$

Since the variation of λ versus bandwidth is very small, in order to have a simpler model it is assumed constant and equal to mean of all the values, which is equal to 2.6 m^{-1}.

IV. CONCLUSION

In this letter, we introduced a model for the estimated distance from TOA of the first path in an indoor multipath environment typically used for WPAN applications. Using results of empirically calibrated Ray Tracing software we showed that in a typical indoor environment how the model relates the distance error to the bandwidth of the system, and demonstrated that the results of the model closely fits the empirical data.

REFERENCES

[1] K. Pahlavan, X. Li, and J. P. Makela, "Indoor Geolocation Science and Technology," *IEEE Commun. Mag.*, vol. 40, no. 2, Feb. 2002, pp. 112-118.

[2] X. Li and K. Pahlavan, K., "Super-resolution TOA estimation with diversity for indoor geolocation", accepted for publication in IEEE Trans. on Wireless Communications, to appear.

[3] B. Alavi and K. Pahlavan, "Modeling of The Distance Error for Indoor Geolocation", *IEEE WCNC 2003*

[4] Chen, P. C., "A Non-Line-of-Sight Error Mitigation Algorithm in Location Estimation," *IEEE WCNC*, 1999, pp. 316-320

[5] K. Pahlavan and A. Levesque, *Wireless Information Networks*, John Wiley & Sons, 1995.

[6] Hassan-Ali, M., and Pahlavan, K., "Site-specific wideband indoor channel modeling using ray-tracing software," *IEE Electronics Letters*, vol. 33, no. 23, Nov. 1997, pp 1983-1984.

[7] Pahlavan, K., Krishnamurthy, P., and Beneat, J., "Wideband Radio Channel Modeling for Indoor Geolocation Applications," *IEEE Commun. Mag.*, vol. 36., no. 4, Apr. 1998, pp. 60-65.

Performance of TOA Estimation Algorithms in Different Indoor Multipath Conditions

Nayef Alsindi, Xinrong Li and Kaveh Pahlavan
Center for Wireless Information Network Studies
Electrical and Computer Engineering Department
Worcester Polytechnic Institute
Worcester, MA 01609, USA
{nalsindi, xinrong, kaveh}@wpi.edu

***Abstract*—Using TOA to determine the distance between the transmitter and the receiver is the most popular technique for accurate indoor positioning. Accuracy of measuring the distance using TOA is sensitive to the bandwidth of the system and the multipath condition between the wireless terminal and the access point. The behavior of the distance measurement error using TOA techniques in LOS and OLOS indoor environments are substantially different. In general, as the bandwidth increases the distance measurement error decreases. However, for the so called undetected direct path (UDP) conditions the system exhibits substantially high distance measurement errors that can not be eliminated with the increase in the bandwidth of the system. In this paper we provide an analysis of the behavior of super-resolution and traditional TOA estimation algorithms in LOS, OLOS and UDP conditions in indoor areas. The analysis is based on the frequency domain measurements of the indoor radio channel propagations in several indoor areas with special attention to the UDP conditions.**

Keywords-indoor geolocation; super-resolution algorithms; time of arrival estimation; indoor radio propagation;

I. INTRODUCTION

In recent years, a growing interest in location-finding systems have emerged for various geolocation applications. Two existing location finding systems, namely Global Positioning System (GPS) and wireless enhanced 911 (E-911), have been used to provide relatively accurate positioning for the outdoor environment [1]. These technologies, although accurate, could not provide the same accuracy when applied to indoor positioning. The different physical requirements of the indoor environment necessitate alternative systems to provide accurate positioning. Therefore, the design and development of indoor positioning systems requires in-depth modeling of the indoor wireless channel.

Although many wideband radio models for telecommunication application exist in literature, their relevance to geolocation systems is distant [2]. In telecommunication application, the sought after parameters are the distance-power relationship and the multipath delay spread of the channel [3]. However, in geolocation application, the parameters of interest are the relative power and the time of arrival (TOA) of the direct line of sight (DLOS) path. Therefore, the accuracy of TOA measurement and modeling of the DLOS path is a measure of the performance of indoor geolocation systems. However due to severe multipath conditions and the complexity of the radio propagation, the DLOS path cannot always be accurately detected [2, 4]. Improving the DLOS detection and TOA estimation requires improving the time domain resolution of the channel response in order to resolve the multipath and enhance the accuracy of estimation.

Spectral estimation methods, namely super-resolution algorithms have been recently used by a number of researchers for time domain analysis of different applications. Specifically, they have been employed in frequency domain to estimate multipath time dispersion parameters such as mean excess delay and RMS delay spread [5]. In addition, [6] used super-resolution algorithms to model indoor radio propagation channels with parametric harmonic signal models. Recently, however, super-resolution algorithms have been applied to accurate TOA estimation for indoor geolocation with diversity combining schemes [7]. The multiple signal classification (MUSIC) algorithm was used as a super-resolution technique and it was shown to successfully improve the TOA estimation.

In indoor positioning, the behavior of TOA estimation in different environments is another important factor in determining the performance of geolocation systems. Besides physical classification of line of sight (LOS) versus obstructed line of sight (OLOS), [2] have shown that there exists further classification that depends on the channel profile and the characteristics of the DLOS path. The first category of this classification is dominant direct path (DDP) where the DLOS path is detected and it is the strongest. The second category, nondominant direct path (NDDP) is when the DLOS path is detected but it is not the strongest. The last category is undetected direct path (UDP) where the DLOS is undetected.

In this paper, a comprehensive measurement database has been created for these classifications with emphasis on finding more UDP cases. The performance and behavior of the DLOS distance error, which is directly related to TOA estimation error, is analyzed in all these different scenarios. In addition, the performance of different TOA estimation algorithms, namely, inverse Fourier transform (IFT), Direct Sequence Spread Spectrum (DSSS) and super-resolution Eigenvector (EV) algorithm is compared for different environments and

bandwidths. The further classification of channel profiles and the performance analysis provide a deeper insight into wireless channel modeling for indoor geolocation.

The paper is organized as follows. Section II describes how the indoor channel profiles were classified. Section III describes the theoretical background of the TOA estimation algorithms used in this paper. Section IV describes how the measurement system was implemented to create the database used in the analysis. Section V provides performance evaluation of the different algorithms in different environments and bandwidths. The conclusion is provided in section VI.

II. Indoor Channel Classifications for TOA Estimation

Wideband radio modeling for indoor geolocation application requires examining the channel profiles at different environments. The behavior of the channel profile or specifically the TOA of the first path depends on the physical location of the receiver with regards to the transmitter. Thus it is pertinent to introduce different measurement classifications to better analyze and characterize the behavior of TOA error. The performance of TOA estimation varies substantially in different environments. Two classification categories to be discussed next are based on the channel profile of the measurement data. The channel profiles were obtained by applying the IFT on the frequency domain measurement followed by a Hanning window.

A. LOS and OLOS

One of the major classifications in the study of TOA modeling is based on physical properties of the indoor environment. Accordingly, LOS and OLOS are easily distinguishable by the measurement scenario. When both transmitter and receiver have no physical obstructions between them the measurement is classified as LOS. When an obstruction exists, such as a wall, the profile is classified as OLOS. For the former case, the DLOS path is the strongest and thus the TOA can be measured with great accuracy. In the latter, however, the DLOS path is obstructed by one to several walls depending on the location of the receiver. The accuracy of TOA in this case, suffers due to the unavailability of a strong DLOS path. In fact for some cases, the first path is undetectable causing the major error in the estimation of TOA.

B. DDP, NDDP and UDP

This classification is based on the channel profile and the strength and availability of the DLOS path. Regardless of physical obstructions, the measurement is classified according to the DLOS path. For this classification, a threshold was used in order to distinguish between a DDP, NDDP and a UDP. Since the noise floor of the measurement system is -100 dBm, and the Hanning window has side lobes of -31 dB below the peak of the profile, a threshold is selected according to the larger value of the two. This ensured that the first peak of the channel profile is classified correctly. DDP is the easiest to detect from the profile because it has a distinct strong first path. This category has an advantage where traditional GPS receivers can lock onto the DLOS path and detect its TOA accurately. When the first path gets weaker but still above the threshold, the profile fits in the NDDP category. For this case, a significant loss of accuracy in TOA estimation can be reduced when a more complex RAKE receiver is used in order to resolve the multipath and intelligently detect the TOA of the DLOS path. A profile is a UDP, when the first path is below the threshold indicating loss of the DLOS path. In this unfavorable situation neither the GPS nor the RAKE receiver can accurately detect the TOA and this, specifically, causes the most significant error in indoor positioning applications. Overall UDP is expected to show substantial degradation in TOA estimation for geolocation application when compared with the other scenarios.

III. TOA Estimation Algorithms

Detecting the DLOS path requires obtaining the time-domain channel profile from the frequency domain measurement data. The following TOA estimiation algorithms provide different time domain resolutions that are directly related to accuracy of TOA estimation.

A. IFT

A simple and conventional TOA estimation algorithm, IFT provides a time domain representation of the channel profile from the frequency domain measurement data. When the time domain response over part of the time period is desired, the chirp-z transform (CZT) is preferred, providing flexibility in the choice of time domain parameters with the cost of longer computational time as compared with the IFT. As mentioned earlier, a Hanning window is also used to avoid leakage and false peaks by reducing the sidelobes of the time domain response with the cost of reduced resolution. The peak detection algorithm then selects the closest peak to the actual TOA. In this paper, the term IFT will generally mean application of the CZT unless otherwise stated.

B. DSSS

Another estimation algorithm uses the cross-correlation techniques with DSSS signals. In order to simulate DSSS signal-based cross-correlation technique, the frequency response of a raised-cosine pulse with rolloff factor 0.25 is first applied to the frequency domain response as a combined response of band-limitation pulse-shaping filters of the transmitter and receiver. Then, the resultant frequency response is converted to time domain using the IFT for TOA estimation.

C. Super-resolution (EV/FBCM)

In this paper, a more complex algorithm, EV is used as a super-resolution technique in TOA estimation for indoor geolocation. The algorithm uses a spectral estimation technique to convert the frequency domain measurement data into the time domain profile needed for determining the TOA

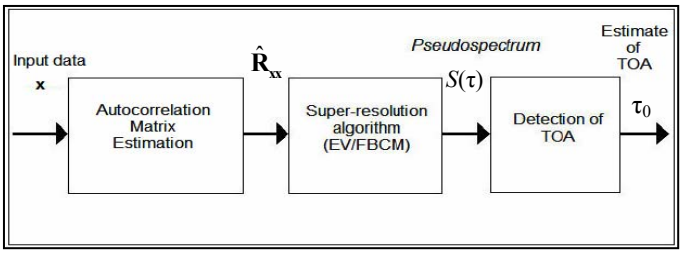

Figure 1. Functional block diagram of the EV/FBCM super-resolution TOA estimation algorithm.

of the DLOS path. The channel frequency domain measurement data are obtained from the measurement database described in section IV. EV super-resolution algorithm is based on eigen-decomposition of the autocorrelation matrix of the input measurement data. The autocorrelation matrix is given by

$$\mathbf{R}_{xx} = E\left\{\mathbf{x}\mathbf{x}^H\right\}, \tag{1}$$

where $\mathbf{x} = \mathbf{H} + \mathbf{w}$ is the measurement data. $\mathbf{H}$ is the measured frequency domain channel impulse response and $\mathbf{w}$ is the additive white measurement noise with zero mean and variance $(\sigma_w)^2$. Superscript H is the Hermitian, conjugate transpose of a matrix. Figure 1 shows a block diagram of the algorithm. The autocorrelation matrix is estimated from the input frequency domain channel measurement data. The L-dimensional space that contains the signal vector $\mathbf{x}$ is split into two orthogonal subspaces, known as signal subspace of dimension L_p and noise subspace of dimension $(L\text{-}L_p)$, by the signal eigenvectors and noise eigenvectors, respectively. The multipath delays τ_k, $0 \le k \le L_p\text{-}1$ can be determined by finding the delay values at which the following pseudospectrum achieves maximum value

$$S_{EV}(\tau) = \frac{1}{\sum_{k=L_p}^{L-1} \frac{1}{\lambda_k} \left|\mathbf{q}_k^H \mathbf{v}(\tau)\right|^2}, \tag{2}$$

where $\mathbf{v}(\tau_k) = [1 \quad e^{-j2\pi\Delta f \tau k} \quad \ldots \quad e^{-j2\pi(L-1)\Delta f \tau k}]^T$, λ_k, $L_p \le k \le L-1$ are the noise eigenvalues and $\mathbf{q}_k$ are the noise eigenvectors. Therefore, maximizing the pseudospectrum in (2) will occur for the delay values corresponding to the noise eigenvalues and eigenvectors which minimize the denominator. In EV algorithm the pseudospectrum of each eigenvector is normalized by its corresponding eigenvalue λ_k. Once the multipath delays in the pseudospectrum are obtained then a peak detection algorithm calculates the TOA of the DLOS path as shown in Fig. 1. In practical implementation the estimate of the correlation matrix is further improved using the *forward-backward correlation matrix* (FBCM). More detailed description of the EV/FBCM algorithm can be found in [7].

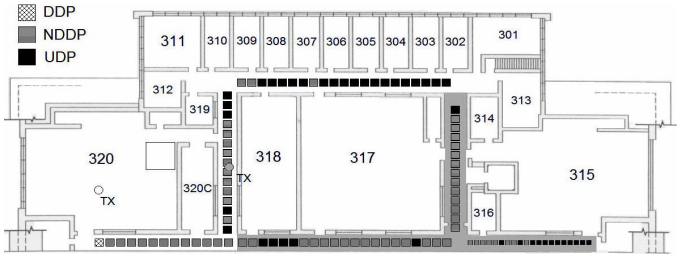

Figure 2. Measurement campaign on the 3rd floor of Atwater Kent building.

IV. Measurement of Different Channel Profile Classes

Analyzing the performance of indoor geolocation systems in different environments requires an experimental basis on which to draw useful conclusions. Measuring different channel profile classes was conducted using the frequency domain measurement system. The creation of a database from these measurements helped in establishing necessary foundations for analysis. In this section, the measurement system and the procedure for creating the database are described.

A. Measurement System

One way to experimentally calculate the TOA is through the use of frequency domain measurement system which is described in [8]. The main component of this system is a network analyzer that sweeps the channel from 900-1100 MHz. After passing through a 30 dBm amplifier, the output is connected to the transmitter antenna by a cable. The receiver is connected to an attenuator and then to the receiver port of the network analyzer. Both antennas are 1 GHz monopole quarter wave adjusted on square plates. The frequency domain measurements were conducted by fixing the transmit antenna and moving the receiver around the desired locations. The analyzer has a sensitivity of -100 dBm.

B. Measurement Database

A measurement database was created by combining previous measurements produced by the Center for Wireless Information Network Studies (CWINS) lab and recent measurements conducted on the third floor of Atwater Kent (AK) building, the electrical engineering department at Worcester Polytechnic Institute (WPI). The previous measurements include the LOS measurements taken on the second and third floor of AK building reported in [9], and mainly OLOS measurements reported in [10]. After classifying these measurements it was apparent that they lacked sufficient UDP cases for statistical analysis. Therefore, the recent measurements were conducted on the third floor of AK building with special attention to generation of more UDP cases. In order to analyze the behavior of the DLOS path in such unfavorable conditions it was necessary to create a database tailored towards this kind of classification.

Extensive measurement campaign was carried out on the 3rd floor of AK building to seek out UDP conditions and understand how and where they are created. The search for UDP required thorough analysis of transmitter-receiver locations within the building in order to vary the attenuation effect on the DLOS path and examine its effect on the channel profile. Figure 2 shows the 3rd floor plan of AK and the respective measurement points. The most effective locations for the receiver in this case were in the corridors, thus increasing the number of obstacles in the DLOS path. The first set of measurements was conducted with the transmitter in room 320 and the receiver moved along the un-shaded region of the corridors comprising 64 measurement points as shown in Fig. 2. The second set of measurements was conducted with the transmitter placed in the corridor to the right of AK 320 and the receiver was moved along the shaded region of the corridors comprising 41 points. The receiver measurement points are 1 meter apart but for those located in the corridor below room 315 they are 50 cm apart. After classification of the data, the 105 measurements comprised of 1 DDP, 62 NDDP and 42 UDP.

From Fig. 2 it is apparent that there are a substantial number of UDP scenarios sparking a concern about the performance of indoor positioning in those regions. The UDP points are clearly labeled with black squares. When these points exist between NDDP points it is mainly because of shadow fading caused by obstacles, in addition to walls, that suddenly attenuate the DLOS path significantly. When the UDP points exist subsequently one after the other then the walls are the main contribution to the loss of the DLOS path. It is interesting to note how UDP scenarios are not localized only to a certain region or corner of the floor plan, but rather they exist in "spots" strengthening the notion that the DLOS path can be lost in locations where system designers might have not predicted because of additional obstacles apart from the walls. The measurement database is used in analyzing the performance of different estimation algorithms in those different multipath conditions. Including the earlier measurements, a total of 256 measurements of which 71, 185, 88, 110 and 58 are LOS, OLOS, DDP, NDDP and UDP respectively.

V. Behavior of Algorithms in Different Environments

In this section, the accuracy of TOA estimation is examined for traditional and super-resolution algorithms in different indoor environments.

A. Performance in LOS versus OLOS

Comparing the two different environments, the performance of an indoor geolocation system varies substantially. The absence of any significant obstructions in the DLOS path provides LOS scenarios with an advantage in terms of mean of ranging error. The significant difference between them is apparent. The obstruction of the first path in OLOS causes substantial error when compared to LOS case.

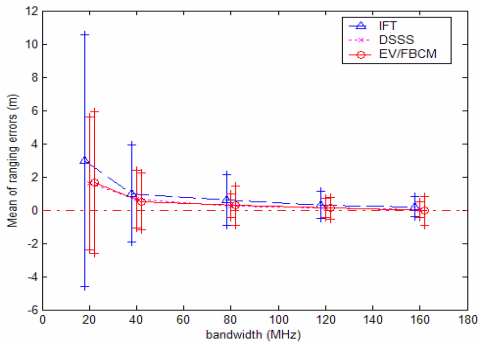

Figure 3. Mean and STD of ranging errors for LOS using different TOA estimation algorithms. The vertical lines corresponds to plus and minus one STD about the mean.

For instance, at 20 MHz OLOS suffers a mean error of 10.7 m while LOS has an error of 2.9 m. As the bandwidth increases, LOS error approaches zero and in the case of 160 MHz it is 0.2 m while OLOS still exhibits a significant 4.1 m error.

The performance of the three TOA estimation algorithms IFT, DSSS and EV/FBCM, is compared for two different scenarios and several bandwidths. In LOS environment, the performance of the algorithms in terms of mean of ranging error is very close to each other. Figure 3 illustrates mean and standard deviation values for the three algorithms in different bandwidths. At lower bandwidths, EV/FBCM performs slightly better than IFT but almost the same as DSSS. At higher bandwidths, the distance error approaches zero and there is no significant advantage for either algorithms. In OLOS scenario, the first path suffers attenuation from walls and other obstructions. As a result the DLOS path is rarely the strongest and that introduces problems for detection. This is shown in Fig. 4 where the distance error for all the algorithms is worst than the LOS case. The EV/FBCM algorithm significantly improves the TOA estimation and, in addition, it outperforms the other conventional algorithms as evident from the figure. As a result, in obstructed conditions more complex TOA estimation algorithms provide means to reducing the error to an acceptable level. On the other hand, use of those algorithms does not provide significant improvement to the TOA estimation in LOS environment.

In general LOS cases are composed mainly of DDP

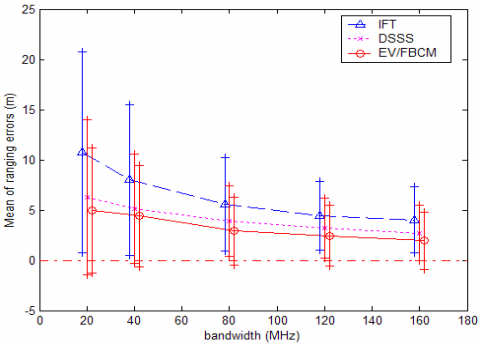

Figure 4. Mean and STD of ranging errors for OLOS using different TOA estimation algorithms.

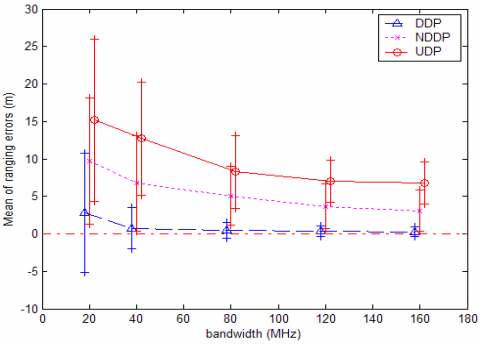

Figure 5. Mean and STD of ranging errors for DDP, NDDP and UDP using IFT algorithm.

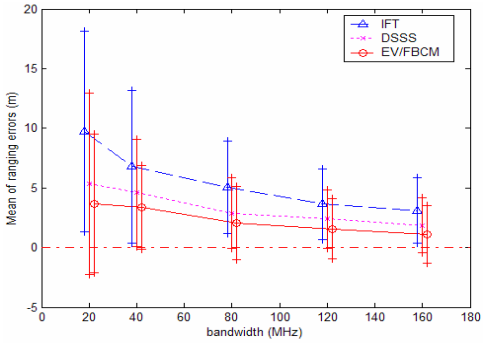

Figure 7. Mean and STD of ranging errors for NDDP using different TOA estimation algorithms.

scenarios. OLOS is composed mainly of NDDP and UDP scenarios.

B. Performance in DDP, NDDP and UDP

With the loss of DLOS path, UDP causes major problems for accurate TOA estimation. As a result, the mean and STD of the distance error are expected to be significant when compared to other cases such as DDP or NDDP. Figure 5 shows the mean and STD of the ranging error for UDP compared to DDP and NDDP using IFT algorithm. It is clear that the mean of ranging error for UDP is substantially larger than the two other cases. In fact at 20 MHz, UDP has a mean error that is 5 times that of DDP and 1.5 times that of NDDP. As the bandwidth increases UDP continues to exhibit significant error values. For example at 160 MHz the mean of distance error for UDP is almost 7 meters while DDP is a mere 0.29 meters. It is important to note that the accuracy of TOA estimation is substantially degraded when a receiver moves from a DDP position to an NDDP or UDP. As will be discussed later, better TOA estimation algorithms reduce average distance error but have limitations for UDP. The loss of the DLOS path creates a situation where a large distance error is unavoidable even with an increase in the bandwidth of the system.

With the second main classification, similarly, the effectiveness of the algorithms is different in each condition. Figure 6 shows a measurement sample of a DDP channel profile at 40 MHz illustrating the performance of the three algorithms. The vertical dash-dot line is the expected TOA. Notice that the DLOS is detected successfully for the three algorithms. EV/FBCM views the time domain channel profile with a higher resolution and thus it provides better accuracy in detection.

In NDDP Fig. 7 shows that EV/FBCM algorithm performs significantly better than the other two algorithms. The main reason is that it has the ability to view the channel profile with higher resolution. In this category the first path usually combines with the subsequent paths and forms a cluster. The conventional algorithms detect the peak of the cluster as the DLOS path and hence the TOA. This erroneous detection causes serious problems for TOA estimation. The higher resolution of the EV/FBCM algorithm "splits" the cluster and provides other paths not detected conventionally. In some cases, the algorithm detects the DLOS path; in other the second or even the third is detected. Regardless of the path detected, Fig. 7 shows that on average EV/FBCM exhibits lower mean of ranging error when compared to the other algorithms.

The performance of EV/FBCM in this scenario can be justified by examining Fig. 8, which shows a typical NDDP profile. The vertical dash-dot line is the expected TOA and it is clear how both the IFT and the DSSS are unable to detect the correct path. However EV/FBCM resolves the cluster and reduces the TOA error by detecting a closer path and in this case it actually detects the first path. Overall it is true to say

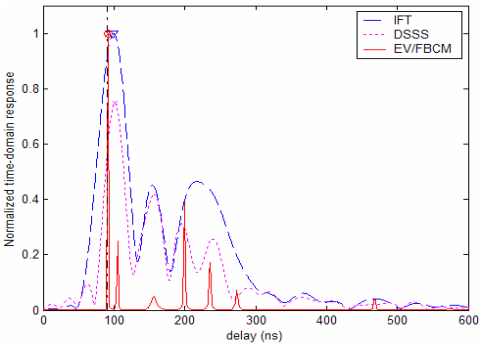

Figure 6. Measured DDP profile obtained with the three estimation algorithms at 40 MHz.

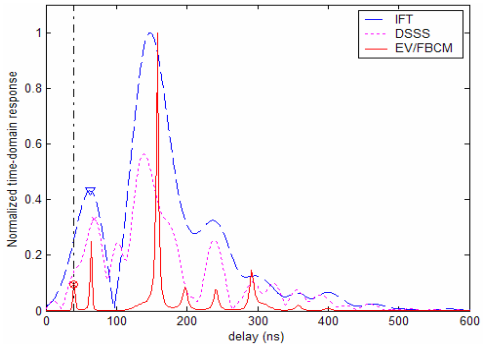

Figure 8. Measured NDDP profile obtained with the three estimation algorithms at 40 MHz.

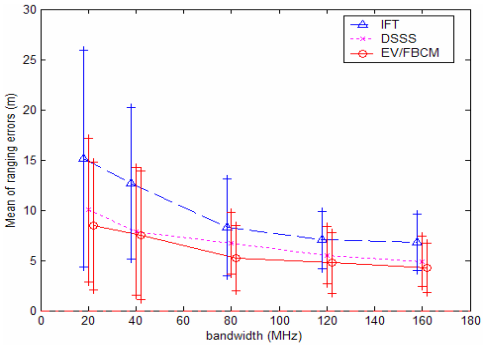

Figure 9. Mean and STD of ranging errors for UDP using different TOA estimation algorithms.

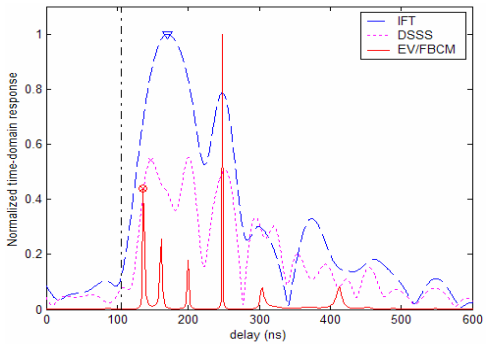

Figure 10. Measured UDP profile obtained with the three estimation algorithms at 40 MHz.

that in NDDP conditions EV/FBCM provides the best performance in terms of mean of ranging errors.

In UDP scenarios, EV/FBCM provides an advantage compared to the other algorithms. Although the DLOS path does not exist, nevertheless, EV/FBCM is expected to perform better than the other algorithms. Figure 9 shows the mean and STD of ranging error for UDP conditions. On average, the EV/FBCM outperforms the other algorithms and exhibits lower error even at higher bandwidths. By examining a measurement sample of a UDP profile, it is possible to see how the three algorithms compare. Figure 10 shows a measured UDP case with the absence of the first path. It is clear that EV/FBCM detects a closer path and improves the TOA estimation when compared to IFT and DSSS. The weakness of the DLOS path makes it difficult to resolve the multipath and detect it. As a result, the UDP condition introduces unavoidable errors and regardless of the bandwidth or the estimation algorithm used, the positioning system will exhibit substantially large errors. This degraded performance requires that in the deployment of an indoor geolocation system care must be taken to avoid coverage areas with UDP conditions. This will further reduce the error and enhance the accuracy of TOA detection and estimation.

VI. CONCLUSION

In this paper the behavior of TOA estimation algorithms and the effect of different multipath conditions have been analyzed. A measurement campaign targeted at gathering UDP indoor channel profiles helped in establishing a comprehensive database for statistical analysis in different multipath conditions. OLOS scenarios exhibit substantial TOA estimation errors compared to LOS. The algorithms are more effective and indeed necessary in OLOS. In DDP the EV/FBCM did not provide any advantage in the TOA estimation when compared to IFT and DSSS. NDDP scenarios introduce a larger margin of error when compared to DDP and can create significant inaccuracies in TOA estimation. It is possible to see that in this case resolving the multipath and detecting the DLOS path is achievable with EV/FBCM as it offers the best performance in this category. UDP showed the worst algorithm performance due to loss of the first path. Increasing the bandwidth of the system can improve the accuracy of TOA estimation. However with the unfavorable UDP condition this has limitations. More importantly, the substantial errors introduced by UDP conditions are unavoidable even with increasing the bandwidth of the system and using complex TOA estimation algorithms.

ACKNOWLEDGMENT

The authors would like to thank Bardia Alavi for his helpful suggestions and insights in the review of the paper. Also, appreciation is expressed to Mohammad Heidari for his help with the measurement campaign.

REFERENCE

[1] M. J. Meyer *et al*., "Wireless Enhanced 9-1-1 Service – Making It a Reality," *Bell Labs Tech. J.,* pp. 188-202, Autumn 1996.

[2] K. Pahlavan, P. Krishnamurthy, and J. Beneat, "Wideband Radio Propagation Modeling for Indoor Geolocation Applications," *IEEE Commun. Mag.*, vol.36, no. 4, Apr. 1998, pp. 60-65.

[3] K. Pahlavan and A. Levesque, *Wireless Information Networks*, New York: Wiley, 1995.

[4] K. Pahlavan, X. Li, and J. Makela, "Indoor geolocation sceince and technology," *IEEE Comm. Mag.*, pp. 112-118, Feb. 2002.

[5] [T. Lo, J. Litva, and H. Leung, "A new approach for estimating indoor radio propagation characteristics," *IEEE Trans. AP*, vol. 42, no. 10, Oct. 1994.

[6] G. Morrison and M. Fattouche, "Super-resolution modeling of the indoor radio propagation channel," *IEEE Trans. VT*, vol. 47, no. 2, pp. 649-657, May 1998.

[7] X. Li and K. Pahlavan, "Super-resolution TOA Estimation with diversity for indoor geolocation," *IEEE Trans. Wireless Comm.,* accepted for publication.

[8] S. J. Howard and K. Pahlavan, "Measurement and Analysis of the indoor Radio Channel in the Frequency Domain," *IEEE Trans. INSTR. Meas.,* no. 39, 1990, pp. 751-55.

[9] E. Zand, "Measurement of TOA Using Frequency Domain Techniques for Indoor Geolocation," M.S. thesis, Worcester Polytechnic Inst., 2003.

[10] J. Beneat, K. Pahlavan, and P. Krishnamurthy, "Radio channel characterization for geolocation at 1 GHz, 500 MHz, 90 MHz and 60 MHz in SUO/SAS," *Proc. IEEE MILCOM'99,* pp. 1060-1063, 1999.

[11] K. Pahlavan and P. Krishnamurthy, *Principles of Wireless Networks – A Unified Approach,* Prentice Hall, 2002.

[12] D. Manolakis, V. Ingle, and S. Kogon, *Statistical and Adaptive Signal Processing*, McGraw-Hill Co., Inc., 2000.

Radio Channel Characterization for Geolocation at 1 GHz, 500 MHz, 90 MHz and 60 MHz in SUO/SAS

Jacques Beneat, Kaveh Pahlavan, and Prashant Krishnamurthy
Center for Wireless Information Network Studies, WPI
100 Institute Road
Worcester, MA 01609, U.S.A.
{beneat, kaveh, prashant}@cwins.wpi.edu
http://www.cwins.wpi.edu

Abstract - In this paper, the results of measurements to characterize the radio channel for geolocation applications are presented. Measurements were made at 1 GHz, 500 MHz, 90 MHz and 60 MHz, in three different environments – commercial, office and residential areas - representative of SUO/SAS scenarios. The characterization of the radio channel is provided through the Cumulative Distribution Function (CDF) of the relative received power and the errors in estimated distances based on the first and strongest paths extracted from the channel impulse responses (CIR). These results are used to evaluate the corresponding performance of a RAKE type receiver that can extract the first path and a traditional type receiver that locks onto the strongest signal.

I. INTRODUCTION

With the success of wireless information systems the possibilities of the radio spectrum for applications which are not primarily for telecommunications are being evaluated. Terrestrial based radio geolocation systems are gaining interest in civilian applications such as intelligent transportation systems, public safety (enhanced 911 services) [1], [2], [3], and in military applications such as those envisioned in the Small Unit Operation Situation Awareness Systems (SUO/SAS) [4], where the location of the warfighters must be known to improve tactical deployment and safety of the soldiers. These new applications involve defining the location in urban and indoor areas where traditional geolocation solutions such as the Global Positioning System (GPS) [5] are unsuitable due to the harsh multipath radio channel conditions.

The wideband measurements and modeling of the radio channel which are available for telecommunication applications [6] are not adequate to evaluate the performance of geolocation systems since their main objective was to determine the relationship between distance and total received power to provide coverage predictions, and to estimate the multipath delay spread of the channel to evaluate the data rate limitations of the receiver. New measurements of the radio channel are needed to determine crucial geolocation parameters such as the relative power and time of arrival (TOA) in the signal arriving from the Direct Line of Sight (DLOS) path and in the signal arriving from the other paths [7], [8]. With this new characterization, the ranging accuracy of current systems can be evaluated and improved designs can be developed.

In this paper, the results of measurements to characterize the radio channel for geolocation applications are presented. The measurements were conducted in three different environments - commercial, office and residential areas - representative of SUO/SAS scenarios. They were made at four different center frequencies using the same locations to estimate the benefits of using one frequency instead of another. A total of 1440 radio channel impulse responses were processed to extract the relative power and TOA of the first detected and strongest paths to characterize the radio channel. The results of this characterization are given in the form of two CDFs: The CDF of the relative received powers in the two paths, and the CDF of the error in estimating the distances using these paths. To illustrate the effect of center frequency, the curves are given for all four frequencies.

The results of characterization are also used to evaluate the performance of a RAKE type receiver with same dynamic range, sensitivity, and bandwidth as the measurement system which would detect the first path and of a traditional type receiver that would lock onto the strongest signal.

II. MEASUREMENT DESCRIPTION

Magnitude and phase measurements of the radio channel were made at four different center frequencies of 1 GHz, 500 MHz, 90 MHz and 60 MHz with bandwidths of 200 MHz, 200 MHz, 100 MHz and 50 MHz respectively, based on the network analyzer system described in [9], [10]. For 1 GHz and 500 MHz center frequencies, quarter wave monopole antennas with rectangular ground plane were used, while for center frequencies of 90 MHz and 60 MHz, a broadband biconical antenna specified for 20 MHz to 300 MHz operation was used.

The measurements were made at three different sites representative of SUO/SAS scenarios. Norton company is a manufacturer of welding equipment and abrasives for grinding machines and the building can be described as a huge open manufacturing floor with heavy metallic machinery and steel sheet external walls with small metallic windows close to the ceiling. Fuller Laboratories is a modern office building with external walls made of brick with some aluminum siding on two sides, metallic window frames and doors. Inside the building there are several laboratory rooms, various offices, lecture halls, and classrooms with internal walls made of sheetrock. Schussler house is a fairly big residential house with wooden exterior walls and sheetrock interior walls. The house is however very old and some portions of the external walls are made of stone. Inside, there are several furnished rooms on the order of a few meters.

0-7803-5538-5/99/$10.00 © 1999 IEEE

For each site, four consecutive snapshots of the radio channel were taken at one given location. The locations were distributed to include indoor-to-indoor, outdoor-to-indoor, and outdoor-to-second floor radio propagation conditions. The same locations were used for all center frequencies and were reported on the corresponding floorplans of the sites so that the physical distances between the transmitting and receiving antennas could be estimated.

The frequency domain measurement data was corrected to remove the effects of system and antennas gains and delays. For each location and each center frequency, four channel impulse responses were produced corresponding to the four snapshots by performing an inverse Fourier transform on the frequency response windowed by a Hanning window. To evaluate the characteristics of the radio channel, the multipath profile of each CIR was constructed using a peak detection algorithm that would associate a tap (magnitude and delay) to each of the peaks in the CIRs. To avoid associating a tap with noise or other unreliable data, only taps above a given threshold were considered.

III. MEASUREMENT RESULTS

For geolocation applications the Direct Line Of Sight (DLOS) path is the most important parameter since its TOA is directly proportional to the physical distance between transmitting and receiving antennas. However, since the measurement system is not ideal – it has finite bandwidth, finite dynamic range, and introduces noise – the DLOS path can never be extracted perfectly from a measurement. The most reasonable approximation is the first detected path in the profile above a given noise floor. The other paths are also important since they can affect the TOA and amplitude of the first path. The most significant of these paths is the strongest path that is commonly detected in receivers locking onto the strongest signal. Therefore, we propose to characterize the radio channel by focusing on the amplitude and TOA/distance of the first and strongest paths as shown in Figure 1.

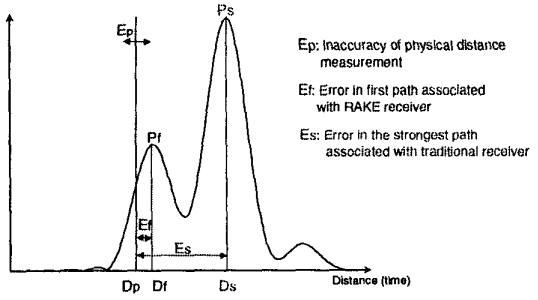

Figure 1: Important geolocation parameters

The expected TOA/distance of the measured physical distance between transmitter and receiver is the reference parameter for evaluating the performance of the geolocation systems. One should note that the measured physical distance is not immune to errors.

In the remainder of this paper, the characteristics of the first and strongest paths will be presented and their effect on the performance of a RAKE and traditional type receivers discussed.

The first characteristic to be given is the CDF of the received power in the first and strongest path at the four center frequencies as shown in Figure 2. At 1 GHz, the received power in the first path is approximately between –115 dB and –50 dB, at 500 MHz between –110 dB and –40 dB, at 90 MHz between –90 dB and –20 dB, and at 60 MHz between –85 dB and –10 dB. There is approximately a 20 dB increase in signal strength per decade of reduction in center frequency and the lowest center frequency provides the highest received power levels. For strong received powers (shorter distances between TX and RX) the first path is also the strongest path and for weaker received powers (larger distances between TX and RX) the probability of having a path stronger than the first path increases. From the curves, the separation between the received power in the strongest path and the first path can exceed 10 dB and as a result, the dynamic range of a RAKE type receiver will become an issue.

In order to quantify the errors in estimating the distances Figure 3 provides the CDF of the error between the physical distance Dp and the distance Df based on the first path and the distance Ds based on the strongest path at the four center frequencies. For RAKE type receivers detecting the first path the probability of making an error less than 10 feet is 91.1% at 1 GHz, 85.6% at 500 MHz, 60% at 90 MHz, and 43.3 % at 60MHz. For traditional receivers locking onto the strongest signal the probabilities become 44.4% at 1 GHz, 41.1% at 500 MHz, 45.6 % at 90 MHz, and 22.2 % at 60 MHz.

Therefore, the traditional type receiver would be quite unsuitable to estimate the distances to 10 feet accuracy in urban and indoor areas. On the other side, the RAKE receiver is a reasonable choice. When using the higher center frequencies where wider bandwidths are available the lowest errors between the physical and estimated distances are obtained. On the other hand at higher frequencies, the relative received powers are smaller and limit the range of the RAKE receiver.

The main problems limiting the ranging accuracy of the RAKE type receiver are illustrated in Figure 4. It shows two main situations where the detected first path is not the DLOS path. In the first situation, the path joining the transmitting and receiving antennas must cross many obstacles such as walls and metallic objects, and the resulting DLOS path is so attenuated that it falls below the measurement system noise floor and can not be detected. In this situation, the detected first path will correspond to the shortest indirect path where several bounces have occurred before reaching the receiver.

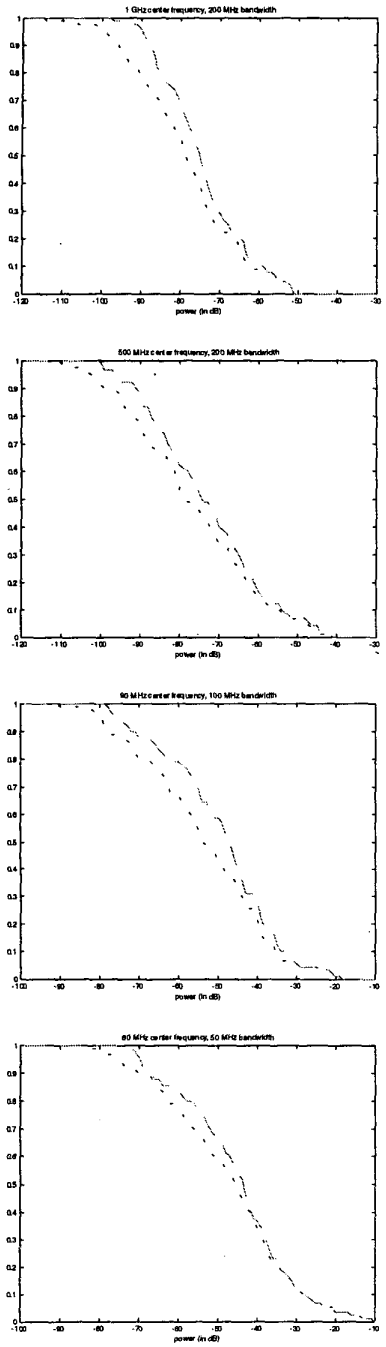

Figure 2: Probability that the relative received power is greater than the abscissa: relative received power in the first path (dash blue) and in the strongest path (dash-dot green).

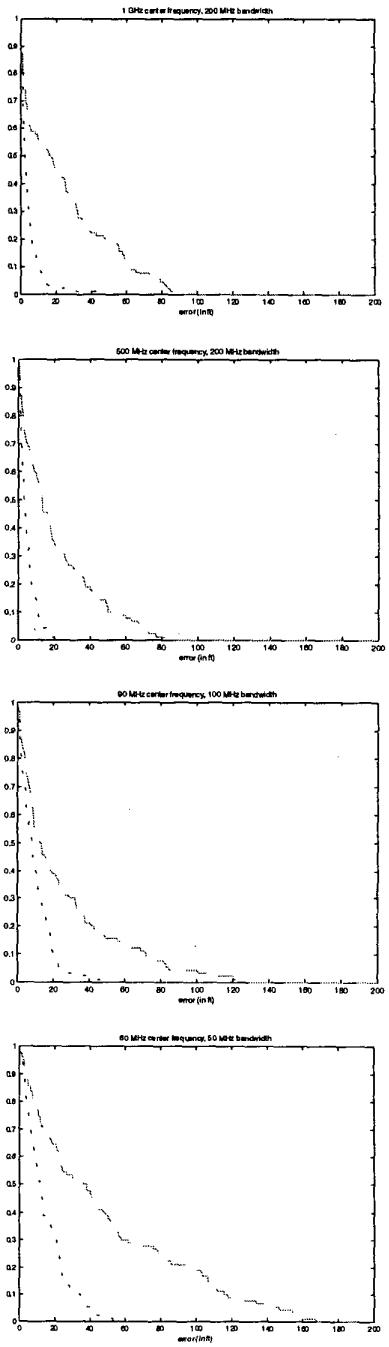

Figure 3: Probability that the error between the physical distance and estimated distance is greater than the abscissa: The estimated distance is based on the first path (dash blue), and the distance is based on the strongest path (dash-dot green)

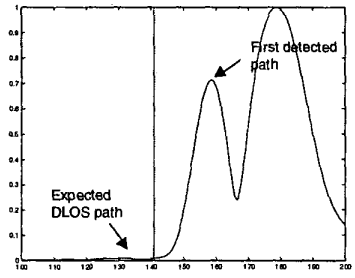

Non-detectable DLOS path

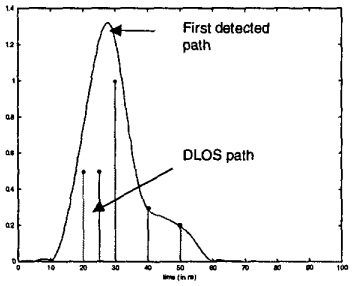

Non-distinguishable DLOS path

Figure 4: Illustration of the situations where the first path is not the DLOS path: Non-Detectable DLOS path and Non-Distinguishable DLOS path.

This case can produce large errors since the TOA of this first detected multipath has no apparent relation to the DLOS path. In the second situation, the limited bandwidth of the system makes it impossible to distinguish the DLOS path from the first few other paths arriving at the receiver. In this case the detected TOA of the first path will correspond to a combination of the TOAs of the DLOS path and the first other paths. The errors in this case should be reasonable since the TOA detected is strongly dependent on the DLOS path.

IV. CONCLUSION

In this paper, the results of measurements to characterize the radio channel for geolocation applications were given. The measurements were taken in commercial, office and residential areas at 1 GHz, 500 MHz, 90 MHz, and 60 MHz, with bandwidths of 200 MHz, 200 MHz, 100 MHz, and 50 MHz, respectively. The important parameters in the channel impulse responses for geolocation applications were shown to be the amplitude and TOA of the first and strongest paths.

The results of characterization were provided though two CDF and were used to evaluate the performance of a RAKE and a traditional type receivers. From the CDF of the relative received power in the two paths it was seen that the received power in the first path would be smaller or at most equal to the power in strongest path. Therefore, the RAKE type receiver will require larger dynamic range in order to track the direct path. It was also seen that at lower frequencies, the received power is higher.

The CDF of the error in estimating the physical distance gave some measure of the errors committed by the RAKE type receiver and the traditional type receiver that locks onto the strongest path. Clearly, the traditional type receiver is not suited to provide distance estimations within 10 feet accuracy in urban and indoor areas. In contrast, the RAKE receiver can satisfy this requirement over 90 % of the time at the center frequency of 1 GHz. The errors in estimating the distances committed by the RAKE receiver are mainly due to the non-detectable DLOS path situations where the direct path falls below the receiver noise floor, and to the non-distinguishable DLOS path situations where the limited bandwidth of the receiver results in large time pulse widths making accurate detection of the direct path difficult.

ACKNOWLEDGEMENT

The authors would like to express their appreciation to Mirela Marku for her help in conducting the measurements at the different sites, to DARPA's SUO-SAS program and Dr. Mark McHenry for partial support of this work. We also thank Paul Creamer and Joseph Pisano of TASC for fruitful discussions and a variety of help.

REFERENCES

[1] M. J. Meyer et al., "Wireless Enhanced 9-1-1 Service - Making It a Reality", *Bell Labs Technical Journal*, pp. 188-202, Autumn 1996.

[2] MicroTRAX Tacking and Location System: http://www.gcsd.harris.com/programs/microtrax/

[3] TruePosition Cellular Location System: http://www.trueposition.com/

[4] DARPA Tactical Technology Office: Situation Awareness System Solicitation Documents: http://web-ext2.darpa.mil/tto/sas-docs.html

[5] E.D. Kaplan, ed., *Understanding GPS: Principles and applications*, Artech House, Boston, 1996.

[6] K.Pahlavan and A. Levesque, *Wireless Information Networks*, John Wiley and Sons, 1995.

[7] K. Pahlavan, P. Krishnamurthy and J. Beneat, "Wideband Radio Propagation Modeling for Indoor Geolocation Applications", IEEE Communications Magazine, April 1998.

[8] P. Krishnamurthy, K. Pahlavan, and J. Beneat, "Radio Propagation Modeling for Indoor Geolocation Applications", Proc. of PIMRC'98, Boston, MA, Sept. 1998, pp. 446-50.

[9] S.J. Howard and K. Pahlavan, "Measurement and Analysis of the Indoor Radio Channel in the Frequency Domain", IEEE Trans. Instr. Meas., no 39, 1990, pp. 751-55.

[10] J. Beneat, P. Krishnamurthy, M. Marku, and K. Pahlavan, "Short Range Geolocation and Telecommunication Channel Measurement and Modeling at 1GHz, 500MHz, 90MHz, and 60MHz", DARPA SUO SAS report, January 1999.

Analysis of the Probability of Detecting the DLOS Path for Geolocation Applications in Indoor Areas

Prashant Krishnamurthy and Kaveh Pahlavan
Center for Wireless Information Network Studies
Department of ECE, Worcester Polytechnic Institute
100 Institute Road, Worcester MA 01609
e-mail: {prashant,kaveh}@wpi.edu

Abstract

Emerging geolocation applications require the accurate detection of the direct line-of sight (DLOS) path in order to correctly estimate the range between a transmitter and a receiver. A mathematical analysis of the probability of detecting the DLOS path with a given indoor radio channel model is provided and verified with simulations. Analytical results for the JTC indoor office channel model C are compared with the results of ray tracing in Atwater Kent Labs at WPI.

1. Introduction

Over the last few years, indoor wireless communications has gained popularity in the form of personal communication services (PCS) for voice and wireless local area networks (WLANS) for data communications [1] resulting in several activities to characterize the indoor radio channel for both narrowband and wideband communications applications [2]. In order to characterize the indoor radio channel for communications, the path loss suffered by the signal in traversing the distance between transmitter and receiver and the root mean square (RMS) multipath delay spread (τ_{rms}) are important [2]. The path loss provides an idea of the signal coverage and τ_{rms} provides an estimate of the maximum possible data rate that can be supported over the channel.

Position location applications are emerging in the market that need a different characterization of the indoor radio channel [3]. The DLOS path corresponds to the straight line connecting the transmitter and the receiver even if there are obstructions like walls in between. The relative power and the delay of the signal arriving via other paths, the channel noise and interference influence the detection of the DLOS path and also the error in estimating the distance (range) between the transmitter and the receiver. A preliminary framework, channel measurements and simulations, and statistics relevant to geolocation applications were considered recently [3,4]. In this paper, we provide a mathematical statement of the problem and analysis of the detection of the DLOS path in indoor areas for channel models that are often used in the literature for telecommunications applications. These models by themselves are insufficient for completely characterizing the radio channel for geolocation applications. However, the analysis in this paper with some additions may be employed to develop models that contain information relevant to both geolocation and communications applications. In Section 2, we describe the geolocation problem and define the relevant parameters that are involved. Section 3 provides the statement of the problem and the analytical solution. Section 4 describes some channel models that are employed indoors for PCS applications and provides the results of the analysis for these models and verifies the results with simulation. A comparison of these results with the results of ray tracing is also provided to emphasize the drawbacks in these models as far as the geolocation problem is considered. Section 5 concludes the paper with future directions and efforts.

2. The Geolocation Problem

Let a sample channel impulse response be given by:

$$h(t) = \sum_{l=0}^{L-1} \alpha_l \delta(t - \tau_l) \exp(j\varphi_l) \qquad (1)$$

where the amplitude, delay and phase associated with the l-th path in the L path channel are given by α_l, τ_l and φ_l respectively. Here we assume that $\tau_i < \tau_{i+1}$ for $i = 0, 1, 2, \ldots L$ and that $\tau_0 = d_{tx\text{-}rx}/c$ always where $d_{tx\text{-}rx}$

0-7803-5565-2/99/$10.00 © 1999 IEEE

refers to the distance between transmitter and receiver in meters and $c = 3\times10^8$ ms^{-1} is the speed of light. This means that the DLOS path always exists (but may or may not be detectable). The amplitude associated with this path is α_0. The TOA of the DLOS path corresponds to τ_0 and an error in estimating it results in a corresponding error in $d_{tx\text{-}rx}$.

We introduce two parameters for obtaining the relevant statistics. We refer to the minimum signal strength in a given path that the receiver can detect as the *receiver sensitivity* Ξ. Thus the signal power in the DLOS path must be larger than Ξ for it to be detected correctly. This simplified criterion implicitly assumes that a particular signal level will be sufficient for correct detection without explicitly investigating the effects of channel noise which will be random. This is because the emphasis here is on modeling of the radio channel rather than receiver design or performance. The effect of phase is also ignored here as it manifests only in receiver performance. In order for the receiver to identify the DLOS path, the signal power in the strongest path *must not be larger* than the signal strength in the DLOS path by more than the receiver dynamic range $\Re$. We define the quantity

$$\Re_0 = \left\{ \frac{\max(\alpha_i^2)_{i=0}^{L-1}}{\alpha_0^2} \right\} \qquad (2)$$

which is the ratio of the ratio of the signal strength in the strongest path to the signal strength in the DLOS path, as another performance measure. It should be observed here that $\Re_0$ can never be negative. We can thus provide the two conditions for correct detection of the DLOS path as:

$$P_{dlos} \geq \Xi \quad \text{and} \quad \Re_0 \leq \Re \qquad (3)$$

where $P_{dlos} = 20\log_{10}(\alpha_0)$ is the signal power in the DLOS path and $\Re_0$ is defined above. If the signal arriving via the DLOS path does not satisfy (3) we assume that the signal arriving via the next earliest path that does satisfy (3) will be detected. If this path is the m-th path, $1 \leq m \leq L-1$, the receiver erroneously estimates the TOA as τ_m. The error in predicted distance will be $\varepsilon_d = (\tau_m - \tau_0)\times c$. The analysis that follows deals only with amplitudes and in terms of amplitude, we let $S^2 = \Xi$, $\rho^2 = \Re$, and $\rho_0^2 = \Re_0$, while retaining the same names as sensitivity and dynamic range for S and ρ respectively.

3. Problem Statement and Solution

The indoor radio channel model (without the phase term) is given by:

$$h(t) = \sum_{i=0}^{L-1} \alpha_i \delta(t - \tau_i) \qquad (4)$$

The multipath amplitudes are given by α_i and the delays are given by τ_i. The amplitudes α_i are independently Rayleigh distributed with mean local strength $E\{\alpha_i^2\} = 2\sigma_i^2$. The probability density function of α_i is given by:

$$f_i(\alpha_i) = \frac{\alpha_i}{\sigma_i^2} \exp\left(\frac{-\alpha_i^2}{2\sigma_i^2} \right), \alpha_i \geq 0 \qquad (5)$$

When i=0, the parameters correspond to the DLOS path. In this analysis, the multipath delays are assumed to be fixed. These assumptions suit the JTC model for instance where the mean local strengths of the paths and fixed path delays are specified.

In detecting the DLOS path, its signal strength and the signal strength in the remaining L-1 paths determine whether or not the DLOS path is detected in addition to the receiver sensitivity and signal-to-noise ratio. The DLOS path can be detected if it is above the noise and the strengths of none of the other paths exceed its own by more than the receiver dynamic range ρ. In particular, if the effects of noise are neglected and it is assumed that the receiver can detect a path as long as its local mean strength is above the sensitivity, we can formulate the problem as follows.

$$P_D(DLOS) = \Pr\{\alpha_1 \leq \rho\alpha_0, \alpha_2 \leq \rho\alpha_0, \ldots \alpha_{L-1} \leq \rho\alpha_0, \alpha_0 \geq S\} \qquad (6)$$

Since each of the random variables in (6) is independent, we can write this probability as follows.

$$P_D(DLOS) = \int_S^\infty f_0(\alpha_0) \int_0^{\rho\alpha_0} f_1(\alpha_1) d\alpha_1 \int_0^{\rho\alpha_0} f_2(\alpha_2) d\alpha_2 \cdots \int_0^{\rho\alpha_0} f_{L-1}(\alpha_{L-1}) d\alpha_{L-1} d\alpha_0 \qquad (7)$$

This can be simplified further as:

$$\int_S^\infty \frac{\alpha_0}{\sigma_0^2} \exp\left(\frac{-\alpha_0^2}{2\sigma_0^2} \right) \prod_{i=1}^{L-1} \left[1 - \exp\left(\frac{-\rho^2\alpha_0^2}{2\sigma_i^2} \right) \right] d\alpha_0 \qquad (8)$$

The closed form of this integral can be expressed as follows:

$$P_D(DLOS) = \exp\left(\frac{-S^2}{2\sigma_0^2}\right) -$$
$$\sum_{i=1}^{L-1} \frac{1}{1+\rho^2\sigma_0^2/\sigma_i^2} \exp\left(-S^2\left[\frac{1}{2\sigma_0^2}+\frac{\rho^2}{2\sigma_i^2}\right]\right) +$$
$$\sum_{i=1}^{L-1}\sum_{j=i+1}^{L-1} \frac{1}{1+\frac{\rho^2\sigma_0^2}{\sigma_i^2}+\frac{\rho^2\sigma_0^2}{\sigma_j^2}} \exp\left(-S^2\left[\frac{1}{2\sigma_0^2}+\frac{\rho^2}{2\sigma_i^2}+\frac{\rho^2}{2\sigma_j^2}\right]\right)$$
$$+\cdots+(-1)^{L-1} \frac{1}{1+\sum_{u=1}^{L-1}\frac{\rho^2\sigma_0^2}{\sigma_u^2}} \exp\left(-S^2\left[\frac{1}{2\sigma_0^2}+\sum_{u=1}^{L-1}\frac{\rho^2}{2\sigma_u^2}\right]\right) \quad (9)$$

When the receiver sensitivity can be assumed to be zero (i.e. it can detect a signal no matter how small it is, implying an infinite SNR), the exponential terms become one *and the probability of detection is simply a function of the ratios of the local mean signal strength of the DLOS path to the local mean signal strength of the other paths multiplied by the receiver dynamic range.*

4. Results for the JTC Model

The Joint Technical Committee on PCS (JTC) model [2,5] has been widely used in simulating the indoor radio channel for PCS applications. In order to incorporate the large amount of variability of delay spread within a given environment, three multipath channels are defined for each indoor radio environment. Channel A is the low delay spread case, channel B is the median delay spread case, and channel C is the high delay spread case. Three such models are specified for each of indoor residential, office, and commercial (e.g. factory or shopping centers) environments. The tapped-delay line model specifies the local mean strength of each of the multipath components, namely $2\sigma_i^2$, as well as the delay associated with the multipath. These delays are discrete and are usually multiples of 25 or 50 ns.

4.1 Infinitely sensitive receiver (S=0)

Figures 1-3 show the results obtained for the JTC models for indoor residential, office and commercial environments respectively with analysis and simulation for the case when S=0 (signal-to-noise ratio is infinite). The analytical results are derived from (9) by using appropriate values for $2\sigma_i^2$ and L. The values of L (number of paths) range between three and eight for the various JTC models. In order to simulate the results, twenty thousand channel profiles were generated using the JTC model parameters in each case. Each model was examined to determine whether the DLOS path can be detected for various values of ρ^2 ranging from 10 dB to 40 dB. The results are shown as discrete points (diamonds) in these figures. The results of simulation match the results of analysis quite closely.

The channel model C for residential and the channel model B for commercial indoor environments are the same (see tables in [2]). In these models, the local mean strength of the DLOS path is smaller than the local mean strength of one of the other multipath components. Consequently, the probability of detecting the DLOS path for these two instances is the smallest for all receiver dynamic ranges and this can be seen from the figures.

4.2 Finite receiver sensitivity ($S > 0$)

When the receiver has a finite sensitivity, the performance will be worse since the probability of detection will be multiplied by exponential terms that are less than one. Since the JTC multipath models are normalized, meaningful results cannot be obtained for arbitrary values of S. The *path loss* suffered by the signal will have to be taken into account and multiplied with the local mean strength of the multipath components and only then can the receiver sensitivity be applied. For a given building, the JTC path loss model provides the path loss as a function of distance d [2]. In particular, for a single-floor office buliding, the path loss is given by:

$$L_p = 49 + 30\log(d) \quad (10)$$

with a standard deviation of 10 dB associated with lognormal fading.

In [3,4], channel profiles from ray tracing simulations (with a floor plan whose parameters were adjusted so that the ray tracing simulations matched measurement results at selected points in the first floor of Atwater Kent Labs at WPI) were used in obtaining statistics useful for geolocation. Around 1700+ receivers were placed in a grid all over the building and the channel profiles observed for a single transmitter (with a transmit power of 27 dBm, center frequency 1 GHz, placed at the center of the building) were considered. Atwater Kent can be categorized as a harsh office

building and Channel C of the JTC indoor office model is suitable for comparison.

Ray tracing channel profiles are examined to determine the probability of detecting the DLOS path for different receiver sensitivities S^2 and dynamic ranges ρ^2. The results are shown in Figures 4 and 5. Analytical results are obtained using (9) and (10) for the JTC indoor office channel model C and they are shown in Figures 6 and 7. The path loss is applied with a correction of 27 dB to account for the transmit power used in thr ray tracing simulations. The average distance (21m) between transmitter and receiver for the 1700+ receivers in the ray tracing simulations is used in (10). The former plot in each case is a two dimensional plot of the probability of detection as a function of ρ^2 with S^2 as a parameter. The latter plot is a three dimensional plot showing the variation of the probability of detection as a function of both ρ^2 and S^2.

The results are comparable in that the order of magnitudes and general shapes of the curves are similar. The probability of detection with ray tracing is the more accurate result and it shows a slower variation with ρ^2. The probability of detection determined through analysis is somewhat optimistic over all values of ρ^2 and S^2. The reasons for this are manifold. A single distance is used in the analysis whereas in reality the probability of detection becomes worse at larger distances. The JTC model in general is not designed for geolocation applications and requires modifications to include information relevant to geolocation. As discussed earlier, P_D(DLOS) is dependent upon the ratios of the local mean strengths of the multipath components. While the JTC models match the RMS multipath delay spreads to those observed with measurements, they do not consider these ratios in developing the model. Also, the analysis here does not include the effects of lognormal fading specified in the model that may further degrade the probability of detection bringing it closer to the values obtained through ray tracing.

5. Conclusions and Future Work

An analysis of the probability of detecting the DLOS path in a discrete multipath Rayleigh fading channel is considered. This probability is dependent upon the receiver sensitivity and dynamic range and for high sensitivities, it is a function of the ratios of the signal strength in the DLOS component to the signal strength of the other components weighted by the dynamic range. Current multipath channel models do not address the issue of detecting the DLOS path and need modifications that provide this information as well. In addition to detecting the DLOS path, the probability of detecting some other path if the DLOS path is NOT detected becomes important to determine the error in range estimates that can occur in a system. This problem is under study at CWINS, WPI. Models such as those developed by JTC ignore the arrival times keeping them discrete and fixed. Modifications that focus on this issue are also being investigated.

Acknowledgements: The authors would like to express their appreciation to DARPA's SUO-SAS program and Dr. Mark McHenry for partial support of this work.

References

[1] K. Pahlavan, A. Zahedi, P. Krishnamurthy, "Wideband Local Access: WLAN and WATM", *IEEE Communications Magazine*, November 1997.

[2] K. Pahlavan and A. Levesque, *Wireless Information Networks*, John Wiley and Sons, New York, 1995.

[3] K. Pahlavan, P. Krishnamurthy, J. Beneat, "Wideband Radio Propagation Modeling for Indoor Geolocation Applications", *IEEE Communications Magazine*, April 1998.

[4] P. Krishnamurthy, K. Pahlavan and J. Beneat, "Radio Propagation Modeling for Indoor Geolocation Applications", *Proc. Of PIMRC'98*, Boston, MA, September 8-11, 1998.

[5] JTC Technical Report on RF Channel Characterization and Deployment Modeling, Air Interface Standards, September 1994.

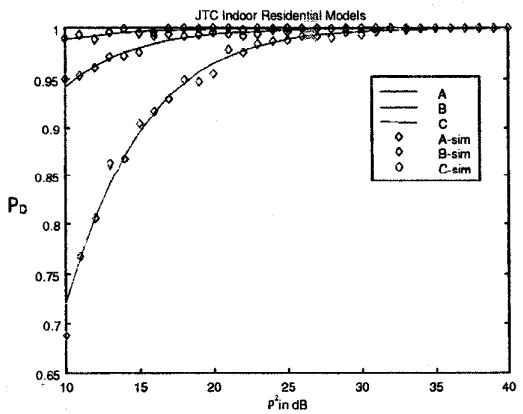

Figure 1: Probability of detecting the DLOS path in indoor residential environments for S=0

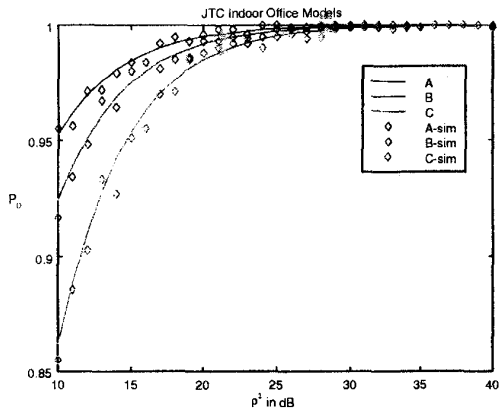

Figure 2: Probability of detecting the DLOS path in indoor office environments for S=0

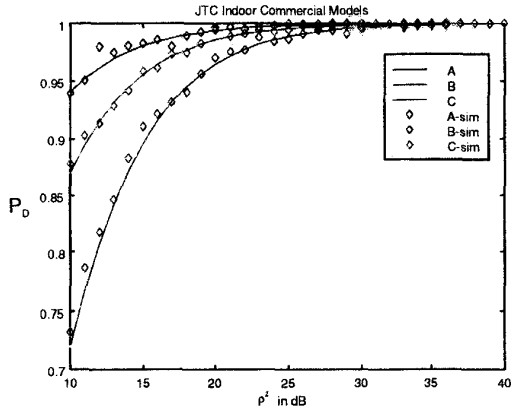

Figure 3: Probability of detecting the DLOS path in indoor commercial environments for S=0

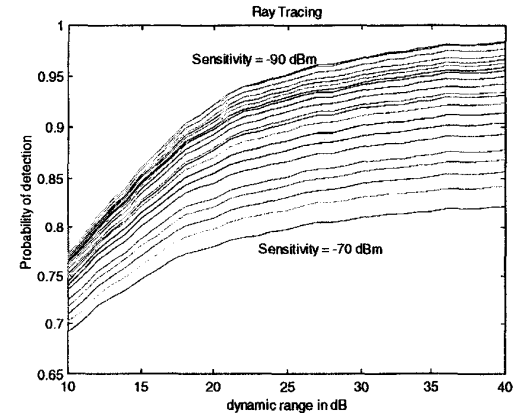

Figure 4: Probability of detecting the DLOS path in Atwater Kent Labs 1st floor (Ray Tracing)

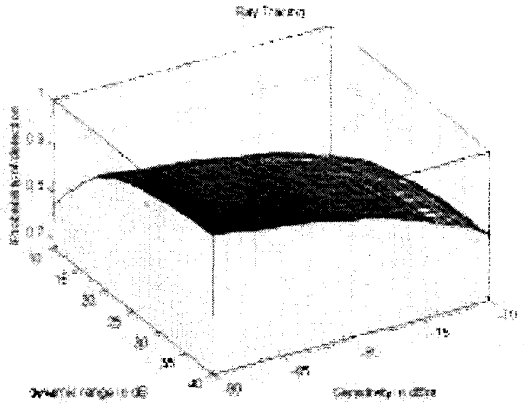

Figure 5: Probability of detecting the DLOS path in Atwater Kent Labs 1st floor (Ray Tracing)

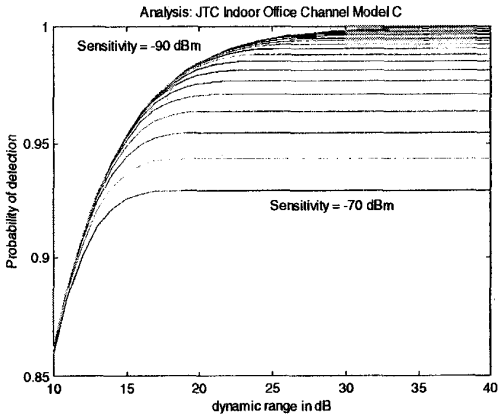

Figure 6: Probability of detecting the DLOS path: JTC Indoor Office Model C

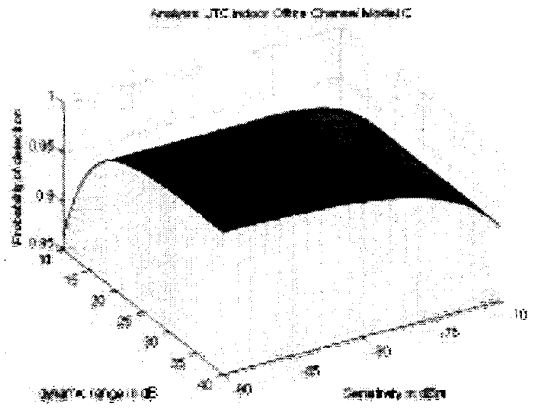

Figure 7: Probability of detecting the DLOS path JTC Indoor Office Model C

Space-Time Measurement of Indoor Radio Propagation

Robert D. Tingley, *Member, IEEE,* and Kaveh Pahlavan, *Fellow, IEEE*

***Abstract*—Most existing techniques for indoor radio propagation measurement do not resolve the angles from which signal components arrive at the receiving antenna. Knowledge of the angle-of-arrival is required for evaluation of evolving systems that employ smart antenna technology to provide features such as geolocation, interference cancellation, and space-division multiplexing. This paper presents a novel technique for the joint measurement of the angles, times and complex amplitudes of discrete path arrivals in an indoor propagation environment. A data acquisition system, based upon a vector network analyzer and multichannel antenna array is described, together with its use to collect channel measurement matrices. The inherent error sources present in these measurement matrices are investigated using a compact indoor anechoic range. Two signal processing algorithms are presented whereby the channel parameters may be estimated from raw measurements. In the first approach, an optimum beamformer is derived which compensates for systematic errors in the data acquisition system. This approach features very low computational complexity, and delivers modest resolution of path components. The second algorithm is based upon the maximum likelihood criterion, using the measured calibration matrices as space-time basis functions. This algorithm provides super-resolution of all path parameters, at the cost of increased computation. Several example measurements are given, and future directions of our research are indicated.**

***Index Terms*—Array signal processing, calibration and verification, high resolution signal processing, indoor radio propagation, propagation measurement.**

I. Introduction

A. Motivation

THE CONCEPT of wireless office information networks was introduced in the early 1980s, with the first commercial products appearing in the early 1990s. Following completion of the IEEE 802.11 Standard, interoperable wireless LAN (WLAN) products have begun to appear. Sales of wireless office products exceeded half a billion dollars last year, and are expected to surpass five billion dollars in the first few years of the new millennium. Today Internet access, cordless telephone, wireless security, headphone, speaker, appliance, and lighting control systems all form important segments of the indoor radio market. The market for all of these applications has grown rapidly in response to consumer demand, and has both exploited and encouraged the development of low-cost chip sets.

Manuscript received August 17, 1999; revised July 24, 2000.

R. D. Tingley is with the Charles Stark Draper Laboratory, Cambridge, MA 02139 USA (e-mail: rtingley@draper.com).

K. Pahlavan is with the Center for Wireless Information Network Studies, Department of Electrical and Computer Engineering, Worcester Polytechnic Institute, Worcester, MA 01609 USA (e-mail: kaveh@ece.wpi.edu).

Publisher Item Identifier S 0018-9456(01)01650-3.

Design assessment and optimization of existing applications have been enabled by a collection of channel modeling and simulation techniques that are geared toward predicting the achievable coverage and data rate [6], [17]. Recently, new applications have been identified that require a more detailed model of the underlying propagation effects. Following a recent FCC ruling intensive development has begun on wireless E-911, which will provide the emergency call center with the estimated location of the caller [2]. At the same time, indoor positioning systems are appearing that allow tracking valuable assets throughout a large facility [1]. As the reliability of these systems becomes well known, their use will inevitably expand to include tracking of personnel in potentially dangerous situations, such as fire fighters, law enforcement officials, and military personnel engaged in urban conflicts [2].

Both adaptive interference cancellation and adaptive space division multiplexing are being studied for incorporation into the next generation of commercial wireless systems. These techniques are based upon the notion that the desired and interfering signals emanate from distinct directions, and as such, may be separated based upon their direction-of-arrival. However, this viewpoint does not consider that, except in the simplest of environs, both the desired and interfering signals arrive from many directions, as affected by the properties of the radio channel.

B. Background

The first indoor radio measurements to include angle-of-arrival information were reported by Lo and Litva in 1992 [7]. They employed a measurement system wherein a 950 MHz carrier was phase modulated by a 40 Mb/s pseudonoise sequence. Each data set was acquired by moving the receiving element through a succession of four points on the radius of a circle, as well as to the center. Bearing information was calculated from each data set by considering the five points to constitute a simple array, and applying standard beamforming techniques. The authors do not provide the system specifications, however based upon the design parameters we expect a spatial resolution of 90°, and a temporal resolution of about 25 ns.

The array measurement system was improved by Rossi *et al.* [8], with the addition of a radial armature that facilitates the automated movement of the receiving element through the various positions. This system also developed bearing estimates using standard beamforming techniques. However, since the measurements in each data set are collected in 1° increments rather than 90° increments, the system features much finer angular resolution. The authors report achieving resolution of 40 ns in time, and 10° in angle-of-arrival.

The highest-performance space-time characterization system presented to date is due to Spencer *et al.* [9], and may be viewed as an extension of the frequency-domain channel sounder of Howard [6]. The new system replaces the omnidirectional receiving element employed in [6] with a 60 cm parabolic dish, mounted atop a computer-controlled turntable. Each data set is acquired by sweeping the network analyzer, followed by dish rotation through 2°, and repeating this sequence until one cycle has been completed. The authors report achieving spatial resolution of 6°, and temporal resolution of 3 ns. Since each data set requires approximately 20 min to acquire, due to setup, dish rotation, and the large number of constituent measurements [10], it may prove difficult to ensure that all constituents are derived from the same underlying propagation scenario. Perhaps more important, since the beamwidth of a parabolic antenna runs inversely with the frequency of operation, an antenna of nearly 2 m diameter is required to maintain the same resolution at 2.4 GHz.

This paper is organized as follows. In Section II, the construction and calibration of an eight-element circular array are presented. In Section III, the spatial filter periodogram algorithm is developed, which provides moderate resolution path parameter estimates. In Section IV, the discrete maximum likelihood algorithm is described, along with its ability to deliver high-resolution estimates of all path parameters. Section V provides a comparison of the two algorithms and several sample measurements, and the paper is concluded in Section VI.

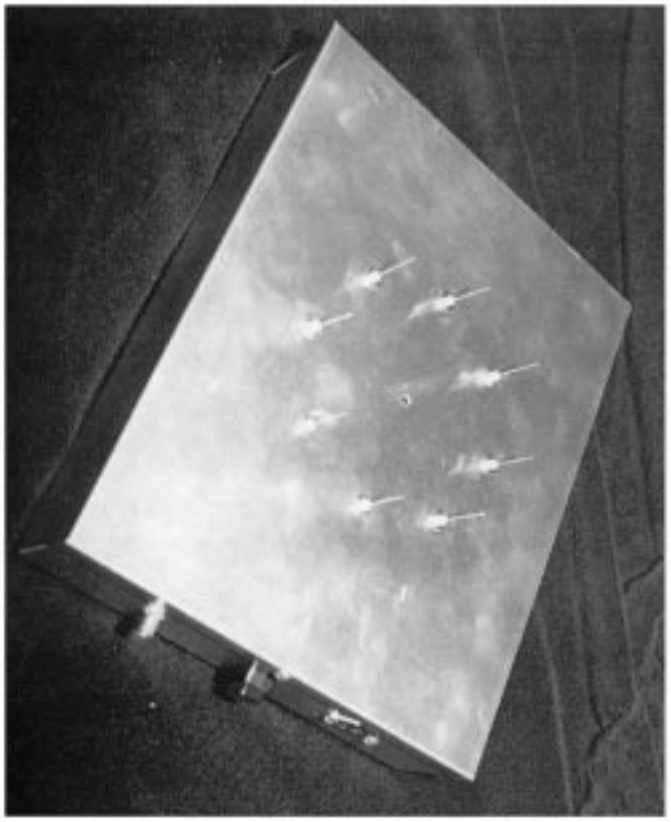

Fig. 1. Eight-element circular array.

II. Data Acquisition System

A. Construction

A data acquisition system which incorporates newly available component technologies holds the promise for delivering several advantages relative to the existing systems. Among the advantages are a simpler setup and measurement process due to minimal component count, elimination of moving parts, and a reliance on off-the-shelf test equipment. At the same time, the acquisition period may be reduced such that the entire data matrix is acquired in less than the channel coherence time. A final advantage is the development of a framework within which to trade excess signal-to-noise ratio for improved resolution by mating the acquisition system with subspace or parametric post processing. Caution is necessary, however, to ensure that the array provides certain characteristics required by the post processing algorithms, such as shift-invariance.

To achieve these goals, the antenna array shown in Fig. 1 was constructed. The array consists of eight nominally-identical quarter-wave monopole elements, mounted at a constant radius and separated by one-third wavelength. The signal received at each element is fed to an eight-channel switch by means of a short run of semi-rigid coaxial cable. The array also provides power to the switch, and a digital interface whereby a personal computer may select the element under test. The internal configuration of the array is shown in Fig. 2.

The array serves as the receiving element of the data acquisition system, as shown in Fig. 3. As in [6] and [9], measurements are conducted in the frequency domain, with the aid of an HP8753D vector network analyzer. The analyzer provides a synthesized microwave source, which is swept from 2.35 to 2.55 GHz, and delivered to an omnidirectional transmit antenna through a 50-m run of double-shielded coaxial cable. A high-power amplifier, located at the base of the transmit antenna, boosts the signal to a level of $+20$ dBm. The transmit spectrum is intercepted by the circular array, where it is amplified by a low-noise amplifier, and applied to the receive channel of the network analyzer.

A standard laptop computer is used to control the measurement setup. To begin acquisition of a data set, the laptop switches the array to the first element, sweeps the network analyzer, retrieves the complex-valued transfer function data (S_{21}), and stores the data to hard disk. The process is repeated for the remaining elements, until all eight transfer functions have been measured and stored. When configured for 101 points and a predetection bandwidth of 3 kHz, a total of 750 ms is required to measure all eight elements and store the corresponding data to disk. The total data acquisition time may be further abbreviated by employing a larger predetection bandwidth, measuring fewer points, or utilizing a network analyzer with faster internal signal processing.

B. Calibration

It was discovered early in the development program that numerous sources of error are present which, left uncompensated, tend to degrade the accuracy of the results. Elements of the array couple strongly with one another, as can readily be demonstrated either through a transmission measurement between adjacent elements, or by measuring the reflection coefficient of

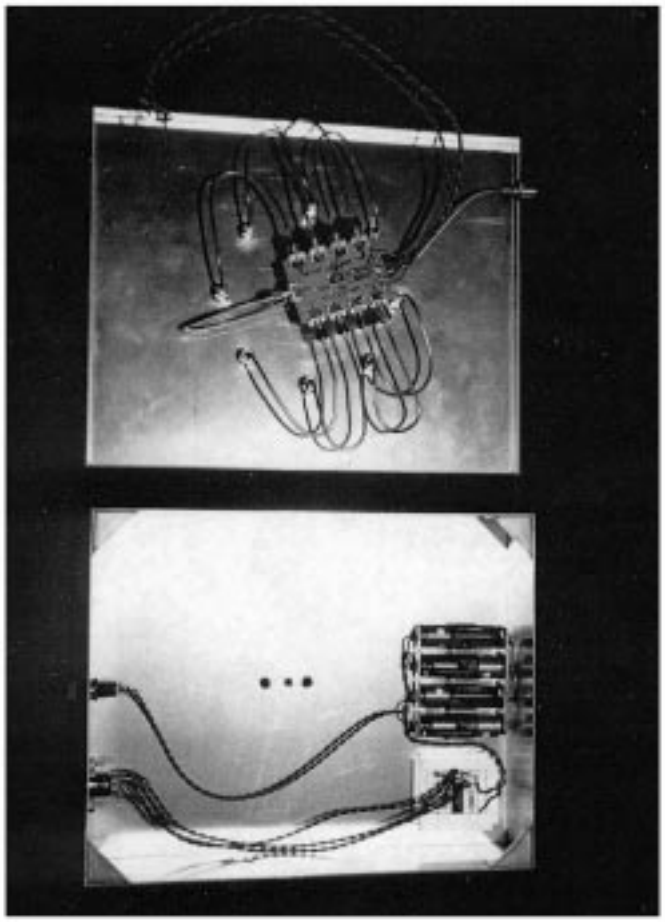

Fig. 2. Array internal construction.

an individual element while adjusting the load placed on either of its immediate neighbors. Related to the coupling effect is a pose-dependent shadowing effect in which the power delivered by an element varies strongly as the element's relation to the source bearing changes. In particular, as an element's position approaches counterpoise with the direction-of-arrival, its power output drops markedly, due to shielding by elements which are blocking its "view" of the source. Still other effects are present, such as the finite dimension of the underlying ground plane, and imperfect knowledge of the relative positions and tuning of the array elements. In aggregate, these effects ensure that the array characteristics may not be described by a simple array factor, as customarily used to develop signal processing algorithms [11]–[13].

In addition to errors caused by the array construction and geometry, numerous circuit and transmission line error sources are present. For example, it was shown that the phase mismatch between switch channel pairs can be as high as 75° at 2.55 GHz. Likewise, the amplitude mismatch between switch channel pairs can be as high as 1.5 dB. Both the amplifiers and the antenna feedlines display a small but significant amount of frequency shaping, and thus may not be considered trivial delay elements.

In order to provide the most generally useful results, system calibration was divided into two portions. In the first portion, the two-port parameters of each circuit element were measured. This characterization included all eight switch channels, the transmit feedline, both amplifiers, and the remaining coaxial runs necessary to complete the system. Armed with such a circuit characterization, subsequent eight-channel measurements are adjusted such that they imply reference planes taken at the base of each individual antenna element.

For the second portion of the calibration, the transmit antenna and receiving array were assembled in a small indoor anechoic range. The antennas were mounted atop turntables, and separated by a distance of 3 m. All measurement gear and personnel were located outside the chamber, in an effort to prevent the addition of spurious reflections. In this configuration, spurious arrivals are attenuated by at least 30 dB relative to the line-of-sight (LOS) arrival. A series of eight-channel frequency domain measurements was conducted. Between each data set, the array was rotated 5.625° in azimuth, relative to its previous orientation. This measurement and rotation sequence was performed for one complete revolution of the array, which resulted in 64 distinct data sets given as

$$\mathbf{U_m} = \begin{bmatrix} u_{1,1,m} & u_{1,2,m} & & u_{1,8,m} \\ u_{2,1,m} & u_{2,2,m} & & \\ & & & \\ u_{101,1,m} & & & u_{101,8,m} \end{bmatrix} \tag{1}$$

where $m = 1, 2, \cdots, 64$. The indices are chosen such that $m = 1$ corresponds to 0°, $m = 2$ corresponds to 5.625°, and so forth. The nth column of $\mathbf{U_m}$ represents the frequency response between the transmit antenna and the nth element of the receiving array. The magnitude of $\mathbf{U_0}$ is presented in Fig. 4. Note that the array elements are numbered in such a fashion that the first element is sighted at 0° azimuth, although this selection was purely arbitrary. The figure displays much higher attenuation at the fifth element, which in this configuration is directly opposite to the angle-of-arrival. This behavior is explained by the shielding effect cited earlier.

III. Spatial Filter Periodogram Algorithm

A. Process Model

In order to facilitate development of signal processing strategies, the discrete arrivals model is augmented as

$$h(t, \theta) = \sum_{l=1}^{L} \beta_l e^{j\phi_l} \delta(t - t_l, \theta - \theta_l). \tag{2}$$

In this formulation, the lth component of the impulse response arrives at the receiver delayed by t_l seconds, and from a bearing of θ_l°. L such components are required to accurately represent the channel response, and each is scaled by a complex factor $\beta_l e^{j\phi l}$. Although this model is generally well accepted, its use can be expected to pose several difficulties when applied to measured channel responses. First, since model components are purely impulsian, surface interactions of a frequency selective nature will not be well represented. In addition, since the elevation angle is not explicitly identified the model can be expected to provide poor performance in the case of arrivals which are not coplanar with the array elements. Data collected in the field confirm that the error accrued due to these effects is small, so

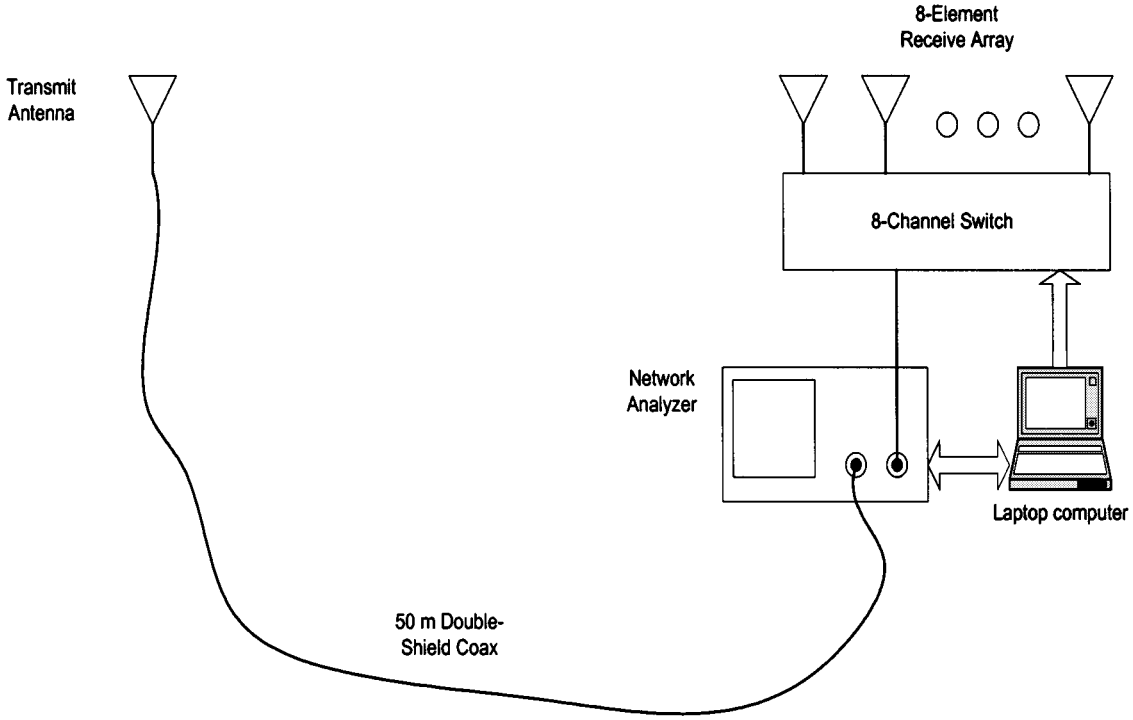

Fig. 3. Measurement system block diagram.

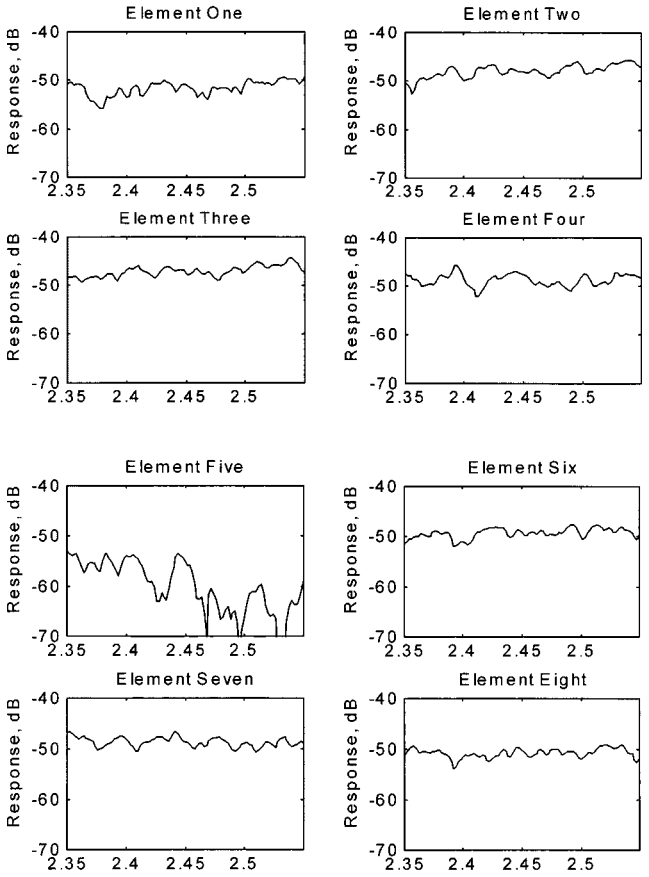

Fig. 4. Example array calibration response.

long as measurements are made in a conventional office environment with both transmitter and receiver on the same floor.

Before proceeding, note that new algorithms have been proposed which estimate the parameters in (2) using extensions to the well-known ESPRIT technique [11], [15], [16]. Although this approach operates on time domain data, and requires a good estimate of the model order, neither of these requirements is insurmountable. The real barrier to direct application is that simple physical arrays do not readily conform with the shift-invariant data model assumed in the algorithm construction.

B. Algorithm Formulation

Rather than employ a conventional beamforming algorithm, the collection of calibration matrices is used to form a least-squares spatial filter. This approach has numerous benefits, including improved resolution, lower sidelobes, and the automatic removal of systematic errors in the array response [5]. In this procedure, we form the cost function

$$f(\mathbf{w}_m) = \sum_{j \neq m} \sum_{l=1}^{101} \left(\sum_{n=1}^{8} u_{l,n,j} w_{n,m} \right) \left(\sum_{n=1}^{8} u_{l,n,j}^{*} w_{n,m}^{*} \right) \tag{3}$$

which is minimized, subject to the additional constraint

$$c(\mathbf{w}_m) = \sum_{l=1}^{101} \left(\sum_{n=1}^{8} u_{l,n,m} w_{n,m} \right) \left(\sum_{n=1}^{8} u_{l,n,m}^{*} w_{n,m}^{*} \right) - 1 = 0. \tag{4}$$

The cost function serves to minimize the array's sensitivity to energy from all directions except the desired, while the constraint guarantees a solution with a fixed, constant gain in the desired direction. This approach is very similar to the well- known minimum-variance, distortionless response method [21], except that in the present case, complete control over the sources guarantees that all energy arrives from the desired direction. As a

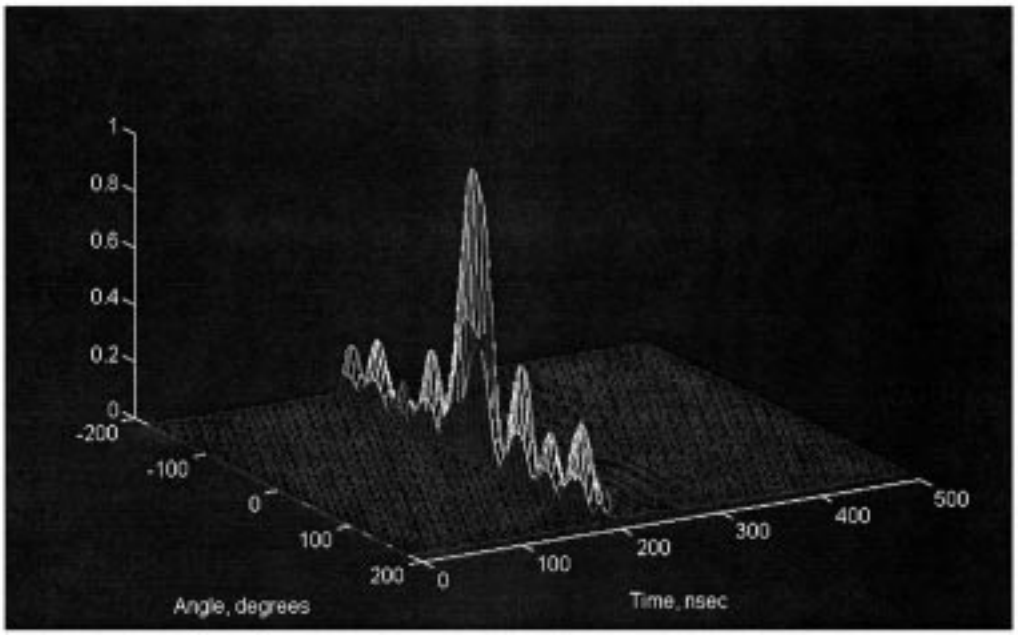

Fig. 5. Space-time impulse response of SFP technique.

result, the optimal solution does not contain deep nulls in the direction of strong interferers. The cost function and constraint are satisfied jointly, using the method of complex Lagrange multipliers, outlined in [21].

The first step in the method is to combine the cost and constraint equations to form the *adjoint equation*

$$\frac{\partial f(\mathbf{w}_m)}{\partial \mathbf{w}_m^*} + \lambda \frac{\partial c(\mathbf{w}_m)}{\partial \mathbf{w}_m^*} = 0. \tag{5}$$

Performing the partial differentiation over each element of the complex-valued tap-weight vector produces a system of equations of the form

$$F_k(\mathbf{w}_m, \lambda) = \sum_{j \neq m} \sum_{l=1}^{101} u_{l,j,k} \sum_{n=1}^{8} u_{l,j,n}^* w_{n,m} + \lambda \sum_{l=1}^{101} u_{l,m,k}^* \sum_{n=1}^{8} u_{l,m,k}^* w_{n,m} = 0 \tag{6}$$

where $k = 1, 2, \cdots, 8$. Since the constraint equation must also be satisfied, we have

$$F_9(\mathbf{w}_m, \lambda) = \sum_{l=1}^{101} \left(\sum_{n=1}^{8} u_{l,n,m} w_{n,m} \right) \cdot \left(\sum_{n=1}^{8} u_{l,n,m}^* w_{n,m}^* \right) - 1 = 0. \tag{7}$$

Taken together, a solution to these nine equations provides the optimal taps for the array processor, as well as the Lagrange multiplier λ. Although (1)–(8) are linear in the independent variables, equation nine is quadratic in the array weights. As a result, standard linear algebraic techniques, such as SVD, cannot be used to compute the solution immediately. An iterative solution technique is described in [20].

The tap weight design algorithm is repeatedly applied, with the results conveniently collected in the form of the spatial filter matrix

$$\mathbf{W} = \begin{bmatrix} w_{11} & w_{12} & \cdots & w_{1M} \\ w_{21} & w_{22} & & \\ \vdots & & \ddots & \\ w_{81} & & & w_{8M} \end{bmatrix}. \tag{8}$$

The mth column of $\mathbf{W}$ provides eight taps which serve to steer the array in the desired direction, while minimizing the energy collected from all other directions. Given an arbitrary measurement matrix

$$\mathbf{V} = \begin{bmatrix} v_{1,1} & v_{1,2} & \cdots & v_{1,8} \\ v_{2,1} & v_{2,2} & & \\ \vdots & & \ddots & \\ v_{101,1} & & & v_{101,8} \end{bmatrix} \tag{9}$$

the space-time impulse response is estimated as

$$\hat{\mathbf{H}} = \mathbf{FXVW} \tag{10}$$

where $\mathbf{F}$ is the inverse Fourier transform matrix, and $\mathbf{X}$ serves as a window function which minimizes the sidelobes present in the equivalent time response. The path parameters of (2) are computed by identifying the local maxima of $\mathbf{H}$, and noting the angle, delay, and complex amplitude at which they occur. The spatial and temporal resolution of the SFP algorithm is investigated in detail in [19], where it is shown to provide an average spatial resolution of approximately 30°, and an average time resolution of 7 ns. In Fig. 5, we present the magnitude of $\mathbf{H}$ for a single arrival, as measured in the anechoic chamber. Prominently displayed are the spatial sidelobes which result from the use of the SFP formulation.

IV. Discrete Maximum Likelihood Algorithm

While the SFP algorithm provides a simple method to estimate the space-time impulse response from a measurement matrix, it suffers from several limitations. The spatial resolution is strictly limited by the number and configuration of array elements, and in the current design stands at 30°. Likewise, the temporal resolution is given by the reciprocal of the sweep bandwidth, and is approximately 7 ns. Both of these limitations are independent of the signal-to-noise ratio of the data acquisition system. A third limitation is that the algorithm tends to introduce bias into the channel parameter estimates as a pair of closely-spaced arrivals appears.

These restrictions may be removed by developing an algorithm based upon the maximum likelihood criteria [12], [18]. Given the arrivals process of (2), an arbitrary measurement $\mathbf{V}$ may be modeled as

$$\hat{\mathbf{V}} = \sum_{l=1}^{L} \beta_l e^{j\phi_l} \mathbf{D}(t_l)\mathbf{U}(\theta_l) \tag{11}$$

where

L number of discrete paths;
$\beta_l e^{j\phi l}$ complex weight of the lth path;
$\mathbf{D}(t_1)$ 101×101 diagonal time delay matrix [19].

The values of L and t_l, θ_l, β_l and ϕ_l where $l = \{1, 2, \cdots, L\}$ are selected to minimize

$$J_{DML} = \sum_{k=1}^{101} \sum_{n=1}^{8} |v_{kn} - \hat{v}_{kn}|^2 . \tag{12}$$

There are at least three strategies by which this cost function may be minimized. Assuming a single component ($L = 1$), one could perform a simple serial search over all possible angles and times of arrival. At each combination, the algorithm calculates the value of $\beta_l e^{j\phi l}$ which serves to drive the cost function to its minimum for the current pose. After all delays and angles have been searched, the algorithm selects that combination which minimizes J_{DML}. The winning combination is weighted by the appropriate value of $\beta_l e^{j\phi l}$, and subtracted from $\mathbf{V}$. This combined search/subtraction algorithm is repeated until L paths have been identified and removed from $\mathbf{V}$. This serial search procedure is essentially identical to the CLEAN algorithm, which was developed for use in astronomy [14]. Its completion requires $L \times D \times M$ function evaluations, where L is the number of paths to identify, D is the number of discrete delays to search, and M is the number of discrete azimuths.

At the opposite extreme from the simple serial search is the full parallel search, wherein all L paths are identified simultaneously. The complex path weight now assumes the form of an $L \times 1$ vector, and on each iteration the values of β and ϕ are chosen which minimize J_{DML}. The search is performed over all delays and angles for all L paths, until the global minimum is reached. This approach will substantially outperform the serial procedure, especially when the number of paths is large. The improvement is derived principally from the fact that the serial search penalizes subsequent searches by accumulating error in the identification of the parameters of each path. The enhanced accuracy comes at a heavy price, however, as the parallel search requires $(D \times M)^L$ evaluations, each of which requires the solution of an Lth order linear system. For a situation with 64 discrete azimuths, 30 discrete arrival times, and 20 paths, the parallel search requires 60 orders of magnitude more computation than the serial search.

Since the full parallel search is impractical for cases with more than three to four discrete arrivals, early experimentation considered the serial approach. The first few paths identified tended to be at the correct arrival times and angles, but displayed increasing error in the complex path amplitude. After eight to ten iterations, the estimated time and angle also begin to fail, evidently due to error accrued from previous path subtractions. These observations suggest a third estimation procedure which alleviates the error accumulation inherent in the standard serial search.

The new algorithm, called the recursive serial search, uses the measured calibration matrices $\mathbf{U_m}$, $m = 1, 2, \cdots, M$ as fundamental basis functions. Using the delay operator matrix $\mathbf{D}(t)$, $D-1$ new versions of each of the calibration matrices are constructed, where the first is delayed τ_o seconds, the second $2\tau_o$ seconds and so forth. This procedure yields the basis matrices $\mathbf{C}_k$, where $k = 1, 2, \cdots, D \times M$. The algorithm then begins with the assumption that a single path is to be found. A search is conducted over all values of k, until that basis is identified which minimizes J_{DML}. This first iteration of the process produces the same result as the first search of the standard sequential detection procedure. However, in the recursive case we do not explicitly remove the identified path. Rather, its index, k_1 is retained in the path history, for use in subsequent searches.

Once the index of the first path has been identified, the model order is incremented to consider a measurement composed of two discrete arrivals. The first arrival, found in the previous iteration, is assumed to be fixed at the index k_1. The second arrival is found by another search over the remaining $D \times M - 1$ values of k. Once found, the second arrival is assigned the index k_2.

At each stage of iteration, the minimum value attained by the cost function is given as

$$J_{DML_{\min}} = m - \mathbf{p}^H \mathbf{R}^{-1} \mathbf{p}, \tag{13}$$

where $\mathbf{p}$ represents the cross correlation between each of the basis functions and the measurement matrix, and $\mathbf{R}$ represents the correlation between the individual basis functions [19]. Also

$$m = \sum_{k=1}^{101} \sum_{n=1}^{8} |v_{kn}|^2 \tag{14}$$

is the total energy contained in the measurement.

The process of incrementing the model order, followed by finding an additional path, is repeated until the desired number of paths have been identified. Since the sequential algorithm seeks to minimize J_{DML} at each stage, paths are identified in order of decreasing energy. This property provides a convenient means to exit the search, by monitoring the optimal value of J_{DML} achieved at each iteration. Once the residual drops below, say 10% of m, we may assume that the model has accounted for most of the energy contained in the measurement, and the algorithm may be terminated. Like the simple sequential search, the recursive search requires $D \times M \times L$ evaluations of the

cost function to identify L paths. However, in the recursive algorithm, these evaluations assume the order of the number of paths found. For example, searching for the Lth path requires evaluation of $D \times M$ systems of L linear equations. Although far more computation is required than the serial search, the algorithm is still quite practical. In most cases, parameter extraction from a measurement consumes from one to three minutes of CPU time on a contemporary Pentium-based personal computer. The DML algorithm is considered in more detail in [19], where the spatial and temporal resolutions are determined to be 2° and 1 ns, respectively, using sample measurements in the anechoic chamber.

V. Verification and Comparison

A. Performance Evaluation

Perhaps the most important stage in the development of any new measurement system is a critical investigation of the system's accuracy when characterizing one or more external standards. For example, a new voltmeter might be evaluated by connecting it to a highly repeatable source, and comparing the meter reading with the source setting, as the source is swept over some range of interest. From a conceptual standpoint, a space-time measurement system could be evaluated by acquiring many distinct data sets, and comparing the estimated path parameters with the known path parameters. However, performing such a direct evaluation is not generally possible, since no technique exists to provide the known path parameters with sufficient accuracy to make this comparison meaningful.

A widely-used approach to performance evaluation of array processors is based upon the premises that a perfect shift-invariant array is available, and that the only perturbation afflicting the measurement system is receiver noise [11], [16]. Numerous computer simulation runs are conducted as the power level of the noise source is adjusted, and the variance of the estimates of one or two arrival angles is compared with results from the Cramer–Rao lower bound [18]. Unfortunately, this scenario does not provide a faithful simulation of a typical channel characterization exercise. Data is typically acquired at a carrier-to-noise ratio of at least 40 dB, and prior to measurement the channel background noise is evaluated to ensure that interference from other users, such as wireless LANs, is not present. When both of these conditions are met, the Cramer–Rao bound provides a lower limit on bearing estimation accuracy that is several orders of magnitude less than 1° [22]. Far more important than noise is the number of paths received, since a typical indoor environment may provide 10–100 arrivals, while the standard algorithms, such as ESPRIT and MUSIC, fail when the number of arrivals exceeds the number of antenna elements [11]. Also, as shown in Section II, the measured array response does not typically conform with the perfect, shift-invariant model assumed in simulation.

As a practical, yet meaningful, alternative to the direct and simulation approaches, it is a straightforward matter to synthesize raw data matrices by combining the measured calibration data according to *a priori* knowledge of the path parameters provided by propagation simulation or statistical models [17]. To be specific, since calibration is performed at a very high carrier-to-noise ratio, each calibration matrix exactly captures the raw array output that is present for a single source arriving from the bearing and distance at which the matrix was acquired. As calibration is performed in the far field of the array, a single arrival at a greater range produces a raw data matrix that is merely a delayed and scaled version of the calibration data acquired at the same bearing. Since radio propagation is well-described as a linear phenomenon, and hence obeys superposition, raw data matrices may be generated by summing a large combination of the measured calibration matrices that have been selected, delayed, and scaled in accordance with known statistical models. The data matrices so generated exactly capture a prescribed physical situation of which we have precise knowledge, and allow the creation of data sets that comprise many more paths than are typically seen in practice.

B. System Validation

The performance of both array processors, coupled with the data acquisition system, was demonstrated by generating several thousand test cases as described in the preceding section. For all cases the path parameters were assumed to be independent and identically distributed, with the angle-of-arrival uniformly distributed between -180 and $+180°$, and the time-of-arrival uniformly distributed between 0 and 200 ns. The path amplitude was taken as unit-variance complex Gaussian, and the number of paths was varied between 1 and 50.

Figs. 6 and 7 demonstrate the typical performance of the SFP and MML algorithm for a channel consisting of 20 known paths. In Fig. 6, the known path parameters are represented by an open circle, whereas the SFP estimates are represented by a cross-hatch. In Fig. 7, the cross-hatches now represent parameter estimates provided by the DML technique. The SFP technique finds many of the paths exactly, but is seen to encounter difficulty for paths that are nearly coincident in time or angle-of-arrival. By contrast, the DML algorithm identifies all paths exactly. This performance is to be expected so long as sufficient carrier-to-noise ratio ($\sim$20 dB) is maintained. More details of the statistical study may be found in [19].

C. Sample Measurements

The data acquisition system, and post processing algorithms are currently being used to enable research of the space-time properties of indoor radio propagation. In Fig. 8 we present a space-time response calculated from data acquired in an indoor LOS environment. We note that significant energy arrives over an expanse of only about 50 ns, and is principally clustered about the bearing at which the transmitter is located. We also notice that the first arrival is by far the largest, and represents the energy conveyed through the direct path.

In Fig. 9, we present a typical response calculated from data acquired in an obstructed LOS environment. This response is vastly different from the LOS case. The delay spread is roughly three times longer, or about 150 ns. The arrivals are no longer tightly clustered about the source bearing, and the first arrival is weaker than many subsequent arrivals. We note that since the DML algorithm provides only path parameter estimates, both Figs. 8 and 9 were generated using the SFP approach.

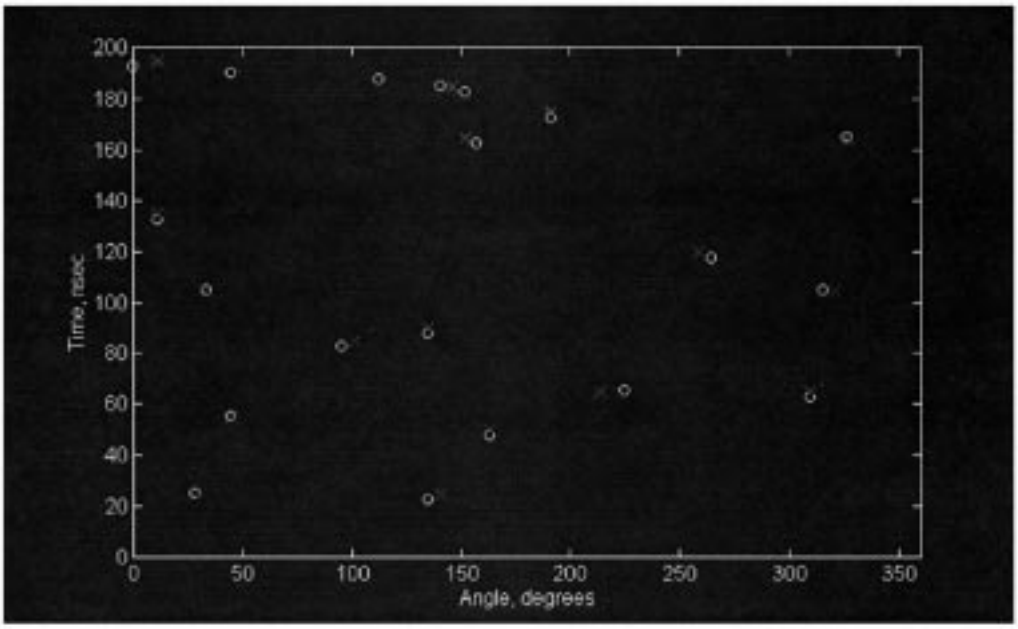

Fig. 6. Parameter estimates produced by SFP algorithm.

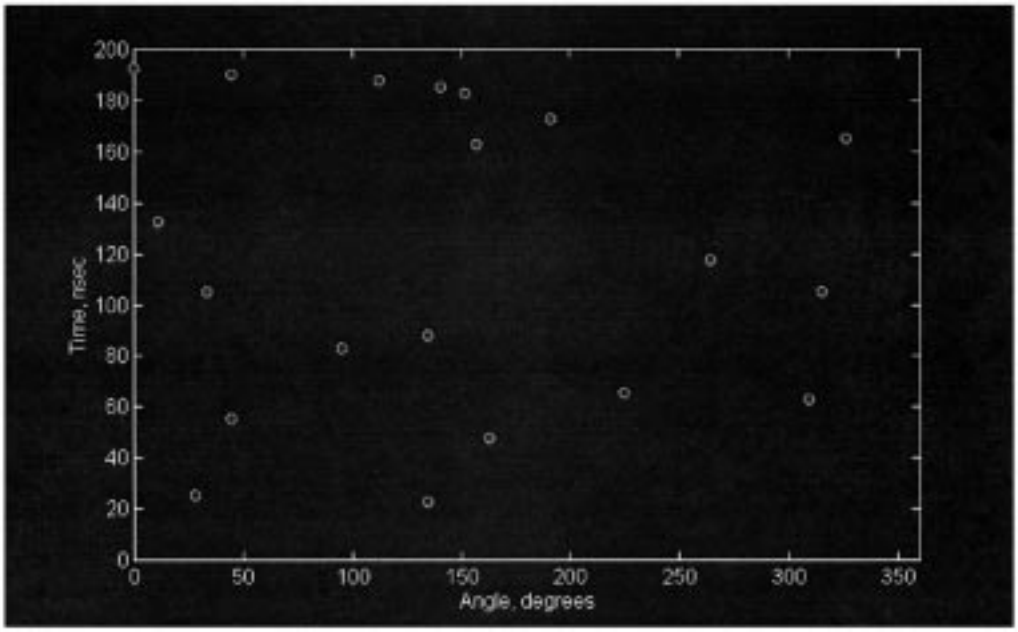

Fig. 7. Parameter estimates produced by DML algorithm.

D. Comparison

The performance of the DML and SFP algorithms, together with the other existing methods, is summarized in Table I. Note that the specifications of the DML algorithm may be adjusted by manipulating the parameters used in the search process, and described in Section IV.

VI. Summary and Conclusions

The analysis of new and emerging wireless applications requires an accurate characterization of the spatial-temporal properties of the environment of interest. This paper has considered an approach which extends the functionality of the frequency-domain channel sounder by inclusion of an antenna array as the receiving element. As compared with existing measurement strategies, the new system features simplified setup, a dramatic reduction in the data acquisition period, and the ability to support high-resolution post processing.

Characterization of the array showed numerous nonidealities which cause the response to depart from the theoretical array factor formulation. As a result, this paper has not considered subspace signal processing, the accuracy of which is critically dependent on the array properties. Rather, two algorithms have been derived which provide a convenient frame-

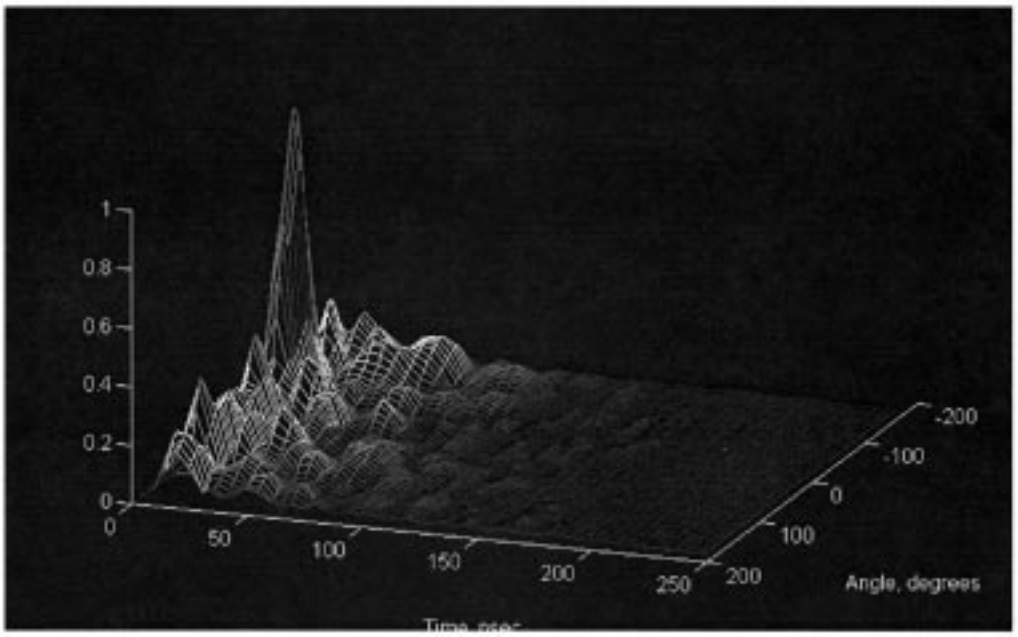

Fig. 8. Example response from indoor LOS environment.

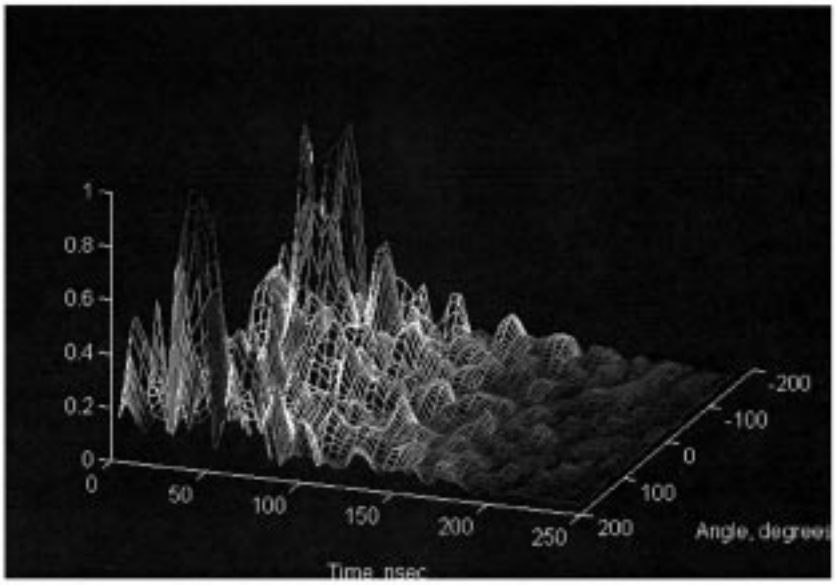

Fig. 9. Example response from indoor obstructed LOS environment.

TABLE I
COMPARISON OF PROPAGATION MEASUREMENT TECHNIQUES

System	Size, at 2400 MHz	Acquisition Time	Processing Time	Temporal Resolution	Spatial Resolution
Lo-Litva	single monpole	~ 1 minute	~ 1 second	~ 25 nsec.	~ 90 degrees
Spencer et al.	2-meter dish	>> 1 minute	>> 1 minute, manual	~ 3 nsec.	~ 6 degrees
Rossi et al.	small array	>> 1 minute	~ 1 second	~ 40 nsec.	~ 10 degrees
SFP	small array	< 1 second	~ 1 second	~ 7 nsec.	~ 30 degrees
DML	small array	< 1 second	~ 1 minute	adjustable, < 1 nsec.	adjustable, < 2 degrees

work within which to incorporate the measured calibration. The spatial filter periodogram algorithm extracts the direction-of-arrival information using a least-squares beamformer, followed by inverse Fourier transformation to calculate the time-of-arrival information. This algorithm is computationally simple, but provides only modest resolution.

The discrete maximum likelihood algorithm is developed using the measured calibration matrices as the fundamental basis functions of a model fitting procedure. The model parameters are determined using a new search procedure, called the recursive serial search, which eliminates the error propagation effects of the CLEAN algorithm, at a modest increase in complexity. Using known chamber responses, the combined discrete maximum likelihood/recursive serial search algorithm has demonstrated the ability to separate arrivals spaced 2° in azimuth, and 1 ns in time.

The data acquisition and post processing techniques described in this paper are currently being used to collect a large volume of data from indoor LOS and obstructed LOS environments. It is envisioned that this data will form the basis of new models for space-time propagation, which may be used to evaluate and optimize systems employing smart antenna technology.

REFERENCES

[1] J. Werb and C. Lanzl, "Designing a positioning system for finding things and people indoors," *IEEE Spectrum*, pp. 71–78, Sept. 1998.

[2] K. Pahlavan, P. Krishnamurthy, and J. Beneat, "Wideband radio propagation modeling for indoor geolocation applications," *IEEE Commun. Mag.*, vol. 36, Apr. 1998.

[3] A. J. Paulraj and C. B. Papadias, "Space-time processing for wireless communications," *IEEE Signal Processing Mag.*, vol. 14, Nov. 1997.

[4] A. Hero, Ed., "Highlights of statistical signal and array processing," in *IEEE Signal Processing Mag.*, Sept. 1998, vol. 15.

[5] R. Tingley and K. Pahlavan, "Propagation measurement using an antenna array," *Electron. Lett.*, Aug. 1999.

[6] S. J. Howard and K. Pahlavan, "Measurement and analysis of the indoor radio channel in the frequency domain," *IEEE Trans. Instrum. Meas.*, vol. 39, pp. 751–755, Oct. 1990.

[7] T. Lo and J. Litva, "Angles of arrival of indoor multipath," *Electron. Lett.*, vol. 28, no. 18, pp. 1687–1688, Aug. 27, 1992.

[8] J. P. Rossi, J. P. Barbot, and A. J. Levy, "Theory and measurement of the angle of arrival and time delay of UHF radiowaves using a ring array," *IEEE Trans. Antennas Propagat.*, vol. 45, pp. 876–884, May 1997.

[9] Q. H. Spencer, B. D. Jeffs, M. A. Jensen, and A. L. Swindlehurst. (1998, Nov.) "Modeling the statistical time and angle of arrival characteristics of an indoor multipath channel". [Online] Available: www.ee.byu.edu/~swindle

[10] Q. H. Spencer, private communication, Nov. 1998.

[11] H. Krim and M. Viberg, "Two decades of array signal processing research: The parametric approach," *IEEE Signal Processing Mag.*, vol. 13, July 1996.

[12] D. H. Johnson and D. E. Dudgeon, *Array Signal Processing*. Englewood Cliffs, NJ: Prentice-Hall, 1993.

[13] S. Haykin, Ed., *Advances in Spectrum Analysis and Array Processing*. Englewood Cliffs, NJ: Prentice-Hall, 1991.

[14] ——, *Array Signal Processing*. Englewood Cliffs, NJ: Prentice-Hall, 1985.

[15] R. Roy and T. Kailath, "ESPRIT—Estimation of signal parameters by rotational invariance techniques," *IEEE Trans. Acoust., Speech, Signal Processing*, vol. 37, July 1987.

[16] A. J. van der Veen, M. C. Vanderveen, and A. Paulraj, "Joint angle and delay estimation using shift-invariance techniques," *IEEE Trans. Signal Processing*, vol. 46, pp. 405–418, Feb. 1998.

[17] K. Pahlavan and A. Levesque, *Wireless Information Networks*. New York: Wiley, 1995.

[18] H. L. Van Trees, *Detection, Estimation, and Modulation Theory*. New York: Wiley, 1968, pt. I.

[19] R. Tingley and K. Pahlavan, "A comparison of two techniques for parameter estimation on an indoor radio channel," in *Proc. Wireless '99*, Calgary, AB, Canada, July 12–14, 1999.

[20] ——, "Measurement of the spatial and temporal propagation characteristics of an indoor radio channel using an antenna array," in *Proc. PIMRC 99*, Sept. 10, 1999.

[21] S. Haykin, *Adaptive Filter Theory*. Englewood Cliffs, NJ: Prentice-Hall, 1991.

[22] R. Tingley, "Space-time parameter estimation and statistical modeling of the indoor radio channel," Ph.D. dissertation, Worcester Polytechnic Inst., Worcester, MA.

Robert Tingley (M'94) received the M.S. and Dr. Phil. degrees in electrical engineering from Worcester Polytechnic Institute, Worcester, MA. He is currently a Communication System Engineer with the Charles Stark Draper Laboratory, Cambridge, MA, where he leads several programs engaged in the development of advanced communication and signal processing systems. His chief research interests include estimation and information theory, and computational electromagnetics.

Kaveh Pahlavan (M'79–SM'88–F'96) is a Professor of electrical and computer engineering and the Director of the Center for Wireless Information Networks Studies at the Worcester Polytechnic Institute, Worcester, MA. His recent research has been focused on indoor radio propagation modeling and analysis of the multiple-access and transmission methods for wireless local networks.

Dr. Pahlavan is the Editor-in-Chief and Founder of the *International Journal of Wireless Information Networks*, the principal author of the book *Wireless Information Networks*, and has contributed to more than 150 technical papers and two patents. He is a Fellow of the IEEE Communications Society and has been Program Chairman and Organizer of IEEE conferences and workshops.

Algorithms, Testbeds, and Performance

- A. Hatami and K. Pahlavan, In-building Intruder Detection for WLAN Access, The IEEE Aerospace and Electronic Systems Society conference, PLANS, Monterey, CA, April 2004.
- M. Kanaan and K. Pahlavan, A comparison of wireless geolocation algorithms in the indoor environment, Proceedings of the IEEE WCNC, April 2004.
- M. Kanaan and K. Pahlavan, CN-TOA a New Algorithm for Indoor Geolocation, IEEE PIMRC, Sep 2004.
- M. Heidari and K. Pahlavan, Performance Evaluation of Indoor Geolocation Systems Using PROPSim Hardware and Ray Tracing Software, IWWAN, Oulu, Finland, June, 2004.
- X. Li and K. Pahlavan, "Super-resolution TOA estimation with diversity for indoor geolocation", *IEEE Trans on Wireless Comm.*, Dec. 2003.
- X. Li and K. Pahlavan, M. Latva-aho, and M. Ylianttila, "Indoor Geolocation using OFDM Signals in HIPERLAN/2 Wireless LANs", IEEE PIMRC'2000, London, Sep. 2000.

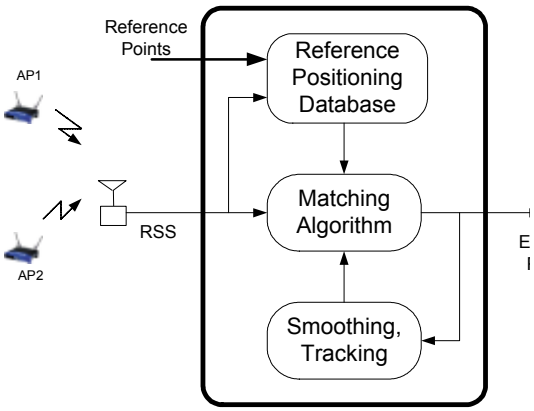

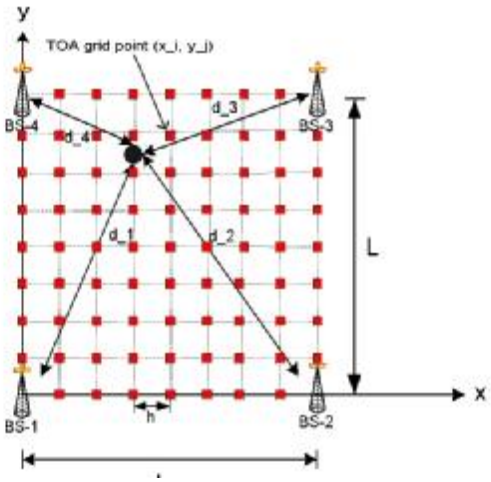

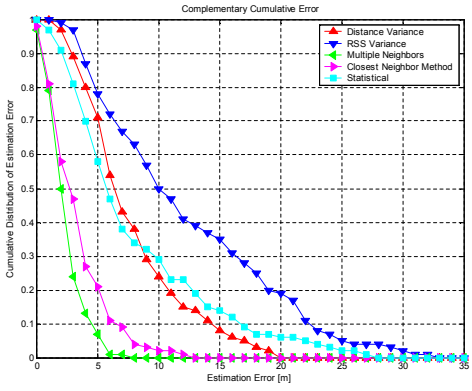

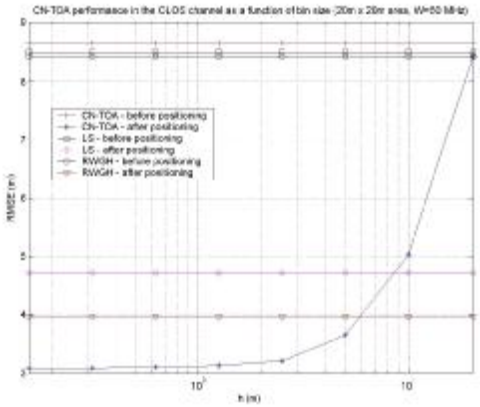

In-Building Intruder Detection for WLAN Access

Ahmad Hatami and Kaveh Pahlavan

Center for Wireless Information Network Studies

Worcester Polytechnic Institute (WPI)

hatami@wpi.edu , kaveh@ece.wpi.edu

Abstract -- In recent years wireless local area network (WLAN) has become a popular choice for local area networking in both enterprise and home networking. Increased data rate and price reduction in IEEE 802.11b-g devices has made WLANs even more attractive in these markets. User mobility has opened a new market for location aware, and pervasive computing applications. As a service to these new applications, security and user authentication plays a more important role in a wireless environment compared to the conventional wired systems. In the corporate WLAN environment, since a mobile wireless networks intruder can access the network without physical presence inside the buildings, the solutions for intruder detection has attracted considerable attention by the research community.

In this paper we first provide an overview of the traditional location sensing and intruder detection algorithms that are using the existing IEEE 802.11 infrastructure. Then we introduce a new algorithm targeted for intruder detection and authentication in a WLAN network. The new algorithm uses indoor radio propagation modeling to reduce complexity of the calibration process used in the existing algorithms. The performance of the existing and the new algorithm in the first floor of the Atwater Kent Laboratory at the Worcester Polytechnic Institute is used as a basis to compare the performances.

I. INTRODUCTION

WLAN made user mobility possible in a local area network, and proliferation of portable computers and hand held devices opened new paradigms in application domain. Location aware and pervasive computing are among these new applications [7]. In this paper our effort is to focus on two such applications in this class, positioning application, and intruder detection application.

Traditional methods for wireless positioning are based on time-of-arrival (TOA) or angle-of-arrival (AOA) measurements from several base stations (BS) and application of triangulation [10] [11]. The Global Positioning System (GPS) is the most widely used location-system in this class. Unfortunately, there are two limitations in GPS based systems. First, these systems do not provide good accuracy inside buildings and other scenarios in which there is no direct line-of-Site (LOS) between the mobile host (MH) and the base station BS [1] [13]. The second limitation is the fact that these systems require each MH to be equipped with an extra piece of hardware which increases the cost, weight, and power consumption of the device. Reference [2] introduced an alternative approach for locating a MH in a WLAN environment. In this method a MH measures the amount of power it receives (Received Signal Strength (RSS)) from each access point (AP). On the next step this data is matched against a well known database which maps a set of RSS values to some well known locations. Reference [3] – [8] enhance this method by applying various techniques which are described in the following sections.

Our implementation is based on RSS information coming from several IEEE 802.11b AP's. We used our ray tracing (RT) software to generate a reference database rather than using on site measurements.

In RSS based systems a MH estimates its location by using RSS from multiple AP's as a location dependent metric. This approach can be easily deployed on top of the existing network infrastructure without any cost for additional devices. There are three main approaches that can be used for using RSS in positioning systems. In the first approach one can use RSS in a path loss model to estimate the distance between a MH and a particular AP. In an ideal scenario MH needs three RSS values from three distinct access points to apply triangulation to determine its location. However, in indoor systems RSS is a highly variable metric, dependent on several known/unknown parameters such as multi-path, interference, local movements, etc. [1], which makes application of this approach very challenging.

The second approach is an exhaustive searching technique. In this approach the system has a stored database that maps location dependent metrics (in this case RSS) to some previously known physical locations (Reference Points). The MH uses RSS to find the closest set of mapping(s) in the database, and declares its location by interpreting this mapping(s) point(s). There are several flavors of this approach, [2], [9] are in this group.

The third approach is the combination of the first two methods in which RSS and triangulation is used to find some first hand estimations and then a set of reference points are used for interpolation. Reference [7] uses this approach.

All systems; using second and third methods; require a reference database as mentioned before. The reference database is a collection of reference points, acquired by on site measurements on various locations, this can be a costly process. The main difference between these systems is in their matching/mapping algorithms, which in turn affects performance of the system.

0-7803-8416-4/04/$20.00 ©2004 IEEE.

II. MATCHING ALGORITHMS USING RSS

The purpose of these algorithms is to search for an RSS vector; $(x'_1, x'_2, \ldots x'_k)$; received from *AP1-APk* in a reference database; containing n distinct reference points $R_1(x_{11}, x_{12\ldots}, x_{1k})$, $R_2(x_{21}, x_{22\ldots}, x_{2k})$, .. $R_n(x_{n1}, x_{n2\ldots}, x_{nk})$ (Signal Space) located at (rx_1, ry_1), (rx_1, ry_1)... (rx_n, ry_n) (Physical Space) respectively; extract the corresponding reference point(s), and declare the current location *L(x,y)* based on that. Note that in the most general case the mapping between signal space and physical space is not unique, in other words there might be several distinct physical locations with the same RSS profile.
In order to evaluate these algorithms we need to consider the following aspects of each algorithm.

Granularity: The reference database is a grid of known locations in which we need to store RSS values. A higher resolution database improves the accuracy of the location estimation.

Complexity: Although by applying more complex algorithms we can improve the performance of the system, but we need to bear in mind that these systems are to be used in a real time fashion in a wireless device with limited processing power.

Reliability and Fault Tolerance: WLAN systems are mostly used inside a building, in locally operated network. These networks are less reliable by nature. We need to make sure that a MH can estimate its location with reasonable accuracy in case of a failure of a single access point.

Deployment Costs and Scalability: The algorithm must be capable of managing increasing number of MH's without imposing any major costs.

Performance Parameters: Accuracy, delay, coverage area, and Capacity are among the metrics used in performance evaluations of different algorithms.

A. Least Mean Square (LMS)

This algorithm uses the Euclidean distance between a measured RSS vector $(x'_1, x'_2, \ldots x'_{kn})$ and the i'th database entry $R_i(x_{i1}, x_{i2\ldots}, x_{ik})$ given by:

$$D_i = \frac{1}{k}\left(\sum_{i=1}^{k}(x'_i - x_{ki})^2\right)^{1/2} \qquad (1)$$

as a metric to find the closest match point in the database $R_M(x_{M1}, x_{M2\ldots}, x_{Mk})$, and declares the corresponding point in the physical space (rx_M, ry_M) as the current location. Note that the outcome of minimum distance may not be unique. The major advantage of this algorithm is its relative simplicity.

B. Least Mean Square with History Monitoring

Reference [9] uses the fact that a MH does not move from a physical location to a different location arbitrarily. In other words, there is a correlation between the previous location of a MH and its current location. This correlation can be applied by restricting the matching process to the reference points where physical distance is not more than a specified value. This distance can be an adjustable system parameter. For a stationary or slow paced MH, moving at a speed of less than 1 m/s and a positioning sampling rate of 1 sec, this distance can vary in the range of 1-10 m depending on the granularity of the database. Some variation of this algorithm can improve the performance of simple LMS algorithm [9].

C. Least Mean Square with Multiple Point Matching (LMS-MP)

This algorithm picks W points closest database entries, instead of a single reference point. These points can be used in an interpolation scheme in order to improve positioning accuracy. Reference [4] eliminates $W-3$ of the farthest points, and declares the average of the remaining three reference points as the current location. In some cases this algorithm provides better accuracy.

D. Prioritized Maximum Power (PMP)

One major disadvantage of the LMS algorithm is the smearing effect introduced by summing all distance errors. The following example illustrates this fact.
The vector (1 , 2 , 0 , 0) has a Euclidean distance of 2 from both vectors $V1 = (1,0,0,0)$, and $V2 = (0,1,1,1)$. It is obvious that *V1* and *V2* are not similar at all, in fact they are perpendicular. Thus, a simple LMS metric can not distinguish between *V1* and *V2*.
We used a modification to the LMS algorithm which alleviates this problem and in some cases provides a better estimation, compared to simple LMS algorithm.
For a measured RSS vector $(x'_1, x'_2, \ldots x'_{kn})$ we sort $(x'_1, x'_2, \ldots x'_{kn})$ in descending order. In this way we can prioritize the contribution of each AP in our mapping scheme. If AP_i is the access point which has the maximum RSS, we restrict our mapping process to a set of reference points in which the corresponding RSS value for AP_i is maximum (*S1*). If the second dominant RSS value is coming from AP_j we restrict our mapping process to a set of reference points in *S1* in which the corresponding RSS value contributed by AP_j is maximum (*S2*). We continue the same process for all the other access points. If the final set is a null set we use the last non null set of points as candidates. At this point we can apply either simple LMS, or LMS-MP on this reduced set of reference points.

III. TEST-BED, SCENARIOS & APPLICATIONS

Our test-bed is located in the first floor of Atwater Kent (AKW1) building in Worcester Polytechnic Institute (WPI). AKW1 has dimensions of 65 meter by 48 meter including multiple rooms and labs. Our WLAN consists of four actual 802.11b access points (AP1- AP4), located on different points in the building. We added a fifth access point (AP5) in ray tracing simulations.

We created a grid with a resolution of one meter (Reference Points), and used ray tracing software to generate a location finger print (RSS form AP1-AP5) for all these points as a function of location. This creates a database of 6600 points with known locations both inside and outside of the building. Our assumption is that RSS varies in different locations depending on multi-path fading, interference, etc. In the data collection process we found both places in which a MH can receive a strong RSS from all the AP's and therefore result in a good reference point, and places with weak RSS from one or multiple AP's.

In upcoming scenarios we want to locate a MH using RSS information received from AP1-AP5, and mapping them to a reference point in our database for two different applications. The first application is positioning. In this application we want to find the exact location of a moving MH. The second application of interest is intruder detection, where we want to identify whether a MH is located inside the building or not rather than finding the exact location of the MH. For this purpose we have used both, measurement data collected by a laptop computer equipped with an 802.11b card, and simulation results of ray tracing software. We found that, by calibrating results of ray tracing we can get a good approximation of measurement data. Since RSS value is a function of several parameters, in our measurements we used four different samples in different directions and averaged the results. We conducted our experiments in two scenarios. In scenario I (Indoor-to-Indoor), MH moves along path P1 which is entirely located inside the building. Figure 1 shows this scenario. In scenario II (Indoor-to-Outdoor), MH moves along path P2. This path starts in an outdoor location and goes through both indoor and outdoor areas of the building. Figure 2 shows this path.

IV. PERFORMANCE EVALUATION USING EXPERIMENTAL RESULTS

In following sections we used positioning error as a random variable and provided complementary cumulative function (CCF) for that. Each point on these graphs CCF(X) represents the probability of a positioning error more than or equal to X meters.

A. PERFORMANCE IN INDOOR AREAS

Figure 3 shows the CCF for scenario I with one meter grid resolution for LMS and PMP algorithms in positioning application. It shows that LMS provides better accuracy since P1 is located inside the coverage area of one or more access points. We have included the same graph with different grid resolutions; Figure 4 shows that as we decrease the grid resolution in points where the error is less than 20 m PMP and LMS algorithms provide comparable results. We observed that LMS or other variations of that can provide a reasonable accuracy when MH moves inside the coverage area. Figure 5 shows the probability of error in intruder detection application for scenario I for both algorithms vs. different grid resolutions. Based on our observations LMS provides better performance in this application as well.

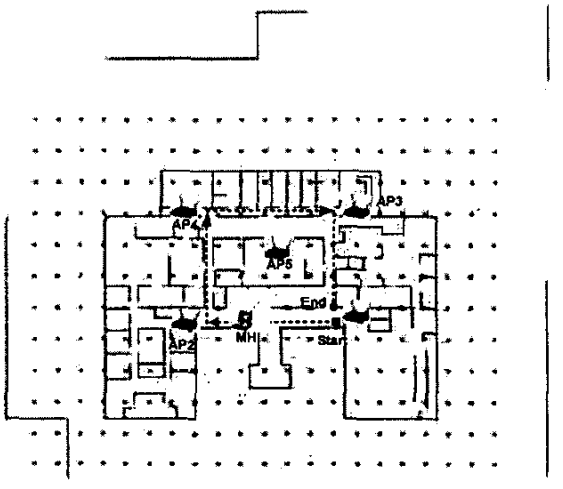

Figure 1: MH moving along P1

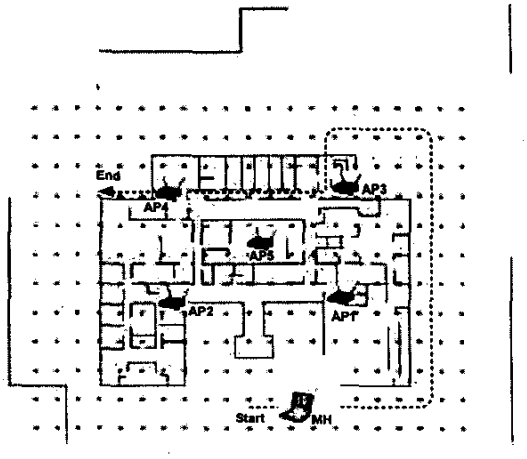

Figure 2: MH moving along P2

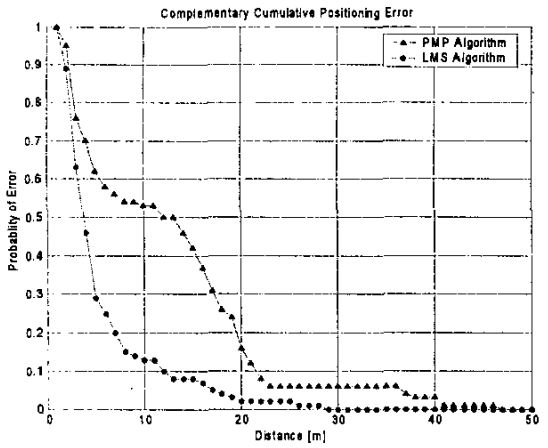

Figure 3: Grid Resolution = 1 [m] (MH moving along P1)

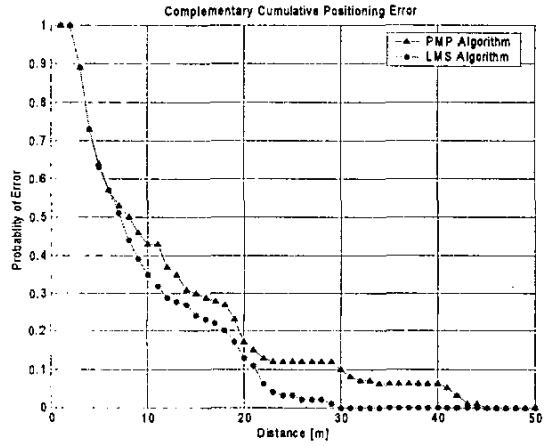

Figure 4: Grid Resolution = 10 [m] (MH moving along P1)

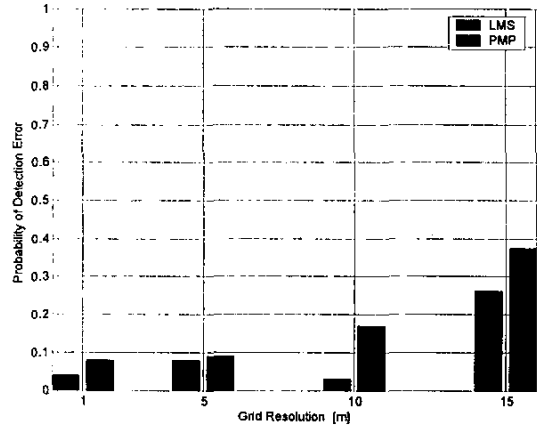

Figure 5: Probability of Detection Error in Intruder Detection Scenario (MH moving along P1)

B. PERFORMANCE IN INDOOR-OUTDOOR AREAS

Figure 6 and Figure 7 show CCF of positioning error when MH moves along path P2 for five and ten meters grid resolution respectively. One major point in on these graphs is the lower accuracy of position estimation, compared to scenario I. The second interesting observation is the similarity between the performance of PMP and LMS algorithms for a high resolution grid. As we decreased the grid resolution we observed that the performance of PMP did not change much, and sometimes even improved. On the other hand performance of LMS algorithm decreased significantly as we reduced grid resolution. This shows that PMP has lower sensitivity to grid resolution compared to LMS in positioning application. Probability of error in intruder detection application is depicted in Figure 8. This figure shows that LMS provides a lower error in intruder detection application compared to PMP, despite its poor location estimation.

Grid resolution determines the number of on site measurements needed. By increasing the grid resolution we can increase the estimation accuracy. This improved performance increases measurement costs and also, a finer grid translates to a larger reference database which in turn dictates more processing power in MH. Grid resolution is one of the major design parameters to be selected during deployment. Figure 9 shows that when MH moves along P1 (inside the coverage area) by increasing grid resolution we can locate it more accurately, as expected. On the other hand Figure 10 ;which is a similar graph for scenario II; shows that increasing grid resolution does not always guarantee higher accuracy.

In WLAN deployments, another major design parameter is the number of access points and their locations. This has a major impact on coverage area, number of hosts, quality of service (QOS) etc. In our experiments, we found that the number of available access points has an effect on estimation accuracy. Figure 11 shows this behavior. As a design guideline we need to use enough number of access points to be able to achieve the desired fault tolerance. Figure 11 and Figure 12 show the impact of number of access points in both applications.

V. CONCLUSIONS

In this paper we discussed positioning application and intruder detection application in WLAN's. We showed that by using the existing wireless infrastructure we can develop these applications without adding any specialized hardware. We discussed about existing positioning systems and their limitations and presented the following enhancements to improve performance.

1. In our RSS based system we used RT software rather than on site measurement, this can be a major cost reduction in a large deployment.

2. We introduced PMP algorithm for positioning algorithm which provides a better performance compared to LMS in positioning application for locations outside the coverage area.

3. We showed that PMP is less susceptible to grid resolution.

4. LMS does not provide accuracy in positioning applications when MH resides outside the coverage area, but it can detect an intruder with a good precision.

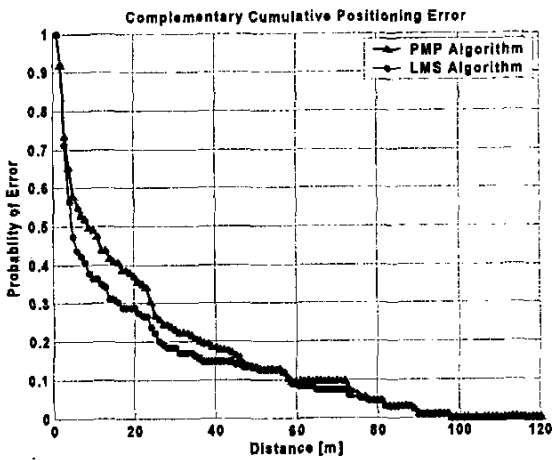

Figure 6: Grid Resolution = 1 [m] (MH moving along P2)

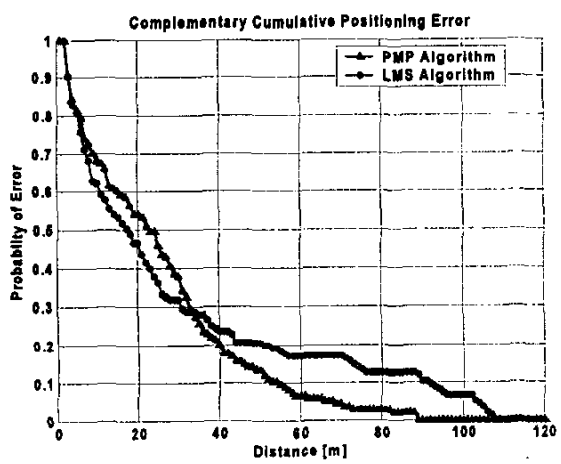

Figure 7: Grid Resolution = 10 [m] (MH moving along P2)

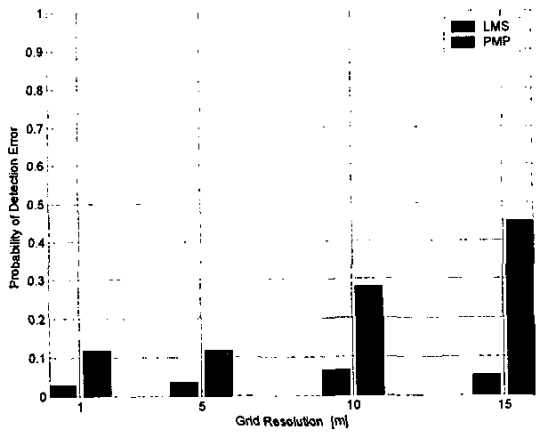

Figure 8: Probability of Detection Error in Intruder Detection Scenario (MH moving along P2)

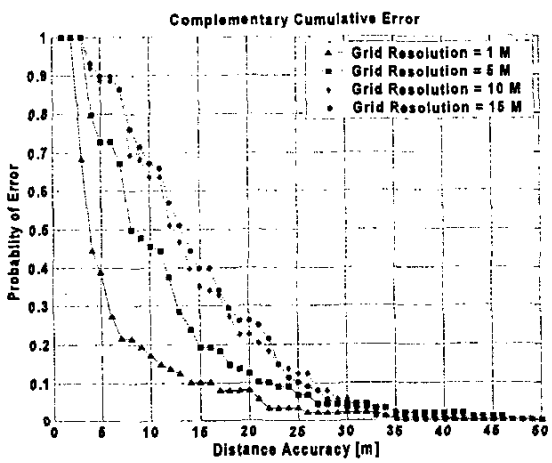

Figure 9: Effect of Grid Resolution in Positioning Accuracy for LMS Algorithm (MH moving along P1)

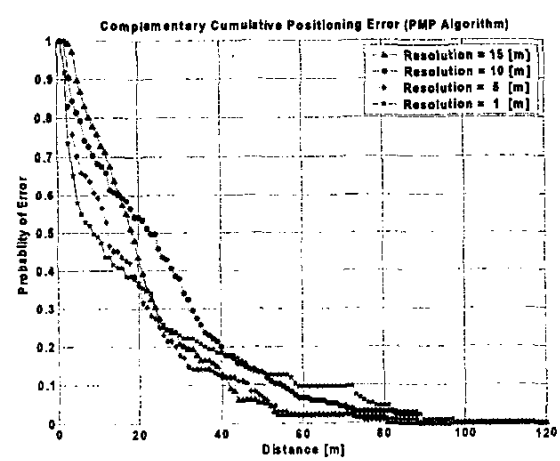

Figure 10: Effect of Grid Resolution in Positioning Accuracy for LMS Algorithm (MH moving along P2)

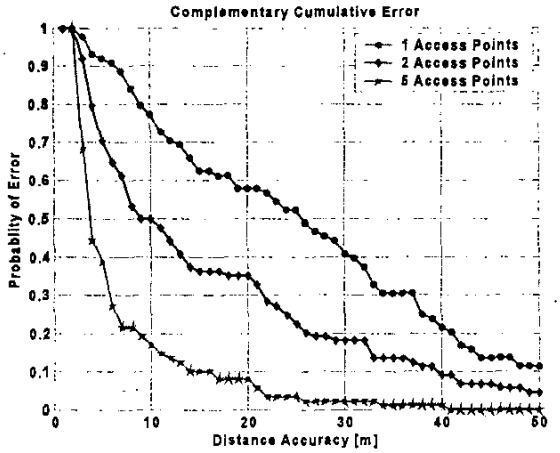

Figure 11: Effect of Number of AP's in Positioning Application (MH moving along P1)

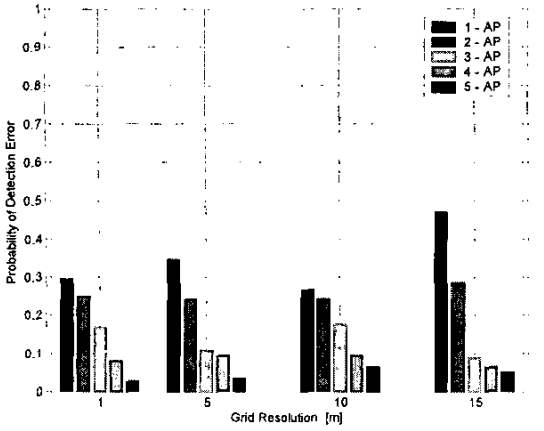

Figure 12: Effect of Number of AP's on Detection Error in Intruder Detection Application (MH moving along P2)

REFRENCES

[1] K. Pahlavan and A. Levesque, *Wireless Information Networks*, John Wiley & Sons, 1995.

[2] P. Bahl and V.N. Padmanabhan, "RADAR: An In-Building RF-Based User Location and Tracking system," Proc. IEEE INFOCOM 2000, Vol. 2, pp. 775-784, Tel-Aviv, Israel, March 2000

[3] P. Bahl and V.N. Padmanabhan, "RADAR: An In-Building RF-Based User Location and Tracking system," Proc. IEEE INFOCOM 2000, Vol. 2, pp. 775-784, Tel-Aviv, Israel, March 2000

[4] P. Prasithsangaree, P. Krishnamurthy, P.K. Chrysanthis, "On Indoor Position Location with Wireless LANs", The 13th IEEE International Symposium on , Volume: 2 , 15-18 Sept. 2002

[5] P. Bahl, V.N. Padmanabhan, and A. Balachandran, "Enhancements to the RADAR User Location and Tracking system," Technical Report MSR-TR-00-12 Microsoft Research, February 2000

[6] Teemu Roos, Petri Myllymaki, Henry Tirri, Pauli Miskangas, and Juha Sievanen, "A Probabilistic Approach to WLAN User Location Estimation", International Journal of Wireless Information Networks, Vol. 9, No. 3, July 2002

[7] Asim Smailagic and David Kogan, "Location Sensing And Privacy In a Context-Aware Computing Environment", IEEE Wireless Communications, Oct. 2002

[8] Teemu Roos, Petri Myllymaki, and Henry Tirri, "A Statistical Modeling Approach to Location Estimation", IEEE Transactions on mobile computing, Vol. 1, No. 1, Jan.-Mar. 2002

[9] Vijay Abhijit, Carla Ellis, and Xiaobo Fan, "Experiences with an Inbuilding Tracking System: Uhuru", PIMRC 2003

[10] Josep Vidal, Montse Najar, Marga Cabrera, and Rene Jativa, "Positioning Accuracy when Tracking UMTS Mobiles in Delay & Angular Dispersive Channels", IEEE Proc. VTC, 2001

[11] Rene Jativa, and Josep Vidal "First Arrival Detection for Positioning in Mobile Channels", IEEE PIMRC, 2002

[12] A. Smailagic, and D. P. Siewiorek, "User-Centered Interdisciplinary Design of Wearable Computers", ACM Mobile Comp. And Comm. Rev., Vol. 3, no. 3, 1999

[13] K. Pahlavan and P. Krishnamurthy, *Principles of WirelessNetworks — A Unified Approach*, Prentice Hall, 2002.

A comparison of wireless geolocation algorithms in the indoor environment

Muzaffer Kanaan
Technology Organization
Verizon Communications
Waltham, MA, 02451, USA
muzaffer.kanaan@verizon.com

Kaveh Pahlavan
Center for Wireless Information Network Studies
Worcester Polytechnic Institute
Worcester, MA 01609, USA
kaveh@wpi.edu

***Abstract*—This paper presents a quantitative comparison of various geolocation algorithms for the indoor wireless environment. Using models recently developed for time-of-arrival (TOA) distance measurement errors in the indoor environment, we characterize the performance of standard least-square (LS), closest-neighbor (CN), and the residual weighting (RWGH) algorithms in Line-of-Sight (LOS), Obstructed LOS (OLOS), and mixed LOS/OLOS channel conditions. We also evaluate the performance of these algorithms in relation to the size of the indoor area over which a user is to be located.**

Keywords-geolocation, wireless networks, indoor, positioning

I. INTRODUCTION

In recent years, there has also been a lot of interest in the geolocation problem for the indoor setting. The applications range from commercial and residential (for example, to track people with special needs, or the elderly in nursing homes), to public safety and military applications (for example, to track inmates in prisons, or navigating policemen, firefighters and soldiers to help them complete their missions) [1]. Because of this, the characterization of the performance of geolocation algorithms is an important issue.

Geolocation systems all depend on an arrangement of base stations (such as in Fig 1 below) performing distance measurements to a user to be located. These measurements can be performed in a variety of ways, such as Angle of Arrival (AOA), Time of Arrival (TOA), or Received Signal Strength (RSS) [1]. Of these, the TOA technique is the most popular for accurate geolocation systems. As the name implies, TOA-based systems use the time of arrival of the first path to estimate distance. However, the unique nature of the indoor propagation environment creates certain challenges in estimating the TOA of the first path accurately [2].

Historically, performance characterization of geolocation systems in the indoor environment has been complicated by the fact that there were no models available for distance measurement errors. Recently, some new models have been developed to address this issue ([3], [4]). These models are based on TOA-estimation techniques, and have characterized the distance errors as a function of the bandwidth of the system used to gather TOA measurements, and in the presence of Line-of-Sight (LOS), and Obstructed LOS (OLOS) propagation conditions. The fundamental contribution of this paper is to characterize the performance of Least-Squares (LS), Closest-Neighbor (CN), and the Residual Weighting (RWGH) algorithms in the presence of these models.

The rest of this paper is organized as follows. Section II undertakes a description of the algorithms used. Section III is devoted to a discussion of the distance error models. Section IV presents results of the performance evaluation. Section V concludes the paper.

II. DESCRIPTION OF THE ALGORITHMS

A. Closest-Neighbor (CN) Algorithm

Consider a group of base stations (BSs), arranged in a regular grid, such as the one shown in Fig.1. In such a scenario, each base station is located at L meters away from its adjacent BSs. In order to locate a particular user, each BS would perform a distance measurement to that user. Let d_i be the distance measurement performed by base station i, which is located at $\boldsymbol{R}_i = [x_i, y_i]^T$. The CN algorithm estimates the location of the user, $\boldsymbol{R}_{est}$, as the location of the BS that is located closest to that user. In other words, $\boldsymbol{R}_{est}$ is that value of $\boldsymbol{R}_i$ for which the corresponding distance measurement, d_i, is the minimum in the set. For example, in Fig 1, the location of the user would be determined as the location of BS 4.

B. Least-Squares (LS) Algorithm

The LS algorithm is fundamentally focused on minimizing the value of the objective function, $f(\mathbf{x})$, usually formulated as:

$$f(\mathbf{x}) = \sum_{i=1}^{N} \left(\sqrt{(x - x_i)^2 + (y - y_i)^2} - d_i \right)^2 \quad (1)$$

where N is the number of reference base stations. The square-root term is readily recognized as the distance between a point (x, y) in the Cartesian coordinate system, and a reference base station located at (x_i, y_i). The difference in the parentheses is commonly called the *residual* of the estimate. Of course, at the true location of the user, each of terms within the summation would be identically zero, such that $f(\mathbf{x}) = 0$. However, in practice, the set of distance measurements, d_i ($1 \le i \le N$), contains some errors, such that the summation in equation (1)

will never be identically zero. The sources of these errors are basically two-fold: systematic (such as those related to synchronization mismatch between a transmitter and receiver), and channel-related (such as those due to Obstructed LOS (OLOS) channel conditions). In this paper, we assume that the systematic errors in the distance measurements are negligible, and that the dominant source of errors is the channel. OLOS channel conditions generally result in the strongest signal being received with longer delay, with the resulting distance measurement being longer than it should be. Under such circumstances, a solution (*x, y*) can be found, which minimizes the value of $f(\mathbf{x})$ in a least-squares sense. For this paper, we used a least-squares algorithm developed by Davidon [5] to minimize $f(\mathbf{x})$, which we discuss below.

The Davidon algorithm is a computationally efficient least-squares algorithm that is based on the Newton-Raphson method, and belongs in the general category of quasi-Newton methods [6]. The Davidon algorithm searches for the point minimizing (1) (generally denoted as the vector, **x**) in an iterative manner, as defined by the equation:

$$\mathbf{x}_{k+1} = \mathbf{x}_k - \mathbf{H}_k \mathbf{g}(\mathbf{x}_k) \quad (2)$$

where $\mathbf{H}_k$ represents an approximation to the inverse of the Hessian of $f(\mathbf{x})$, $\mathbf{G}(\mathbf{x})$, whose elements are defined as:

$$G_{jk}(x_1, x_2, \ldots x_N) \equiv \frac{\partial^2 f(x_1, x_2, \ldots x_N)}{\partial x_j x_k} \quad (3)$$

and $\mathbf{g}(\mathbf{x})$ is the gradient of $f(\mathbf{x})$, defined as:

$$\mathbf{g}(\mathbf{x}) = \nabla f(\mathbf{x}) \quad (4)$$

As can be seen from (3), $\mathbf{G}(\mathbf{x})$ is a matrix of second derivatives. It can be shown that $\mathbf{G}(\mathbf{x})$ is both symmetric, and positive-definite. However, computing the Hessian and its inverse at every iteration point (as the Newton-Raphson method generally requires) can be computationally prohibitive. Therefore, the Davidon algorithm tries to construct an approximation to it. Of course, in doing this, one would have to ensure that the approximation, $\mathbf{H}_k$, stays both symmetric and positive-definite from one iteration to the next. To accomplish this, $\mathbf{H}_k$ is updated according to the equation:

$$\mathbf{H}_{k+1} = \mathbf{H}_k + \frac{\lambda_k - 1}{\rho_k} \mathbf{r}_k \mathbf{r}_k^T \quad (5)$$

where:

$$\mathbf{r}_k = \mathbf{H}_k \mathbf{g}(\mathbf{x}_{k+1}) \quad (6)$$

and

$$\rho_k = \left(\mathbf{g}(\mathbf{x}_{k+1})\right)^T \mathbf{H}_k \left(\mathbf{g}(\mathbf{x}_{k+1})\right) = \mathbf{r}_k^T \mathbf{g}(\mathbf{x}_{k+1}) \quad (7)$$

Equation (7) is readily recognized as a quadratic form. Therefore, as long as $\mathbf{H}_k$ is positive-definite, ρ_k will be greater than zero, and will be zero only if $\mathbf{g}(\mathbf{x})$ is zero. As such, (7) is often used as an explicit stopping criterion for the algorithm. Of course, in practice, ρ_k will never be identically zero, but can be compared to some small tolerance value, ε, so that computations stop when $\rho_k \le \varepsilon$.

All this leaves us with the task of setting λ_k, which is somewhat more complex. As can be inferred from (5), this quantity is of central importance in ensuring that the $\mathbf{H}_k$ matrices remain positive-definite throughout successive iterations. It can be shown ([5]) that:

$$\lambda_k = \frac{\gamma_k}{\gamma_k + 1} \quad (8)$$

where:

$$\gamma_k \equiv -\frac{\mathbf{r}_k^T \mathbf{g}(\mathbf{x}_k)}{\rho_k} \quad (9)$$

Choosing λ_k in accordance with (8) and (9) generally ensures that $\mathbf{H}_k$ remains positive-definite from one iteration to the next, unless $\gamma_k = -1$. Because of this possibility, the Davidon algorithm provides a slightly different way of mapping γ_k values to λ_k values. Specifically, two numbers, and , are defined. The values of these can be picked at will. Then, the Davidon algorithm defines the following transformation:

$$\Lambda(\gamma) = \begin{cases} \alpha & -\dfrac{\beta}{\beta+1} < \gamma < \dfrac{\alpha}{1-\alpha} \\ \beta & -\dfrac{\beta}{\beta-1} < \gamma < \dfrac{\beta}{\beta+1} \\ \dfrac{\gamma}{\gamma+1} & \text{elsewhere} \end{cases} \quad (10)$$

C. *Residual Weighting (RWGH) Algorithm*

The RWGH algorithm has been investigated in [7], and [8] as a way of mitigating the effects of errors in distance measurements brought about by OLOS channel conditions. Although originally formulated in the context of geolocation in terrestrial cellular systems, this algorithm was included in this study to evaluate its performance in an indoor setting, and can be basically viewed as a form of weighted least-squares algorithm.

The fundamental concept behind this algorithm is as follows: since OLOS channel conditions introduce errors that are strictly positive, distance measurements corrupted by OLOS errors would give rise to location estimates with higher residuals than would be the case with no OLOS errors. Therefore, if the number of distance measurements is greater than the minimum required (which, for a TOA-based system, is three), then the distance measurements can be grouped in various ways and intermediate LS estimates derived from those sub-groups. Some of these intermediate estimates would have lower residuals than others. The final estimate of the location can then be formed as a linear combination of these intermediate estimates, with each intermediate estimate weighted by the inverse of its associated residual. This means that, in the computation of the final estimate, those

intermediate estimates with lower residuals would be assigned more weight. In this manner, the overall accuracy of the location estimate can be improved. Specifically, given M ($M > 3$) distance measurements, the algorithm calls for the formation of N different distance measurement combinations, where

$$N = \sum_{i=3}^{M} \binom{M}{i} \quad (11)$$

with each combination being represented by an index set $\{S_k \mid k = 1,2,.....N\}$. An intermediate LS estimate is then computed for each set of measurements. Note that the sets S_k will not necessarily all be of the same size. Therefore, the residuals in the intermediate LS estimates may depend on the size of the set. In order to remove this dependence, a *normalized* residual is computed for every intermediate estimate, $\mathbf{x}_k'$, as:

$$\tilde{R}_{es}(\mathbf{x}'_k, S_k) = \frac{R_{es}(\mathbf{x}'_k, S_k)}{\text{size of } S_k} \quad (12)$$

The final estimate, $\mathbf{x}'$, can then be computed as:

$$\mathbf{x}' = \frac{\sum_{k=1}^{N} \mathbf{x}'_k \left(\tilde{R}_{es}(\mathbf{x}'_k, S_k) \right)^{-1}}{\sum_{k=1}^{N} \left(\tilde{R}_{es}(\mathbf{x}'_k, S_k) \right)^{-1}} \quad (13)$$

III. OVERVIEW OF THE CHANNEL MODELS

The behavior of the channel under LOS and OLOS conditions is very different. Within the context of the geolocation problem, the different channel conditions can introduce different amounts of errors to the distance measurements. This, in turn, affects the accuracy of the final location estimate. We assume the following model for the distance measurement errors. Let $d_{a,i}$ represent the actual distance of the user from base station *i,* assuming no systematic or channel-related errors. The distance measurement, as reported by base station i in the presence of errors, can be modeled using the equation:

$$d_i = d_{a,i}(1+\eta) \quad (14)$$

where η is a random variable, whose distribution depends on the particular channel scenario [4]. Specifically, it has been shown that, for the LOS case, η has a Gaussian distribution with a zero mean, and a variance that depends on the system bandwidth used to make the distance measurements. For the OLOS case, it has been shown that η has a hybrid distribution, which is a linear combination of Gaussian and exponential distributions, with the parameters again being a function of the system bandwidth. This paper uses the parameters as specified in [4] for the performance evaluations.

IV. PERFORMANCE EVALUATION

The performance of the three algorithms described in section II is evaluated through simulations. The regular grid arrangement of four base stations is assumed, as shown in Fig 1. A number of random user locations are simulated. Each of the BSs performs a distance measurement to that user, which are corrupted, in accordance with (14), and using the particular distribution for η [4]. Three different channel scenarios are simulated: LOS, OLOS, and mixed LOS/OLOS. The mixed LOS/OLOS scenario is simulated using a binomial random variable, such that the channel is likely to be LOS with probability p, and OLOS with probability $1-p$. The results are presented for the case of p = 0.3. System bandwidths in the range of 50 – 1000 MHz are considered for the distance error models, as given in [4]. The performance metric is the average estimation error, E_{av}, defined as:

$$E_{av} = E\{|\mathbf{R}_{est} - \mathbf{R}_{act}|\} \quad (15)$$

where $\mathbf{R}_{act}$, and $\mathbf{R}_{est}$ are the actual and estimated locations of a user.

The first set of simulation results (Figures 2 through 4), show a comparison of the LS and RWGH algorithms for LOS, OLOS and mixed LOS/OLOS scenarios. These results have been obtained over a 15m x 15m area. The corresponding results for the CN algorithm are not shown, since this algorithm will have large estimation errors associated with it due to its simplicity. For this reason, the authors feel that directly comparing CN with LS and RWGH in this context is not necessarily fair. The next set of results (Fig 5) presents a performance comparison for the CN algorithm for the three channel scenarios in a 15m x 15m area. The rest of the results compare the performance of the three algorithms in a 15m x 15m area, versus 30m x 30m area (LS in Figs. 6 through 8, RWGH in Figs. 9 through 11, and CN in Figs. 12 through 14), for all the three different channel scenarios.

On the basis of the results presented in Figs. 6 through 14, an *average degradation factor*, K_{av}, has been calculated for all the three algorithms within each channel scenario. These values are shown in Table I, and are calculated as follows. For a given algorithm, and channel scenario, the ratio of E_{av} values at 30m x 30m to the values for 15m x 15m are calculated for each measurement bandwidth value. K_{av} is then calculated as the average of all the ratio values. Essentially, K_{av} allows an insight into the amount of performance degradation (i.e. reduction in estimation accuracy indicated by the increase in E_{av}) that can be expected as the size of the area is increased. The exact amount of performance degradation will, of course, vary as a function of the system bandwidth; nevertheless, K_{av} will be helpful in giving a rough idea.

TABLE I. AVERAGE DEGRADATION IN ESTIMATION ACCURACY

Algorithm	Channel Scenario	K_{av}
LS	LOS	2.011
	OLOS	2.048
	MIXED LOS/OLOS	2.052
RWGH	LOS	2.024
	OLOS	1.920
	MIXED LOS/OLOS	1.897
CN	LOS	2.002
	OLOS	1.991
	MIXED LOS/OLOS	1.991

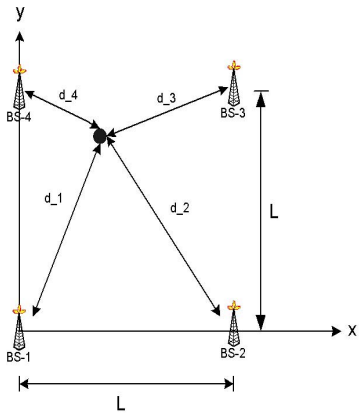

Figure 1. The basic configuration for a geolocation system

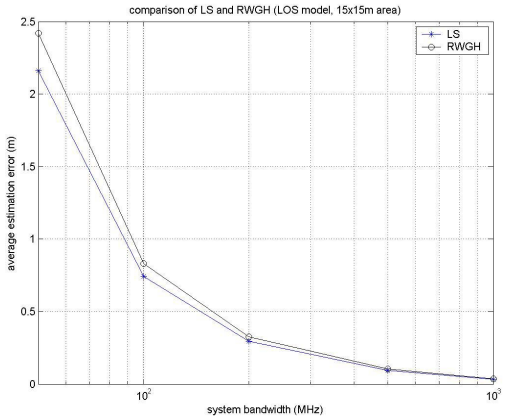

Figure 2. LS/RWGH comparison for LOS channel

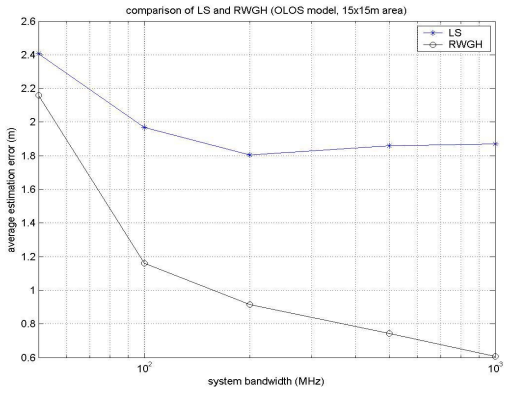

Figure 3. LS/RWGH comparison for OLOS channel

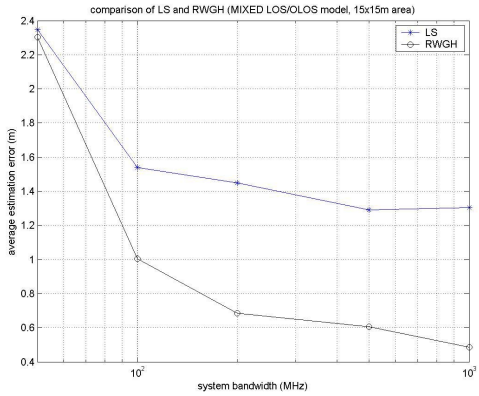

Figure 4. LS/RWGH comparison for mixed LOS/OLOS channel

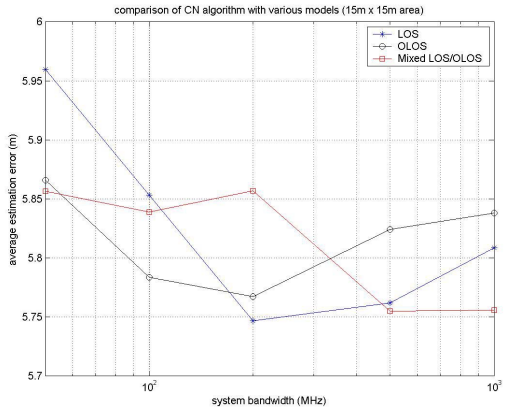

Figure 5. CN comparison for the three channel scenarios

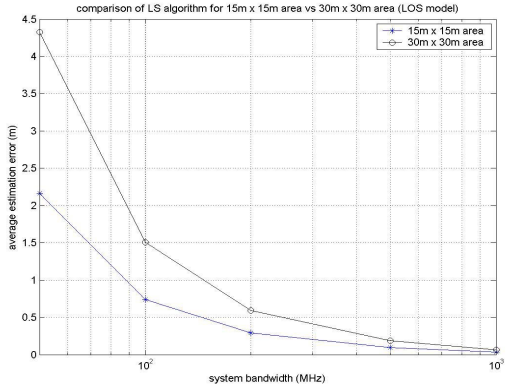

Figure 6. LS comparison in LOS case (area increase)

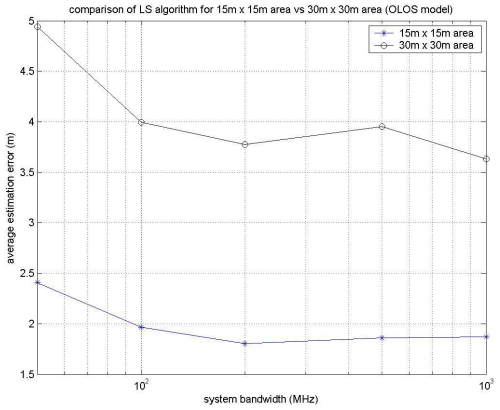

Figure 7. LS comparison in OLOS case (area increase)

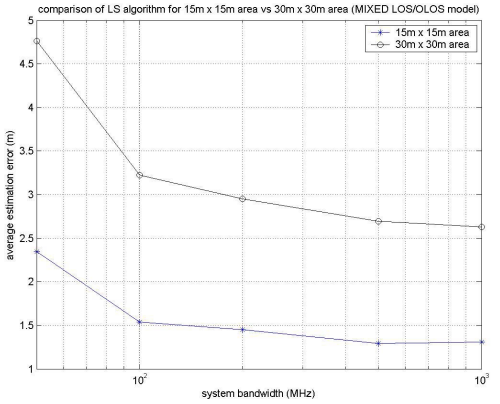

Figure 8. LS comparison in mixed LOS/OLOS case (area increase)

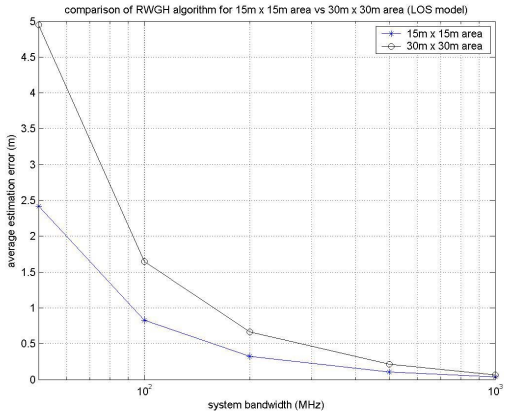

Figure 9. RWGH comparison in LOS case (area increase)

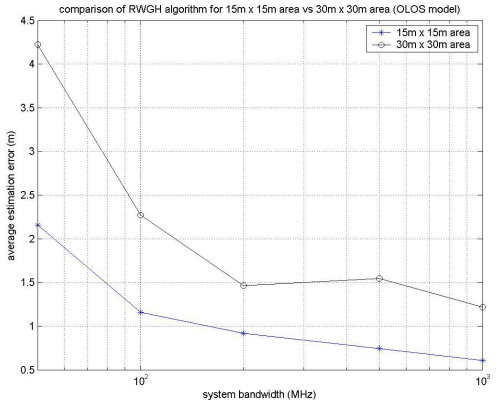

Figure 10. RWGH comparison in OLOS case (area increase)

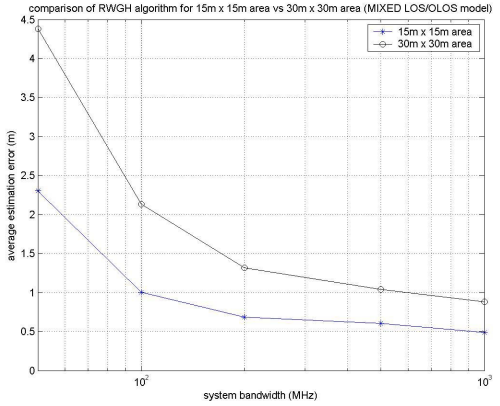

Figure 11. RWGH comparison in mixed LOS/OLOS case (area increase)

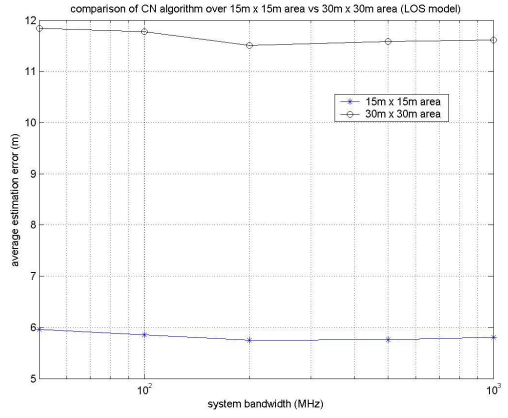

Figure 12. CN comparison in LOS case (area increase)

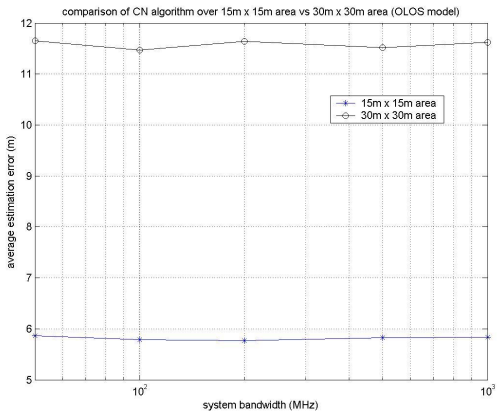

Figure 13. CN comparison in OLOS case (area increase)

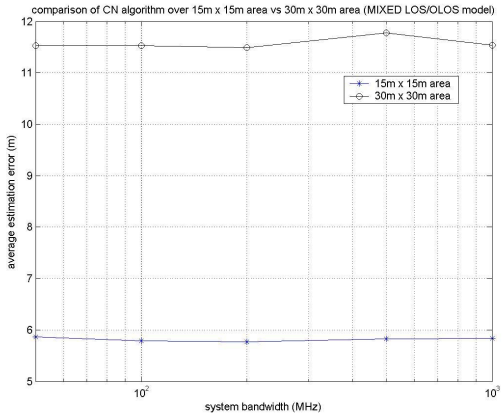

Figure 14. CN comparison in mixed LOS/OLOS case (area increase)

V. CONCLUSIONS

Based on the results presented in the previous section we can draw a number of conclusions:

1. Regardless of the particular type of channel scenario, the CN algorithm has the worst performance of the three algorithms considered. This is expected, since the algorithm provides an estimate that is only as accurate as the location of the BS that is closest to the user.
2. The difference in performance between the LS and RWGH algorithms rapidly diminishes beyond a measurement bandwidth of 100 MHz, for the LOS case. In other words, as long as the system bandwidth is above 100 MHz, RWGH provides no additional advantage from a performance perspective in the LOS case. For the OLOS and mixed LOS/OLOS cases, however, the performance of RWGH is significantly better than that of LS algorithm. This point is currently under further investigation.
3. Based on the distance error model parameters considered in this paper, it can be said that increasing the size of the area over which a user is to be located (while keeping the number and location of BSs fixed) makes the resulting location estimates less accurate. This point makes intuitive sense, in that as the area gets larger, the LOS paths from the BS to the user will suffer more path loss, and the OLOS paths will suffer more delay (due to multipath). These factors will affect the TOA measurements, and therefore, the distance measurements that a given BS will make. From the results given in Table I, it can be seen that a four-fold increase in the size of the area translates to an approximately two-fold increase in estimation error, regardless of the algorithm, and the particular channel scenario.

ACKNOWLEDGMENT

The authors would like to thank Bardia Alavi and the rest of their colleagues at the Center for Wireless Information Network Studies for the many helpful discussions regarding this paper. In addition, the principal author would like to thank one of his former colleagues, Dr. David F. Freeman, for his help regarding the Davidon LS algorithm. Verizon Communications did not sponsor, participate in, or provide technical guidance/review of, the work reported in this paper.

REFERENCES

[1] K. Pahlavan, X. Li, J. Mäkelä, "Indoor geolocation science and technology", IEEE Communications Magazine, pp. 112-118, February 2002.

[2] K. Pahlavan, P. Krishnamurthy, J. Beneat, "Wideband radio propagation modeling for indoor geolocation applications", IEEE Communications Magazine, pp. 60-65, April, 1998.

[3] B. Alavi, K. Pahlavan, "Modeling of the distance error for indoor geolocation", Proceedings of the IEEE Wireless Communications and Networking Conference (WCNC), 2003, vol. 1, pp. 668-672, March, 2003.

[4] B. Alavi, K. Pahlavan, "Bandwidth effect on distance error modeling for indoor geolocation", Proceedings of the IEEE Personal Indoor Mobile Communications Conference (PIMRC), 2003.

[5] W.C. Davidon, "Variance algorithm for minimization", Computer Journal, Vol. 10, pp. 406-410, 1968.

[6] R. Fletcher, Practical Methods of Optimization, John Wiley & Sons, 1987.

[7] P-C. Chen, "Mobile position location estimation in cellular systems", PhD Thesis, WINLAB, Electrical and Computer Engineering Dept., Rutgers University, 1999.

[8] P-C. Chen, "A non-line-of-sight error mitigation algorithm in location estimation", Proceedings of the IEEE Wireless Communications and Networking Conference, 1999.

CN-TOAG: A NEW ALGORITHM FOR INDOOR GEOLOCATION

Muzaffer Kanaan

Technology Organization
Verizon Communications
Waltham, MA, 02451, USA
muzaffer.kanaan@verizon.com

Kaveh Pahlavan

Center for Wireless Information Network Studies
Worcester Polytechnic Institute
Worcester, MA 01609, USA
kaveh@wpi.edu

***Abstract*—This paper presents the CN-TOAG (Closest-Neighbor with TOA grid) algorithm, a new geolocation algorithm, which presents certain performance improvements in the indoor environment. We describe this algorithm, and quantitatively compare its performance to the standard Least-Squares (LS), as well as weighted least-squares (RWGH) algorithms in the presence of Obstructed LOS (OLOS) channel conditions. The results indicate that the CN-TOAG algorithm can outperform the other two algorithms in the indoor environment.**

Keywords-geolocation, wireless networks, indoor, positioning

I. INTRODUCTION

In recent years, there has also been a lot of interest in the geolocation problem for the indoor setting. The applications range from commercial and residential (for example, to track people with special needs, or the elderly in nursing homes), to public safety and military applications (for example, to track inmates in prisons, or navigating policemen, firefighters and soldiers to help them complete their missions) [1]. Because of this, the characterization of the performance of geolocation algorithms is an important issue.

Geolocation systems all depend on an arrangement of base stations (such as in Fig 1 below) performing range measurements to a user to be located. These measurements can be performed in a variety of ways, such as Angle of Arrival (AOA), Time of Arrival (TOA), or Received Signal Strength (RSS) [1]. Of these, the TOA technique is the most popular for accurate geolocation systems. As the name implies, TOA-based systems use the time of arrival of the first path to estimate range. However, the unique nature of the indoor propagation environment creates certain challenges in estimating the TOA of the first path accurately [2].

Historically, performance characterization of geolocation systems in the indoor environment has been complicated by the fact that there were no models available for range measurement errors. Recently, some new models have been developed to address this issue ([3], [4]). These models are based on TOA-estimation techniques, and have characterized the range errors as a function of the bandwidth of the system used to gather TOA measurements, and in the presence of Line-of-Sight (LOS), and Obstructed LOS (OLOS) propagation conditions.

Given the propagation conditions (as embodied in the range measurement error models), one can then develop algorithms for estimating the location of a user accurately. This paper proposes a new algorithm, known as CN-TOAG (Closest-Neighbor with TOA grid), and compares its performance to standard as well as weighted least-squares methods.

The rest of this paper is organized as follows. Section II undertakes a description of the algorithms used. Section III is devoted to a discussion of the ranging error models. Section IV presents results of the performance evaluation. Section V concludes the paper.

II. DESCRIPTION OF THE ALGORITHMS

A. *Closest-Neighbor with TOA Grid (CN-TOAG) Algorithm*

Before discussing the CN-TOAG algorithm, it would be instructive to review the standard Closest-Neighbor (CN) algorithm.

Consider a group of base stations (BSs), arranged in a regular grid, such as the one shown in Fig.1. In such a scenario, each base station is located at L meters away from its adjacent BSs. In order to locate a particular user, each BS would perform a range measurement to that user. We let d_i denote the range measurement performed by base station i, which is located at $\boldsymbol{R}_i = [x_i, y_i]^T$, and denote the set of range measurements performed by each BS by $\mathbf{D}$. The CN algorithm estimates the location of the user, $\boldsymbol{R}_{est}$, as the location of the BS that is located closest to that user. In other words, $\boldsymbol{R}_{est}$ is that value of $\boldsymbol{R}_i$ for which the corresponding range measurement, d_i, is the minimum in the set. For example, in Fig 1, the location of the user would be determined as the location of BS 4.

The CN-TOAG algorithm is a variation of this idea. Specifically, with the CN-TOAG algorithm, the whole area covered by the array of BSs is divided into a grid of points, with each point being equidistant from each of its adjacent neighbors, as shown in Fig. 2. As can be seen, this is equivalent to subdividing the area covered by the array of BSs into equal-sized squares of size h meters. There is a set of range measurements associated with each point on the grid, one from each base station. In our current example, since there are four BSs involved, each point, (x_i, y_j), on the grid has a vector of four range measurements associated with it. We denote such a vector of range measurements associated with a particular point on the grid by $\boldsymbol{r}_{ij}$, and call it the *range signature* associated with the point (x_i, y_j). Conceptually speaking, having a range signature associated with each point on the grid is almost equivalent to performing TOA-based range measurements to

0-7803-8523-3/04/$20.00 ©2004 IEEE.

each point on the grid, and we will call the overall construct a *TOA grid.*

Since the range values forming the range signature for a given point can be based on straightforward geometric calculations (assuming the locations of the BSs are known accurately), the range signature is exact. Therefore, the user location can be estimated by comparing the vector of range measurements to the range signature at each point, and noting the degree of similarity between them. Specifically, for each point on the TOA grid, (x_i, y_j), an error figure, e_{ij}, is calculated as:

$$e_{ij} = ||\mathbf{D} - \mathbf{r}_{ij}|| \quad (1)$$

The estimated location, $\boldsymbol{R}_{est}$, is that point, (x_i, y_j), on the grid which corresponds to the minimum value of e_{ij}.

As may be expected, the granularity of the TOA grid, as given by h, is a big determinant of the estimation accuracy for this algorithm.

B. Least-Squares (LS) Algorithm

The LS algorithm is fundamentally focused on minimizing the value of the objective function, $f(\mathbf{x})$, usually formulated as:

$$f(\mathbf{x}) = \sum_{i=1}^{N} \left(\sqrt{(x - x_i)^2 + (y - y_i)^2} - d_i \right)^2 \quad (2)$$

where N is the number of reference base stations. The square-root term is readily recognized as the range between a point (x, y) in the Cartesian coordinate system, and a reference base station located at (x_i, y_i). The difference in the parentheses is commonly called the *residual* of the estimate. Of course, at the true location of the user, each of terms within the summation would be identically zero, such that $f(\mathbf{x}) = 0$. However, in practice, the set of range measurements, d_i ($1 \le i \le N$), contains some errors, such that the summation in equation (2) will never be identically zero. The sources of these errors are basically two-fold: systematic (such as those related to synchronization mismatch between a transmitter and receiver), and channel-related (such as those due to Obstructed LOS (OLOS) channel conditions). In this paper, we assume that the systematic errors in the range measurements are negligible, and that the dominant source of errors is the channel. OLOS channel conditions generally result in the strongest signal being received with longer delay, with the resulting range measurement being longer than it should be. Under such circumstances, a solution (x, y) can be found, which minimizes the value of $f(\mathbf{x})$ in a least-squares sense. For this paper, we used a least-squares algorithm developed by Davidon [5] to minimize $f(\mathbf{x})$, which we discuss below.

The Davidon algorithm is a computationally efficient least-squares algorithm that is based on the Newton-Raphson method, and belongs in the general category of quasi-Newton methods [6]. The Davidon algorithm searches for the point minimizing (2) (generally denoted as the vector, $\mathbf{x}$) in an iterative manner, as defined by the equation:

$$\mathbf{x}_{k+1} = \mathbf{x}_k - \mathbf{H}_k \mathbf{g}(\mathbf{x}_k) \quad (3)$$

where $\mathbf{H}_k$ represents an approximation to the inverse of the Hessian of $f(\mathbf{x})$, $\mathbf{G}(\mathbf{x})$, whose elements are defined as:

$$G_{jk}(x_1, x_2, \ldots x_N) \equiv \frac{\partial^2 f(x_1, x_2, \ldots x_N)}{\partial x_j x_k} \quad (4)$$

and $\mathbf{g}(\mathbf{x})$ is the gradient of $f(\mathbf{x})$, defined as:

$$\mathbf{g}(\mathbf{x}) = \nabla f(\mathbf{x}) \quad (5)$$

As can be seen from (4), $\mathbf{G}(\mathbf{x})$ is a matrix of second derivatives. It can be shown that $\mathbf{G}(\mathbf{x})$ is both symmetric, and positive-definite. However, computing the Hessian and its inverse at every iteration point (as the Newton-Raphson method generally requires) can be computationally prohibitive. Therefore, the Davidon algorithm tries to construct an approximation to it. Of course, in doing this, one would have to ensure that the approximation, $\mathbf{H}_k$, stays both symmetric and positive-definite from one iteration to the next. To accomplish this, $\mathbf{H}_k$ is updated according to the equation:

$$\mathbf{H}_{k+1} = \mathbf{H}_k + \frac{\lambda_k - 1}{\rho_k} \mathbf{r}_k \mathbf{r}_k^T \quad (6)$$

where:

$$\mathbf{r}_k = \mathbf{H}_k \mathbf{g}(\mathbf{x}_{k+1}) \quad (7)$$

and

$$\rho_k = (\mathbf{g}(\mathbf{x}_{k+1}))^T \mathbf{H}_k (\mathbf{g}(\mathbf{x}_{k+1})) = \mathbf{r}_k^T \mathbf{g}(\mathbf{x}_{k+1}) \quad (8)$$

Equation (8) is readily recognized as a quadratic form. Therefore, as long as $\mathbf{H}_k$ is positive-definite, ρ_k will be greater than zero, and will be zero only if $\mathbf{g}(\mathbf{x})$ is zero. As such, (8) is often used as an explicit stopping criterion for the algorithm. Of course, in practice, ρ_k will never be identically zero, but can be compared to some small tolerance value, ε, so that computations stop when $\rho_k \le \varepsilon$.

All this leaves us with the task of setting λ_k, which is somewhat more complex. As can be inferred from (6), this quantity is of central importance in ensuring that the $\mathbf{H}_k$ matrices remain positive-definite throughout successive iterations. It can be shown ([5]) that:

$$\lambda_k = \frac{\gamma_k}{\gamma_k + 1} \quad (9)$$

where:

$$\gamma_k \equiv -\frac{\mathbf{r}_k^T \mathbf{g}(\mathbf{x}_k)}{\rho_k} \quad (10)$$

Choosing λ_k in accordance with (9) and (10) generally ensures that $\mathbf{H}_k$ remains positive-definite from one iteration to the next, unless $\gamma_k = -1$. Because of this possibility, the Davidon algorithm provides a slightly different way of mapping γ_k values to λ_k values. Specifically, two numbers, α and β, are defined. The values of these can be picked at will.

Then, the Davidon algorithm defines the following transformation:

$$\Lambda(\gamma)=\begin{cases}\alpha & -\frac{\beta}{\beta+1}<\gamma<\frac{\alpha}{1-\alpha}\\ \beta & -\frac{\beta}{\beta-1}<\gamma<\frac{\beta}{\beta+1}\\ \frac{\gamma}{\gamma+1} & \text{elsewhere}\end{cases} \quad (11)$$

C. *Residual Weighting (RWGH) Algorithm*

The RWGH algorithm has been investigated in [7], and [8] as a way of mitigating the effects of errors in range measurements brought about by OLOS channel conditions. Although originally formulated in the context of geolocation in terrestrial cellular systems, this algorithm was included in this study to evaluate its performance in an indoor setting, and can be basically viewed as a form of weighted least-squares algorithm.

The fundamental concept behind this algorithm is as follows: since OLOS channel conditions introduce errors that are strictly positive, range measurements corrupted by OLOS errors would give rise to location estimates with higher residuals than would be the case with no OLOS errors. Therefore, if the number of range measurements is greater than the minimum required (which, for a TOA-based system, is three), then the range measurements can be grouped in various ways and intermediate LS estimates derived from those sub-groups. Some of these intermediate estimates would have lower residuals than others. The final estimate of the location can then be formed as a linear combination of these intermediate estimates, with each intermediate estimate weighted by the inverse of its associated residual. This means that, in the computation of the final estimate, those intermediate estimates with lower residuals would be assigned more weight. In this manner, the overall accuracy of the location estimate can be improved. Specifically, given M ($M > 3$) range measurements, the algorithm calls for the formation of N different range measurement combinations, where

$$N=\sum_{i=3}^{M}\binom{M}{i} \quad (12)$$

with each combination being represented by an index set $\{S_k / k = 1,2,.....N\}$. An intermediate LS estimate is then computed for each set of measurements. Note that the sets S_k will not necessarily all be of the same size. Therefore, the residuals in the intermediate LS estimates may depend on the size of the set. In order to remove this dependence, a *normalized* residual is computed for every intermediate estimate, $\mathbf{x}_k'$, as:

$$\tilde{R}_{es}(\mathbf{x'}_k, S_k)=\frac{R_{es}(\mathbf{x'}_k, S_k)}{\text{size of } S_k} \quad (13)$$

The final estimate, $\mathbf{x}'$, can then be computed as:

$$\mathbf{x'}=\frac{\sum_{k=1}^{N}\mathbf{x'}_k\left(\tilde{R}_{es}(\mathbf{x'}_k, S_k)\right)^{-1}}{\sum_{k=1}^{N}\left(\tilde{R}_{es}(\mathbf{x'}_k, S_k)\right)^{-1}} \quad (14)$$

III. OVERVIEW OF THE CHANNEL MODELS

The behavior of the channel under LOS and OLOS conditions is very different. Within the context of the geolocation problem, the different channel conditions can introduce different amounts of errors to the range measurements. This, in turn, affects the accuracy of the final location estimate. We assume the following model for the range measurement errors. Let $d_{a,i}$ represent the actual range of the user from base station i, assuming no systematic or channel-related errors. The range measurement, as reported by base station i in the presence of errors, can be modeled using the equation:

$$d_i = d_{a,i}(1+\eta) \quad (15)$$

where η is a random variable, whose distribution depends on the particular channel scenario [4]. Specifically, it has been shown that, for the LOS case, η has a Gaussian distribution with a zero mean, and a variance that depends on the system bandwidth used to make the range measurements. For the OLOS case, it has been shown that η has a hybrid distribution, which is a linear combination of Gaussian and exponential distributions, with the parameters again being a function of the system bandwidth. This paper uses the parameters as specified in [4] for the performance evaluations.

IV. PERFORMANCE EVALUATION

The performance of the three algorithms described in section II is evaluated through simulations. The regular grid arrangement of four base stations over an area of size 20m by 20m is assumed, as shown in Fig 1. A number of random user locations are simulated. Each of the BSs performs a range measurement to that user, which are corrupted, in accordance with (15), and using the particular distribution for η [4]. For the purposes of this paper, only the OLOS channel scenario is considered. System bandwidths in the range of 50 – 1000 MHz are considered for the range error models, as given in [4]. The choice of these bandwidth figures for this study is purely arbitrary; these bandwidth values are sufficient to present a good representative sample of the results. There are two performance metrics depicted in the results presented below. The first is the root-mean-square positioning error ($RMSE_{pos}$), defined as:

$$RMSE_{pos}=\sqrt{E\left\{(|\mathbf{R}_{est}-\mathbf{R}_{act}|)^2\right\}} \quad (16)$$

where $\mathbf{R}_{act}$, and $\mathbf{R}_{est}$ are the actual and estimated locations of a user. The other performance metric is the root-mean-square ranging error ($RMSE_{ran}$), defined as:

$$RMSE_{ran} = \sqrt{E\left\{(|\mathbf{d} - \mathbf{d}_{act}|)^2\right\}} \quad (17)$$

where $\mathbf{d}_{act}$ is the vector of actual (uncorrupted) range measurements, and $\mathbf{d}$ is the vector of range measurements that the BSs would report in practice (i.e. the range measurements corrupted by OLOS channel conditions).

The results are presented in Figures 3 through 6. In Figures 3 through 5, the performance of the CN-TOAG algorithm is compared against the LS and RWGH algorithms for three system bandwidth values: 50 MHz, 500 MHz, and 1000 MHz. In each of these figures, the RMSE for ranging, as well as the RMSE for positioning is depicted for each algorithm (the RMSE for ranging and positioning are referred to in the plots as RMSE 'before' and 'after' positioning respectively). Figure 6 aims to show how the performance of the CN-TOAG algorithm (i.e. the $RMSE_{pos}$ value) varies as the system bandwidth is varied.

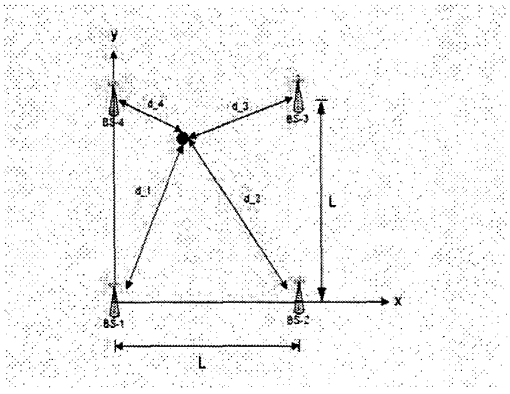

Figure 1 Basic structure of a geolocation system

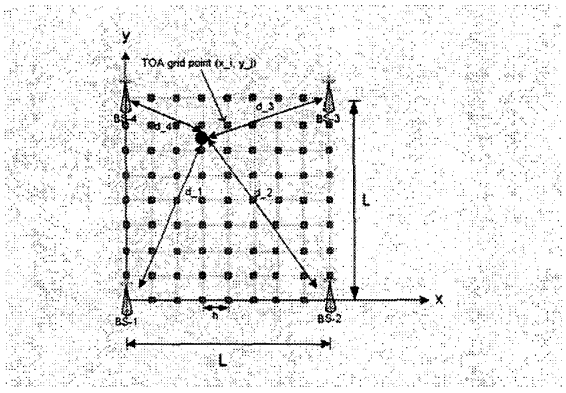

Figure 2 A geolocation system showing the TOA grid for the CN-TOAG algorithm

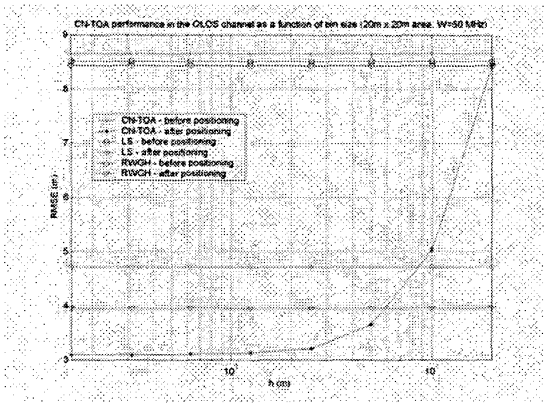

Figure 3 Comparison of CN-TOAG performance versus LS and RWGH algorithms (system bandwidth = 50 MHz)

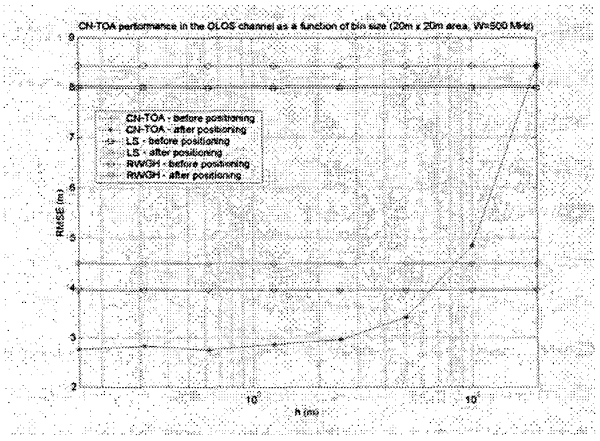

Figure 4 Comparison of CN-TOAG performance versus LS and RWGH algorithms (system bandwidth = 500 MHz)

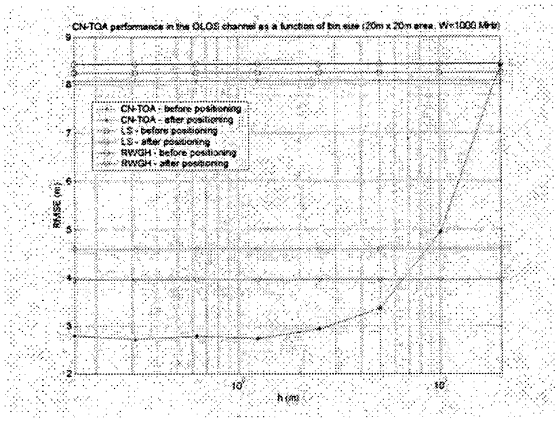

Figure 5 Comparison of CN-TOAG performance versus LS and RWGH algorithms (system bandwidth = 1000 MHz)

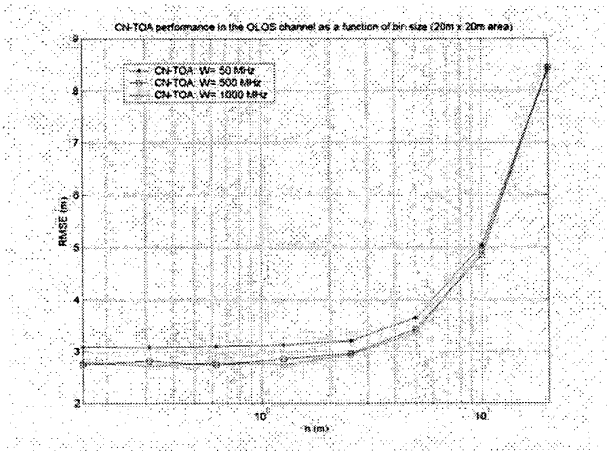

Figure 6 CN-TOAG performance at the various bandwidth values

V. CONCLUSIONS

On the basis of the results presented in the previous section, we can draw a number of conclusions:

1. CN-TOAG can achieve exactly the same level of performance as the LS and RWGH algorithms in the indoor OLOS environment, provided that the TOA grid is granular enough (i.e. h is small enough). From the results of our system scenario, we note that, regardless of the system bandwidth used to make the range measurements, CN-TOAG can achieve exactly the same performance as LS using h = 8.5 m. In the case of RWGH, the grid has to be only slightly more granular for CN-TOAG to achieve the same performance, with h in the 6 – 6.5 m range.
2. CN-TOAG performance does not appear to improve appreciably beyond a certain value of h. For the system scenario considered in this paper, this value of h is about 1.25 m.
3. From the results, we note that the CN-TOAG performance essentially stays the same between system bandwidth values of 500 and 1000 MHz. As the bandwidth of the system used to make the range measurements is increased, the range measurements themselves would be more accurate, which is normally expected to translate to a more accurate location estimate. However, for the CN-TOAG algorithm, the results suggest that beyond a certain point, increasing the system bandwidth any further will not necessarily result in greater accuracy in the location estimates. This issue is currently under further investigation.

ACKNOWLEDGMENT

The authors would like to thank Bardia Alavi and the rest of their colleagues at the Center for Wireless Information Network Studies for the many helpful discussions regarding this paper. In addition, the principal author would like to thank one of his former colleagues, Dr. David F. Freeman, for his help regarding the Davidon LS algorithm. Verizon Communications did not sponsor, participate in, or provide technical guidance/review of, the work reported in this paper. The second author's work on this paper was partially supported by the National Science Foundation grant number 0084112.

REFERENCES

[1] K. Pahlavan, X. Li, J. Mäkelä, "Indoor geolocation science and technology", IEEE Communications Magazine, pp. 112-118, February 2002.

[2] K. Pahlavan, P. Krishnamurthy, J. Beneat, "Wideband radio propagation modeling for indoor geolocation applications", IEEE Communications Magazine, pp. 60-65, April, 1998.

[3] B. Alavi, K. Pahlavan, "Modeling of the distance error for indoor geolocation", Proceedings of the IEEE Wireless Communications and Networking Conference (WCNC), 2003, vol. 1, pp. 668-672, March, 2003.

[4] B. Alavi, K. Pahlavan, "Bandwidth effect on distance error modeling for indoor geolocation", Proceedings of the IEEE Personal Indoor Mobile Communications Conference (PIMRC), 2003.

[5] W.C. Davidon, "Variance algorithm for minimization", Computer Journal, Vol. 10, pp. 406-410, 1968.

[6] R. Fletcher, Practical Methods of Optimization, John Wiley & Sons, 1987.

[7] P-C. Chen, "Mobile position location estimation in cellular systems", PhD Thesis, WINLAB, Electrical and Computer Engineering Dept., Rutgers University, 1999.

[8] P-C. Chen, "A non-line-of-sight error mitigation algorithm in location estimation", Proceedings of the IEEE Wireless Communications and Networking Conference, 1999

Performance Evaluation of Indoor Geolocation Systems Using PROPSim Hardware and Ray Tracing Software

Mohammad Heidari *Student Member, IEEE*, Kaveh Pahlavan, *Fellow, IEEE*

Center for Wireless Information Network Studies
Worcester Polytechnic Institute
100 Institute Rd., Worcester , MA 01605
(508) 831-5018, (508) 831-5634
mheidari@wpi.edu , kaveh@ece.wpi.edu
http://www.cwins.wpi.edu

Abstract— **In this paper we present a real-time channel simulation environment for performance evaluation of the indoor geolocation systems using RSS. The EKAHAU positioning software is used as the test positioning system for performance evaluation. The core of the testbed hardware is the PROPSim real-time channel simulator originally developed for real time performance evaluation of wireless communication modems. We interface the hardware to 2D Ray tracing software to make it suitable for simulation of the indoor location identification. This paper provides implementation details of this testbed and presents the preliminary results of our performance evaluation.**

***Index Terms*—Indoor Geolocation, performance evaluation, RSS fingerprinting algorithm, and Testbed.**

I. INTRODUCTION

Recently indoor geolocation applications have attracted considerable attention in the field of telecommunication.

Accurately predicting the location of an individual or an object definitely can be an ambiguous and difficult task because of the harsh wireless environment. The indoor radio propagation channel is characterized as site-specific, severe multipath, and low probability of a Line Of Sight (LOS) signal propagation path between the transmitter and receiver [1]. Applications for indoor geolocation systems consist of three main categories; commercial, public safety and military applications. In commercial applications the main need is for locating patients in a hospital or important objects in warehouses. Public safety application comprises of locating inmates in prison or firefighters in a building. In military applications the main interest is tracing soldiers in combat. Recently there are software packages available in the market which can locate the predefined object almost precisely but still there is a strong interest for more accurate systems comparable to outdoor geolocation systems like GPS.

Basically the indoor geolocation procedure begins with collecting metrics according to the position of the mobile terminal relative to the reference point. Almost any sort of metric which is used in telecommunication systems can also be used in geolocation systems. Direction of Arrival (DOA) and Received Signal Strength (RSS) are the most popular ones but one can use Time of Arrival (TOA) and Phase of Arrival (POA) as well. They are used widely in location estimation systems. GPS, which is the most famous positioning system, works with the TOA of the signal.

The second step is to process the gathered metrics and estimate the location of the desired object. This step usually requires signal processing knowledge unless fingerprinting method is being used. In this method before any location estimation one should build a grid network for the place and collect the metric according to the location of each node in grid. After building the database for a new location one can measure the metric and compare it with database to find the best node that could be referred to the desired point. In any other methods metrics should be processed. Figure 1 demonstrates a block diagram of the positioning process. The more reliable measured metrics we have, the less complex the estimation algorithm would be.

The idea of developing a real-time testbed for indoor geolocation systems can help us to evaluate the performance

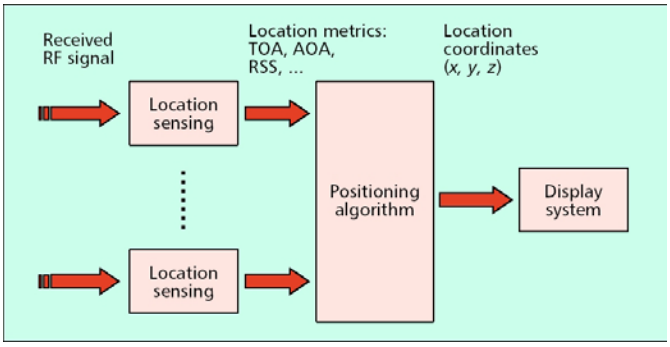

Figure 1: Block Diagram of positioning systems

of a positioning system in a specific building. No work has been done in terms of performance evaluation of indoor geolocation systems so this real-time testbed will help us to assess the performance of such systems.

There are two approaches for building an infrastructure for positioning systems. The first approach is to use the existing infrastructure for WLAN systems and develop a signaling system while the second approach requires designing a specific infrastructure for positioning.

The accuracy of location estimation is a function of the accuracy of location metrics and the complexity of positioning algorithms. Since the metrics for geolocation applications are AOA, RSS, and TOA, models for geolocation application must reflect the effects of channel behavior on the estimated value of these metrics at the receiver. The existing narrowband indoor radio channel models designed for telecommunication applications [2] can be used to analyze the RSS for geolocation applications. The emerging 3D channel models developed for smart antenna applications [4] might be used for modeling of the AOA for indoor geolocation applications. However, the existing wideband indoor multipath channel measurement and models [1] are not suitable for analysis of the behavior of TOA for geolocation applications.

The outline of this paper is as follows. Section 2 of this paper will review the testbed design for Real-Time positioning systems. In section 3 the results of the real-time testbed will be discussed. Section 4 includes the conclusion and future work.

II. DESCRIPTION OF THE TESTBED

In this section the general design of the testbed will be described and each block is going to be described briefly.

A. General architecture

Running massive measurement is one of the ways to evaluate the performance of a positioning system. This way also is not repeatable and every time we gather the measurement data we may get different errors. But with this Testbed one can sit in the lab and evaluate the performance of a positioning system without gathering real data from different locations. Also the scenario is repeatable with this Testbed, so we can compare the results of one positioning system with another one and compare the results.

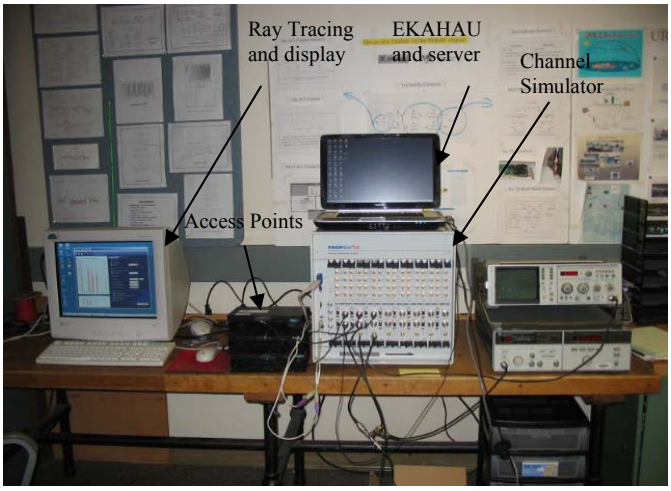

Figure 2: Depiction of Testbed

The intuition here is to use a real-time channel simulator for performance evaluation of a positioning system. With the aid of this real-time channel simulator we can simulate the channel between transmitter and receiver antenna. We can divide the testbed into two main parts, software and hardware. EKAHAU and Ray Tracing blocks are software oriented while PROPSim is hardware.

Figure 2 shows us a picture of the testbed and figure 3 shows us a Block diagram of designed testbed. Ray tracing and modeling blocks have been implemented in PC while EKAHAU and display have been implemented in the laptop. Real-time channel simulator block is connected to the access points with cables while channel models have been fed to channel simulator through a parallel interface.

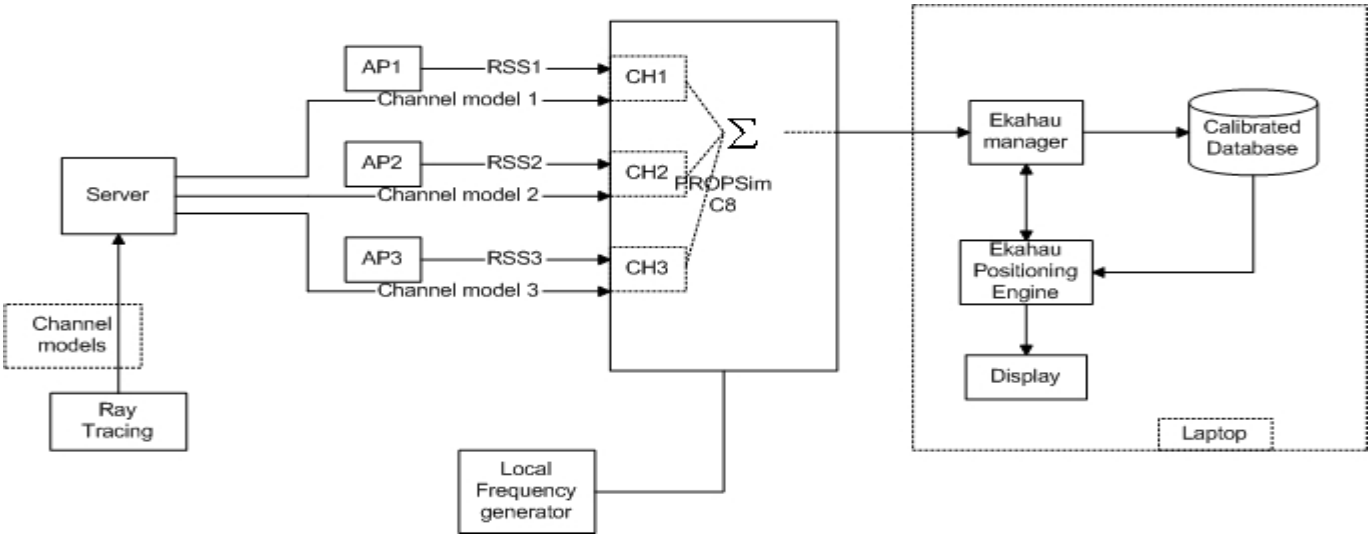

Figure 3: Block Diagram of the testbed

B. *Details of the elements of the testbed*

EKAHAU is a positioning system using RSS method and fingerprinting. This software communicates with the access points in the building to locate an object. First you have to define paths and trails for the software. Every several meters you can read the power of different access points in the building and this will be your database when you walk through all the routine paths in the building and collect data. The more data you collect, the more accurate your location estimation can be. After collecting data, you can locate your desired object. The location estimation is done based on fingerprinting method.

The core for Real-Time channel simulation is PROPSim. Basically the channel simulator works based on the tapped-delay line method where it can generate different models and channels between the input and output of the each PROPSim's channel. For our purpose, since we had 3 access points we needed 3 inputs from PROPSim and just one output. Each channel's bandwidth is 70 MHz so it is quite enough for RSS or AOA measurement methods but for TOA method there will be shortage in our setup system.

We used a 2-D ray tracing software, PlaceTool, developed at CWINS to simulate the channels as the inputs of PROPSim. This software yields all of the possible paths between transmitter and receiver regarding the reflection and transmission of the walls and the floorplan of the building.

III. PERFORMANCE EVALUATION

The scenario here is the third floor of Atwater Kent building in WPI University. The experiment was repeated for different scenarios.

A. *Effects of testbed parameters*

In order to evaluate the effects of testbed parameters we created different scenarios. First we had access point and 3 scenarios regarding the number of points which were used to train EKAHAU.

The channel responses were provided by PlaceTool Ray Tracing software. After simulation in PROPSim, the power from the access points fed into EKAHAU software as our database for fingerprinting. The grid network for location estimation consisted of 66 points. Similar to this experiment we trained the EKAHAU with 10 points and 27 points. Then we increased the number of access points having similar 3 scenarios for training points. Summary of this experiment is in the following figures.

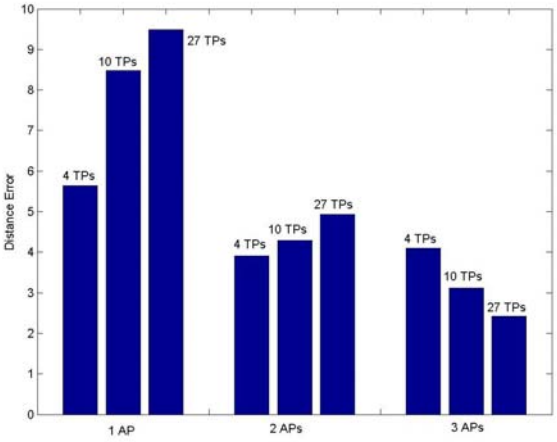

Figure 2: Standard deviation of error for different access points and different training points

Figure 4 discusses about the effect of parameters in mean of distance error. As it can be observed from the figure if you increase the number of access points the mean of error generally decreases. Change of the number of training points also affects the statistics of error. Figure 5 shows us how these parameters affect the standard deviation of error. As it can be seen, for the scenarios with 1 access point or 2 access points the increase in the number of training points increases the standard deviation. This is contrary to our expectation that an increase in training point should lead to a decrease in distance error values. One possible explanation is that with less than three access points EKAHAU is unable to build an accurate

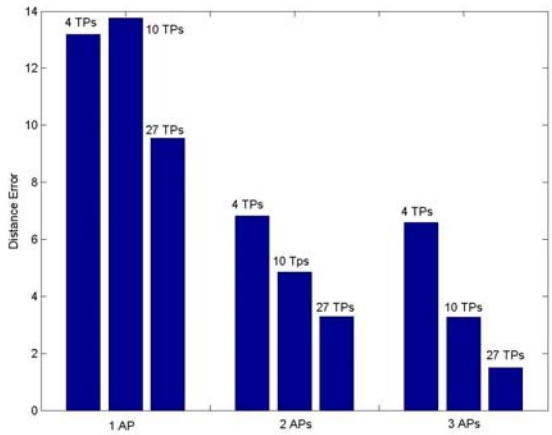

Figure 3: Mean of error for different access points and different training points

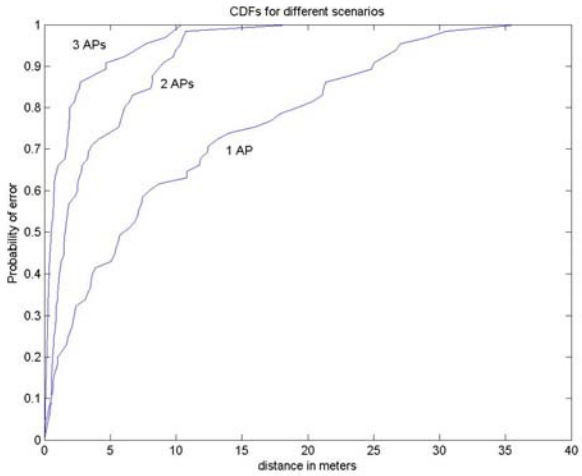

Figure 4: CDF of the error for different number of access points

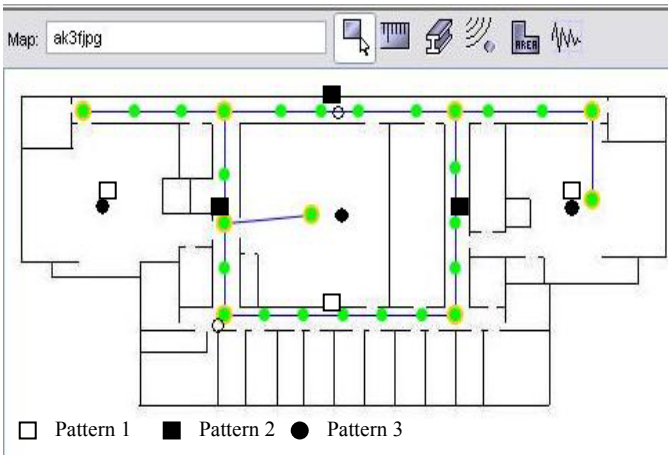

Figure 5: schematic of the location of access points for random deployment experiment

database which leads to substantially larger errors.

As it was expected the number of access points and number of training points are both important to determine the accuracy of the system. The more access points we have in the building, the more accurate the positioning system would be. The effect of training point is also important. For example with increasing the number of training points from 4 to 27 we can halve the error in mean. This will also happen if we increase the number of access points which means change in the infrastructure of the WLAN. The sample Cumulative Distributive Function (CDF) for different experiments has been shown in figure 6. As it can be noticed from figure 6, by having 3 access points and enough number of training points the error would be less than 5 meters with the probability of 0.9 while with 1 access point and the same number of training points the error is just less 21 meters %90 of the time

B. Effects of deployment strategy

This subsection focuses on finding the effect of the location of access points on the accuracy of the system. We defined 3 scenarios with 3 access points in each and we changed the location of access points for each scenario. The 3 configuration for location of access points is shown in the figure 7.

Each scenario contains 25 training points and the grid network for error estimation consisted of 100 points. We tried to arrange the access points in a manner which an actual user would arrange for telecommunication purposes. This kind of installation is the case if we want to use the existing infrastructure for positioning purposes [6].

So in the first look it can be seen that if you place the location of access points close to each other the accuracy degrades. This is mainly because when two access points are closer to each other, the number of points which may have similar power profile increases.

The next observation is that a configuration designed for telecommunication systems might not be suitable for positioning systems. For example for better coverage we may prefer to arrange the access points in a straight line, but it is obvious that this scenario is not appropriate for positioning systems. As you can see from figure 8, even the best installation for telecommunication purpose would end up with 3.5 meters error on average in location estimation and even for the second experiment the mean of error is 8 meters which is completely not suitable for indoor positioning. The other remark to be made is that since patterns 1 and 3 has almost the same access points locations, the CDF of error should be similar which in figure 8 this similarity is shown.

Figure 9 shows us the mean and standard deviation of error for this experiment. As we can see pattern 1 and pattern 3 have both close mean and variance. pattern 2 in which location of access points were close to each other was considered as the worst case since the average error is 8 meters in pattern 2.

IV. CONCLUSION AND FUTURE WORK

In this experiment it was concluded that there are several factors that affect the accuracy of location estimation using RSS method. Increasing the number of training points enhances the accuracy of estimation. Besides the fact that

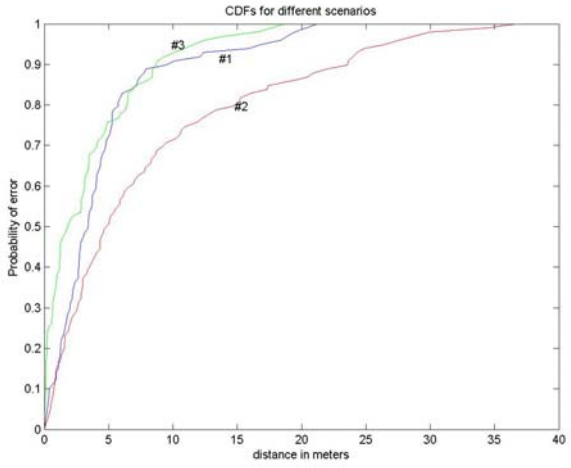

Figure 7: CDF of error for random deployment

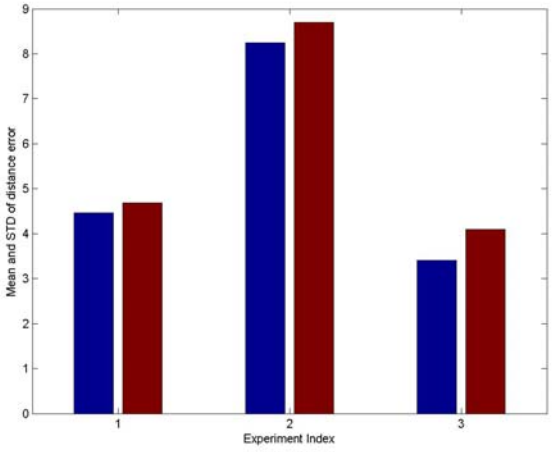

Figure 6: Mean and Standard Deviation of error for three patterns of random deployment

number of access points will affect the accuracy, the location of them is also an important parameter which should be considered. The relationship between the location of access points and accuracy of system can be found with further research.

Future work can be done in terms of channel model developing which instead of Ray Tracing channel models you can simply use your own model and see how accurate it works for indoor geolocation. Another feature which this Testbed is capable of handling is that you can define the same scenario for another positioning system and by comparing the results you are able to say which one is more accurate. Generalization of this Testbed is that you could be able to simulate the other methods of positioning rather than fingerprinting. You can define AOA in PROPSim and consequently you are able to use AOA methods of positioning. Finally this testbed can applied to TOA method if a larger bandwidth is used for channel modeling..

REFERENCES

1. K.Pahlavan and A. Levesque, *Wireless Information Networks*, John Wiley & Sons, 1995
2. K. Pahlavan, P. Krishnamurthy, J. Beneat , “Wideband Radio Propagation Modeling for Indoor Geolocation Applications” *IEEE Communication Mag*. Vol 36, no 4, Apr. 1998, pp 60-65.
3. J. Kolu, T. Jamsa, ”A Verification Platform for Cellular Geolocation Systems” Elektrobit Oy, Finland, May 2002
4. M. Hassan-Ali and K. Pahlavan, “A New Statistical model for Site-Specific Indoor Radio Propagation Prediction Based on Geometric Optics and Geometric Probabilty” *IEEE JSAC Wireless,* Jan 2002
5. T. Roos, P. Myllymaki, and H. Tirri ”A Statistical Modeling Approach to Location Estimation ” *IEEE Transactions on mobile computing*, VOL. 1, No. 1, Jan-March 2002
6. M. Unbehaun, “On the Deployment of Unlicensed Wireless Infrastructure”, PHD Dissertation, Royal Institute of Technology, Stockholm, 2002

Super-Resolution TOA Estimation With Diversity for Indoor Geolocation

Xinrong Li, *Student Member, IEEE,* and Kaveh Pahlavan, *Fellow, IEEE*

***Abstract*—This paper presents an in-depth investigation of frequency-domain super-resolution time-of-arrival (TOA) estimation with diversity techniques for indoor geolocation applications. A methodology for performance evaluation of super-resolution techniques based on the measurements of indoor radio propagation channels is presented. The performance of super-resolution techniques is compared with the performance of conventional TOA estimation techniques. The effects of diversity techniques on the performance of super-resolution techniques are evaluated. The measurement and simulation methods presented in this paper can be used to establish empirical performance bounds for real implementation of super-resolution indoor geolocation systems.**

***Index Terms*—Channel measurement, diversity techniques, indoor geolocation, performance evaluation, spectrum estimation, super-resolution, time-of-arrival (TOA) estimation.**

I. Introduction

With the emergence of location-based applications and next-generation location-aware wireless networks, location finding techniques are becoming increasingly important [1]. Location finding based on time-of-arrival (TOA) is the most popular method for accurate positioning systems. The basic problem in TOA-based techniques is to accurately estimate the propagation delay of the radio signal arriving from the direct line-of-sight (DLOS) propagation path. However, in indoor and urban areas, due to severe multipath conditions and the complexity of the radio propagation, the DLOS cannot always be accurately detected [2], [3]. Increasing time-domain resolution of channel response to resolve the DLOS path improves the performance of location finding systems employing TOA estimation techniques.

Super-resolution techniques have been studied in the field of spectral estimation [4]. Recently, a number of researchers have applied super-resolution spectral estimation techniques for time-domain analysis of different applications. These applications include electronic devices parameter measurement [5], [6] and multipath radio propagation studies [7]–[11]. In [7], the super-resolution technique was employed in the frequency domain to estimate multipath time dispersion parameters such as mean excess delay and root-mean-square delay spread. A similar method was used in [8] to model indoor radio propagation channels with parametric harmonic signal models. Here, we address the application of super-resolution techniques to accurate TOA estimation for indoor geolocation. In the literature, the time-delay estimation problem has been studied with a variety of super-resolution techniques, such as minimum-norm [9], root multiple signal classification (MUSIC) [10], and total least square-estimation of signal parameters via rotational invariance techniques (TLS-ESPRIT) [11]. While super-resolution techniques can increase time-domain resolution, it also increases complexity of system implementation. In this paper, we present an investigation of frequency-domain super-resolution TOA estimation techniques for indoor geolocation. We present and evaluate techniques that can be used in practical implementation to improve the performance of TOA estimation. To demonstrate usefulness, the performance of super-resolution techniques is compared with that of two conventional TOA estimation techniques. In addition, two diversity combining schemes are presented for super-resolution TOA estimation techniques and the effects of diversity techniques are evaluated based on these two schemes.

In the literature, the performance of super-resolution techniques for time-domain analysis is typically evaluated either by computer simulation with simple two-path channel model [9] or by using specially designed simple circuits [6]. In this paper, the performance of super-resolution TOA estimation techniques is studied through computer simulations based on measurements of indoor radio propagation channels. Due to the complexity of multipath indoor radio channels, performance analysis based on experimental channel measurement data reveals much more realistic statistical results than computer simulations with simple theoretical channel models. Furthermore, as the channel measurement system that we used provides a convenient means for conducting extensive measurements in indoor areas, the measurement and simulation methods presented in this paper can be used to conveniently establish empirical performance bounds for real implementation of super-resolution indoor geolocation systems.

The rest of the paper is organized as follows. In Section II, the MUSIC super-resolution algorithm is applied to the frequency-domain channel measurement data for TOA estimation. Then several issues in practical implementation are addressed in Section III. Section IV presents diversity techniques that can be applied to super-resolution TOA estimation. Simulation results based on measurement data are presented in Section V, which is followed by conclusions.

Manuscript received December 8, 2001; revised July 2, 2002; accepted October 4, 2002. The editor coordinating the review of this paper and approving it for publication is K. B. Lee. This work was supported in part by the National Science Foundation under Grant ECS-0084112.

The authors are with the Department of Electrical and Computer Engineering, Worcester Polytechnic Institute, Worcester, MA 01609 USA (e-mail: xinrong@wpi.edu; kaveh@wpi.edu).

Digital Object Identifier 10.1109/TWC.2003.819035

II. Super-Resolution Techniques

The multipath indoor radio propagation channel is normally modeled as a complex lowpass equivalent impulse response given by

$$h(t) = \sum_{k=0}^{L_p-1} \alpha_k \delta(t - \tau_k) \tag{1}$$

where L_p is the number of multipath components, and $\alpha_k = |\alpha_k| e^{j\theta_k}$ and τ_k are the complex attenuation and propagation delay of the kth path, respectively, while the multipath components are indexed so that the propagation delays τ_k, $0 \le k \le L_p - 1$ are in ascending order. As a result, τ_0 in the model denotes the propagation delay of the DLOS path, i.e., the TOA, which needs to be detected for the purpose of indoor geolocation. Taking the Fourier transform of (1), the frequency-domain channel response can be expressed as

$$H(f) = \sum_{k=0}^{L_p-1} \alpha_k e^{-j2\pi f \tau_k}. \tag{2}$$

The parameters α_k and τ_k are random time-variant functions because of the motion of people and equipment in and around buildings. However, since the rate of their variations is very slow as compared with the measurement time interval, these parameters can be treated as time-invariant random variables within one snapshot of measurement [12]. The phase of the complex attenuation θ_k is normally assumed random from one snapshot to another with a uniform probability density function $U(0, 2\pi)$ [13]. On the other hand, these parameters are frequency-dependent since they are related to radio signal characteristics such as transmission and reflection coefficients. However, as shown in [14], for frequency bands used in this paper, these parameters can be assumed frequency-independent.

In this paper, we consider super-resolution TOA estimation based on frequency-domain measurement of indoor channel response. In practice, discrete samples of frequency-domain channel response can be obtained by sweeping the channel at different frequencies [15], by using a multicarrier modulation technique such as orthogonal frequency-division multiplexing (OFDM), or in a direct-sequence spread spectrum (DSSS) system by deconvolving the received signal over the frequency band of high signal-to-noise ratio [7], [9]–[11].

If we exchange the role of time and frequency variables in (2), we can observe that it becomes a harmonic signal model

$$H(\tau) = \sum_{k=0}^{L_p-1} \alpha_k e^{-j2\pi f_k \tau} \tag{3}$$

which is well known in spectral estimation field [4]. Consequently, any spectral estimation techniques that are suitable for the harmonic signal model can be applied to the frequency response of multipath indoor radio channel to perform time-domain analysis. In this paper, we use the MUSIC algorithm [16], as an example of super-resolution techniques, in TOA estimation for indoor geolocation applications.

The discrete measurement data are obtained by sampling channel frequency response $H(f)$ at L equally spaced frequencies. Considering additive white noise in the measurement process, the sampled discrete frequency-domain channel response is given by

$$x(l) = H(f_l) + w(l) = \sum_{k=0}^{L_p-1} \alpha_k e^{-j2\pi(f_0 + l\Delta f)\tau_k} + w(l) \tag{4}$$

where $l = 0, 1, \ldots, L-1$, and $w(l)$ denotes additive white measurement noise with mean zero and variance σ_w^2. We can then write this signal model in vector form

$$\mathbf{x} = \mathbf{H} + \mathbf{w} = \mathbf{V}\mathbf{a} + \mathbf{w} \tag{5}$$

where

$$\begin{aligned}
\mathbf{x} &= [\,x(0) \quad x(1) \quad \ldots \quad x(L-1)\,]^T \\
\mathbf{H} &= [\,H(f_0) \quad H(f_1) \quad \ldots \quad H(f_{L-1})\,]^T \\
\mathbf{w} &= [\,w(0) \quad w(1) \quad \ldots \quad w(L-1)\,]^T \\
\mathbf{V} &= [\,\mathbf{v}(\tau_0) \quad \mathbf{v}(\tau_1) \quad \ldots \quad \mathbf{v}(\tau_{L_p-1})\,] \\
\mathbf{v}(\tau_k) &= [\,1 \quad e^{-j2\pi\Delta f \tau_k} \quad \ldots \quad e^{-j2\pi(L-1)\Delta f \tau_k}\,]^T \\
\mathbf{a} &= [\,\alpha'_0 \quad \alpha'_1 \quad \ldots \quad \alpha'_{L_p-1}\,]^T \\
\alpha'_k &= \alpha_k e^{-j2\pi f_0 \tau_k}
\end{aligned}$$

and the superscript T denotes the matrix transpose operation.

The MUSIC super-resolution techniques are based on eigendecomposition of the autocorrelation matrix of the preceding signal model in (5)

$$\mathbf{R}_{xx} = E\{\mathbf{x}\mathbf{x}^H\} = \mathbf{V}\mathbf{A}\mathbf{V}^H + \sigma_w^2 \mathbf{I} \tag{6}$$

where $\mathbf{A} = E\{\mathbf{a}\mathbf{a}^H\}$ and the superscript H denotes conjugate transpose operation, i.e., Hermitian, of a matrix. Since the propagation delays τ_k in (1) can be theorectically assumed all different, and the matrix $\mathbf{V}$ has full column rank, i.e., the column vectors of $\mathbf{V}$ are linearly independent. If we assume the magnitude of the parameters α_k is constant and the phase is a uniform random variable in $[0, 2\pi]$, the $L_p \times L_p$ covariance matrix $\mathbf{A}$ is nonsingular. Then, from the theory of linear algebra, it follows that assuming $L > L_p$, the rank of the matrix $\mathbf{V}\mathbf{A}\mathbf{V}^H$ is L_p, or equivalently, the $L - L_p$ smallest eigenvalues of $\mathbf{R}_{xx}$ are all equal to σ_w^2. The eigenvectors (EVs) corresponding to $L - L_p$ smallest eigenvalues of $\mathbf{R}_{xx}$ are called noise EVs, while the EVs corresponding to L_p largest eigenvalues are called signal EVs. Thus, the L-dimensional subspace that contains the signal vector $\mathbf{x}$ can be split into two orthogonal subspaces, known as signal subspace and noise subspace, by the signal EVs and noise EVs, respectively. The projection matrix of the noise subspace is then determined by

$$\mathbf{P}_w = \mathbf{Q}_w (\mathbf{Q}_w^H \mathbf{Q}_w)^{-1} \mathbf{Q}_w^H = \mathbf{Q}_w \mathbf{Q}_w^H \tag{7}$$

where $\mathbf{Q}_w = [\,\mathbf{q}_{L_p} \quad \mathbf{q}_{L_p+1} \quad \ldots \quad \mathbf{q}_{L-1}\,]$ and $\mathbf{q}_k$, $L_p \le k \le L-1$ are noise EVs. Since the vector $\mathbf{v}(\tau_k)$, $0 \le k \le L_p - 1$ must lie in the signal subspace, we have

$$\mathbf{P}_w \mathbf{v}(\tau_k) = 0. \tag{8}$$

Thus, the multipath delays τ_k, $0 \le k \le L_p - 1$ can be determined by finding the delay values at which the following MUSIC pseudospectrum achieves maximum value:

$$\begin{aligned}
S_{\mathrm{MUSIC}}(\tau) &= \frac{1}{||\mathbf{P}_w \mathbf{v}(\tau)||^2} = \frac{1}{\mathbf{v}^H(\tau)\mathbf{P}_w\mathbf{v}(\tau)} = \frac{1}{||\mathbf{Q}_w^H \mathbf{v}(\tau)||^2} \\
&= \frac{1}{\sum_{k=L_p}^{L-1} |\mathbf{q}_k^H \mathbf{v}(\tau)|^2}.
\end{aligned} \tag{9}$$

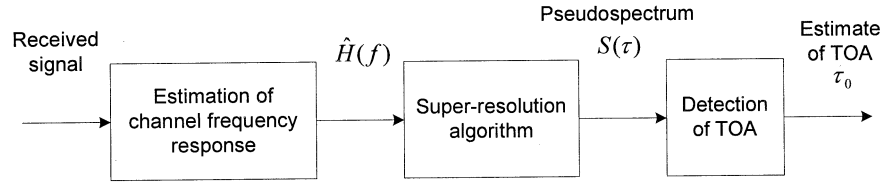

Fig. 1. Functional block diagram of the receiver of super-resolution TOA estimation systems.

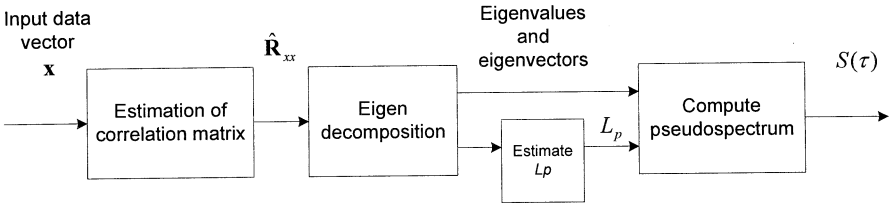

Fig. 2. Functional block diagram of the MUSIC super-resolution TOA estimation algorithm.

Fig. 1 shows a functional block diagram of the receiver of super-resolution TOA estimation systems. The received signal is first used to estimate channel frequency response. Then, a super-resolution algorithm is used to transform the channel frequency response to time domain pseudospectrum, as defined in (9). The estimate of TOA is then obtained by detecting the first peak of the pseudospectrum in the delay axis using a peak detection algorithm. In the next section, issues in the practical implementation of super-resolution TOA estimation techniques will be presented.

III. Issues in Practical Implementation

Note that in the analysis, we considered the theoretical or true correlation matrix $\mathbf{R}_{xx}$. In practice, the correlation matrix must be estimated from the measured data samples. Fig. 2 illustrates a functional block diagram of the MUSIC super-resolution TOA estimation algorithm. The input data vector, i.e., the estimate of channel frequency response given in (5), is first used to estimate the correlation matrix $\mathbf{R}_{xx}$. Then, the eigenvalues as well as the corresponding EVs of the correlation matrix are computed. The parameter L_p is determined through the analysis of the eigenvalues and EVs of the correlation matrix, which is discussed in details later in this section. Finally, the pseudospectrum is obtained using (9).

If we have P snapshots of measurement data, the estimate of the correlation matrix is obtained from

$$\hat{\mathbf{R}}_{xx} = \frac{1}{P}\sum_{k=1}^{P}\mathbf{x}^{(k)}\mathbf{x}^{(k)H} \tag{10}$$

but if only one snapshot of measurement data of length N is available, the data sequence is divided into M consecutive segments of length L and then the correlation matrix is estimated as

$$\hat{\mathbf{R}}_{xx} = \frac{1}{M}\sum_{k=0}^{M-1}\mathbf{x}(k)\mathbf{x}(k)^{H} \tag{11}$$

where $M = N - L + 1$ and $\mathbf{x}(k) = [x(k) \quad \ldots \quad x(k+L-1)]^T$. In this section, we will focus on the second method, where only one snapshot of measurement data is used in estimating data correlation matrix as in (11). Methods based on multiple snapshots will be discussed in Section IV for application with diversity techniques.

As we mentioned earlier, for the super-resolution TOA estimation techniques, the measurement data vector $\mathbf{x}$ is obtained by sampling channel frequency response uniformly over a given frequency band. In order to avoid aliasing in the time domain, similar to the time-domain Nyquist sampling theorem, the frequency-domain sampling interval Δf is determined to satisfy the condition $1/\Delta f \geq 2\tau_{\max}$, where $\tau_{\max} = \max(\tau_{L_p-1})$ is the maximum delay of the measured multipath radio propagation channel. For example, for indoor geolocation applications, the frequency sampling interval Δf is normally set to be 1 MHz, which accommodates application scenarios where the maximum delay $\tau_{\max}$ is less than 500 ns or, equivalently, the maximum length of the multipath signal propagation path is less than 150 m. Thus, with a bandwidth of 20 MHz, the length of one measurement data sequence is 21, which is far too short to accurately estimate the correlation matrix. As we will discuss, a number of issues arise and a number of techniques can be used to improve the performance when the estimate of the correlation matrix is used in the implementation of super-resolution techniques.

A. Improved Estimation of Correlation Matrix With Limited Measurement Data

The measurement data are assumed to be stationary. Thus, the correlation matrix of the data is Hermitian (conjugate symmetric) and Toeplitz (equal elements along all diagonals). However, the estimate of the correlation matrix $\hat{\mathbf{R}}_{xx}$, based on the actual measurement data of small finite length N, is not Toeplitz. The estimate of the correlation matrix can be improved using the following *forward–backward correlation matrix* (FBCM):

$$\hat{\mathbf{R}}_{xx}^{(\mathrm{FB})} = \frac{1}{2}(\hat{\mathbf{R}}_{xx} + \mathbf{J}\hat{\mathbf{R}}_{xx}^{*}\mathbf{J}) \tag{12}$$

where the superscript $*$ denotes conjugate, superscript FB stands for forward–backward estimation, and $\mathbf{J}$ is the $L \times L$ exchange matrix whose components are zero except for ones on the antidiagonal. It can be easily shown that $\hat{\mathbf{R}}_{xx}^{(\mathrm{FB})}$ is persymmetric, that is, $\mathbf{J}\hat{\mathbf{R}}_{xx}^{(\mathrm{FB})}\mathbf{J} = \hat{\mathbf{R}}_{xx}^{(\mathrm{FB})*}$, and its elements

are conjugate symmetric about both main diagonals. This technique is widely used in spectral estimation with the name *modified covariance method* [4], in linear least-square signal estimation with the name *forward–backward linear predication* [4], and in antenna array signal processing with the name *modified spatial smoothing preprocessing* [6], [17]. Here, we call the correlation matrix in (11) the *forward correlation matrix* (FCM) in contrast to the FBCM in (12).

In our development of basic theories, we assumed that the magnitude of the parameters α_k in (1) is constant and the phase θ_k is a uniformly distributed random variable so that the correlation matrix $\mathbf{A}$ in (6) is full-rank (nonsingular), but if the phase of α_k is nonrandom, which is true if only one snapshot of measurement data is used in estimating the correlation matrix $\mathbf{R}_{xx}$, the rank of the correlation matrix $\mathbf{A}$ decreases to one and the matrix becomes singular. In such a situation, the MUSIC algorithm does not work properly, but fortunately, for the signal model (4), the estimation of data correlation matrix using (11) has decorrelation effects. The decorrelation effects in forward and forward–backward correlation matrices were analyzed in [6], [17], and [18]. For the forward estimation method, following the derivation in [18] for the two-source model, the correlation coefficient between α_i' and α_j', i.e., the ith and jth element of $\mathbf{a}$, can be derived as

$$\rho_{ij}^{(\mathrm{FCM})} = \frac{A_{ij}}{\sqrt{A_{ii}A_{jj}}} = Ke^{-j\phi} \tag{13}$$

where

$$K = \frac{\sin[M\pi\Delta f(\tau_i - \tau_j)]}{M\sin[\pi\Delta f(\tau_i - \tau_j)]}$$
$$\phi = -(\theta_i - \theta_j) + 2\pi f_0(\tau_i - \tau_j) + \pi(M-1)\Delta f(\tau_i - \tau_j)$$

and A_{ij} is the (i,j)th element of the parameter correlation matrix $\mathbf{A}$. It is noted that the decorrelation effects of the forward estimation method depend on the number of segments M, the frequency sampling interval Δf, and time-delay difference $(\tau_i - \tau_j)$. Similarly, the correlation coefficient of the forward–backward estimation method can be derived as

$$\rho_{ij}^{(\mathrm{FBCM})} = K\cos\left(\phi + \frac{\psi}{2}\right)e^{j\psi/2} \tag{14}$$

where

$$\psi = 2\pi(L-1)\Delta f(\tau_i - \tau_j)$$

which depends, in addition, on the length of the segments L, phase difference of parameters $(\theta_i - \theta_j)$, and the lowest frequency of the spectrum f_0. Detailed derivations of (13) and (14) can be found in the Appendix. From

$$\left|\rho_{ij}^{(\mathrm{FBCM})}\right| = \left|\rho_{ij}^{(\mathrm{FCM})}\right| \times \left|\cos\left(\phi + \frac{\psi}{2}\right)\right| \tag{15}$$

we can clearly observe that FBCM has better decorrelation effects than the FCM. Fig. 3 shows examples of the decorrelation effects versus the number of segments calculated from (13) and (14), respectively. Later in this paper, we compare the performance of the forward and forward–backward estimation methods by computer simulations.

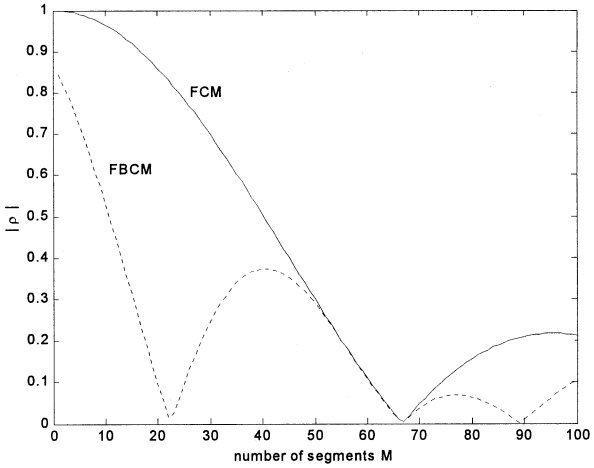

Fig. 3. Correlation coefficients of FCM and FBCM, with $\Delta f = 1$ MHz, $(\tau_i - \tau_j) = 15$ ns, $(\theta_i - \theta_j) = 0$, $f_0 = 900$ MHz, and $L = 13$.

B. Determination of Parameters L and L_p

If we use only one measurement data snapshot of length N points to estimate the TOA, the first step is to determine the value of L for estimation of $\hat{\mathbf{R}}_{xx}$ as in (11). With large values of L, the potential for higher resolution of the MUSIC algorithm increases, which is similar to that in array signal processing where increasing L means an increase in subarray aperture and, thus, an increase in resolution capability [19], [20]. On the other hand, from (11), we can see that for a fixed value of N, the value of M decreases as L increases. The decrease in M increases fluctuations in the matrix $\hat{\mathbf{R}}_{xx}$, resulting in large perturbations of the eigenvalues and EVs of $\mathbf{R}_{xx}$, and reduces the number of coherent α_k that can be detected [20], [21]. Consequently, the value of L needs to be selected so that it provides a balance between resolution and stability of the algorithm. Different values of L have been used in the literature; for example, [22] used $N/2$ and $N/3$, [19] used $3N/4$, and [9] adopted $3N/5$. In this paper, we use a value of $2N/3$, which was determined through computer simulations.

Another parameter that needs to be determined in using a super-resolution technique is the number of multipath components L_p. If the true correlation matrix $\mathbf{R}_{xx}$ is available, L_p can be easily determined by observing eigenvalues of the correlation matrix since in theory, the $L - L_p$ smallest eigenvalues of $\mathbf{R}_{xx}$ are all equal to σ_w^2, and the remaining L_p eigenvalues are all larger than σ_w^2, but in practical implementation, especially when the correlation matrix is estimated from a limited number of data samples, the noise eigenvalues are all different, which makes it challenging to clearly distinguish signal eigenvalues and noise eigenvalues. In [23], the information theoretic criteria for model selection, including Akaike information theoretic criteria and Rissanen minimum descriptive length criteria (MDL), are applied to this problem. The MDL criterion for estimation of L_p is used in this paper, which is given as [23]

$$\mathrm{MDL}(k) = -\log\left(\frac{\prod_{i=k}^{L-1}\lambda_i^{1/(L-k)}}{\frac{1}{L-k}\sum_{i=k}^{L-1}\lambda_i}\right)^{M(L-k)} + \frac{1}{2}k(2L-k)\log M \tag{16}$$

where λ_i, $0 \le i \le L-1$ are the eigenvalues of correlation matrix in descending order. The estimate of L_p is determined as the value of $k \in [0, L-1]$ for which the MDL is minimized. In [24], Xu *et al.* showed that when the forward–backward estimation method is used, the MDL criteria in (16) cannot directly apply and the second term of the criteria must be modified to $(1/4)k(2L-k+1)\log M$.

C. EV Method

One implicit assumption in the MUSIC method is that the noise eigenvalues are all equal, i.e., $\lambda_k = \sigma_w^2$ for $L_p \le k \le L-1$, that is, the noise is white. However, as we just discussed, when the correlation matrix is estimated from a limited number of data samples in practice, the noise eigenvalues are not equal. A slight variation on the MUSIC algorithm, known as the EV method, can be used to account for the potentially different noise eigenvalues [4], [25]. The pseudospectrum of the EV algorithm is defined as

$$S_{\mathrm{EV}}(\tau) = \frac{1}{\sum_{k=L_p}^{L-1} \frac{1}{\lambda_k} |\mathbf{q}_k^H \mathbf{v}(\tau)|^2} \tag{17}$$

where λ_k, $L_p \le k \le L-1$ are the noise eigenvalues. In effect, the pseudospectrum of each EV is normalized by its corresponding eigenvalue. If the noise eigenvalues are equal, the EV method and the MUSIC method are identical. The performance of the MUSIC and EV methods were compared in [25], and it was shown that the EV method is less sensitive to inaccurate estimate of the parameter L_p, which is highly desirable in a practical implementation. As presented later in this paper, the EV method is shown by computer simulations to have slightly better performance than the MUSIC method. In Section IV, we investigate diversity techniques that can be used to further improve the performance of super-resolution TOA estimation techniques.

IV. Diversity Techniques

Diversity techniques such as time diversity, space diversity, and frequency diversity are widely utilized in wireless communication systems to improve link performance [1], [13], [26]. Diversity techniques take advantage of the random nature of the radio propagation channel by finding and combining uncorrelated signal paths. In essence, all diversity techniques used for wireless communication systems can be used for TOA estimation systems with the general structure shown in Fig. 4, where the diversity system has P branches. The TOA is estimated independently at each diversity branch of receiver, and then a combining algorithm is used to process the TOA estimates from all branches to obtain an optimum estimate. A variety of different combining algorithms can be designed for different diversity techniques. The simplest one is the equal-gain combining algorithm given by

$$\hat{\tau}_0 = \frac{1}{P} \sum_{k=1}^{P} \hat{\tau}_0^{(k)}. \tag{18}$$

In some cases, more complex variable-gain combining is also possible, where the estimate of each diversity branch

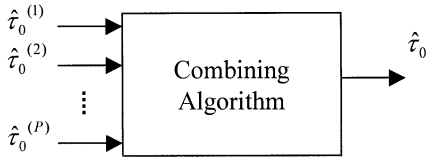

Fig. 4. General structure of TOA estimation with diversity techniques.

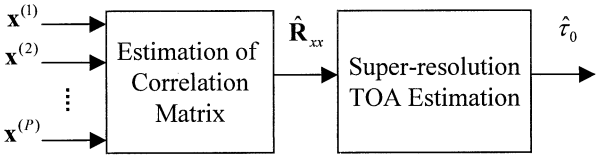

Fig. 5. Estimation of correlation matrix with diversity techniques for super-resolution TOA estimation, correlation matrix based diversity combining scheme (CMDCS).

is weighted with a coefficient that reflects the quality of time-delay estimation at each branch. More research work is needed to design optimum combining algorithms for diversity techniques.

For the super-resolution TOA estimation techniques presented in this paper, diversity techniques can also be applied, as shown in Fig. 5. Instead of combining independent time-delay estimates as in Fig. 4, the measurement data at diversity branches are combined to estimate the correlation matrix using (10). For the convenience of referencing, we call the structure in Fig. 4(a) the *general diversity combing scheme* (GDCS), and the structure in Fig. 5(a), the *correlation matrix-based* diversity combing scheme (CMDCS). In super-resolution TOA estimation techniques, the major computational load is in the eigen analysis, i.e., computing eigenvalues and EVs, of the correlation matrix. As a result, CMDCS is computationally superior to GDCS since the CMDCS scheme performs eigen analysis only once, but the GDCS scheme needs to perform independent eigen analysis P times.

On the other hand, by applying the CMDCS scheme, the underlying assumption concerning the radio propagation channel is that the amplitude attenuation and time delay for each path, and the number of signal paths are the same from the transmitter to all diversity branches of the receiver. This restricts CMDCS to only quasistationary scenarios, where the channel remains unchanged while the P diversity measurement data are collected. This is one disadvantage of the CMDCS scheme as compared with the GDCS scheme, which has no such restriction in application. This condition for applicability also makes it challenging to use CMDCS for space diversity since in space-diversity situations, the radio propagation channel from the transmitter to diversity branches of the receiver are most likely not the same. Similarly, CMDCS is not suitable for time diversity. As we discussed in Section III, the super-resolution technique cannot work properly when the phase of each signal path remains unchanged together with the amplitude attenuation and time delay for each path, and the number of signal paths. For quasistationary scenarios, it is unknown whether the phase is random or not for repeated measurements while the number of signal paths and the amplitude attenuation and time delay for each path all remain unchanged, but simulation results utilizing

measurement data collected on indoor radio channels, which will be presented in Section V, show that time-diversity with CMDCS yield almost no improvement over nondiversity techniques. In contrast, frequency-diversity can be well fitted into CMDCS. By using frequency-diversity, the kth measurement data vector $\mathbf{x}^{(k)}$, $1 \le k \le P$ are obtained using kth carrier frequency. A quantitative relationship between the improvement of TOA estimation accuracy and frequency diversity is not known, but the effects of frequency diversity can be conveniently analyzed using the correlation coefficients similar to the way by which we analyzed the forward–backward correlation method.

For frequency diversity, if the carrier frequency f_0 is uniformly distributed

$$f_0 \sim U\left(f_c - \frac{\Delta F}{2}, f_c + \frac{\Delta F}{2}\right) \tag{19}$$

where f_c is center frequency, and ΔF is the range of the frequency distribution, the correlation coefficient between α_i' and α_j' can be derived as

$$\rho_{ij}^{(\mathrm{FD})} = \frac{\sin(\pi\Delta F(\tau_i - \tau_j))}{\pi\Delta F(\tau_i - \tau_j)} e^{j[(\theta_i - \theta_j) - 2\pi f_c(\tau_i - \tau_j)]} \tag{20}$$

where the superscript FD stands for frequency diversity. Similarly, if the frequency diversity method is used for the FCM, then the correlation coefficient becomes

$$\rho_{ij}^{(\mathrm{FCM,FD})} = K' e^{-j\phi'} \tag{21}$$

where

$$K' = K\frac{\sin(\pi\Delta F(\tau_i - \tau_j))}{\pi\Delta F(\tau_i - \tau_j)}$$
$$\phi' = -(\theta_i - \theta_j) + 2\pi f_c(\tau_i - \tau_j) + \pi(M-1)\Delta f(\tau_i - \tau_j)$$

and that for FBCM becomes

$$\rho_{ij}^{(\mathrm{FBCM,FD})} = K' \cos\left(\phi' + \frac{\psi}{2}\right) e^{j\psi/2}. \tag{22}$$

We notice that by using the frequency diversity method, the coherence between multipath components is decorrelated according to the *sinc* finction as ΔF and absolute value of delay difference $(\tau_i - \tau_j)$ increase. Fig. 6 shows correlation coefficients of forward and forward–backward correlation matrices with frequency diversity, calculated from (21) and (22), using the same parameters as in Fig. 3. We can clearly observe that the frequency diversity technique further improves the decorrelation effects in both forward and forward–backward correlation matrices. Details of the derivations of (20)–(22) are presented in the Appendix.

V. Simulation Results Based on Measurement Data

In this section, we further investigate the performance of super-resolution and diversity techniques by means of computer simulations based on the measured frequency response of indoor radio propagation channels. The frequency response of the indoor radio channel can be measured with a network analyzer, as reported in [15] and [27]. The main component of our measurement system is a network analyzer that generates a swept frequency signal and analyzes the resulting received signal. The measurement data reported in [28], collected using a network analyzer, is used in this paper to evaluate the performance of super-resolution TOA estimation techniques. Magnitude and phase measurements of radio channels were performed at center frequency 1 GHz with bandwidth of 200 MHz. The measurements were conducted at three different buildings that represent highly likely places for deployment of indoor geolocation systems, including a manufacturing building at the Norton Company, Worcester, MA, a modern academic building, the Fuller Laboratory at Worcester Polytechnic Institute, Worcester, MA, and a residential house, the Schussler House at Worcester Polytechnic Institute. Thirty locations were selected at each site for measurement at places where indoor geolocation systems will be likely used. Four consecutive snapshots of the radio channel were taken at each receiver location while preventing movement around the vicinity of the antennas of transmitter and receiver. During the measurement, a transmitter was fixed at one location while a receiver was moved around. The measurement locations were distributed so as to include indoor-to-indoor, outdoor-to-indoor, and outdoor-to-second floor radio propagation conditions. For each measurement location, the physical distance between the antennas of transmitter and receiver were determined either directly or from the blueprint of building floorplans. After the measurement, the frequency domain measurement data were calibrated to remove the effects of system and antenna gains and delays [15].

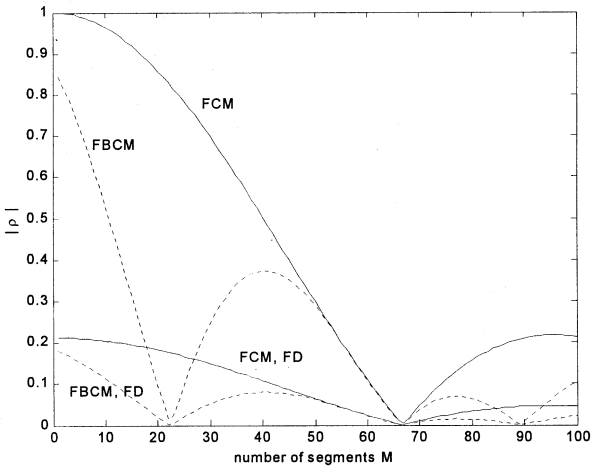

Fig. 6. Correlation coefficients of FCM and FBCM with and without frequency diversity, with $\Delta f = 1$ MHz, $(\tau_i - \tau_j) = 15$ ns, $(\theta_i - \theta_j) = 0$, $f_c = 1$ GHz, $L = 13$, and $\Delta F = 100$ MHz.

The signal bandwidth is one of the key factors affecting the accuracy of TOA estimation in multipath propagation environments [3]. To study the performance of TOA estimation using signals of various bandwidths, in the simulations, we use only a segment of each frequency domain measurement data to reflect the band-limitation effects. For example, with a 1-MHz frequency-domain sampling interval, a data segment of 21 samples, centered at 1 GHz, of each measurement data is used in simulations for a bandwidth of 20 MHz.

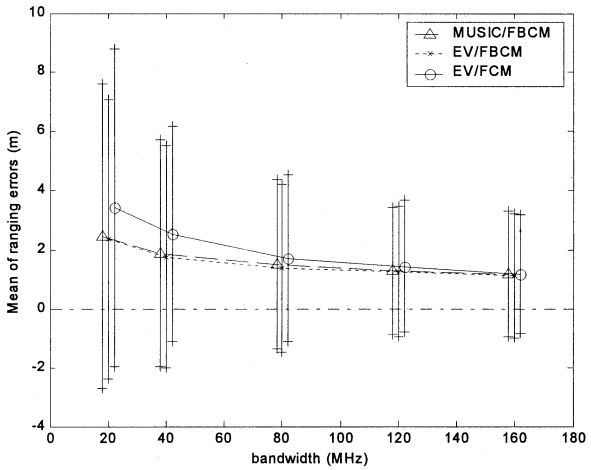

Fig. 7. Mean and STD of ranging errors using different techniques. The vertical line corresponds to plus and minus one STD about the mean.

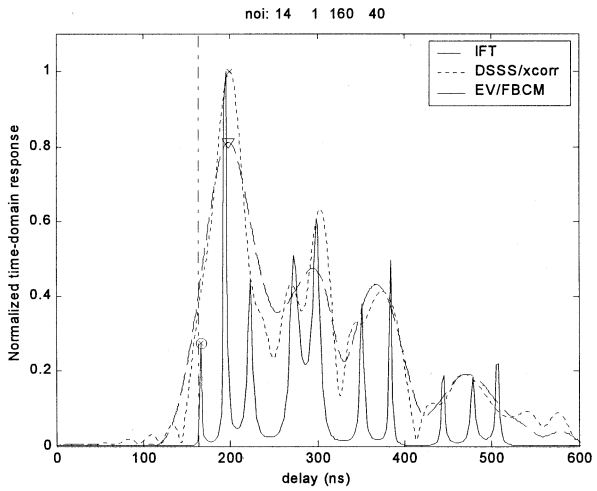

Fig. 8. Estimated TOA of the DLOS path and normalized time-domain responses obtained using three different techniques. The vertical dashed–dotted line denotes the expected TOA.

A. Performance of Super-Resolution Techniques

As we mentioned earlier, the EV method is a variant of the MUSIC method and it is preferred when the correlation matrix is estimated from a limited number of data samples. To compare the performance of EV and MUSIC methods, both algorithms are applied to the measured data with forward–backward estimation of the correlation matrix. Fig. 7 presents the mean and standard deviation (STD) of the ranging errors versus signal bandwidth. To clearly relate the results to geolocation applications, time delay τ is converted to distance d by the relationship $d = c \times \tau$, where $c = 3 \times 10^8$ m/s is the constant speed of light in free space. We can observe that both mean and STD of the ranging errors decrease as the bandwidth increases. The EV method (i.e., EV/FBCM) has slightly better performance than the MUSIC (i.e., MUSIC/FBCM) for low signal bandwidth in terms of smaller STD of ranging errors. As a result, in the following, we use the EV algorithm for further investigation.

We analyzed FCM-based and FBCM-based super-resolution TOA estimation techniques through the decorrelation effects in the estimated correlation matrix. Since there is no analytical way to quantitatively relate the improvement in the accuracy of TOA estimation to the method of correlation matrix estimation, we compare the two methods using statistical simulation results. Fig. 7 also presents simulation results for the EV algorithm with FCM. Comparing EV/FBCM and EV/FCM, it is clear that the FBCM-based method performs better than the FCM-based method in terms of smaller mean and STD of ranging errors, which is consistent with the analytical analysis. It is also noted that both techniques have similar performance when the signal bandwidth is large, e.g., bandwidth larger than 120 MHz.

B. Comparison of Super-Resolution and Conventional Techniques

In order to demonstrate the usefulness of the super-resolution technique, we compare its performance with two conventional time-delay estimation techniques. In the first of the other two techniques, the frequency-domain channel response is converted directly to time domain using the inverse Fourier transform (IFT), and then, propagation delay of the DLOS is detected. When the time-domain response over part of the time period is desired, the chirp-z transform (CZT) is preferred, providing flexibility in the choice of time-domain parameters with the cost of longer computational time as compared with IFFT (inverse fast Fourier transform) [29]. The time-domain resolution with CZT is the same as with the IFFT. On the other hand, a proper window function is needed to avoid leakage and false peaks by reducing the sidelobes of the time-domain response, which result from finite bandwidth, with the cost of reduced time-domain resolution. In our simulations, we employ CZT with the Hanning window to convert frequency channel response to the time domain.

The second technique uses the traditional cross-correlation techniques with DSSS signals (DSSS/xcorr). To simulate DSSS signal-based cross-correlation technique using measured frequency channel response data, frequency response of a raised-cosine pulse with rolloff factor 0.25 is first applied to the frequency channel response as a combined response of band-limitation pulse-shaping filters of the transmitter and receiver. Then, the resultant frequency response is converted to the time domain using the IFT for TOA estimation.

Fig. 8 shows normalized time-domain responses obtained from simulations of the three techniques using a sample channel measurement data. We observe that the super-resolution technique shows much higher time-domain resolution than the other two, and it accurately detects the delay of the DLOS path while the other two fail. Fig. 9(a) presents mean and STD of ranging errors versus the bandwidth of the system. Fig. 9(b) presents probabilities of measurement locations where absolute ranging errors are smaller than 3 m. In general, the super-resolution technique has the best performance and it is preferred, especially when the signal bandwidth is small. It should be noted that, as shown in the simulation results, while using super-resolution technique and larger bandwidth can improve the statistical performance of TOA estimation, it cannot eliminate large estimation errors at some locations. This is because of the possibility of no-LOS propagation (NLOS)

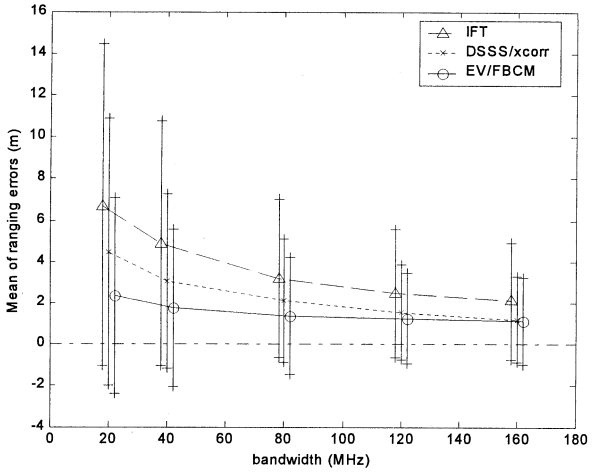

(a)

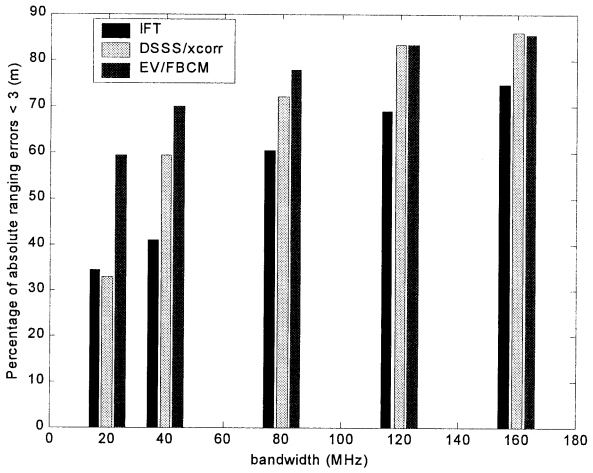

(b)

Fig. 9. Simulation results. (a) Mean of ranging errors using three different TOA estimation techniques. The vertical line corresponds to one STD. (b) Percentages of measurement locations where absolute ranging errors are smaller than 3 m.

condition between the transmitter and the receiver. Such a condition needs to be dealt with in the positioning process to achieve high positional accuracy in a geolocation system [3].

C. Effects of Time Diversity

Here, we study the effects of time diversity with the two diversity combining schemes, i.e., GDCS and CMDCS, that we discussed in Section IV. Time diversity is simulated by running simulations using the four measurements of each location, collected consecutively while stopping movement in the vicinity of the transmitter and the receiver antennas during the measurement. This represents the situation in which the system is used for quasistationary applications with four time-diversity branches. Fig. 10 presents simulation results for the EV/FBCM method with two diversity-combining schemes, i.e., EV/FBCM/TD4-CMDCS and EV/FBCM/TD-GDCS. Simulation results for the EV/FBCM method without time diversity are also shown in the figure as a reference for comparison. From the results, we can observe that there is almost no difference between the performances of the CMDCS-based method and the nondiversity method while the GDCS-based

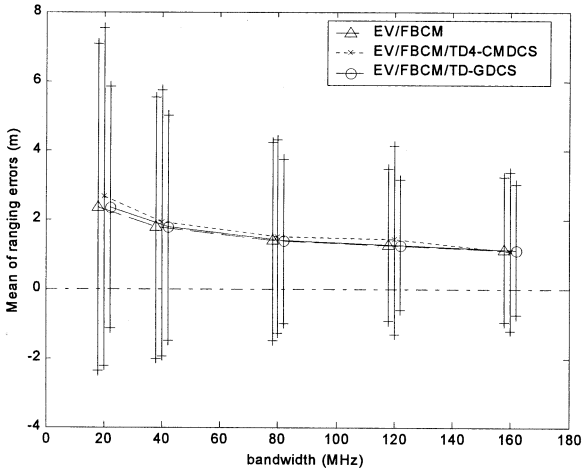

Fig. 10. Mean and STD of ranging errors with time diversity.

method has clearly better performance in terms of smaller STD of ranging errors. This verifies our earlier comment that the CMDCS is not suitable for time-diversity systems. In contrast, GDCS can be used in time-diversity systems to improve the system statistical performance to some extent.

D. Effects of Frequency Diversity

The use of frequency diversity is simulated by running simulations based on segments of data samples that are obtained by dividing each measurement data sequence of frequency channel response into a number of equally spaced segments. Since the measurement data at each location are of 200-MHz bandwidth, to avoid overlapping among diversity segments, the effect of frequency diversity is evaluated only for a bandwidth of 20 MHz. It should be noted that in real implementation, overlapping segments can be used for frequency diversity. In our simulations, the overlapping is avoided in order to avoid correlation between measurement noises in the overlapping segments since the segments are obtained from one measurement. Four equally spaced segments are first used for each measurement data sequence to compare frequency and time-diversity techniques using the same number of diversity branches. Both GDCS and CMDCS schemes are used for EV/FBCM (i.e., EV/FBCM/FD4-GDCS and EV/FBCM/FD4-CMDCS), and the results are compared with that of EV/FBCM and EV/FBCM/TD-GDCS, as shown in Fig. 11(a). The cumulative distribution function (CDF) is used for comparison. From the figure, we note that all three diversity techniques perform better than the nondiversity EV/FBCM method and frequency diversity with CMDCS has the best performance. In order to examine the effects of the number of diversity branches, we increase the number of diversity branches to ten, which is the maximum number of segments that we can achieve from 200-MHz measurement data without overlapping segments. Then, in Fig. 11(b), the simulation results of GDCS and CMDCS schemes with ten diversity branches (i.e., EV/FBCM/FD10-GDCS and EV/FBCM/FD10-CMDCS) are compared with that of nondiversity EV/FBCM and frequency diversity with four diversity branches, i.e., EV/FBCM/FD4-CMDCS, which has the best

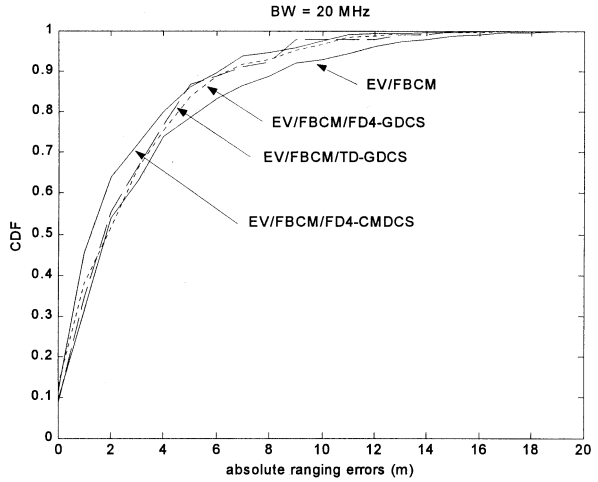

(a)

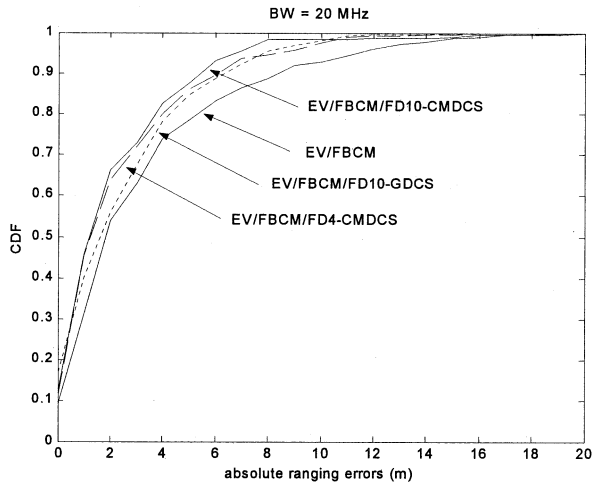

(b)

Fig. 11. CDF of ranging errors for a bandwidth of 20 MHz with frequency diversity.

performance in Fig. 11(a). From the results, it is clear that EV/FBCM/FD10-CMDCS has the best performance and even the EV/FBCM/FD4-CMDCS has slightly better performance than EV/FBCM/FD10-GDCS, though it has a smaller number of diversity branches. Consequently, we can conclude that frequency diversity can further improve the ranging performance and for frequency diversity, the CMDCS scheme is preferred to the GDCS.

VI. Conclusion

In this paper, we have applied super-resolution spectral estimation techniques to the measured channel frequency response to accurately estimate TOA for indoor geolocation applications. Our results show that super-resolution techniques can significantly improve the performance of TOA estimation as compared with conventional techniques including direct IFT and DSSS signal-based cross-correlation techniques. We have shown that a number of techniques are able to further improve the performance of super-resolution techniques, including the EV method, forward–backward estimation of correlation matrix, time diversity, and frequency diversity. For time diversity, the general diversity combining scheme is preferred while for frequency diversity, the correlation matrix-based scheme is preferred. Another important factor that affects the performance of TOA estimation is signal bandwidth. For all techniques the performance improves as signal bandwidth increases. On the other hand, as bandwidth increases, there is less difference in performance between different techniques. Also, it should be noted that due to the possibility of the NLOS condition between transmitter and receiver, using super-resolution techniques and large bandwidth cannot eliminate large ranging errors at some locations.

Appendix

The parameter correlation matrix is defined in (6) as

$$\mathbf{A} = E\{\mathbf{a}\mathbf{a}^H\}. \tag{A1}$$

Thus, using the forward estimation method, the (i,j)th element of the correlation matrix $\mathbf{A}$ can be obtained as

$$\begin{aligned} A_{ij} &= E\{\alpha_i' \alpha_j'^*\} \\ &= \frac{1}{M}\sum_{k=0}^{M-1} (\alpha_i e^{-j2\pi(f_0+k\Delta f)\tau_i}) \times (\alpha_j e^{-j2\pi(f_0+k\Delta f)\tau_{ji}})^* \\ &= \frac{1}{M}\alpha_i\alpha_j^* e^{-j2\pi f_0(\tau_i-\tau_j)} \sum_{k=0}^{M-1} e^{-j2\pi k\Delta f(\tau_i-\tau_j)} \\ &= \frac{1}{M}\alpha_i\alpha_j^* e^{-j2\pi f_0(\tau_i-\tau_j)} \frac{1-e^{-j2\pi M\Delta f(\tau_i-\tau_j)}}{1-e^{-j2\pi\Delta f(\tau_i-\tau_j)}} \\ &= \alpha_i\alpha_j^* e^{-j2\pi f_0(\tau_i-\tau_j)} e^{-j\pi(M-1)\Delta f(\tau_i-\tau_j)} \\ &\quad \times \frac{\sin[M\pi\Delta f(\tau_i-\tau_j)]}{M\sin[\pi\Delta f(\tau_i-\tau_j)]} \end{aligned} \tag{A2}$$

and it easily follows that

$$A_{ii} = |\alpha_i|^2 \tag{A3}$$

where $\alpha_i = |\alpha_i| e^{j\theta_i}$. From the definition of the correlation coefficient between the ith and jth parameters, defined as in [18], we can obtain that

$$\rho_{ij}^{(\mathrm{FCM})} = \frac{A_{ij}}{\sqrt{A_{ii}A_{jj}}} = Ke^{-j\phi} \tag{A4}$$

where K and ϕ are defined in (13).

The FBCM is defined in (12)

$$\hat{\mathbf{R}}_{xx}^{(\mathrm{FB})} = \frac{1}{2}(\hat{\mathbf{R}}_{xx} + \mathbf{J}\hat{\mathbf{R}}_{xx}^*\mathbf{J}) \tag{A5}$$

where $\hat{\mathbf{R}}_{xx}$ and $\mathbf{J}\hat{\mathbf{R}}_{xx}^*\mathbf{J}$ are forward and backward correlation matrices, respectively. The backward correlation matrix can be equivalently calculated using (11) with the data vector

$$\mathbf{x} = [\,x(L-1) \quad x(L-2) \quad \ldots \quad x(0)\,]^H \tag{A6}$$

so that the element of the parameter vector $\mathbf{a}$ in (5) becomes

$$\alpha_k' = \alpha_k^* e^{j2\pi(f_0+(L-1)\Delta f)\tau_k}. \tag{A7}$$

Thus, using the backward estimation method, the (i,j)th element of the parameter correlation matrix can be obtained as (A8), shown at the top of the page, where A_{ij} is given by (A2). Then, the (i,j)th element of the parameter correlation matrix using the forward–backward estimation method can be obtained as

$$A_{ij}^{(\mathrm{FB})} = \frac{1}{2}\left(A_{ij} + A_{ij}^{(\mathrm{B})}\right). \tag{A9}$$

$$
\begin{aligned}
A_{ij}^{(\mathrm{B})} &= \frac{1}{M}\sum_{k=0}^{M-1}\left(\alpha_i^* e^{j2\pi(f_0+k\Delta f+(L-1)\Delta f)\tau_i}\right)\times\left(\alpha_j^* e^{j2\pi(f_0+k\Delta f+(L-1)\Delta f)\tau_{ji}}\right)^* \\
&= \frac{1}{M}\alpha_i^*\alpha_j e^{j2\pi(f_0+(L-1)\Delta f)(\tau_i-\tau_j)}\sum_{k=0}^{M-1} e^{j2\pi k\Delta f(\tau_i-\tau_j)} \\
&= \frac{1}{M}\alpha_i^*\alpha_j e^{j2\pi(f_0+(L-1)\Delta f)(\tau_i-\tau_j)}\frac{1-e^{j2\pi M\Delta f(\tau_i-\tau_j)}}{1-e^{j2\pi\Delta f(\tau_i-\tau_j)}} \\
&= \alpha_i^*\alpha_j e^{j2\pi(f_0+(L-1)\Delta f)(\tau_i-\tau_j)} e^{j\pi(M-1)\Delta f(\tau_i-\tau_j)}\frac{\sin[M\pi\Delta f(\tau_i-\tau_j)]}{M\sin[\pi\Delta f(\tau_i-\tau_j)]} \\
&= A_{ij}^* e^{j2\pi(L-1)\Delta f(\tau_i-\tau_j)} \qquad \text{(A8)}
\end{aligned}
$$

Finally, the correlation coefficient between the ith and jth parameters can determined by

$$
\begin{aligned}
\rho_{ij}^{(\mathrm{FBCM})} &= \frac{A_{ij}^{(\mathrm{FB})}}{|\alpha_i||\alpha_j|} \\
&= \frac{1}{2}\left(Ke^{-j\phi}+Ke^{j(\phi+\psi)}\right) \\
&= K\cos\left(\phi+\frac{\psi}{2}\right)e^{j\psi/2} \qquad \text{(A10)}
\end{aligned}
$$

where ψ is given in (14).

For frequency diversity, we assume the carrier frequency is uniformly distributed as given in (19). The elements of the parameter correlation matrix are derived as follows:

$$
\begin{aligned}
A_{ij}^{(\mathrm{FD})} &= E\{\alpha_i'\alpha_j'^*\} \\
&= \frac{1}{\Delta F}\int_{f_c-\Delta F/2}^{f_c+\Delta F/2}\alpha_i\alpha_j^* e^{-j2\pi f_0(\tau_i-\tau_j)}df_0 \\
&= \alpha_i\alpha_j^* e^{-j2\pi f_c(\tau_i-\tau_j)}\frac{\sin[\pi\Delta F(\tau_i-\tau_j)]}{\pi\Delta F(\tau_i-\tau_j)} \qquad \text{(A11)}
\end{aligned}
$$

and the correlation coefficient is easily obtained

$$
\begin{aligned}
\rho_{ij}^{(\mathrm{FD})} &= \frac{A_{ij}^{(\mathrm{FD})}}{|\alpha_i||\alpha_j|} \\
&= \frac{\sin(\pi\Delta F(\tau_i-\tau_j))}{\pi\Delta F(\tau_i-\tau_j)}e^{j[(\theta_i-\theta_j)-2\pi f_c(\tau_i-\tau_j)]}. \qquad \text{(A12)}
\end{aligned}
$$

The correlation coefficients of forward and forward–backward estimation methods, given in (21) and (22), are easily obtained by noticing that

$$
\begin{aligned}
\rho_{ij}^{(\mathrm{FCM,FD})} &= E\left\{\rho_{ij}^{(\mathrm{FCM})}\right\} \\
\rho_{ij}^{(\mathrm{FBCM,FD})} &= E\left\{\rho_{ij}^{(\mathrm{FBCM})}\right\} \qquad \text{(A13)}
\end{aligned}
$$

where the statistical expectation $E\{\cdot\}$ is performed with respect to the uniformly distributed carrier frequency.

ACKNOWLEDGMENT

The authors would like to thank members of the CWINS at WPI, who have contributed in various ways to this work. In particular, they would like to thank Dr. J. Beneat and Dr. P. Krishnamurthy, for their work in building the database of channel measurements that were used in this paper, and Dr. A. Levesque and Dr. R. Tingley, for their comprehensive reviews that have greatly improved the manuscript.

REFERENCES

[1] K. Pahlavan and P. Krishnamurthy, *Principles of Wireless Networks—A Unified Approach*. Englewood Cliffs, NJ: Prentice-Hall, 2002.
[2] K. Pahlavan, P. Krishnamurthy, and J. Beneat, "Wideband radio propagation modeling for indoor geolocation applications," *IEEE Commun. Mag.*, vol. 36, pp. 60–65, Apr. 1998.
[3] K. Pahlavan, X. Li, and J. Makela, "Indoor geolocation science and technology," *IEEE Commun. Mag.*, vol. 40, pp. 112–118, Feb. 2002.
[4] D. Manolakis, V. Ingle, and S. Kogon, *Statistical and Adaptive Signal Processing*. New York: McGraw-Hill, 2000.
[5] W. Beyene, "Improving time-domain measurements with a network analyzer using a robust rational interpolation technique," *IEEE Trans. Microwave Theory Tech.*, vol. 49, pp. 500–508, Mar. 2001.
[6] H. Yamada, M. Ohmiya, Y. Ogawa, and K. Itoh, "Superresolution techniques for time-domain measurements with a network analyzer," *IEEE Trans. Antennas Propagat.*, vol. 39, pp. 177–183, Feb. 1991.
[7] T. Lo, J. Litva, and H. Leung, "A new approach for estimating indoor radio propagation characteristics," *IEEE Trans. Antennas Propagat.*, vol. 42, pp. 1369–1376, Oct. 1994.
[8] G. Morrison and M. Fattouche, "Super-resolution modeling of the indoor radio propagation channel," *IEEE Trans. Veh. Technol.*, vol. 47, pp. 649–657, May 1998.
[9] M. Pallas and G. Jourdain, "Active high resolution time delay estimation for large BT signals," *IEEE Trans. Signal Processing*, vol. 39, pp. 781–788, Apr. 1991.
[10] L. Dumont, M. Fattouche, and G. Morrison, "Super-resolution of multipath channels in a spread spectrum location system," *Electron. Lett.*, vol. 30, pp. 1583–1584, Sept. 1994.
[11] H. Saarnisaari, "TLS-ESPRIT in a time delay estimation," in *Proc. IEEE 47th VTC*, 1997, pp. 1619–1623.
[12] Saleh and R. Valenzuela, "A statistical model for indoor multipath propagation," *IEEE J. Select. Areas Commun.*, vol. SAC-5, pp. 128–137, Feb. 1987.
[13] K. Pahlavan and A. Levesque, *Wireless Information Networks*. New York: Wiley, 1995.
[14] G. Yang, "Performance evaluation of high speed wireless data systems using a 3D ray tracing algorithm," Ph.D. dissertation, Worcester Polytech. Inst., Worcester, MA, 1994.
[15] S. Howard and K. Pahlavan, "Measurement and analysis of the indoor radio channel in the frequency domain," *IEEE Trans. Instrum. Meas.*, vol. 39, pp. 751–755, Oct. 1990.
[16] R. Schmidt, "A signal subspace approach to multiple emitter location and spectral estimation," Ph.D. dissertation, Stanford Univ., Stanford, CA, 1981.
[17] R. Williams, S. Prasad, A. Mahalanabis, and L. Sibul, "An improved spatial smoothing technique for bearing estimation in a multipath environment," *IEEE Trans. Acoust., Speech, Signal Processing*, vol. 36, pp. 425–432, Apr. 1988.
[18] V. Reddy, A. Paulraj, and T. Kailath, "Performance analysis of the optimum beamformer in the presence of correlated sources and its behavior under spatial smoothing," *IEEE Trans. Acoust., Speech, Signal Processing*, vol. ASSP-35, pp. 927–936, July 1987.
[19] D. Tufts and R. Kumaresan, "Estimation of frequencies of multiple sinusoids: Making linear prediction perform like maximum likelihood," *Proc. IEEE*, vol. 70, pp. 975–989, Sept. 1982.
[20] H. Krim and M. Viberg, "Two decades of array signal processing research," *IEEE Signal Processing Mag.*, vol. 13, pp. 67–94, July 1996.

[21] J. Liberti and T. Rappaport, *Smart Antennas for Wireless Communications: IS-95 and Third Generation CDMA Applications*. Englewood Cliffs, NJ: Prentice-Hall, 1999.
[22] S. Lang and J. Mclellan, "Frequency estimation with maximum entropy spectral estimators," *IEEE Trans. Acoust., Speech, Signal Processing*, vol. ASSP-28, pp. 716–724, Dec. 1980.
[23] M. Wax and T. Kailath, "Detection of signals by information theoretic criteria," *IEEE Trans. Acoust., Speech, Signal Processing*, vol. ASSP-33, pp. 387–392, Apr. 1985.
[24] G. Xu, R. Roy, and T. Kailath, "Detection of number of sources via exploitation of centro-symmetry property," *IEEE Trans. Signal Processing*, vol. 42, pp. 102–112, Jan. 1994.
[25] D. Johnson and S. DeGraaf, "Improving the resolution of bearing in passive sonar arrays by eigenvalue analysis," *IEEE Trans. Acoust., Speech, Signal Processing*, vol. ASSP-30, pp. 638–647, Aug. 1982.
[26] T. Rappaport, *Wireless Communications Principles and Practice*. Englewood Cliffs, NJ: Prentice-Hall, 1996.
[27] S. Howard and K. Pahlavan, "Autoregressive modeling of wide-band indoor radio propagation," *IEEE Trans. Commun.*, vol. 40, pp. 1540–1552, Sept. 1992.
[28] J. Beneat, K. Pahlavan, and P. Krishnamurthy, "Radio channel characterization for geolocation at 1 GHz, 500 GHz, 90 MHz and 60 MHz in SUO/SAS," in *Proc. IEEE MILCOM*, 1999, pp. 1060–1063.
[29] B. Ulriksson, "Conversion of frequency-domain data to the time domain," *Proc. IEEE*, vol. 74, pp. 74–76, Jan. 1986.

Xinrong Li (S'00) received the B.E. degree from the University of Science and Technology of China, Hefei, China, in 1995 and the M.E. degree from the National University of Singapore, in 1999. He is currently pursuing the Ph.D. degree in wireless communications and networks at the Worcester Polytechnic Institute (WPI), Worcester, MA.

From 1995 to 1997, he was a System Engineer at the Shenyang Institute of Automation, Chinese Academy of Sciences, Shenyang, China. Since 1999, he has been working as a Research Assistant at the Center for Wireless Information Network Studies, WPI, on various research projects sponsored by Nokia, TEKES, Sonera, United Technologies Research Center, and the National Science Foundation. During the summer of 2002, he worked on system capacity and performance measurement and analysis of 3G all-IP CDMA2000 1xEV-DO Network Infrastructure Systems at Airvana, Inc., Chelmsford, MA. His research interests include statistical signal processing, indoor geolocation, performance analysis of wireless communication and network systems, and measurement and modeling of indoor radio propagation channels.

Kaveh Pahlavan (M'79–SM'88–F'96) is a Professor of Electrical and Computer Engineering, a Professor of Computer Science, and Director of the Center for Wireless Information Network Studies, Worcester Polytechnic Institute, Worcester, MA. He is also a Visiting Professor of the Telecommunication Laboratory and the Centre for Wireless Communications (CWC), University of Oulu, Oulu, Finland. His area of research is broadband wireless indoor networks. He has contributed to numerous seminal technical publications in this field. He is the principal author (with A. Levesque) of the *Wireless Information Networks* (New York: Wiley, 1995) and (with P. Krishnamurthy) *Principles of Wireless Networks–A Unified Approach* (Englewood Cliffs, NJ: Prentice-Hall, 2002). He has been a consultant to a number of companies including CNR Inc, GTE Laboratories, Steinbrecher Co., Simplex, Mercury Computers, WINDATA, SieraComm, 3COM, and Codex/Motorola in MA; JPL, Savi Technologies, RadioLAN in CA; Aironet in OH; United Technology Research Center in CT; Honeywell in AZ; Nokia, LK-Products, Elektrobit, TEKES, and Finnish Academy in Finland; and NTT in Japan. Before joining WPI, he was the Director of Advanced Development at Infinite Inc., Andover, MA, working on data communications. He started his career as an Assistant Professor at Northeastern University, Boston, MA.

He is the Editor-in-Chief of the *International Journal on Wireless Information Networks*. He was the Founder, Program Chairman, and Organizer of the IEEE Wireless LAN Workshop, Worcester, MA, in 1991 and 1996, and the Organizer and Technical Program Chairman of the IEEE International Symposium on Personal, Indoor, and Mobile Radio Communications (PIMRC), Boston, MA, in 1992 and 1998. He was selected as a member of the Committee on Evolution of Untethered Communication, U.S. National Research Council, in 1997 and has led the U.S. review team for the Finnish Research and Development Programs in Electronic and Telecommunication, in 1999. For his contributions to the wireless networks, he was the Westin Hadden Professor of Electrical and Computer Engineering at Worcester Polytechnic Institute from 1993 to 1996 and become a fellow of Nokia in 1999. From May of 2000, he was the first Fulbright-Nokia scholar at the University of Oulu. Because of his inspiring visionary publications and his international conference activities for the growth of the wireless LAN industry, he is referred to as one of the founding fathers of the wireless LAN industry. Details of his contributions to this field are available at www.cwins.wpi.edu.

Indoor Geolocation using OFDM Signals in HIPERLAN/2 Wireless LANs

Xinrong Li and Kaveh Pahlavan
Center for Wireless Information Network Studies
Worcester Polytechnic Institute, USA
{xinrong, kaveh}@ece.wpi.edu

Matti Latva-aho and Mika Ylianttila
Centre for Wireless Communications
University of Oulu, Finland
{matla ,over}@ees2.oulu.fi

ABSTRACT

With the finalization of new series of IEEE 802.11 and ETSI HIPERLAN standards, it becomes very important and interesting to study the methods to integrate geolocation functionalities into the next generation wireless LANs. In this paper we investigate geolocation methods and system architectures using OFDM signals in HIPERLAN/2 wireless LANs. We propose a novel method to measure geolocation metrics by exploiting the HIPERLAN/2 MAC frame structure. Computer simulation results are presented to show the performance of the geolocation systems using OFDM signals.

I. INTRODUCTION

Providing geolocation services and integrating context awareness is becoming one of the future trends of wireless data communication systems. As a result of FCC ruling concerning the enhanced wireless E911 services, considerable interests have been attracted to geolocation techniques. Similar to the geolocation applications in cellular systems, there are increasing needs in indoor environments (e.g. hospital, warehouse and emergency site) to locate expensive equipments or people (e.g. patients, children, firefighters, soldiers and policemen) [1][2]. These incentives have led to research in designing accurate geolocation systems in indoor environment where the severe multi-path radio propagation and lack of line-of-sight signal makes it very difficult for traditional GPS systems and cellular geolocation systems to provide adequate accuracy.

Geolocation information can be extracted either from a dedicated infrastructure and signaling system (e.g. GPS systems) or from an existing infrastructure and signaling system designed for wireless voice or data communications (e.g. providing geolocation services within existing cellular systems) [2]. Compared to the method of using dedicated systems, extracting geolocation information from existing signaling systems is more challenging. However, exploiting existing infrastructures and signaling system for geolocation purpose is more attractive because by using this method, geolocation related services can be easily integrated into existing wireless communication systems without significant changes in both mobile terminals and network infrastructures. With the finalization of new series of IEEE 802.11 and ETSI BRAN HIPERLAN standards, new features are being integrated into the next generation wireless LANs and it becomes very important and interesting to study the methods to integrate geolocation functionality into wireless LANs.

During the past decade, geolocation methods in DSSS (Direct Sequence Spread Spectrum) systems have been well studied. The autocorrelation properties of PN sequences make DSSS systems very suitable for ranging and geolocation applications. More recently, OFDM has been adopted by ETSI HIPERLAN/2 and IEEE 802.11a as physical layer standard for next generation wireless LANs. However, no similar studies of using OFDM systems for geolocation applications have been reported in the literature. In this paper, we investigate geolocation methods and system architectures using OFDM signals in HIPERLAN/2 wireless LANs. We propose a novel method to measure geolocation metrics TOA (Time of Arrival) and TDOA (Time Difference of Arrival) by exploiting the HIPERLAN/2 MAC frame structure.

The paper is organized as follows. In Section 2, we review those aspects of HIPERLAN/2 standards that are relevant to geolocation considerations. Then in the following section, we investigate geolocation methods and architectures in HIPERLAN/2 wireless LANs. In Section 4, we present a burst synchronization method in HIPERLAN/2 OFDM systems that can be used to extract geolocation metrics from OFDM signals. In Section 5, simulation results are presented to show the performance of OFDM based geolocation systems.

II. REVIEW OF HIPERLAN/2

The HIPERLAN is a collective reference to High Performance Radio Local Area Networks standards developed or been developing by ETSI (European Telecommunications Standards Institute) project BRAN (Broadband Radio Access Networks) [4][5]. The HIPERLAN/2 network operates in 5 GHz band, and it supports short-range broadband wireless access, 30m in typical indoor environment and up to 150m in typical outdoor or large open indoor environment.

A HIPERLAN/2 network typically has a configuration as shown in Figure 1. A number of Access Points (AP), each of which covers a certain area, are connected to a core network and form together a radio access network. The mobile terminal (MT) associates with one of the APs and communicate with the associated AP over the radio channel. Handoff between APs will be performed for the roaming MTs when necessary. HIPERLAN/2 defines two basic operation modes, the mandatory

0-7803-6465-5/00 $10.00 © 2000 IEEE

Centralized Mode and the optional Direct Mode. In the Centralized Mode, APs are connected to a core network that serves MTs associated to it. All traffic must pass through AP even if the data exchange is between two MTs in the same serving area of the AP. In the optional Direct Mode, the medium access is still controlled by a central controller but this controller needs not necessarily be connected to a core network. The MTs may communicate directly between each other. In a HIPERLAN/2 network, data transmission between MT and AP is connection-oriented. There are two types of connections, bi-directional point-to-point and unidirectional point-to-multipoint (from AP to MT). The connections between MTs and AP, which are time-division multiplexed over the air interface, are established prior to the transmission using signaling functions.

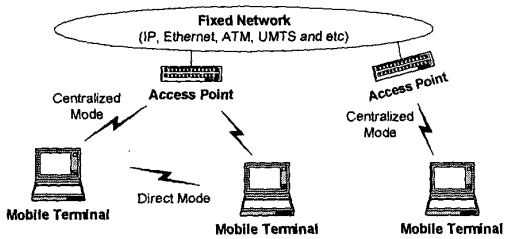

Figure 1: The HIPERLAN/2 network.

HIPERLAN/2 protocol has three basic layers: Physical (PHY) layer, Data Link Control (DLC) layer, and Convergence layer (CL). The PHY layer defines basic data transmission functions via radio channel. The DLC layer consists of Medium Access Control (MAC) function, Error Control (EC) function and Radio Link Control (RLC) function. The Convergence layer works as an intermediate component between the DLC layer and a variety of fixed networks, e.g. IP, Ethernet, ATM, UMTS and etc., to which HIPERLAN/2 network is connected.

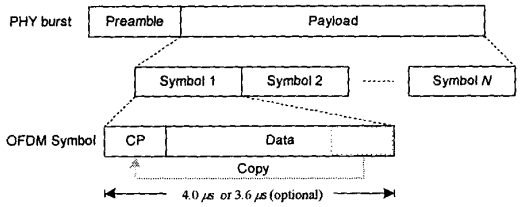

Figure 2: HIPERLAN/2 physical layer burst format with OFDM signaling.

The PHY layer of HIPERLAN/2 is based on a multicarrier modulation scheme OFDM (Orthogonal Frequency Division Multiplexing). The basic idea of the OFDM is to divide a wideband selective channel into a number of independent narrowband sub-channels so that the narrowband sub-channels can be viewed as non-selective or flat fading. OFDM can be efficiently implemented using FFT (Fast Fourier Transform) and IFFT (Inverse FFT) at the receiver and the transmitter respectively. In such a scheme, to avoid inter-symbol-interference (ISI) and to combat multipath effects, a cyclic prefix (CP), which is a copy of the ending part of OFDM symbol, is added at the beginning of each symbol as temporal guard interval as illustrated in Figure 2. As shown in Figure 2, the basic signal format on the PHY layer is a RF burst started with a preamble that is followed by a payload data part. Five different types of PHY bursts are defined with different burst preamble formats to distinguish between each other: Broadcast Burst, Downlink Burst, Uplink Burst with Short Preamble, Uplink Burst with Long Preamble and Direct Mode Burst.

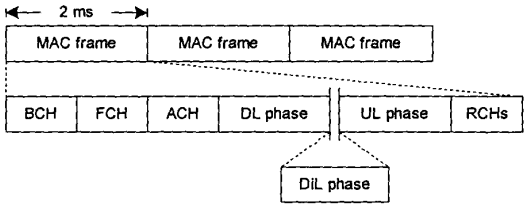

Figure 3: MAC frame structure for HIPERLAN/2.

The Data Link Control layer constitutes the logical link between AP and MTs. The functional entities in DLC layer are Medium Access Control function, Error Control function and Radio Link Control function. In HIPERLAN/2, the MAC protocol is based upon a dynamic TDMA/TDD scheme with centralized control. The Basic MAC frame structure is shown in Figure 3. The duration of each MAC frame is 2ms. Each MAC frame consists of transport channels BCH (Broadcast Channel), FCH (Frame Channel), ACH (Access Feedback Channel), a DL (Down-Link) and UL (Up-Link) phase, and one or many RCHs (Random Channel). A DiL (Direct Link) phase is also contained between DL phase and UL phase if Direct Mode is used. The duration of the BCH is fixed while the duration of the FCH, DL phase, DiL phase, UL phase and the number of RCHs are dynamically adapted by the AP according to the current traffic condition. The BCH (downlink only) contains control information that reaches all the MTs. It provides information about transmission power levels, starting point and length of the FCH and RCH, wake-up indicator, and identifiers for identifying both the HIPERLAN/2 network and the AP. The FCH (downlink only) contains an exact description of how the DL phase, UL phase and RCH are configured in the current MAC frame. The ACH (downlink only) contains information on previous access attempts made in the RCH. The DL and UL phase (bi-directional) is for the traffic of PDU (Protocol Data Unit) trains to and from the MTs respectively. The RCH (uplink only) is used by the MTs to request transmission resources for the DL or UL phase in upcoming MAC frames, and to convey some RLC signaling messages. Collisions may occur in RCH and the results from RCH access will be reported to MTs in ACH.

III. HIPERLAN/2 GEOLOCATION METHODS AND ARCHITECTURES

As we noted in the last section, HIPERLAN/2 MAC protocol is based upon dynamic TDMA/TDD scheme with centralized control. Each MAC frame of fixed length (2ms) is divided into a number of transport channels of varying length. The MAC frame synchronization between AP and MTs is established with the aid of physical layer Broadcast Burst that is transmitted at the beginning of transport channel BCH (i.e. the beginning of each MAC frame). The starting time points of other transport channels are determined with time offset from the starting point of MAC frame and are known to both AP and mobile terminals. These features of MAC frame structure can be exploited in measuring geolocation metrics TOA and TDOA from OFDM burst signals. In this section, we examine different geolocation methods in light of different geolocation architectures in HIPERLAN/2 wireless LANs.

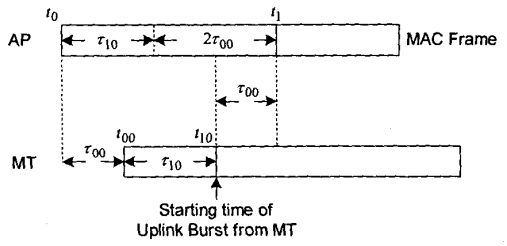

Figure 4: AP-based TOA geolocation method.

Geolocation system architectures can be roughly grouped into two categories, mobile-based and network-based architectures. In both cases, more than three Geolocation Base Stations (GBS) are needed to geometrically locate MT using multiple TOA/TDOA measurements [2]. In mobile-based architecture, MT extracts geolocation metrics from received radio signals that are transmitted by GBSs. The location information can be relayed to a Geolocation Control Station (GCS) if necessary. In network-based architecture, GBS measures radio signals transmitted by MT and then GBS or GCS extracts geolocation metrics from the measurements. The selection of geolocation system architecture depends on where the geolocation information is needed, i.e. in MT or in GCS, and some other implementation considerations in specific application scenarios. In this paper, we only focus on geolocation methods for network-based architecture. The functionality of GBS can be either implemented in AP or in a separate Geolocation Reference Point (GRP). The selection of implementation methods between AP-based and GRP-based approaches also depends on the specific application scenarios and implementation considerations. For example, in some application scenarios, only one AP is available and thus we need a few separate GRPs operating around AP to provide geolcoation services. As we will discuss later in this section, different approach requires different geolocation methods and results in different signaling requirements in HIPERLAN/2 networks.

In AP-based architecture, TOA from MT to AP can be measured basing on round-trip time of flight as illustrated in Figure 4, where t_0 and t_1 are the times (measured at AP) of transmitting Broadcast Burst and receiving Uplink Burst from MT respectively, while t_{00} and t_{10} are the times (measured at MT) of receiving Broadcast Burst from AP and transmitting Uplink Burst respectively. The delay τ_{10} is the offset of UL phase within the MAC frame, which is known to both MT and AP, and the delay τ_{00} is the TOA to be measured. The request for location services can be initiated either from GCS, which is connected to the network through wired or wireless connection, or from MT through AP (or GCS). AP assigns UL phase in current MAC frame to the target MT and the MT sends a signal within UL phase. The MT determines the starting time t_{00} of current MAC frame by measuring the receiving time of the Broadcast Burst from AP, and AP determines t_1 by measuring the receiving time of the Uplink Burst from the MT. Since the delay τ_{10} is known to both AP and MT, the TOA from MT to AP can be calculated at AP as follows:

$$\tau_{00} = \frac{1}{2}[(t_1 - t_0) - \tau_{10}]. \quad (1)$$

To perform geolocation function at GCS, TOA measurements from MT to at least three APs are required. But it should be noted that to measure TOA from MT to multiple APs, forced handoffs are needed to associate MT to different APs, which requires significant coverage overlap between adjacent APs. This is the major drawback of AP-based geolocation method.

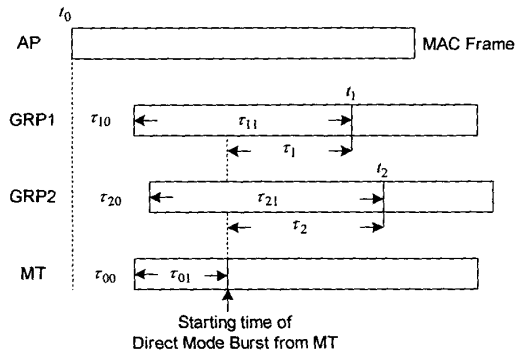

Figure 5: GRP-based TDOA geolocation method.

If the functionality of GBS is implemented in a separate Geolocation Reference Point (GRP) instead of in AP, TDOA method can be used as illustrated in Figure 5, where t_0 is the starting time of a MAC frame at AP while t_1 and t_2 are the times of receiving Direct Mode Burst at GRP1 and GRP2 respectively. The delay τ_{01} is the offset of DiL phase within MAC frame; delays τ_{00},

τ_{10} and τ_{20} are transmission delays from AP to MT, GRP1 and GRP2 respectively. In this method, after the request for geolocation services is initiated by MT or GCS, AP assigns the optional DiL phase in the current MAC frame to the MT and the MT transmits a Direct Mode Burst within the DiL phase. Then GRP measures the receiving time of the Direct Mode Burst from the MT. The TOAs from AP to GRPs τ_{10} and τ_{20} can be accurately estimated at GCS since the distances between each GRP and AP are known. Consequently, the TDOA from MT to GRP1 and GRP2 can be calculated as follows:

$$\begin{aligned} TDOA_{21} &= \tau_2 - \tau_1 \\ &= [(\tau_{20} + \tau_{21}) - (\tau_{00} + \tau_{01})] \\ &\quad - [(\tau_{10} + \tau_{11}) - (\tau_{00} + \tau_{01})] \\ &= (\tau_{20} + \tau_{21}) - (\tau_{10} + \tau_{11}) \end{aligned} \tag{2}$$

Using this method, GCS acts as a master that collects measurements of receiving time of Direct Mode Burst from multiple GRPs and calculates TDOAs as well as estimating position of MT basing on TDOAs. As a result, after measuring receiving time of Direct Mode Burst, GRPs have to request a UL phase to report the measurement to GCS. Using the GRP-based TDOA method, only one AP is needed to perform geolocation function and no forced handoff between APs are needed.

IV. BURST SYNCHRONIZATION METHODS IN HIPERLAN/2 OFDM SYSTEMS

Using the geolocation methods discussed in the preceding section, we need to determine the receiving time of physical layer burst signals at MT and AP (or GRP) that is also known as symbol timing synchronization. Symbol timing for OFDM signals is very different from that of a single carrier signals because no eye-opening point, which is the best sampling time, can be found [6]. In this section, we present burst synchronization methods in HIPERLAN/2 OFDM systems that can be used for geolocation purpose.

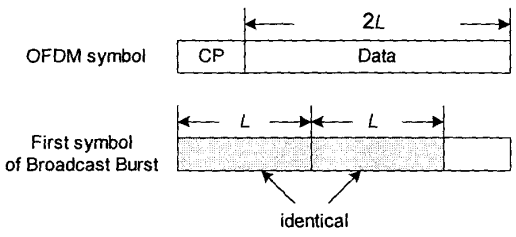

Figure 6: Training symbol in HIPERLAN/2 burst preamble.

In burst transmission mode, receiver must continuously scan for incoming data and the symbol synchronization time is required to be as short as possible. In HIPERLAN/2, the burst preamble consists of special training symbols that are used to accomplish the timing synchronization and frequency offset correction within the duration of several OFDM symbols. The first symbol in the Broadcast Burst preamble consists of two identical parts in the time domain as illustrated in Figure 6. The timing synchronization can be performed by searching for the training symbol with two identical halves. A timing metric M is formed by performing sliding correlation of two consecutive parts of the received signal $r(k)$ (each of which has a length of L) as follows [6]:

$$M(d) = \frac{|P(d)|^2}{[R(d)]^2}, \tag{3}$$

where

$$\begin{aligned} P(d) &= \sum_{m=0}^{L-1} r^*(d+m) \cdot r(d+m+L) \\ R(d) &= \sum_{m=0}^{L-1} |r(d+m+L)|^2 \end{aligned} \tag{4}$$

and * denotes complex conjugate operation. Figure 7 shows the timing metric output of the sliding correlation described above where the first vertical line indicates the starting point of the first symbol and the last vertical line is the starting point of the second symbol. Our simulation results show that this timing synchronization method works well in AWGN channel and an exponential channel that will be described in the next section. Statistical results of the timing metric obtained from our simulations (which are omitted here due to lack of space) also closely match the theoretical results presented in [6].

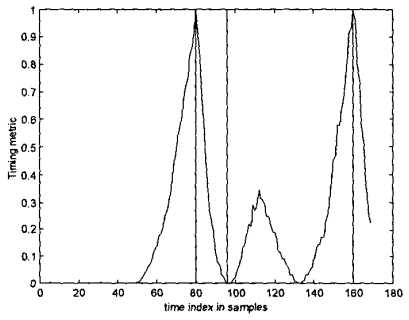

Figure 7: Timing metric without noise.

V. SIMULATION RESULTS

To study the performance of geolocation systems, ranging accuracy must be obtained first. Then the ranging accuracy can be mapped into positioning accuracy by simulations or by statistical methods. We obtained statistical results of timing errors from computer simulations using the timing synchronization method presented in the preceding section. Parameters for computer simulations are summarized in Table 1. A raised-cosine lowpass filter is used to take account of band-limitation condition that has impacts on the accuracy of timing synchronization. At the receiver an up-sampling rate of 10 is used, which is needed to make adequately high resolution in delay/distance estimation.

Two channel models are used in our simulations, AWGN channel and frequency selective channel with an exponential power delay profiles as described in [6]. AWGN channel is used to show the performance in a benign channel while the exponential channel represents a more realistic environment. For the frequency selective channel, 5 paths are chosen with path delays of 0, 2, 4, 6, and 8 samples, where sampling rate is 20MHz, so that the channel impulse response is shorter than the guard interval. The amplitude of each path is calculated from the exponential distribution:

$$A_i = \exp(-\tau_i / 8) \qquad (5)$$

where A_i is the amplitude of the ith path and τ_i is the delay of the ith path in samples. The phase of each path is chosen from a uniform distribution from 0 to 2π.

Table 1: Parameter values for HIPERLAN/2 OFDM transceiver simulations.

PARAMETER	VALUE
Number of OFDM sub-carriers	52
Sub-carrier frequency spacing	0.3125 MHz
Sampling rate	20MHz
Samples per symbol	80
Samples in cyclic prefix	16
Raised-cosine lowpass filter	$T = 1/(20\text{MHz}), \alpha = 0.25$
Up-sampling rate at receiver	10

Figure 8 shows simulation results of timing errors for the two aforementioned channel models. We can observe that compared to the AWGN channel, the mean and standard deviation of timing errors became worse for exponential channel. Since the sampling period at the receiver is $T_s = 5\text{ns}$ (with up-sampling rate 10), one sample timing error maps to 1.5m ranging error. As a result, the mean of ranging errors remains around 3m for AWGN channel and 7.5m for exponential channel when signal-to-noise ratio is greater than 9dB. The timing synchronization method used in our simulations is pretty simple since only one OFDM training symbol is used. Some other timing methods are needed to further improve the accuracy in real multi-path indoor environment.

VI. CONCLUSIONS

In this paper we presented indoor geolocation methods and system architectures for HIPERLAN/2 wireless LANs. A novel method is proposed to measure TOA and TDOA from OFDM signal by exploiting MAC frame structure in HIPERLAN/2 wireless LANs. A symbol timing synchronization method is used to obtain the statistical results of timing errors that were mapped into ranging accuracies. The simple timing method used in this paper can result in a mean ranging errors around 7.5m in the exponential channel. Other timing methods have to be combined to further improve the performance.

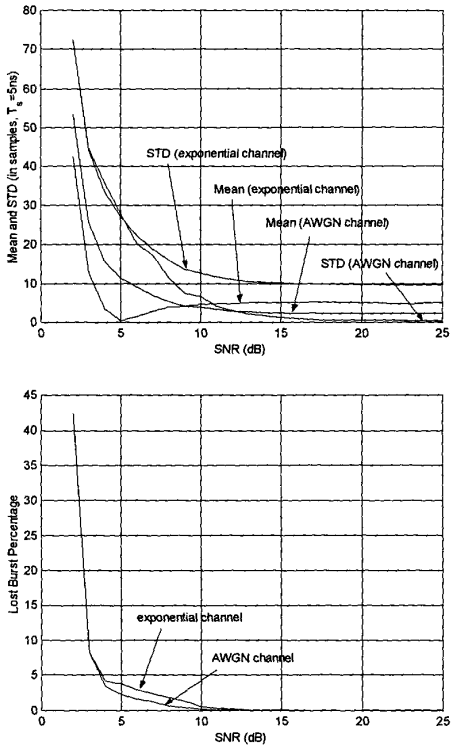

Figure 8: Mean and STD (standard deviation) of timing errors for AWGN and exponential channels.

ACKNOWLEDGEMENT

The authors would like to express their appreciation to TEKES, Nokia, and Finnish Defense Forces for supporting most parts of this project. We also thank Dr. Jacques Beneat, our colleague at CWINS, for fruitful discussions and a variety of help.

REFERENCES

[1] K. Pahlavan, P. Krishnamurthy and J. Beneat, "Wideband radio propagation modeling for indoor geolocation applications" *IEEE Comm. Magazine*, pp. 60-65, April 1998.

[2] K. Pahlavan, X. Li, *et al.*, "An overview of wireless indoor geolocation techniques and systems", *Proceeding of MWCN'2000*, Paris, Franse, May 2000.

[3] C. Sinner and R. Sigle, "Toward wireless multimedia communications. Current stands and future directions", *Int'l J. of Wireless Information Networks*, vol. 5, No.1, pp. 61-73, January 1998.

[4] ETSI, *Technical Report: TR 101 031 v2.2.1-- Requirements and architectures for wireless broadband access*, January 1999.

[5] Martin Johnsson, "HiperLAN/2– The broadband radio transmission technology operating in the 5GHz frequency band", *HiperLAN/2 Global Forum (http://www.hiperlan2.com)*, 1999.

[6] T.M. Schnidl and D.C. Cox, "Robust frequency and timing synchronization for OFDM", *IEEE Trans. Comm.*, vol. 45, No. 12, pp. 1613-1621, December 1997.